Final Technical report for Alberta Innovates –Bio Solutions and Program Partners

Project Number: VCS-11-008

Project title: Research to Support Recovery and Long Term Conservation of Grizzly Bears in Alberta.

July 2015

Prepared by:

Dr. Marc Cattet. Canadian Wildlife Health Cooperative, Saskatoon, Saskatchewan, Canada.

Dr. Nicholas Coops. Department of Forest Management, UBC. Vancouver, British Columbia, Canada.

Dr. David Janz. Department of Toxicology, Western College of Veterinary Medicine, University of Saskatchewan, Saskatoon, Saskatchewan, Canada.

Dr. Scott Nielsen. Department of Renewable Resources, University of Alberta. Edmonton, Alberta, Canada.

Gordon Stenhouse. Foothills Research Institute, Hinton, Alberta, Canada.

Table of Contents

Introduction

This document represents the full technical summaries of Alberta Innovates Bio Solutions Grant number VCS-11-008 "*Research to support recovery and long term conservation of grizzly bears in Alberta*", which was supported by Alberta Innovates Bio Solutions and government and industry partners (listed in Appendix A). This project was undertaken and completed over a three year period (2011-2014) by a multi-disciplinary research team within the Foothills Research Institute's Grizzly Bear Program as part of an ongoing long term program within provincial grizzly bear range in Alberta.

This report is presented in chapter format by research themes and the authorship of each chapter identified within each subject area.

Readers are referred to published papers listed for additional detail if required.

On behalf of our research team and all those who assisted with many aspects of this 3 year research effort, I want to thank our program partners for supporting this research effort.

Sincerely,

Gordon Stenhouse
Research Scientist and FRI Program Lead
July 29, 2015

Research Theme: Tracking and Monitoring Landscape Condition and Change

Overview

Author: Nicholas Coops

In the interest of developing a scientifically-informed platform for the projection of future landscape and habitat conditions for grizzly bears, we first require base maps of current landscape conditions and need to develop an understanding of the spatial and temporal patterns of landscape change. Such base products are fundamental. Thus, these studies are aimed to provide land and resource managers with regularly updated spatially-explicit map products to identify and understand landscape conditions in Alberta's grizzly bear range. In addition, we need to generate new GIS tools to predict landscape change and the impact of abiotic environmental drivers (e.g., climate and fire), natural biotic drivers (e.g., mountain pine beetle), and human activity (e.g., forest harvesting, oil/gas development, etc.).

Climate variability appears to affect grizzly bear populations through changes in the access and abundance of critical food resources (Theme II) thereby affecting the individual health of animals (Theme IV) and thus populations (Theme V). However, climatic variables are not the only factors driving change in Albertan grizzly bear habitat on the eastern slopes of the Rocky Mountains. Indeed, White et al.'s (2014) STAARCH-powered disturbance characterizing maps indicate that anthropogenic impacts are the most influential causes of land cover and habitat change in their 130 727 km^2 study area. Specifically with regard to grizzly bear habitat, change-inducing human activities relating to forest harvest, oil/gas drilling (well sites), and road construction were found to occur across the greatest areas, much greater than those areas disturbed by fire. The results matched well with Pasher et al.'s (2013) mapping of anthropogenic polygons across the entirety of the boreal. Some challenges remain, however, in that fire disturbance detection was lower than anticipated likely due to misclassification of fire to forest harvest. These results, localized to grizzly habitat area, have broad implications for management and planning practices, as the effects on bear-habitat interaction include aspects both positive (increased forage) and negative (increased human–bear interactions). Disturbance mapping and characterization, such as the work done here, is only one aspect however of the broader goal of base mapping grizzly bear habitat.

Another aspect of this project involved predicting the location of viable understory food species and resources that are a critical part of quality bear habitat. Nijland etal. (2014) contributed to this by comparing which model(s) would be most accurate at predicting 14 key grizzly bear understory foraging species. Against standard climate- and land cover-based landscape models, they incorporated Light Detection and Ranging (LiDAR) metrics to determine which fine-scale variables could improve model accuracy and for which species. The climate-LiDAR model demonstrated high performance capabilities for 8 of the 14 species under investigation at the fine scale, with the evidence suggesting that wet area information was critical for 6 of the 8 high-accuracy species. Given that LiDAR data is available, these results indicate that integrating LiDAR with climate variables is valuable for forest managers and environmental planners in the future in determining areas suitable for grizzly bear habitat, with particular attention being paid not as importantly to canopy cover but to the fine-scale terrain conditions that affect distributions of understory species relied on seasonally by grizzly bears.

Completing the first research theme, Nijland et al. (2015) integrated optical, multispectral Landsat data with LiDAR data to classify grizzly habitat. Optical data are not well-suited to discriminate topographical information or canopy structure, but still provide a favourable mix of availability, cost, and resolution, addition to being able to distinguish between coniferous stands and deciduous stands. The integrating approach presented, developing a new habitat classifier in western Alberta, comprised direct LiDAR measure of tree canopy height and cover with optical species-type estimates (coniferous versus deciduous). The result of this research was a highly transferrable transferable and versatile wildlife habitat classifier heuristic. Most salient to the project goals are the opportunities this heuristic presents to be an adaptable classification system that supports informed decision-making for wildlife management.

Study Summaries

Characterizing a Decade of Disturbance Events Using Landsat and MODIS Satellite Imagery in Western Alberta, Canada for Grizzly Bear Management

Carson F.H. White, Nicholas C. Coops, Wiebe Nijland, Thomas Hilker, Trisalyn A. Nelson, Michael A. Wulder, Scott E. Nielsen, Gordon Stenhouse

Canadian Journal of Remote Sensing, 40:336–347, 2014

Abstract. Mapping and quantifying the area and type of disturbance within forests is critical for sustainable forest management. Grizzly bear (*Ursus arctos*) have large home ranges and diverse habitat needs and as a result, information on the extent, type, and timing of disturbances is important. In this research we apply a remote-sensing-based disturbance mapping technique to the southeastern extent of a grizzly bear range. We apply a data fusion approach with MODIS250mand Landsat 30m spatial resolution imagery to map disturbances biweekly from 2001–2011. A regression tree classifier was applied to classify the disturbance events based on spatial and temporal characteristics. Fire was attributed as a disturbance based on a national fire database. Results indicate that across the 130,727 km^2 study area, 4,603 km^2 of forest were disturbed over the past decade (2001–2011), impacting 0.35% of the study area annually. Overall, 68.7% of the disturbance events were attributed to forest harvest, followed by well sites 13.4%, fires 9.3% and road development, 8.6%. Primary source habitat contained 3.8% of disturbed land, and primary sink areas had 5.9% disturbed land. Our findings quantify habitat change, which can aid managers by identifying significant areas for grizzly bear conservation.

Introduction. The goal of sustainable forest management is to maintain biodiversity, ecosystem structure, and ecosystem services (Amoroso et al. 2011) while allowing persistence of renewable resources for future yield. Forested ecosystems are highly dynamic and often subject to a wide range of disturbances, which can include both biological (e.g., disease, insects) and nonbiological (e.g., fire, wind throw) events as well as anthropogenic disturbances including mining, forest harvest, road building, and infrastructure development (Nielsen, Boyce, et al. 2004). The wildlife habitat will return to a natural state after fire and forest harvest, given time, whereas roads or well sites represent more permanent changes and are often viewed as habitat loss (Roever et al. 2008). Disturbances can cause mortality to organisms and alter the spatial fragmentation of the landscape, with potentially significant impacts on wildlife habitat (Gardner 1998; Nielsen, Munro, et al. 2004). The amount and extent of fragmentation, available and edge habitat quality, and resource availability are closely related to disturbance regimes and influence forest productivity and biodiversity (Berland et al. 2008; Linke et al. 2005).

In this study, we extend this work in 3 critical ways. First, we extend the size of the area of interest to cover the complete area of grizzly bear source and sink areas. Second, we temporally extend the approach to cover a decade of change in the region. Finally, we attribute the detected disturbance events as forest cutblocks, fire, well sites, or roads using a series of rules defined within the study area. This unique combination of the increased focus area, the extended time period, and the attributed disturbance types, we believe, provides the most comprehensive analysis of the disturbance regime in the area. Our approach was as follows. First, disturbance events were detected using the STAARCH approach. A decision tree approach was then applied to attribute disturbance events based on both spatial and temporal characteristics, allowing us to assess how much of this disturbance is anthropogenic or nonanthropogenic in nature. We distinguished among forest harvest, resource exploration and installations, and road development, as well as fire disturbance (based on polygons from the national fire database). Classifying disturbance by type allows anthropogenic change to be quantified and the persistence of cover change to be calculated. We examined disturbance regimes across the entire region, by season and by type. Finally, to demonstrate how these data can be used, we compared disturbance events with grizzly bear habitat states (Nielsen et al. 2006) to observe spatial patterns of disturbance with safe harbor and attractive sink habitats. Our observations aim to provide an indication of how these datasets can be used to fill missing elements to grizzly bear comprehensive management strategies, which is quantifying habitat loss and bear-disturbance interactions that can be applied over large areas.

Methods. *Disturbance Detection.* The STAARCH algorithm relates biweekly change in forest cover at 30 m spatial resolution (Hilker et al. 2009). In brief, the algorithm utilizes a minimum of 2 Landsat observations of the same location at the start and end of the study period, in addition to a sequence of MODIS 250 m images at a biweekly interval (Gao et al. 2006). First, the spatial extent of disturbances occurring from one Landsat observation to the next is mapped using 2 or more cloud-filtered scenes (Irish et al. 2006). Disturbances are mapped using a spectral disturbance index (Healy et al. 2005) based on the brightness, greenness, and wetness indices following calculation of the TCT (Kauth and Thomas 1976). Second, a time series of MODIS imagery is used to determine the time of disturbance at biweekly time steps. To do so, the MODIS-based disturbance index is computed based on the MODIS land bands and is compared to identify significant changes in the time series of biweekly observations. The STAARCH algorithm has been applied and validated in previous research within the same study area (Hilker et al. 2009). This work demonstrated the accuracy and applicability of the STAARCH-based disturbance detection technique for identifying and categorizing disturbance based on spatial and temporal metrics. Hilker et al. (2009) found that the STAARCH approach had an accuracy rate of 87%, 87%, and 89% in 2002, 2003, and 2005, respectively, for correctly identifying disturbances in the correct year, based on an independently derived disturbance mapping dataset derived from aerial photography. The spatial accuracy of the detection area itself was 93% when compared to the validation dataset. Areas where the algorithm had poorer accuracy were wetter sites, and as a result, disturbances within flood plains and bogs might be more poorly represented. Similarly successful disturbance detection is dependent on cloud-free viewing, so in some cases there was an 8-day delay in time attribution due to cloud-obscured MODIS data. Overall, however, we are confident in the accuracy of the approach and its applicability for assessing and attributing disturbances in this region. As persistent cloud and snow cover makes delineation of disturbance events extremely difficult in winter, the STAARCH methodology is applied only to growing season images (March to October). As a result, areas disturbed in winter will appear in the first image in the growing season of the following year (Hilker et al. 2009). For this project, a total of 64 Landsat 5 TM scenes covering an area of 16 path/rows, acquired between July 2001 and August 2011 were obtained free of charge and ready for analysis (Woodcock et al. 2008) from the USGS GLOVIS archive.1 Images were selected to minimize cloud cover (where possible to below 30%) as well as the temporal separation between adjacent scenes across the study area. All images were expressed as top-of-atmosphere reflectance and were corrected using a dark object subtraction technique (Song et al. 2001). Land cover data was obtained from the Landsat 7 land cover classification of Canada that was produced for the Earth Observation for Sustainable Development of forests (EOSD) initiative (Wulder,White, Cranny, et al. 2008) representing circa year 2000 conditions.

Data Analysis. Our processing methodology was as follows: first, the STAARCH algorithm was applied to identify disturbance patches. These patches were input to FRAGSTATS to calculate the required metrics for use in the decision tree developed by Hilker et al. (2011) to attribute each patch as either well site, road, or forest harvest. The fire disturbance layer was then overlaid with the patch identification layer produced from STAARCH and the decision tree, and patches identified as fire by the fire database had their attribution changed to fire, regardless of the decision tree attribution. Polygons attributed as fire by the decision tree, but not contained within the fire polygons, were attributed to forest harvest. Disturbance polygons were then analyzed temporally (monthly and annually), for the distribution of anthropogenic and natural disturbance events. Second, disturbance polygons were overlaid with the grizzly bear habitat states to observe disturbance by type on known grizzly bear habitat. We estimate confidence intervals on the disturbed areas based on the accuracy statements developed by Hilker et al. (2009) and Hilker et al. 2011). In Hilker et al. (2009), estimates of the accuracy of detecting disturbed areas is, on average, 88%. Hilker et al. (2011) evaluated the accuracy of the disturbance attribution, which was between 83–89%.

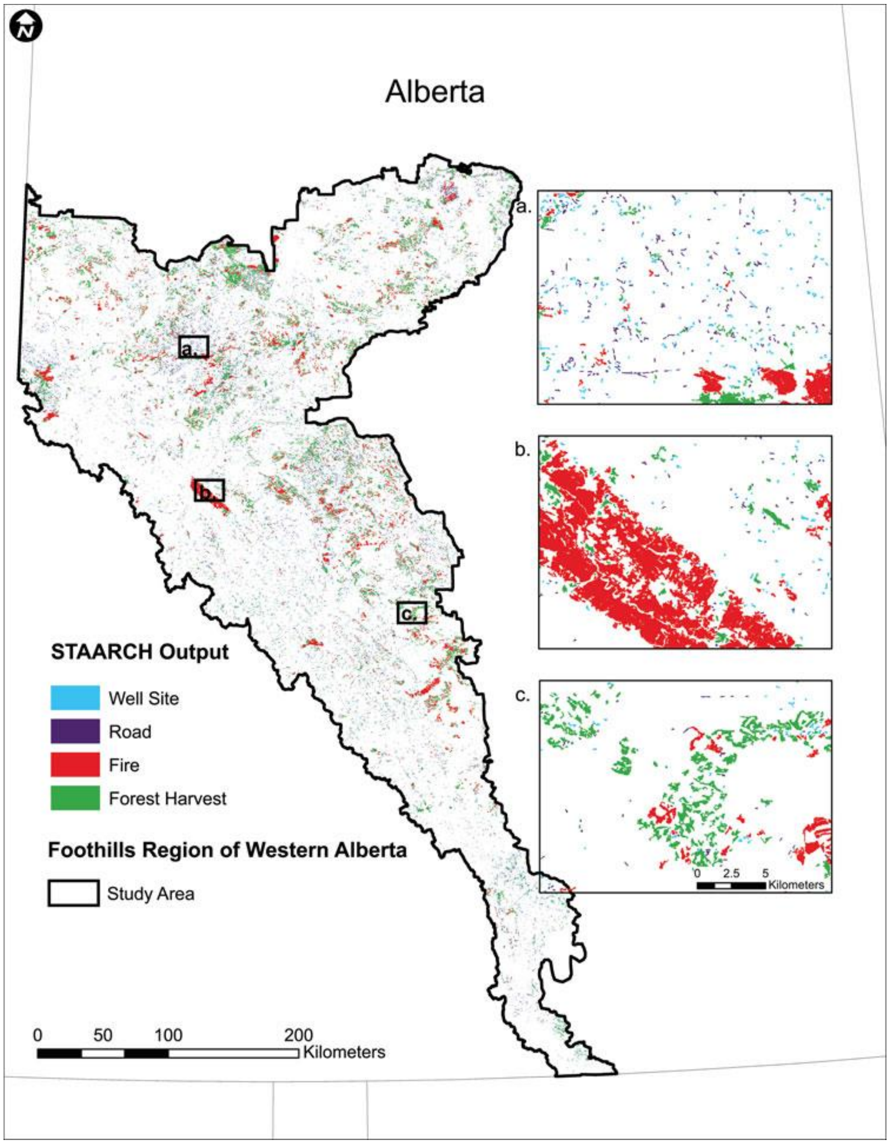

Figure 2. STAARCH output for the Grizzly bear study area classified by the type of disturbance.

Results. Summer (July and August) and fall (September and October) periods account for most of the disturbance area. The summer and fall months (July to October) have the highest proportion of forest harvesting, although this sometimes decreases temporarily during dry periods because of fire risk. Road construction remains relatively consistent throughout the year; well site construction is comparatively slower from June to August, and forest fires account for a variable portion of disturbance during the detection period, peaking in late summer and early fall. Generally, September observes the highest amount of forest disturbance through the decade, accounting for 1,032 km^2 of disturbance (22%), with forest harvesting accounting for 63.5% of that change. Well sites and roads have the smallest footprint in disturbance area, averaging 0.03 km^2 and 0.02 km^2, respectively, followed by forest harvest (0.13 km^2) and fire disturbance (0.26

km^2). Nonanthropogenic disturbance (fire) has 2% of the number of disturbance events, yet 9% (±} 0.5%) of the total area observed. Well sites and roads compose 63% of the disturbance events (35% and 28%, respectively), although compose only 22% (±} 2%) of the total disturbed area (13% and 9%, respectively). Forest harvest is 35% of the total disturbance events and occupies 69% (±} 5.5%) of the disturbed area in the study area.

Habitat State Attribution. Grizzly bear source (primary and secondary) areas had lower total disturbed area than did sink areas or noncritical habitat. Primary habitat areas had a total of 672 km^2 of anthropogenic disturbance and 195 km^2 of nonanthropogenic disturbance (2.9% and 0.9% of the area, respectively). Secondary habitat areas had a total of 501 km^2 of anthropogenic disturbance and 104 km^2 of nonanthropogenic disturbance (2.7 km^2 and 0.6 km^2). Primary sink areas had a total of 1,055 km^2 of anthropogenic disturbance (5.9% of the area), and secondary sink areas had a total of 658 km^2 of anthropogenic disturbance (5.3% of the area). Anthropogenic disturbance is responsible for 97% of the disturbance in both primary and secondary sink habitats and 95% in noncritical habitats. Figure 7 shows the annual area disturbed in each individual grizzly bear habitat state. Primary and secondary habitat and primary sinks showed declining trends in disturbance area from 2001–2011, except in years 2008 and 2009, which were the highest years of total disturbance, after 2002. Between the years of 2001 and 2005, total disturbed area of both primary and secondary habitat was 933 km^2, compared with 539 km^2 from 2006–2011. Total disturbed area for both primary and secondary sink areas from 2001–2005 was 1092 km^2, and from 2006–2011 was 680 km^2. Both source and sink areas show a decline in the amount of disturbed area from 2001–2011.

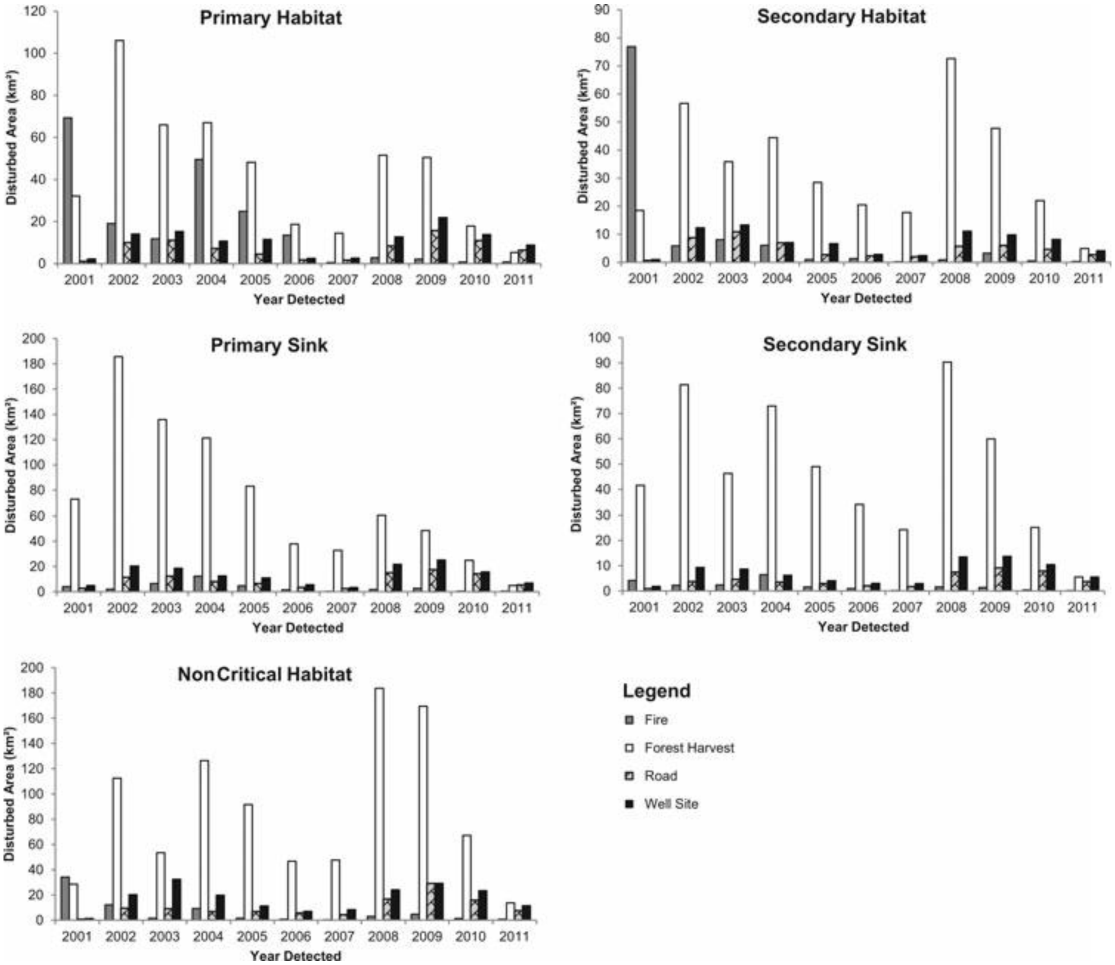

Figure 7. Total disturbed area (square kilometers) classified by year, for individual habitat states (primary habitat, secondary habitat, primary sink, secondary sink and noncritical habitat) from 2001–2011.

Discussion. Our analysis aimed to detect both anthropogenic and nonanthropogenic disturbances for western Alberta, as there is no timely, publicly available, comprehensive data source for the region on well sites, road building, and forest harvest activities, derived in a consistent and transparent manner. The Canadian National Fire Database has publicly accessible historical fire polygons and these were used to allocate fire attribution on the intersecting STAARCH polygons, regardless of the decision tree results. Well sites, roads, fires, and forest harvests were selected as the critical disturbance types for observation, because they represent the most common and spatially unique disturbances in the region. We applied an existing model, which used a unique combination of time of disturbance as well as spatial features of the detected patch, to attribute the detected disturbances. The use of an automated change detection and attribution framework is an important goal for both remote sensing scientists and natural resource managers because it reduces subjectivity and improves the timeliness of change data

(Stewart et al. 2009). The use of shape and contextual attributes adds additional dimensions to disturbance patches and evidence from a number of studies supports the use of shape-based and reflectance-based attributes (Stewart et al. 2009). Our approach, which incorporates the temporal dimension of when the disturbance events occurred throughout the year, is novel. Surface or open-pit mining, pipelines, and seismic lines also exist, although these were omitted from our analysis because mines account for a small proportion of the study area only (0.55 ha/km^2; Linke and McDermid 2012). Pipelines and seismic lines also were omitted because they have a narrow disturbance footprint (Stewart et al. 2009), which cannot be reliably detected in our data fusion approach.

The rate and size of disturbance shows a degree of agreement with other studies. Linke and McDermid report 0.62% annual rate of change/disturbance, comparing well to the observations in this article. Stewart et al. (2009) identified similar levels of well site disturbance, but higher levels of road disturbances over their smaller, more industrial area. Pasher et al. (2013), in a recent study, report 60% of mapped anthropogenic polygons across the whole boreal were cutblocks, followed by mines (0.9%), oil and gas infrastructure (0.1%), well sites (0.4%). The relative proportions of anthropogenic disturbances matches well with our findings. Finally, our results attribute the area of fire disturbance at rates lower than anticipated, likely due to a misclassification with harvest. In 2003 for example, a significant fire year, the levels of area burnt detected in this study, compared to the large fire database, are much lower; in some cases less than half. This suggests that fire patterns and size are similar in spatial characteristics to harvest events, a goal of sustainable forest management objectives in the area.

Conclusion. In this article we demonstrate the ability to map and attribute disturbances as detected by the STAARCH algorithm across the foothills of western Alberta. This is made possible by fusing fine spatial resolution of Landsat images (30 m) with the high temporal resolution of MODIS (biweekly) images, which have lower spatial resolution of 250 m. Anthropogenic disturbances (forest harvest, well sites, and road construction) are the most influential disturbances on the landscape of southwestern Alberta, in terms of number and area affected. These disturbances have both positive (increased forage) and negative (increased human–bear interactions) implications on important grizzly bear habitats. Our research represents a viable monitoring tool for land managers through the quantification of the disturbed area and characterization of the type of disturbance.

Fine-spatial scale predictions of understory species using climate- and LiDAR-derived terrain and canopy metrics

Wiebe Nijland, Scott E. Nielsen, Nicholas C. Coops, Michael A. Wulder, Gordon B. Stenhouse

Journal of Applied Remote Sensing 083572, 2-16, 2014

Abstract. Food and habitat resources are critical components of wildlife management and conservation efforts. The grizzly bear (*Ursus arctos*) has diverse diets and habitat requirements particularly for understory plant species, which are impacted by human developments and forest management activities. We use light detection and ranging (LiDAR) data to predict the occurrence of 14 understory plant species relevant to bear forage and compare our predictions with more conventional climate- and land cover-based models. We use boosted regression trees to model each of the 14 understory species across 4435 km^2 using occurrence (presence–absence) data from 1941 field plots. Three sets of models were fitted: climate only, climate and basic land and forest covers from Landsat 30-m imagery, and a climate- and LiDAR-derived model describing both the terrain and forest canopy. Resulting model accuracies varied widely among species. Overall, 8 of 14 species models were improved by including the LiDAR-derived variables. For climate-only models, mean annual precipitation and frost-free periods were the most important variables. With inclusion of LiDAR-derived attributes, depth-to-water table, terrain-intercepted annual radiation, and elevation were most often selected. This suggests that fine-scale terrain conditions affect the distribution of the studied species more than canopy conditions.

Introduction. Developing a comprehensive understanding of food and habitat resources' use for large mammals is a critical component for their conservation and management, as well as for assessing the cumulative effects of human impacts and estimating habitat-based carrying capacities for species of management concern (Gordon et al., 2004). This is particularly true for the grizzly bear (*Ursus arctos*) population in western Alberta, Canada, where resource extraction is expanding (e.g., forestry, exploration and mining, and urban expansion) along with human use of the landscape, resulting in concern for the long-term survival of the species in this region (Clark et al., 1996; Nielsen et al., 2004; Nielsen et al., 2006; Nielsen et al., 2008).

This study aims to evaluate the integration of LiDAR data into large area studies on species distribution. To do so, we assess the effectiveness of using LiDAR remote sensing data to predict species occurrence for 14 understory plant species relevant to bear habitat and food. We compare these with more conventional climate- and land cover-based models of species occurrence to evaluate whether LiDAR data improve our understanding of the local distribution of bear foods. We compiled and derived a number of topographic and canopy metrics from airborne LiDAR data and combined them with climate and land cover data to model the distribution of 14 key plant species in the Alberta foothills region. Model performance and spatial patterns of the three sets of models were compared. In addition, we assessed variable importance within the models to increase our understanding of the main environmental drivers of plant distribution in the study area and our ability to capture those drivers with different data sources.

Methods. *Climate Covariates*: Spatial predictors of the region included a number of seasonal and annual climate variables which were derived from long-term (1961 to 1990) climate records, using the CLIMATE-WNA (Wang et al., 2012) which uses a PRISM down-sampling (Daly et al., 1994) approach to create surfaces at a 500 × 500-m resolution. These included mean maximum and minimum temperatures, growing degree days (base 0°C), frost-free periods, mean annual precipitation during the growing season, and summer moisture index.

Land and forest cover covariates: Landsat-derived land cover information was available for the study region and included information on land cover, canopy cover (%), and percent of pixels dominated by conifer overstory species (McDermid et al., 2009). The products were based on Landsat images acquired between 2005 and 2009 and have a 30 × 30-m resolution with typical geolocation accuracy within one pixel (Lee et al., 2004).

LiDAR data covariates: LiDAR data were provided by the Alberta Environment and Sustainable Resource Department, who compiled a globally unique compilation of LiDAR datasets acquired from 2003 to 2008. The compiled LiDAR dataset covers the majority of the forested areas of the province of Alberta extending over 25 million ha. The LIDAR dataset was compiled by the Government of Alberta from a variety of sources including forestry, mining, and exploration companies. The extremely large area covered by the compilation allows broad-scale environmental issues (such as species–habitat relations) to be addressed. Typical characteristics of the multiple data acquisitions were multiple returns, small footprint, acquisition from a fixed wing platform with nominal postspacing of approximately 0.75 points per square meter, and vertical and horizontal accuracies typically within 40 cm (Davenport et al., 2004). To minimize the impact of different survey configurations and acquisition dates (e.g., hit density or leaf-on/off), the data were thinned to produce a consistent 1-m spacing dataset, which, despite being lower than many typical LiDAR datasets (Wulder et al., 2008), ensured consistent density and coverage over the entire 4435 km^2 study area. From the thinned LiDAR point cloud, a bare Earth digital elevation model (DEM) and a canopy height model were provided at 1-m raster resolution. From the bare Earth DEM, the slope aspect and elevation were extracted for each plot location. A suite of forest canopy metrics was then developed for each 25 × 25 mpixel, including a calculation of percentiles from 5th to the 95th in steps of 5%, where a given height percentile was calculated as the height greater than a given percentage of LiDAR first returns (Means et al., 2000). Mean height, maximum height, the fraction of points above 2 m, relative height ratio (mean height/max height), skewness of the percentile height, and standard deviation of heights were also computed for each plot. In addition to the canopy and topographic metrics, information on the annual radiation regime for the bare Earth DEM, canopy height, and terrain and canopy elevations for each plot was calculated from the LiDAR data using a hemispherical viewshed algorithm (Rich et al., 2000; Fu and Rich, 2002), which incorporates extraterrestrial solar flux, the relative optical path (determined by the solar zenith angle and elevation above sea level), the duration of a defined time interval, and the effect of the surface orientation (Garnier and Ohmura, 1968). Lastly, a wet-areas mapping (WAM) layer was available, providing an estimate of the depth-to-water table using the shape and orientation of the terrain (White et al., 2012). The WAM was based on the same LiDAR elevation models, created a 1-m raster resolution, and resampled to 25 m. For the LiDAR-derived variables, we made a selection capturing different aspects of terrain and vegetation cover while limiting the overall number of variables and multicollinearity, based on other studies including those done by Coops et al. (2010) and Ferster et al. (2009). Previous LiDAR approaches involving the direct detection of understory structure (Martinuzzi et al., 2009; Wing et al., 2012) were not possible due to insufficient point density and limitations in separating low vegetation and ground returns in the compiled dataset. As a result, overstory and terrain characteristics were used as surrogate predictors of understory structure.

Modeling: Boosted Regression Trees. Distribution models were built for the 14 plant species using boosted regression trees from the “gbm” package in R statistical software (R Development Core Team, 2013), it follows the methods described in Friedman (2001; 2002). Boosted regression tree modeling is a relatively new technique which is gaining popularity in the distribution modeling community (Elith et al., 2008). Benefits include flexibility in combining different types of variables (e.g., continuous, categorical, and nominal), flexibility in statistical distributions, and a demonstrated high-predictive power (Elith et al., 2008). Up to 1500 individual trees were fit with a five-level tree depth and a learning rate of 0.005 to avoid over fitting of collinear variables. The optimum number of trees was selected using a 10-fold cross-validation within the training data. To verify the selected model, we made a random 80-20 split of all plot data before the model building and calculated the model fit using the separated 20% of the plots. Model performance was assessed using the “area under the receiver-operator characteristic curve” (AUC) (Jiménez-Valverde, 2011) with values ranging from 0.5 to 0.7 generally viewed as “low” model accuracy, values between 0.7 and 0.9 considered “good,” and values greater than 0.9 considered “high” model accuracy (Swets, 1988; Manel et al., 2001). The kappa coefficient, although disputed by some (Pontius and Millones, 2001), was also calculated. It is a widely used metric particularly useful in ecological research (see review by Monserud and Leemans, 1992). This statistic calculates the proportion of specific agreement across presence and absence classes.

Results. Overviews of the three sets of models developed for individual species show a wide variety of model accuracy. Model AUC values ranged from 0.70 to 0.85, while K statistic values ranged between 0.09 and 0.48 (i.e., poor to moderate, based on Landis and Koch’s (1977) thresholds for the K statistic). Apart from the three model sets shown, we also tested models using LiDAR- or Landsat-based information only, but these had poor performance with an average validation AUC of around 0.65 as they fail to capture the larger-scale patterns in the study area. The most accurately predicted species was *Hedysarum alpinum* (sweet vetch), while the poorest was *Equisetum arvense* (horsetail). *H. alpinum* is a critical spring root-digging resource for bears, whereas horsetail produces a high-protein, succulent, and herbaceous food resource at green-up.

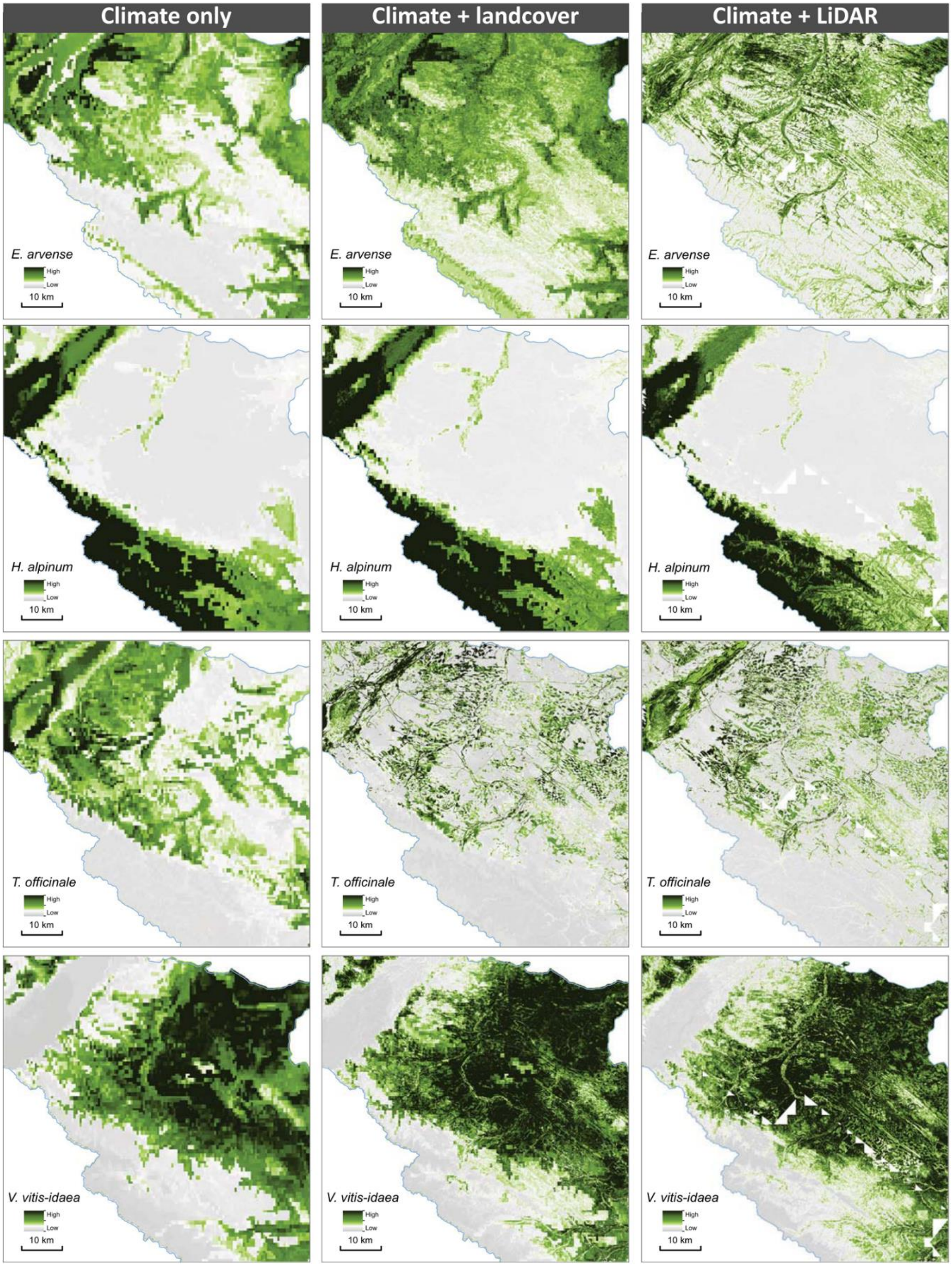
Climate only
Climate + landcover
Climate + LiDAR
E. arvense
H. alpinum
T. officinale
V. vitis-idaea
High
Low
10 km

Figure 2. Probability of occurrence maps based on climate (left), climate + forest cover (middle), and climate + LiDAR (right) data for *Equisetum arvense, Hedysarum alpinum, Taraxacum officinale*, and *Vaccinium vitis-idea*.

Overall, 8 of the 14 most accurate species models were developed using a combination of climate- and LiDAR-derived variables, with an average increase in AUC of 5% and the greatest model improvement of up to 12% for *Arctostaphylos uva-ursi* (bearberry). For three species, the most accurate model derived was from climate and broader-scale land and forest cover information, and three were equally supported.

The individual response graphs of the most important variables of the combined models for four species indicate the relationship between species occurrence and environmental drivers. For *E. arvense*, it is apparent that the species occurrence is driven by the presence of wet areas within the landscape at lower elevations. The *H. alpinum* model did not incorporate any LiDAR-derived terrain or canopy information and had a bimodal response for degree days, reflecting its occurrence in cold, high-elevation meadows, and warmer low-elevation sites in stream valleys. *T. officinale* is predicted to occur in sites with longer frost-free periods and lower-mean canopy height, predominantly in sites having vegetation cover less than 5 m in height. Lastly, *V. vitis-idea* occurs in sites with intermediate frost-free period lengths and in cooler, lower-elevation sites.

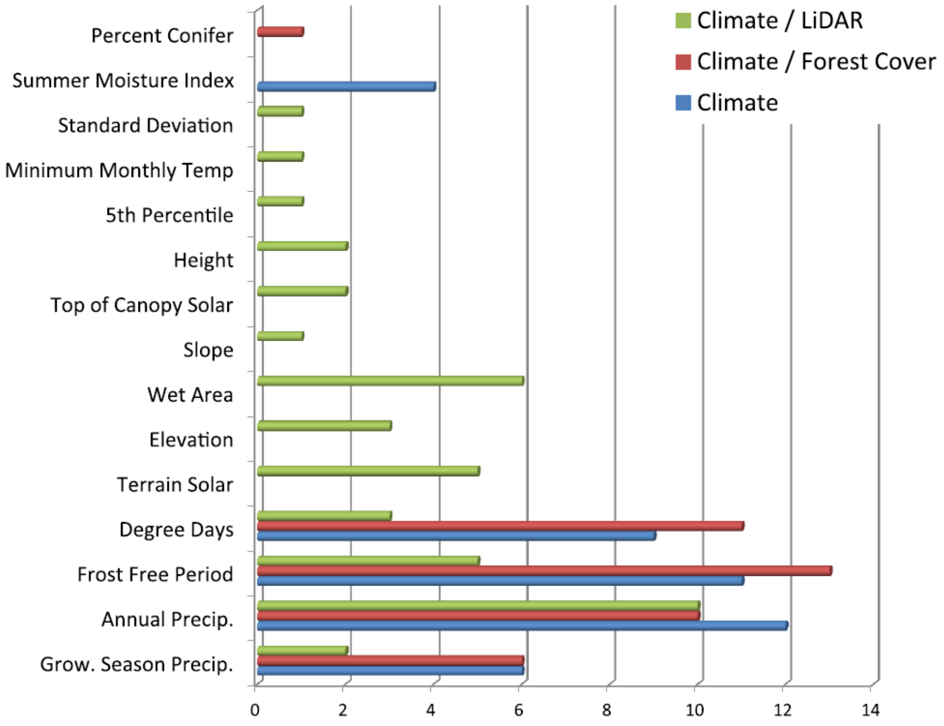

Fig. 3 Frequency of variables selected in the top-three predictors for each species for the three model suites.

Conclusions. In this study, we investigated the added benefit of incorporating LiDAR-derived terrain and forest canopy information into understory species models relevant for grizzly bear species habitat modeling. Our use of boosted regression trees for model development enabled the combination of multiple data types as well as the inclusion of complex relationships, which are often not possible to represent within standard linear models. Boosted regression trees allow representation of the main variables used in the developed models, as well as response graphs between individual plant occurrence and the most important variables. The past 5 years has seen these models increasingly selected in ecological research because of a number of features, including an ability to deal with collinear datasets, to exclude insignificant variables, and to allow for asymmetrical distribution of samples (De'Ath, 2002; Schwalm et al., 2006; Melendez et al., 2006). We recognize that a limitation of boosted regression approaches is that many observations are required for reliable model building, making model development of rare and more localized understory species more problematic, and should be undertaken with caution (Coops et al., 2011).

Our results demonstrate that the models developed with a combination of both broad-scale climate data as well as with LiDAR-derived terrain and canopy information provided the best overall performance, capturing more fine-scale spatial variation than models using climate data alone. The inclusion of the LiDAR attributes suggest that these variables provide a more detailed explanation of the fine-scale site conditions, such as access to water, and solar radiation regime at the site caused by terrain shading, in addition to overall site elevation and slope (White et al., 2012). Information on canopy height, gaps, shading, and height variations also appear to affect the distributions for some species, but to a lesser degree than the finer site condition measured by LiDAR. The inclusion of site level measures from LiDAR resulted in a reduction of importance for growing degree days and frost-free periods. This shift implies that the inclusion of LiDAR data allows a more comprehensive description of the thermal and radiation regimes of individual sites, replacing the need for broader-scale descriptions of the thermal load of each site.

Integrating optical satellite data and airborne laser scanning in habitat classification for wildlife management

W. Nijland, N.C. Coops, S.E. Nielsen, G. Stenhouse

International Journal of Applied Earth Observation and Geoinformation, 38, 242–250, 2014

Abstract. Wildlife habitat selection is determined by a wide range of factors including food availability, shelter, security and landscape heterogeneity all of which are closely related to the more readily mapped landcover types and disturbance regimes. Regional wildlife habitat studies often used moderate resolution multispectral satellite imagery for wall to wall mapping, because it offers a favourable mix of availability, cost and resolution. However, certain habitat characteristics such as canopy structure and topographic factors are not well discriminated with these passive, optical datasets. Airborne laser scanning (ALS) provides highly accurate three dimensional data on canopy structure and the underlying terrain, thereby offers significant enhancements to wildlife habitat mapping. In this paper, we introduce an approach to integrate ALS data and multispectral images to develop a new heuristic wildlife habitat classifier for western Alberta. Our method combines ALS direct measures of canopy height, and cover with optical estimates of species (conifer vs. deciduous) composition into a decision tree classifier for habitat – or landcover types. We believe this new approach is highly versatile and transferable, because class rules can be easily adapted for other species or functional groups. We discuss the implications of increased ALS availability for habitat mapping and wildlife management and provide recommendations for integrating multispectral and ALS data into wildlife management.

Introduction. Wildlife respond to a large number of factors when selecting habitat, involving complex behavioral decisions which are made at multiple spatial scales (Ciarniello et al., 2007; Herfindal et al., 2009; Johnson et al., 2002). Broad scale spatial variation in biodiversity is thought to respond to three major drivers; climatic stability, productivity, and habitat structure (MacArthur, 1972) –with empirical evidence demonstrating the importance of each of these variables (Coops et al., 2008). Bioclimatic models are often applied to estimate broad-scale distribution of species (Guisan and Zimmermann, 2000; Rahbek and Graves, 2001; Willis and Whittaker, 2002). However, at finer spatial scales land cover, disturbance, and habitat heterogeneity are more important factors affecting local distribution and habitat selection of species (Iverson and Prasad, 1998; Thuiller, 2004).

Many have tried to bridge the gap between the need for structural information and the inability of direct optical classification to provide information for management and decision-making. Solutions may include the use of ancillary data, texture information, object based analysis, post classification procedures, or other remotely sensed data like radar (Lu and Weng, 2007; Roberts et al., 2007). The most common source of ancillary data is elevation models (Franklin et al., 2002; Johnson et al., 2003; McDermidet al., 2009) and topographic derivatives like slope and aspect. Texture information is used in the form of gray-level co-occurrence matrices (Franklin et al., 2002), spatial autocorrelation (Magnussen et al., 2004), or variogram functions (Zhang et al., 2004), based on homogeneity assumptions within the forest stand and the information content of shaded vs. sunlit parts in the canopy. In post classification methods the fine scale patterning of simple land-cover types (e.g., treed, herb, bare) or vegetation indices can be used to define habitat classes (Sluiter et al., 2004). Radar in particular is able to partially penetrate vegetation canopies, but the efficacy in detecting structure is highly dependent on the microwave wavelength, vegetation height and moisture content (Imhoff et al., 1997). All of these potential solutions can improve classification results in certain cases, but can be laborious, costly and require extensive training data or manual steps which may lead to interpreter-related differences and locally optimised but regionally less applicable results.

ALS data can provide specific information on forest structure, such as understory and midstory cover assessment, topographic morphological variables, such as slope and aspect, as well as the presence of old, tall trees or snags. As a result, the use of ALS technology has increased for assessments of wildlife habitat. Hyde et al. (2005) utilized ALS data to characterize montane forest canopy structure in the Sierra National Forest for large-area habitat mapping. They found that the accurate prediction of canopy height, canopy cover, and biomass was an important prerequisite predicting wildlife habitat showing significant promise in its use. Vierling et al. (2008) provide a review of the current status of ALS remote sensing and habitat characterization and conclude that, although a growing number of studies highlight interest in ALS advances, few studies have actually used the data to quantitatively address these relationships.

In this research, we introduce an approach to integrate ALS and multispectral satellite images to develop a new heuristic wildlife habitat classifier for western Alberta. The classifier uses vegetation structure, species composition, and terrain characteristics derived from available ALS and multispectral data directly in a decision tree. We evaluate the accuracy of the habitat layers and discuss the added value of the created products for the classification. Based on our results, we look at implications of increased ALS availability for habitat mapping and wildlife management, and make recommendations on the application of ALS in regional habitat mapping efforts.

Methods. *Classification scheme.* The habitat classification scheme developed is based on a merging of a standardised landcover classification based on the Alberta Vegetation Inventory (AVI) (Nesby, 1997) combined with a Landsat-based Grizzly bear habitat classifier presented by McDermid et al. (2005, 2009). Cut-off values of percent canopy cover were taken from the existing classification as they are currently well understood and used by the management community. The classes are well proven and used in other related models, such as habitat selection functions which makes it desirable to build upon these existing classes. The AVI is an interpreter-derived delineation of vegetation units based on aerial photography and field sampling of forest characteristics, including timber productivity, tree species composition, height, and crown closure. The scheme closely matches the Canada wide forest classification by Wulder et al. (2008b,c) and Wulder et al. (2006) – the Earth Observation for Sustainable Development of Forests (EOSD) – with exclusion of classes irrelevant to the study area (like bryoid tundra). In accordance with McDermid et al. (2005) and Nielsen et al. (2009), additional habitat classes for alpine barren areas, alpine meadows, and dense coniferous forests based on their relevance for Grizzly bear were included. Alpine meadows have specific food resources like alpine sweetvetch (*Hedysarum alpinum*) (Coogan et al., 2012; Nijland et al., 2012), plus both alpine meadows and alpine barren areas are expected to be stable, while meadow and barren land cover types in lowlands are often the result of disturbances and may quickly develop more vegetation cover. Dense coniferous forest is separated as a distinct class because of their relevance for denning sites (Ciarniello et al., 2005; Pigeon et al., 2014), but usually lower yield of fruiting species (Nielsen et al., 2004b). These classes were not separated previously, because they were not reliably detected in previously used multispectral classifiers. They are more likely however to be successfully separated using topographical and canopy structure information from ALS. We chose to split them from existing classes to allow for a backwards compatible generalization of the newly created habitat types with existing maps.

Classification models. The overall classification approach integrates a spectral classifier to separate water and bare ground from the vegetated classes, which are further divided based on height, density and species composition measures. Conifer cover is modeled using a linear model based on leaf-on—leaf-of NDVI (Tucker, 1979) difference, and tasseled-cap (Kauth and Thomas, 1976) brightness. Vegetation structure is directly derived from ALS metrics without regression models. In all forest structure models, areas with a vegetation height less than 4mwere excluded as they are not considered as forest in our classification. The hydrologic model for depth-to-water table is described in White et al. (2012) and uses topographic routing of water over the terrain surface together with fixed area for flow initiation to derive the water table height. The parts of the study area that have no ALS data present are in-filled using a standard maximum likelihood classifier on the Landsat visible, near infrared and short wave infrared spectral bands, DTM, and Percent Conifer layers. We evaluate the agreement between our integrated classification with the classification without ALS data using an equalized random sample of 1000 points per class taken from the area where both classifications area available. While this cannot be interpreted as a validation of our results, the comparison reflects on the improvement our integrated classification provides over a more traditional classifier.

Results. *Pre classification models.* ALS derived maximum canopy height and points above 2mwere selected to represent canopy height and cover directly without using any models. The relations between the selected variables and field based measurements of canopy structure were strong (R2 vegetation height: 0.87, vegetation cover over 2m: 0.60) and visual evaluation of the relations reveal no bias in the estimators. The accuracy of using direct ALS variables (RMSE canopy height: 3.08 m, canopy cover: 16.2%) is acceptable for our classification scheme. Conifer cover was modeled using a linear model based on leaf-on— leaf-of NDVI difference, and tasseled-cap brightness (R2: 0.60, RMSE: 0.18). The linear model was then thresholded into three classes, conifer, mixed, and deciduous based on maximum likelihood showing acceptable class separation.

Classification. The decision tree classification shows the input data and the subsequent class decisions. Of the total study area 63% was classified as forested, 12% as herb and shrub, 5% as wetland and 20% as barren land. The proportion of land cover classes over the region corresponds well with existing landcover products: EOSD (Wulder et al., 2008b; Wulder et al., 2006) (forest:60%, wetlands:6%, herb and shrub:16%, barren:18%), and the classification made for the Grizzly bear project (McDermid et al., 2009) (forest:61%, wetland: 4%, herb and shrub 14%, barren: 21%).

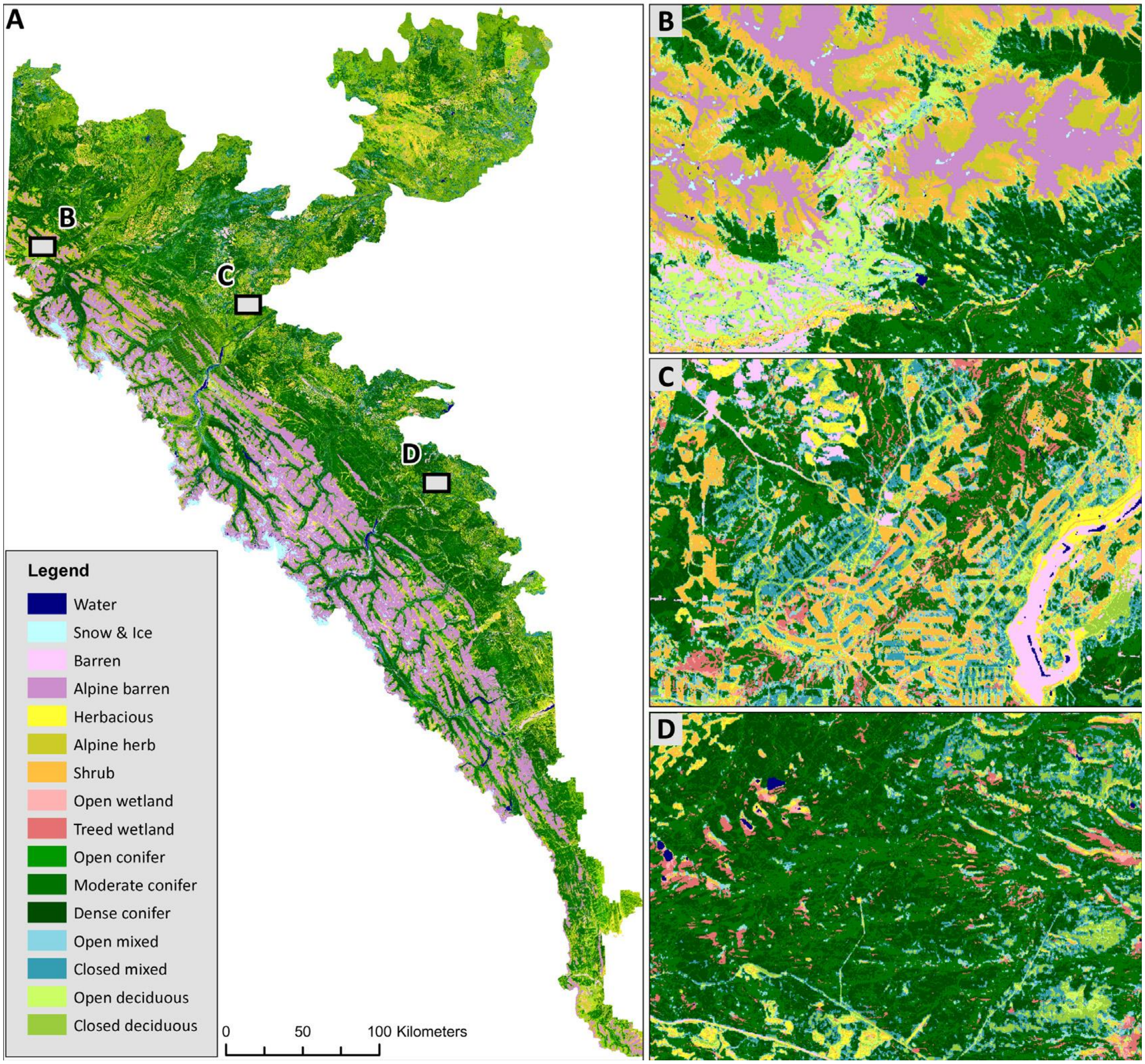

Fig. 6. Overview map of the classification results for the whole study area (A) and three detail sites as indicated in the first panel. (B) mountainous area with a recovering fire scar in the SW corner, (C) mosaic of regenerating forest harvests with a coal mine site in the east, (D) mostly continuous conifer forest interspersed with wetlands and mixed\deciduous patches.

Comparison of our integrated classification with a traditional Landsat based maximum likelihood classifier gives an indication of the gained by including ALS based terrain and structural information. Considerable disagreement exists between the herbaceous, shrub, wetland, and open forest classes. The shrub class has high levels of confusion with almost all vegetated classes except the moderate and dense conifer. Wetlands are confused among themselves for treed and open, and specifically treed wetlands are often confused with mixed and deciduous forest.

Within each of the forest types the open and closed classes are often confused. The non-vegetated classes like water, snow, and barren have high levels of agreement between the two classifiers as do the forest types. The high agreement within these classed is as expected as separation between them in our integrated classifier is already made based on spectral information.

Discussion. Availability of ALS data into habitat classifications allows more direct estimates of vegetation structure in the classification scheme which has been shown to be of direct relevance to habitat evaluation and wildlife management (Vierling et al., 2008). By using ALS data in combination with optical data direct information on vegetation characteristics can be integrated using a heuristic-based classifier that directly employs the class definitions as set based on the management needs. Our results indicate that users can gain considerable accuracy improvements over solely Landsat-based classifications

Integrating ALS derived structural information into habitat classifications allows habitat classification to be tailored for specific species or functional groups. In this approach, we used continuous input layers for which the class rules can be adapted to create new products without the need of additional input data. ALS supports this system specifically by providing information difficult to obtain using passive optical sensing systems such as small scale topographical features and vertical vegetation structure. Improvements are also possible for classes which describe the understory which can be detected from ALS, but often have non-unique spectral signatures because of canopy cover. Key habitats where the fusion of ALS and optical data are likely to be beneficial include wetland areas, alpine areas, forest-cover density and species composition.

We recognise ALS is not ubiquitously available over all jurisdictions; however, this is quickly changing. Through the combined effort of industry and provincial government an almost wall to wall ALS coverage of the forested areas in Alberta has been acquired. This paper demonstrates how valuable these types of data are, not only in engineering and resource management, but also for improving wildlife management and supporting ecological values and other benefits of forests. The current map product is created for regional applications and uses a raster resolution of 25m for summarizing the ALS derived canopy metrics. The generalization of data to this 25mgrid size facilitated integration with multispectral images and minimised the impact of different survey configurations of the merged large area ALS dataset. The approach of using naïve estimators from ALS to represent vegetation structure does produce relatively high RMSE values, but the relationship is highly transferable and has minimal bias. Loss in detail compared to the state of the art in laser scanning is in exchange for the gain in integration of ALS and multispectral satellite data for large area applications supporting more effective habitat and wildlife management.

Conclusions In this paper, we present a new habitat classification for grizzly bear management in Alberta, Canada. We combine optical satellite images and ALS into a heuristic, decision tree based habitat classifier. Based on the integrated use of optical and ALS data we are able to describe the major axes of landscape variability including species composition and vegetation structure and to use these data directly in the landcover classifier. The classifier allows for more detailed habitat classes in alpine areas, wetlands and overstory density and structure and represents a step forward from currently available products. This proposed system is versatile in the sense that the class rules can be easily adapted for other species or functional groups without the need of additional inputs or training data. Integration of multispectral satellite images and ALS enables an adaptable classification system that supports informed decision making for wildlife management.

Research Theme: Development of a spatially explicit software application to address future landscapes and climate change

Overview

Author: Nicholas Coops

Accurate modeling of future landscape conditions under climate change involves accounting for a variety of data inputs, including current landscape conditions, land cover change, bear foods, energy, phenology, bear health, population status, and climatic variables. Ongoing research into the use of the STAARCH algorithm is important for the first aspect, providing a spatial database of land cover, canopy closure and disturbances that will then be integrated into energy and food surfaces from other research themes (III and IV). This information then incorporates the relationships defined in Theme II between landscape change, energy availability, and grizzly bear habitat to produce spatially explicit predictive models able to determine in which areas bear presences will be higher or lower. This was the most challenging and ambitious set of goals in the research: the modeling of future landscapes requires an abundance of information and also an understanding of the relationships that grizzly bears have with the land and that way that it changes through time and in response to anthropogenic disturbances.

A network of consumer-grade digital SLR cameras was set up to test their efficacy in monitoring grizzly bear habitat understory vegetation phenology, or the pattern of seasonal changes in vegetation development. Most often, the 2G-RB index was used to measure the seasonal half-max green-up and senescence value for various plant species (e.g., *Hedysarum alpinum*, *Equisetum arvense*, *Shepherdia canadensis*) by applying the index to repeat photography taken at regular daylight intervals between April and September. This, too, was the way in which the length of the growing seasons was calculated: the duration of time between the half-max for green-up and that of senescence was determined to be the growing season. Nijland et al. (2013) employed this network of phenology cameras to map phenological events to nutritional quality of *H. alpinum*, and Nijland et al. (2014) then determined that infrared-converted cameras performed below the standard set by traditional consumer-grade RGB SLR digital cameras. In Vartanian et al. (2014) this digital repeat photography captured imagery at three different locations across an elevational gradient and at different fields of view (i.e., fine versus broad). This allowed for comparison within and between species of critical importance to grizzly bear health, nutrition, and habitat quality, and provided information as to which was the most effective way to monitor phenological patterns for species of importance to grizzly bear populations, having direct implications for how we bring information from megafauna-specific nutritional landscape monitoring forward into predictive habitat mapping, especially in the context of changing understory compositions and distributions in a boreal ecozone affected by climate change.

Further, this research laid the groundwork for establishing ground-based methods of detecting vegetational response to changes in climate conditions; Nijland et al. (submitted) compared the capacity of Landsat imagery to monitor canopy-level phenology based on optical indices with that of ground-based understorey-level phenology camera networks, determining that Landsat was able to track the phonological trajectory observed by the ground-based networks. The prospect of using Landsat data, a both freely-available and high-spatial resolution data archive, to monitor phenological patterns throughout recent landscape histories is significant: monitoring grizzly bear habitat in remote areas remains a challenge, but improvements to current and future models could be made if confidence in Landsat imagery to detect phenology increases. This would provide high-quality inputs for the grizzly habitat- and population-prediction models developed in the second half of this research goal.

Assessment of phenological patterns in grizzly bear habitat ranges was only one component of a larger set of necessary data inputs for effective model predictions of habitat quality. Erickson et al. (2015) employed the TACA-GEM model to determine establishment and regeneration regimes for a number of coniferous and deciduous species in the Albertan foothills study area. Biospheric climate feedbacks were found to have reduced the regenerational probabilities of a variety of tree species, particularly in that their simulations suggest that warmer and more variable climatic conditions are diminishing the conditions for extent and adjacent tree species.

From regeneration to disturbance regimes, forest dynamics are subject to a number of increasing pressures influencing the nature of tree regeneration and migrational patterns. The information determined by the Erickson et al. (2015) simulations were then brought forward into a process-based fusion model parameterized for the project, combining both the TACA-EM and LANDIS-II models to predict regeneration patterns under climate change and expanding anthropogenic disturbance in the region (Erickson et al., submitted). Of particular importance both for grizzly habitat detection and prediction, fire regimes were found to be changing: they suggested that a shift toward smaller, more frequent fires and diminishing regeneration conditions were reducing the ability of forests to track warming, amplifying climatic disequilibrium and reducing resilience of the systems. Tree species regeneration niches moved toward higher elevations and latitudes, driven by changes in soil water balance, as boreal fire regimes migrated northward. Erickson et al. (submitted) also anticipated that ecosystems to the south will migrate into the Alberta study region in the coming years. This process-based fusion model provides a more robust and effective method of predicting suitable grizzly bear habitat, more inclusive in its incorporation of a large variety of ecological inputs and therefore more able to provide managers with the information they need to account for grizzly bear population and ecosystem health under a changing climate.

Study Summaries

Vegetation phenology can be captured with digital repeat photography and linked to variability of root nutrition in *Hedysarum alpinum*

W. Nijland, N.C. Coops, S.C.P. Coogan, C.W. Bater, M.A. Wulder, S.E. Nielsen, G. McDermid, G.B. Stenhouse

Applied Vegetation Science, 16, 317–324, 2013

Abstract

Question: Can repeat (time-lapse) photography be used to detect the phenological development of a forest stand, and linked to temporal patterns in root nutrition for *Hedysarum alpinum* (alpine sweetvetch) an important grizzly bear food species?

Location: Eastern foothills and front ranges of the Rocky Mountains in Alberta, Canada. The area contains a diverse mix of mature and young forest, wetlands and alpine habitats.

Methods: We deployed six automated cameras at three locations to acquire daily photographs at the plant and forest stand scales. Plot locations were also visited on a bi-weekly basis to record the phenological stage of *H. alpinum* and other target plant species, as well as to collect a root sample for determination of crude protein content.

Results: Repeat photography and image analysis successfully detected all key phenological events (i.e. green-up, flowering, senescence). Given the relation between phenology and root nutrition, we illustrate how camera data can be used to predict the spatial and temporal distribution and quality of a key wildlife resource.

Conclusions: Repeat photography provides a cost-effective method for monitoring vegetation development, food availability, and nutritional quality at a forest stand scale. Since wildlife responds to the availability and quality of their food resources, detailed information on changes in resource availability helps with land-use management decisions and furthers our understanding of grizzly bear feeding ecology and habitat selection.

Introduction. Seasonal changes in vegetation phenology are critical drivers of food availability and quality for a wide variety of animal species. Food availability affects large-scale movements in migratory species such as caribou (Sharma et al. 2009; Festa-Bianchet et al. 2011), as well as the seasonal foraging habits of species within their home ranges (Nielsen et al. 2003, 2010). This is the case for grizzly bears (*Ursus arctos*), which are considered generalists with diverse diets that change during the course of the year. Individual bears may travel large distances to locate high-quality food sources (Rogers 1987), with a diet comprised of seasonally abundant and nutrient-rich food (Hamer & Herrero 1987; Hamer et al. 1991; Craighead & Sumner 1995; McLellan & Hovey 1995; Munro et al. 2006).Within their remaining range in western Canada, grizzly bears have three distinct foraging seasons: hypophagia, early hyperphagia, and late hyperphagia (Nielsen et al. 2006). During hypophagia, grizzly bears feed on the roots of *Hedysarum* spp. (sweetvetch) and other early herbaceous material. During early hyperphagia their diet extends to green herbaceous material such as *Heracleum lanatum* (cow-parsnip) and *Equisetum* spp. (horsetail), while in the later season berries such as *Shepherdia canadensis* (buffalo berry) and *Vaccinium* spp. (huckleberry, blueberry and lingonberry) make up the majority of their diet. As fruit consumption declines in the autumn, grizzly bears once again dig for sweetvetch roots (Nielsen 2005; Munro et al. 2006; Nielsen et al. 2006, 2010). While animal matter and insects are an important food resource for grizzly bears during spring and early summer, a wide variety of vegetable matter, including roots, forbs and fruit, makes up the majority of their diet from late June through to early October. The amount of animal matter consumed by grizzly bears can also vary by season (moose and other ungulate calves), distribution and abundance (Munro et al. 2006).

Despite the demonstrated capacity to monitor vegetation phenology remotely, changes in vegetation greenness detected by cameras do not necessarily directly correspond to other factors affecting use of those resources, such as nutrient quality. For example, in the case of grizzly bears, the nutritional content of *Hedysarum alpinum* (alpine sweetvetch) roots varies significantly throughout the growing season, with highest nutritional concentration occurring prior to and during the initial green-up phase (Hamer et al. 1991; Coogan et al. 2012). Once the aboveground biomass component of *H. alpinum* has reached its peak, corresponding to the mid-point of the growing season, the nutritional value of the roots substantially decreases when compared to the initial green-up earlier in the season or senescence in the autumn (Coogan et al. 2012). As a result, there is a need to link remote sensing-derived observations of greenness to not only vegetation activity, but also to the nutritional value of the above- and below-ground components of the vegetation.

The main objectives of this study are two-fold. First, examine changes in vegetation phenology of key individual plant species critical to grizzly bear diet using very high spatial resolution digital camera data. Changes in vegetation phenology (spectral greenness) for individual plants were examined over a full growing season and compared to phenophase observations of the above-ground vegetation component, as well as to the nutritional content of the below-ground roots. The second objective of the study is to demonstrate if individual species-based models, such as *H. alpinum*, can be scaled up using stand-scale digital camera observations. If these relationships exist, then the distribution and timing of forage availability can be predicted at broader scales.

Methods. Digital camera setup Six standard commercially available digital camera systems manufactured by Harbortronics (Gig Harbor, Washington, WA, USA) were installed at the three sites. The camera systems include a Pentax K100D digital SLR camera (Pentax Corporation, Tokyo, Japan) mated to an intervalometer. The camera was sealed in a fiberglass case with a solar panel and lithium ion battery to provide power. At each of the three plots, one camera was mounted 3 m above the ground on a tall and dominant tree and pointed north (as described in Bater et al. 2011a) with images capturing conditions of the forest stand. A second camera was mounted close to the first camera, but with a reduced field of view (ca. 5 9 5 m) in order to monitor a small number of individual plants, hereafter referred to as the plant scale. To minimize directional effects caused by solar movements, all cameras acquired five images per day between noon and 13:00 hr, local time, at regular intervals. Digital images were archived as full resolution JPEG files (3008 9 2008 pixels) and ancillary data included a time stamp for easy reference of the date of acquisition.

Table 2. Phenological phases as observed in the field plots, based on Dierschke (1972).

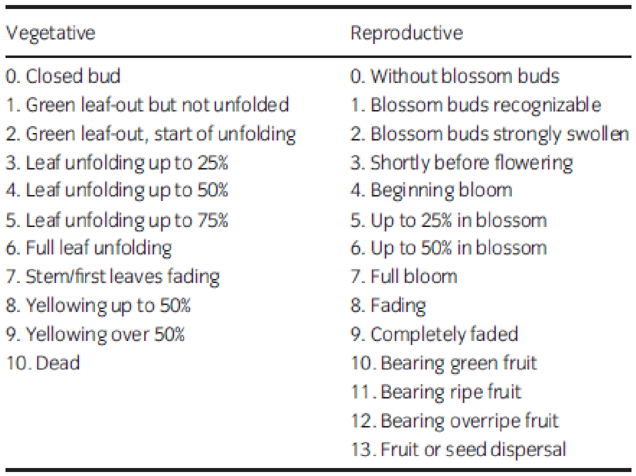

Vegetative	Reproductive
0. Closed bud	0. Without blossom buds
1. Green leaf-out but not unfolded	1. Blossom buds recognizable
2. Green leaf-out, start of unfolding	2. Blossom buds strongly swollen
3. Leaf unfolding up to 25%	3. Shortly before flowering
4. Leaf unfolding up to 50%	4. Beginning bloom
5. Leaf unfolding up to 75%	5. Up to 25% in blossom
6. Full leaf unfolding	6. Up to 50% in blossom
7. Stem/first leaves fading	7. Full bloom
8. Yellowing up to 50%	8. Fading
9. Yellowing over 50%	9. Completely faded
10. Dead	10. Bearing green fruit
	11. Bearing ripe fruit
	12. Bearing overripe fruit
	13. Fruit or seed dispersal

Field validation, phenophase codes and root nutrition Data. Two sets of imagery acquired at the three sites provided a range of homogenous understorey and overstorey species-specific regions of interest, observable on the digital camera imagery. All sites were visited weekly between April and October 2010 to record the phenophase codes (Table 2) of the vegetation, following the practices of Dierschke (1972). In the further analyses, we use summarized phenological scale with pre-leaf: Vegetative ≤4, leaf: Vegetative ≥5, flower: Reproductive ≥6, seed: Reproductive ≥10 and dormant: Vegetative ≥9 (Table 2). The green-up, flower and senescence dates are defined as the first occurrence of leaf, flower and dormant, respectively. Observable species included *H. alpinum* (alpine sweetvetch), *Sheperdia canadensis* (buffalo berry), *Lathyrus ochroleucus* (cream pea), *Vaccinium vitis-idaea* (lingonberry), *Arctostaphylos uva-ursi* (bearberry) and *Dryas octopetala* (mountain avens). In addition to the phenophase observations, *H. alpinum* plants just outside of the observable images were also sampled for nutritional content. In total, 66 samples were collected and analysed for crude protein content following the procedures described in Coogan et al. (2012). All protein measurements were normalized as a fraction of the total dry matter. To allow comparisons between the camera information, phenology data and root protein data, root samples were grouped into five phenological stages (pre-leaf, leaf, flower, seed and dormant).

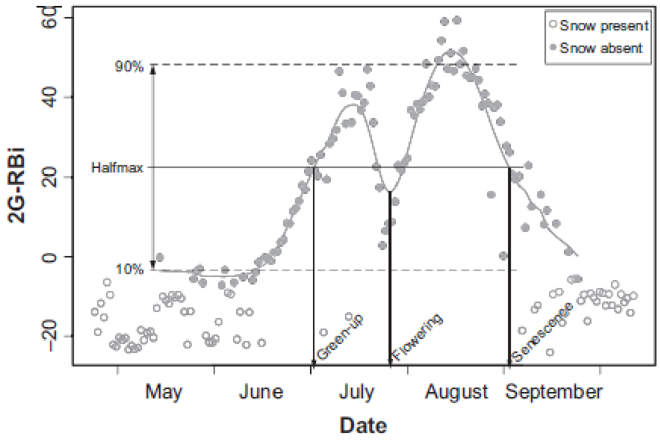

Fig. 2. Seasonal metrics calculated from the 2G-RBi time series from each pixel.

Image analysis. In order to extract a single spectral index indicative for vegetation activity from the blue, green and red spectral channels we calculated the 2G-RB index (Richardson et al. 2007), hereafter noted as 2G-RBi. The 2G-RBi compares the green channel of the RGB image to the red and blue channels to derive excess greenness corrected for illumination differences. All images where snow was present in the scene were removed from further analysis, and a smoothing spline with rigidity of 2/3 was fitted to the 2G-RBi data for each pixel, similar to that of Richardson et al. (2009). Key dates from the fitted spline were then extracted, including date of green-up, end of season and flowering of the *H. alpinum* (Fig. 2). To do so, green-up was defined as the first date that greenness was higher than that of pixels robust half-max (90th percentile–10th percentile/2); senescence was defined as the last date that greenness was higher than that of pixels robust half-max. The robust half-max was chosen above a standard half-max or inflexion point to account for the increased amount of scattering present in the by-pixel data, as opposed to analysis of averages over larger predefined areas. The half-max is commonly used to detect the dates of start of season in camera- (Richardson et al. 2009; Bater et al. 2011a) or satellite-based phenology detection (Schwartz et al. 2002). Flowering of *H. alpinum* was detected as a local minimum in the greenness curve between the green-up date and the end of season. This minimum is caused by the pink flowers of *H. alpinum* that have a negative 2G-RBi.

Results. Approximately 850 images were obtained from each camera, covering the period from mid-April to mid-October. Figure 3(a) provides an example of a typical field of view at the plant scale during flowering of *H. alpinum*. The image clearly shows the leaf structure and flowers of the plant. The 2G-RBi image is shown in Fig. 3(b), with white areas indicative of very green vegetation and darker areas showing non-vegetated scene components. The derived start and end of growing season images are shown in Fig. 3(c,d), respectively.

Camera-derived dates of phenological events and the field-observed dates are strongly correlated (r2 = 0.89, P < 0.01, N = 16), except for evergreen Ericaceae shrubs (e.g., *V. vitis-idaea, A. uva-ursi*), which did not exhibit easily detectable changes in phenology or greenness and show up as clear outliers below the 1:1 line. The relationship between the field-measured phenophase and the protein content of *H. alpinum* is shown in Fig. 5, and demonstrates a reduction in protein content while plants are actively growing. The pre-leaf phenological stage had the highest nutritional value, while the flower and seed phenophases had the lowest nutritional values. Also apparent is the high nutritional load of the below-ground component when the species are dormant, and the variability of root protein across the three sites.

Discussion. Discussion While broad-scale patterns in phenology can provide an overall assessment of available food resources and inter-annual changes in forest productivity, a key limitation of working at this scale is an inability to detect subtle or species-specific phenological events that occur at the temporal and spatial scale at which animals perceive their environment and that are critical for food modelling (Nielsen et al. 2003, 2010). In this paper, we use two sets of cameras configured to capture imagery at the plant- and forest stand-scale. This paired design allowed the precise timing of initial leaf unfolding and the development of fruits to be observed and subsequently linked to the nutritional value of the below-ground food resource. Placing cameras in close proximity to plants offers the advantage of continuous data and the possibility of a reduced frequency of field visits for collection of phenological data (phenophase monitoring). This study confirms that ground-based cameras can be employed to simultaneously monitor phenology of multiple plant species within the image footprint, and that images capturing different scales can be linked with landscape assessments of vegetation nutritional value. The phenological development of *H. alpinum* indicates that high protein roots were available before the start of July and again after the end of August (Coogan et al. 2012). This pattern corresponds well with root consumption patterns observed in grizzly bear faeces (Munro et al. 2006) and GPS telemetry data on habitat selection (Coogan et al. 2012), which show most root consumption in late April to June, and resuming from August to October.

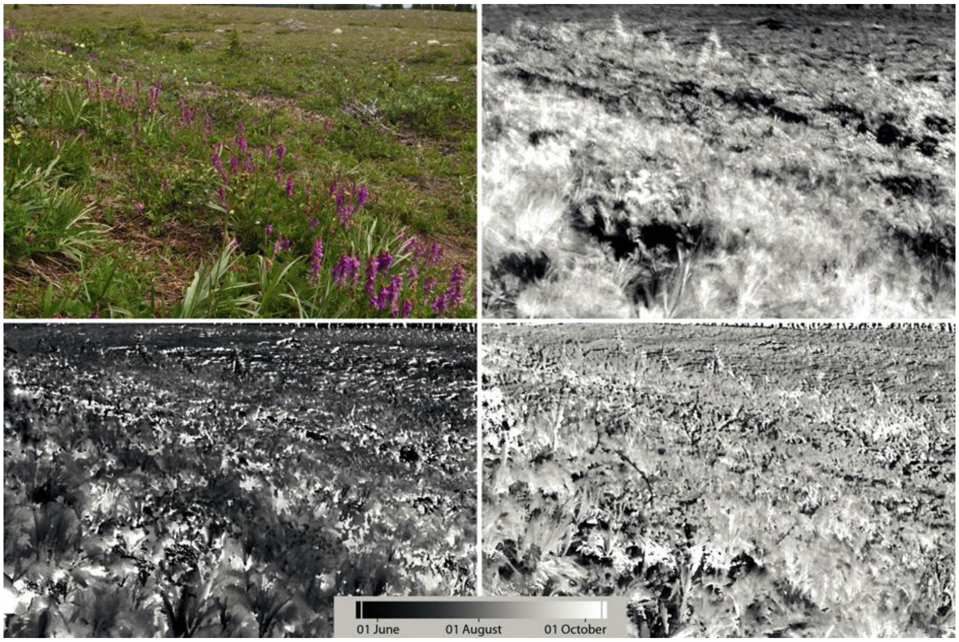

Fig. 3. Examples of phenology camera data, (a) RGB image, (b) 2G-RB index image, (c) Green-up, (d) Senescence.

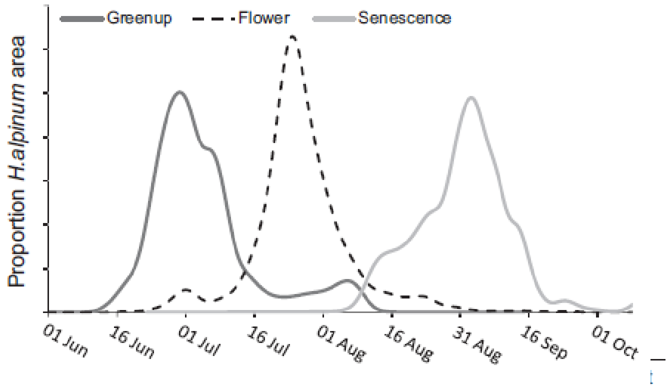

Fig. 7. Histograms of green-up, flowering and senescence for *H. alpinum* from the Cardinal Divide stand-scale camera perspective.

Fig. 5. Average crude protein content of *H. alpinum* roots sampled in three locations in west-central Alberta, Canada, in different phenological stages. Error bars are 1 SE above and below the mean. Based on data from Coogan et al. (2012).

From a wildlife management and monitoring point of view, we believe it is the linking of Figs 5 and 7 in this work that provides the most important insights. While there is considerable variability around the root nutritional value at the sampled sites (initial high nutritional value, followed by a reduction at flowering and seed production, and an increase again at dormancy), the pattern of nutritional status throughout the season is similar to many understorey species. Most of these species allocate more resources above the ground for reproduction at certain times of the year, thereby reducing resources below the ground and at other times. With few above-ground resources to support at pre-leaf and dormant stages, the below-ground component of the vegetation gains comparatively more resources and thus nutrient content. This pattern of below-ground nutrient availably is the inverse of the camera observable greenness, and thus the link is an inverse one for forest managers. The portion of the scene shown in Fig. 7 at each of the key, above-ground phenological phases can essentially be inversely multiplied by the nutritional value in Fig. 5 to provide a landscape estimate of the nutrient carrying load of this specific vegetation type for wildlife. In this example at Cardinal Divide, nutritional availability of food is highest between 1 June and 1 July (before maximum green-up) and after 15 August (during senescence). The capacity to provide explicit dates of when these maximum nutritional load events occur across the landscape is of significant benefit to managers, as it provides key time periods when bear activity in these areas is most likely, or conversely least likely, to occur due to root forage quality and availability. While other food sources, and management activities, will of course also impact bear movements and locations, this information provides one key perspective on the overall bear landscape. Multiple cameras at multiple sites characterizing the key bioclimatic zones across the region would, when combined, provide a region-wide bear forage availability map that could be updated in real time and provide an immediate perspective on the nutritional load for the bears within this area.

Conclusions. In this paper, we describe a system and approach to detect the phenological development of individual plant species from daily camera images at both a plant and forest stand scale. The phenological development of certain species is closely linked with the nutritional value of above- and below-ground parts of these plants, and therefore the availability of high-quality forage for grizzly bear. The use of repeat photography provides a cost-effective way to assess vegetation development and food availability at a forest stand scale, improving information availability for management of bear habitat and providing a tool for increasing our understanding of grizzly bear feeding ecology.

Monitoring plant condition and phenology using infrared sensitive consumer grade digital cameras

Wiebe Nijland, Rogier de Jong, Steven M. de Jong, Michael A. Wulder, Chris W. Bater, Nicholas C. Coops

Agricultural and Forest Meteorology, 184, 98– 106, 2014

Abstract. Consumer-grade digital cameras are recognized as a cost-effective method of monitoring plant health and phenology. The capacity to use these cameras to produce time series information contributes to a better understanding of relationships between environmental conditions, vegetation health, and productivity. In this study we evaluate the use of consumer grade digital cameras modified to capture infrared wavelengths for monitoring vegetation. The use of infrared imagery is very common in satellite remote sensing, while most current near sensing studies are limited to visible wavelengths only. The use of infrared-visible observations is theoretically superior over the use of just visible observation due to the strong contrast between infrared and visible reflection of vegetation, the high correlation of the three visible bands and the possibilities to use spectral indices like the Normalized Difference Vegetation Index. This paper presents two experiments: the first study compares infrared modified and true color cameras to detect seasonal development of understory plants species in a forest; the second is aimed at evaluation of spectrometer and camera data collected during a laboratory plant stress experiment. The main goal of the experiments is to evaluate the utility of infrared modified cameras for the monitoring of plant health and phenology. Results show that infrared converted cameras perform less than standard color cameras in a monitoring setting. Comparison of the infrared camera response to spectrometer data points at limits in dynamic range, and poor and separation as the main weaknesses of converted consumer cameras. Our results support the use of standard color cameras as simple and affordable tools for the monitoring of plant stress and phenology.

Introduction. Information on vegetation development from satellite images commonly relies on indices which compare the reflectance of vegetation in multiple spectral regions. The most common indices utilize the differential response of vegetation in near infrared (NIR) and red (R) or other visible bands. The normalized difference vegetation index (NDVI) (NIR − R/NIR + R) (Tucker, 1979) is the most commonly used index (Liang et al., 2011; Soudani et al., 2012).Many studies have successfully used ground based infrared or mixed-spectrum cameras to study plant health, vegetation cover, or vegetation vigor, such as in precision agriculture (Bauer et al.,2011; Huang et al., 2010; Knoth et al., 2010), ecology (Aber et al.,2009), and archeology (Verhoeven et al., 2009), among others. The studies focus mostly on the spatial domain, while few studies analyzed time-series of IR or mixed imagery (Lelong, 2008). Many long-term near sensing phenology studies however, rely on indices of greenness, either 2G − RB, excess greenness, or

G/RGB, green chromatic coordinate (Richardson et al., 2007; Sonnentag et al., 2012;Woebbecke et al., 1995). The difference in usage between satellite versus ground-based systems has principally been driven by atmospheric and economic considerations. Both air- and space-borne remote sensing systems are influenced by atmospheric scattering in the blue and green range and therefore better results are often obtained using longer wavelengths such as red and NIR. Satellite sensors are designed for Earth observation and thus include NIR detection capabilities, while consumer cameras are designed for taking pictures of cats and thus resemble the human vision system which has considerable overlap between especially red and green sensitivity (Konica and Minolta., 1998; Poynton, 1995). Atmospheric scattering is of little concern for near sensing as the target and the sensor are spatially much closer and shorter wavelengths like blue and green are less affected because of the reduced path length. Secondly, near sensing approaches often utilize inexpensive consumer-grade sensors (digital cameras), which facilitate autonomous remote operation and establishment of observational networks covering significant geographical areas or environmental gradients (Bater et al., 2011). In contrast, sensors that can acquire NIR image data are inclined to be more expensive, reducing both their flexibility in deployment and quantity of units deployed. The differences between spectral characteristics and approaches of remote and near sensing systems raise questions about the compatibility of the two approaches (Coops et al., 2012; Fisher et al., 2006). Additional research is required to improve our under-standing of how these data compare both spatially and temporally, as well as how they can capture varying degrees of plant stress.

In this paper we discuss the use of single-capture infrared images for monitoring phenology and plant health. To do so we undertake two case studies, the first of which compares the performance of IR and true color cameras to detect seasonal development of understory plant species within a forest canopy. In contrast to the theoretical advantage of IR based systems, true color cameras outperform the IR converted sensors. Therefore, we use the second study to further explore response of IR and true color cameras to changes in plant health in a controlled laboratory environment. This study combines images and spectrometer data of a 52 day stress experiment on *Buxus sempervirens* plants. We use the spectrometer data to simulate the response of different camera systems to changes in plant health to help explain the performance of standard and converted consumer cameras in vegetation studies. Our main objective is evaluating the utility of consumer grade digital cameras, specifically with infrared conversions, for vegetation monitoring and phenology studies.

Methods. *Infrared conversion of consumer-grade digital cameras*. Consumer-grade digital cameras are fitted with either a CCD (charge coupled device) sensor or a CMOS (complementary metal-oxide-semiconductor) sensor. The silicon-based sensor substrate is

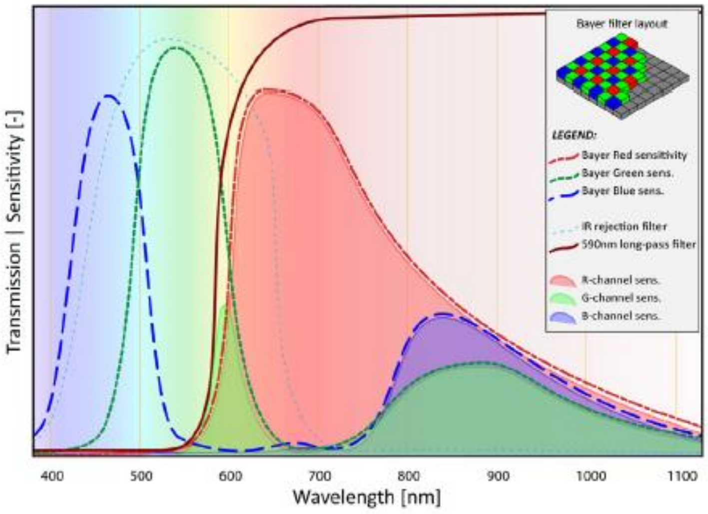

Fig. 1. Idealized filter profiles (lines) and channel sensitivity (surface) for camera with internal *IR* rejection filter replaced by a 590 nm long pass filter (after: LDP 2012, Nijland, 2012; Buil, 2012).

generally sensitive to wavelengths between 350 nm and 1100 nm, including ultraviolet (UV) and NIR (Brooker, 2009). To obtain true-color images, most sensors have a Bayer color filter array (Bayer, 1976; Hirakawa and Wolfe, 2008), which combines a blue, a red and two green sensor cells into one true-color image pixel (Figure 1). However, the filter materials (partly) transmit UV and IR radiation and therefore the cameras are fitted with a rejection filter that cancels out these wavelengths. It becomes possible to use standard CCD/CMOS sensors for IR imaging if the rejection filter is removed. A number of companies offer such conversions (e.g. Life Pixel Infrared Conversion Services, Mukilteo WA (www.lifepixel.com); LDP LCC, Carlstadt, NJ (www.maxmax.com)),or market purpose built digital cameras that are based on converted RGB sensors (Tetracam Inc, Chatsworth CA (www.tetracam.com)).The IR rejection filter is replaced by a filter that allows transmittance of IR and selected regions of the visible spectrum. The Bayer color filter array, on the other hand, is fused to the sensor substrate and cannot be removed. As a result, when using RGB cameras with the IR filter removed, the transmission profiles of the Bayer color channels remain, and depending on the filter choice each channel is sensitive to its original color and/or to IR radiation. Fig. 1 shows the sensitivity of a camera with the IR rejection filter replaced by a 590 nm long-pass filter. In this example, the R-channel records Red + IR, the G-channel records IR plus some component of the Green, and the B-channel records IR only.

Fig. 2. Examples of images acquired at the botanical garden at UBC in RGB (left) and IR-590 (right). The numbered rectangles identify species of interest.

The filter choice influences the spectral sensitivity and dynamic range of the sensor. A low cutoff wavelength gives better separation between the color bands and thus allows for using these color differences in calculating band indices. However, these filters often result in a large exposure difference between R, G and B, requiring exposure compensation and causing loss of usable dynamic range. In addition to their confounded spectral response, digital RGB cameras have a limited dynamic range and acquire images using automated exposure control setting which may involve in-camera image preprocessing; usually, this preprocessing cannot be tuned. As a result, band ratio indices have to be used to negate changes in brightness and produce images which are

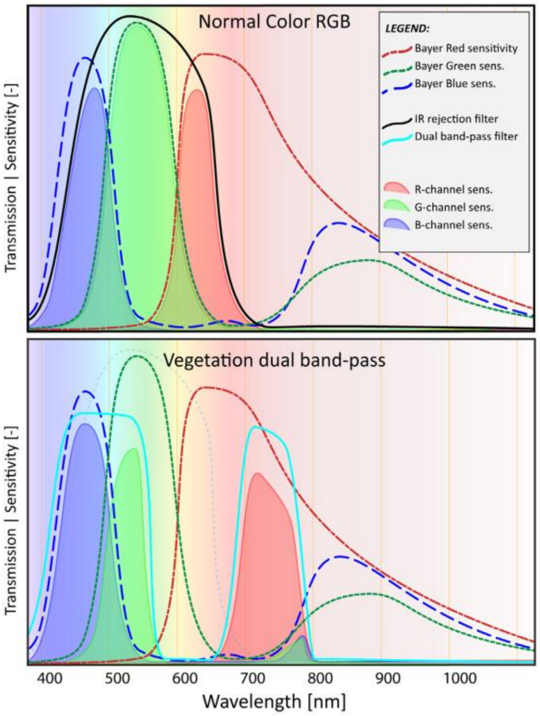

less sensitive to image brightness and exposures, such as the excess greenness (2G − RB) or green chromatic coordinate (G/RGB) in standard color images. With long-pass filters that transmit (a part of) red light (Figure 1), indices that leverage the difference between the B (IR-only) and R (Red + IR), like the blue channel chromatic coordinate (IR − B/IR − RGB), are most promising. Additionally, the green channel may be used, although it has less potential due to its dual sensitivity in both the green and IR regions. Since the Bayer red pixels are by design sensitive for red and infrared light, it is not possible to obtain separate measurements of red and infrared with a single exposure. This, in turn, makes it impossible to calculate a true NDVI from a single image.

Laboratory experiment. We simulated the responses of different camera filters to changes in plant health using the ASD spectra and theoretical camera response curves. The simulations were used to assess the effect of different filter configurations separated from issues related to the exposure and processing of images. The simulations were made with seven different configurations: Standard camera IR-rejection filter (normal RGB, Fig. 4); uniform 100 nm RGB; 590 nm long-pass filter (Fig. 1); 715 nm long-pass filter; 830 nm long-pass filter; red rejection dual band pass filter (Fig. 4);and Thematic Mapper bands 4, 3, and 2 (Markham and Helder, 2011) (G 0.52–0.60; R 0.63–0.69; NIR 0.76–0.9 nm, with uniform response within those ranges). The simulated responses were then used to calculate band indices to capture the development of the plant phenology and stress. For this experiment we considered: uniform 100 nm Green chromatic coordinate (G/R + G + B), TMNDVI (NIR − R/NIR + R), IR intensity (720–920 nm), camera green chromatic coordinate (G/RGB), 590 nm long-pass blue chromatic coordinate (IRB/IRR+ IRG+ IRB), and red rejection band pass NDVI (NIR – B/NIR + B). All of the indices were calculated as deviation from the initial value to make them more comparable and remove slight individual differences between groups.

Figure 4. Idealized filter profiles for a normal (true-color) RGB camera and a camera with a red-rejection dual-band-pass filter as used for the camera simulations.

Results. *Field experiment.* Exploratory analysis of image-derived indices showed variation in the correlation between IR indices and greenness-based indices, especially for the IR-blue chromatic coordinate. In order to get a more detailed understanding of the sensitivity of these indices to changing illumination and phenological condition we looked at the hourly and yearly patterns of three species and compared them to a constant, non-vegetation surface

Hourly patterns. The hourly profiles of green and IR based indices show the yearly averaged values by each hour and corresponding standard deviations (Fig. 5). For the greenness based indices, the 2G-RBi has a much stronger diurnal signal than the G/RGB as this index is by design more sensitive to changes in illumination. From the IR images, we derived blue channel brightness (sensitive from 800 to1100 nm) and blue chromatic coordinate (B/RGB), which leverages the difference between the blue and other image channels. Again, the blue chromatic coordinate has less hourly variability, indicating a lower sensitivity to illumination changes. In both the greenness and IR based indices, different species showed different daily cycles, likely due to shading since the direct illumination varied tempo-rally among the individual plants. This effect is strongest around noon, with highest illumination and therefore strongest contrast between shaded and non-shaded species. Fig. 5 illustrates that the difference between the three plant species and the non-vegetation area is more apparent in the greenness-based indices than in the IR-based indices.

Yearly development. Seasonal trends were shown in our assumedly constant target (wood-chip path), the deciduous bog blueberry (*V. uliginosum*), and the evergreen salal (*G. shallon*). As anticipated, the wood chip shows no clear trend, with most of the small variations likely related to daily illumination conditions. Neither does the IRB chromatic coordinate show any clear trends related to the phenological development of the plants. Conversely, the green chromatic coordinate of the bog blueberry shows a very strong spring leaf flush and decreasing green values as the leaf ages during the growing season. The evergreen salal has high greenness values throughout the year, with a distinct peak during the summer months when new (bright green) leafs unfold. The IRB intensity follows the general trends that can be observed in the greenness, but seems to be less sensitive to the color differences between young and fully developed leafs. The IR values show intraday scatter caused by its sensitivity to illumination conditions.

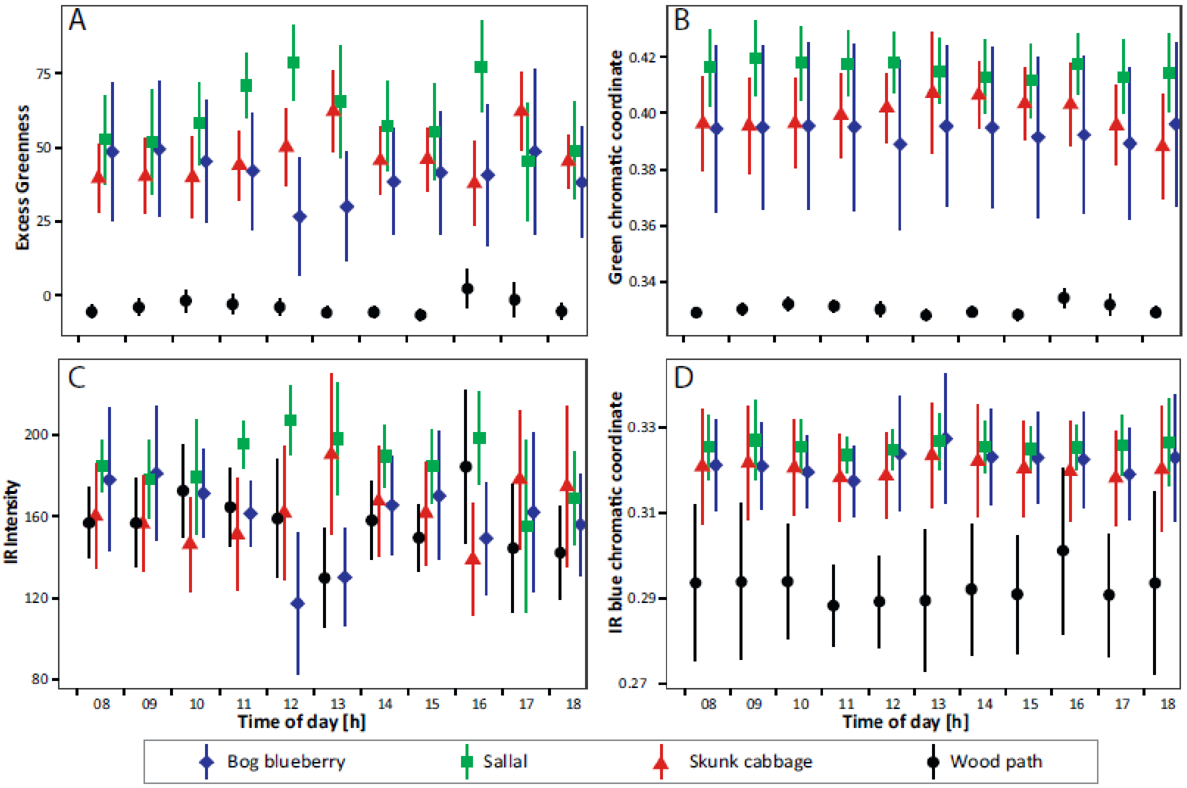

Fig. 5. Hourly patterns of four vegetation indices as averages over the whole year, the lines indicate one standard deviation. Shown are: *V. uliginosum*, Bog blueberry; *G.shallon*, Salal; *L.americanus*, Skunk cabbage; and wood-chip path as non-vegetated reference.

Discussion. In this study, we used consumer-grade digital cameras for monitoring plant health and phenology. The performance of near-infrared images was compared against true-color RGB images. The latter were found to outperform infrared images, especially in an uncontrolled (field) environment. The underperformance of infrared imagery for vegetation monitoring is attributable to limitations in dynamic range and band separation. These two issues are discussed below. The limited dynamic range of consumer grade CCD/CMOS sensors forces the use of camera auto exposure and prevents con-version of digital numbers into calibrated radiance values. If a scene has notable changes in brightness over the monitoring period, the camera has to compensate its exposure, which obscures the detection of actual changes. In complex scenes, local differences in direct versus diffuse illumination may further obscure the changes of interest. Furthermore, consumer cameras apply non-linear trans-formations to the image data in ways that are beyond user control (Wüller et al., 2007). It is therefore not possible to effectively correct for the changes in illumination and exposure. The lack of calibrated data can be addressed by using color indices that are insensitive to brightness, like the green chromatic coordinate, which is used in many visible-color vegetation studies. In IR cameras that are converted using a long pass filter, such indices have to be constructed using the red and blue channels, leveraging the difference between IR + Red and IR-only information. However, our study shows that the IRB chromatic coordinate is insensitive to plant health or phenology, both in the field situation and in the lab experiment (Figures 6, not shown, and 7). In the experiments we have considered other band combinations and indices, but none exhibit a clear response in agreement with vegetation trends. Effects of illumination changes can be reduced by selecting images under specific conditions as demonstrated by Ide and Oguma (2010), i.e. using overcast conditions only. However, eliminating images limits data availability and can decrease the temporal resolving power of the analysis.

Conclusions. In this study, we investigated the potential use of IR-sensitive consumer-grade digital cameras for the detection of trends in plant phenology and health in a field situation and during a con-trolled laboratory experiment. Consumer grade digital cameras are promising tools in monitoring plant health, phenology, and vegetation development at local scales, or by deploying them in a network over larger regions. Results show that IR-converted cam-eras underperform in a monitoring setting compared to standard color cameras due to these systems' limitations in dynamic range and poor band separation. Simulations show that a conversion with a red-rejection dual-band-pass filter (i.e. blue, green and infrared sensitivity) largely overcomes these issues, making it a promising tool for vegetation monitoring studies. Consumer-grade RGB cameras are already widely used in vegetation monitoring settings and our results further support and promote their use as simple and affordable tools for reliable detection and monitoring of plant stress, development and phenology.

Assessing the Impact of Field of View on Monitoring Understory and Overstory Phenology Using Digital Repeat Photography

M. Vartanian, W. Nijland, N.C. Coops, C. Bater, M.A. Wulder, G. Stenhouse

Canadian Journal of Remote Sensing, 40:85–91, 2014

Abstract. Phenological patterns of the components within forest ecosystems, such as understory vegetation, are important indicators of climate variability, productivity, and additional ecosystem services such as food and habitat availability for wildlife. Proximal sensing systems can provide detailed phenological records at a relatively low cost. As interest in these datasets increases, we need additional information regarding the effect of different approaches on the scale of observations and camera field of view. In this research, we examine the impact of field of view on the capacity of cameras to detect changes in phenology of individual species in an image time series. We examine two co-located series of oblique images acquired using a fine and broad field of view and compare a number of phenological indicators, including the start and end of season derived for individual plant species. Our results indicate both fine and broad field of view camera systems are highly effective at detecting key markers of plant phenology with no significant differences between the two. This result supports environmental monitoring using cost-effective broad field of view cameras, or even—subject to some constraints—readily available camera stations installed for tourism or traffic monitoring.

Introduction. In a remote sensing context, variations in the reflectance of vegetation cover can be used as indicators of phenological changes (Badeck et al. 2004) and, as a result, data from a number of instruments and sensor types are used to monitor vegetation changes at both local and global scales. At the stand level, the increasing popularity and use of inexpensive visible spectrum digital cameras has offered a new source of information for the monitoring and measurement of phenological events at the local scale (Woebbecke et al. 1995; Richardson et al. 2007; Ide & Oguma 2010). Repeat photography allows a very fine temporal sampling, often at daily or hourly intervals, for monitoring vegetation phenology (Graham et al. 2010; Richardson et al. 2010; Bater et al. 2011a; Nijland et al. 2013). This type of proximal sensing system has a number of benefits, including high temporal frequency data acquisition and cost effectiveness. Permanent proximal sensing systems are deployed in a wide range of configurations ranging from webcams (Richardson et al. 2007; Morris et al. 2013) to dedicated single-lens reflex (SLR) camera systems (Bater et al. 2011b; Sonnentag et al. 2012; Nijland et al. 2014), and mounted on existing towers or buildings (Graham et al. 2010; Sonnentag et al. 2012) to positions right next to individual plants (Graham et al. 2006). However, as novel techniques proliferate, comparisons between approaches are not often undertaken, resulting in a wide variety of methods with little examination of issues such as field of view or scene extent and the associated trade-offs. In this communication we examine the impact of field of view on the capacity of imagery, acquired from a digital camera network, to detect changes in phenology of specific plant species or individuals in the image. To do so we examine a series of oblique images acquired at narrow and broad fields of view. Identical plants were located on both sets of images, with the start and end of the season's phenological indicators derived for individual plants, from each scene, and compared by species. Phenological events were also recorded in the field and statistically compared to the camera derived dates. We conclude with recommendations on appropriate fields of view for vegetation monitoring.

Digital Camera Network. Six digital camera units were installed (Harbortonics, Fort Collins, CO, USA) at three study locations in western Alberta. The primary component of each camera unit was a Pentax K100D digital SLR (Pentax Corporation, Tokyo, Japan) installed with lithium ion batteries and supplemented by a solar panel for power throughout the study period. Five images were acquired between noon and 13h local time for each day of the study in JPEG format (3008 × 2008 pixels) and were stored on memory cards, retrieved at the completion of data collection. At each location, for the duration of the study period (late April to early October 2010), two cameras were positioned on suitable trees in order to collect both broad and narrow field of view oblique images (see Figure 1). The field of view of an image is a function of the angle of view and the object distance. In this case, given that the cameras were identical, the field of view is principally a function of the distance between the camera and the vegetation. All cameras were positioned facing north, with the broader field of view images acquiring data over a greater spatial range (500–2000m2) than the narrow field of view (<5m2) cameras. The motivation and discussion of the network is provided by Bater et al. (2011b).

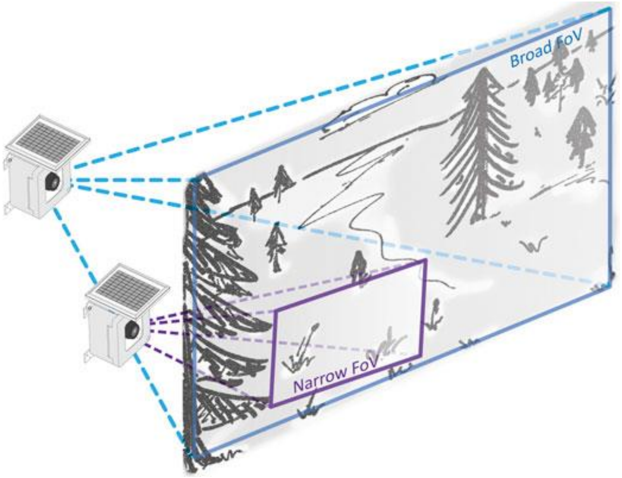

Figure 1: Geometry of images.

Image Analysis. Images were processed and analyzed in the R programming environment (R Development Core Team 2012) using GDAL for reading the image data (Bivand et al. 2013) to obtain the start and end of the growing season. To do so, we located individual plants per frame in both the broad and narrow field of view images, delineated pixel coordinates, and extracted average RBG values per individual. RGB values were then used to calculate the 2G-RB index (Richardson et al. 2007) to minimize light intensity differences between averaged daily images:

$$2G - RBi = 2\mu G - (\mu R + \mu B)$$

where μ is the is the image digital numbers in bands R: red, G: green, and B: blue. A smoothing spline function with rigidity of 2/3 was fitted to the data point (5 each day) to decrease scatter caused by plant movement or changes in lighting conditions, the smooth curve was used in the further analyses. Beginning of season and end of season dates were calculated from the temporal sequence of 2G-RBi values using the half-maximum method, which has been used both in local phenological monitoring as well as larger scale investigations (Schwartz et al. 2002; Richardson et al. 2009; Bater et al. 2011a). Beginning of season was defined as the first day above the derived half-maximum value, and end of season as the first day below. To ensure integrity of the derived values, images recording excessive rain or snow were removed from analysis and values normalized by the 10 and 90 percentiles to remove outliers from the remaining data (i.e., the lowest and highest 10 % of data points were removed) (Nijland et al. 2013). Finally, deviance plots were produced for each species and field of view.

Statistical Analyses Between Fields of View. The impact of recording imagery with narrow and broad fields of view was assessed in a number of ways. First, *t*-tests were undertaken to assess if differences existed between the broad and narrow fields of view, beginning of season and end of season estimates, when compared to the field data. Using *t*-tests and correlation analysis, we then assessed if the broad and narrow field of view estimates beginning of season and end of season differed from each other.

Results. Each camera acquired between 800–880 images per site with a few data breaks because of power or storage failures. In total, 11 individuals from eight species were identified across all images, and differences in phenology were compared across the three key stages of the annual vegetation development, the greening phase, approximately comprising the first third of the curve; the peak and/or flowering phase, comprising the middle third; and the yellowing or senescing phase, approximately comprising the last third, as well as the beginning and end of season estimates.

When compared to the field-observed phenological stage, results indicated no significant difference between the broad or narrow fields of view with field measured beginning of season values ($p > 0.05$). In contrast, end of season validation data was found to be significantly different ($p < 0.003$) to both the broad and fine field of view images, with differences of 14 and 21 days, respectively, suggesting that 2G-RBi is not as effective at determining end of season compared to the beginning. When comparing the broad and fine field of view estimates to each other, both the beginning and end of season estimates were not statistically different, with mean differences on average by all species of between 0.75 and 2.71 days, respectively.

Discussion. In this study we evaluated broad and narrow field of view images to detect changes in phenology in forest understory plant species. Bater et al. (2011b) proposed that proximity may play a role in event monitoring efficacy; that is, images that contain more spatial detail may be able to collect more accurate species specific phenological information, and further, that the need for validation field visits would be reduced if species-specific events could clearly be discerned on the time-series imagery. Likewise, Nijland et al. (2013) highlighted other potential advantages offered by close proximity phenological monitoring, including an amelioration of perspective issues and increased spatial resolution. In contrast to these expectations, the results of this analysis suggest that broad field of view images perform in a similar manner when compared to images captured using a narrow field of view.

To date, most studies investigating the role of digital camera imagery for environmental monitoring have used cameras with a broad field of view (Richardson et al. 2007; Graham et al. 2010). In this study, we found that broad scale image series detected phenological events as accurately as closer placed, fine scale images. Installing cameras with a wider field of view is more cost effective when the phenology of multiple species can be detected in the same image. Furthermore our results support the investigation toward the use of readily available camera stations that have been installed for other purposes such as traffic monitoring or tourism to monitor phenology. The field of view is often broad and highly oblique, but will likely still be suitable for accurate extraction of the main vegetation phenophases.

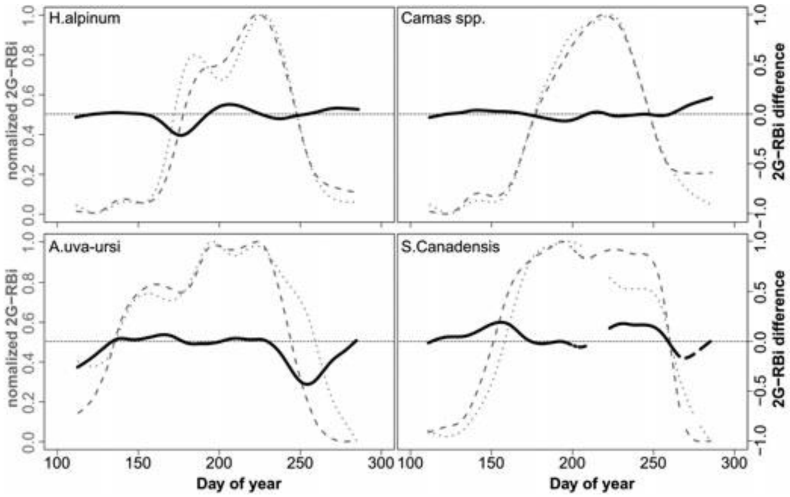

FIG. 4. Deviation 2G-RBi plots (Broad – Narrow) by species. The gray lines are the normalized splines for narrow (dots) and broad (dash) fields of view, the black solid lines shows the difference between the two.

Conclusions. In this research we conclude that narrow- (<5 m2) and broad (500–2000 m2) field of view repeat photography systems perform equally in the detection of phenological patterns for individual species in the view. The field of view can thus be chosen freely depending on the specific project needs, but we advocate the use of a broader field of view because of associated scale and cost advantages. This finding goes against the intuition that closer camera placement will result in more reliable detection of phenology in individual plant species. In addition, we demonstrate the ability to detect phenological curves for multiple plants with different growth patterns within the field of view.

Imaging understorey phenology: scaling from camera plots to landscapes

W. Nijland, Doug K. Bolton, N.C. Coops, and G. Stenhouse

Submitted to Remote Sensing of Environment, 2015

Abstract. Information on the spatial and temporal patterns of plant phenology is important to develop a more comprehensive understanding of food availability and habitat for many animal species. The combination of broad scale, regional climatic, and more localized, site-level drivers presents a challenge when upscaling phenology from the plot to the region. Likewise, developing relationships between ground- or camera-based estimates and satellite imagery remains difficult due to the trade-off between temporal and spatial resolution. Landsat imagery, with its 16 day temporal resolution, is often thought of as being insufficient for timely observation of changes in vegetation throughout the year. However the free, and readily availability of the Landsat archive has enabled a major shift in the way Landsat imagery is processed moving towards pixel, rather than scene, based analyses. In this paper we build on previous research by examining the applicability and accuracy of Landsat derived phenology curves beyond deciduous stands into more mixed stands and conifer dominated forest types. In addition, we discuss the application of these Landsat phenology curves to phenology of understorey species which are linked to habitat selection for free roaming wildlife, in particular grizzly bears. The agreement between Landsat- and camera-derived estimates of key phenological events was stronger for green-up (RMSE = 7 days) than for senescence (RMSE = 14 days). Our results show that yearly adjustment of green-up and senescence dates using available Landsat observations improved the agreement with camera-derived estimates when compared to average annual curves. Transition dates accepted as valid ranged from 25% for alpine herbaceous pixels to 75% for closed deciduous, demonstrating the variable success of this approach across land cover types. Transition dates were rejected if pixels lacked a strong enough green-up signal in Landsat spectral indices or if the estimated dates fell outside of the valid range. We conclude by investigating the spatial patterns of seasonal phenology at the Landsat scale, and assess the relative importance of regional vs. microsite conditions as well as the utility of these data for resource and wildlife management.

Introduction. Spatial and temporal patterns in plant phenological events such as leaf emergence and senescence are important factors driving the carbon cycle of terrestrial ecosystems (Badeck et al., 2004; Keeling et al., 1996; Myneni et al., 1997) as well as in the provisioning of food availability and habitat use by many animal species (Nielsen et al., 2003; Sharma et al., 2009; Visser and Both, 2005). The precise timing of phenological events both within and between years, is driven by a combination of regional climate conditions (Cleland et al., 2007; Menzel, 2000), and more localized processes like snow-melt (Schwartz 2003 Chap 14;Julitta et al., 2014), or overstorey structure (Liang et al., 2012), as well as specific traits of individual plant species (Uemura, 1994).

In this paper we examine the applicability of Landsat derived phenology curves beyond deciduous stands into more mixed stands and conifer dominated forest types. In addition, we apply the technique to examine phenology of understorey species which are linked to habitat selection for free roaming wildlife, in particular grizzly bear (*Ursus arctos*). Our study area is focused the eastern flank of the Rocky Mountains in Alberta, Canada which has a regionally important and threatened population of grizzly bear (Festa-bianchet, 2010), as well as various economic values in forestry, resource extraction (e.g. oil/gas and mining), and tourism. We mine the Landsat archive from 1986 onwards to derive phenological patterns based on the Enhanced Vegetation Index (EVI) at 30m spatial resolution. The long term phenological curves for each pixel are analyzed as well as yearly differences in the timing of green-up and senescence. To validate the approach, we compare the Landsat derived estimates to a network of phenological cameras throughout the region. We conclude by investigating the spatial patterns of seasonal phenology at the Landsat scale, and assess the relative importance of regional vs. microsite conditions as well as the utility of these data for resource and wildlife conservation management.

Methods.

Phenology Model. To represent the phenological development in each pixel, a double sigmoid function was fit to the EVI values against the day of year, following the methods of (Fisher et al., 2006).

$$EVI = f(t) = V_{min} + V_{amp}\left(\frac{1}{1 + e^{m_1 + m_2 t}} - \frac{1}{1 + e^{m_3 + m_4 t}}\right)$$

Where t = day of year, Vmin = average off-season EVI, Vamp = seasonal EVI amplitude and m1-4 are parameters that depend on the timing and rate of the vegetation green-up (m1,2) and senescence (m3,4). All 6 parameters are fit simultaneously to all of the clear pixel observations from DOY 80–340 in an iterative least squares fitting procedure. From the curve, we then calculated the maximum EVI, amplitude, day of year for green-up and senescence (defined as the curves half-max point in spring or autumn, Waring et al., 2006), and season length as the difference between the green-up and senescence date. Initially, the logistic model was fit for all pixels with sufficient observations, however not all pixels will necessarily return a reasonable fit. In particular a key assumption of the logistic fitting is a clearly defined transition between the dormant and the green phase. Therefore, pixels with an EVI amplitude less than 0.1 were flagged as having poor model fits. Models that predicted phenological events outside the main growing season (green-up < 135 days, 175 < seasonal max day of year < 225, and senescence >280 days) were also flagged. Once the long term mean curve is fit to the data, annual deviations in green-up and senescence dates were derived by shifting the curve to fit available points within 20 days and 1/5th of the EVI range of the fitted transition point, following a similar method proposed by Melaas et al. (2013) .

We assess our results by examining the proportion of acceptable vs rejected (i.e., flagged) pixel fit using the method above. We first compared accepted and rejected fits by terrain, examining the impact of elevation and slope on estimation of the transition values. Second, we use a 16 class land cover map based on a combination of Landsat and LiDAR data (Nijland et al., 2015) to stratify the area and examine the predictions by major land cover types. The accuracy of the predicted transition dates is evaluated by comparing them to the dates derived from the phenology camera network deployed in the study area.

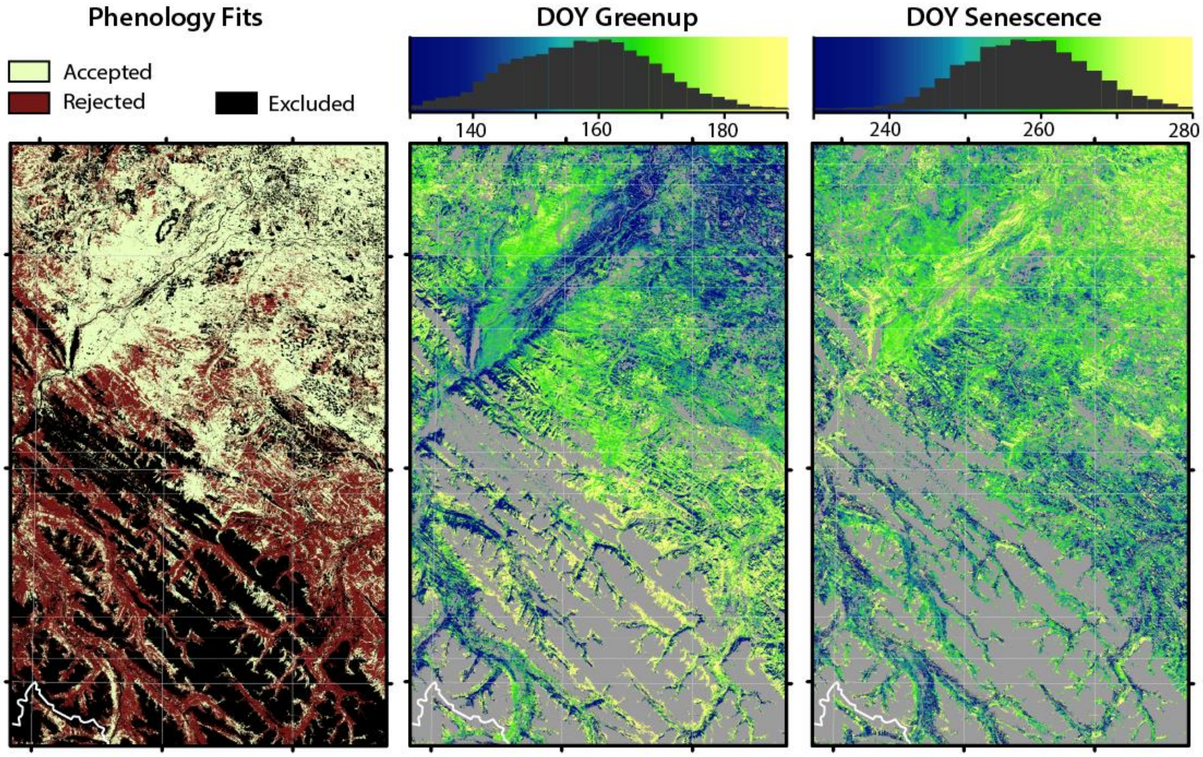

Figure 5: Spatial patterns of a) phenology fit succes, b) fitted green-up day of year, c) fitted senescence day of year.

Results. *Fit Accuracy.* To assess the accuracy of the Landsat derived green-up and senescence dates for individual years we compared predictions to the average phenology dates derived from the ground based camera network. Figure 6 shows the Landsat EVI observations and fitted phenology curves for three camera locations. Note the differences in amplitude and season length between the vegetation types and elevation of the locations. Both the start and end of season root mean square error (RMSE) of Landsat vs. camera dates was reduced by adjusting the dates to the correct observation year with increased accuracy of 2 days for green-up, and 1 day for the senescence. Overall the correspondence between the camera and Landsat derived dates was improved more for the green-up than the senescence with an RMSE of 7 and 14 days respectively. These errors are similar as those between the camera- and field-dates (C. C. W. Bater et al., 2011; Nijland et al., 2012; Vartanian et al., 2014). The dates of the camera derived phenological events, alongside the average and year specific dates from the Landsat data are shown in Figure 7, the camera locations are plotted in order of their elevation.

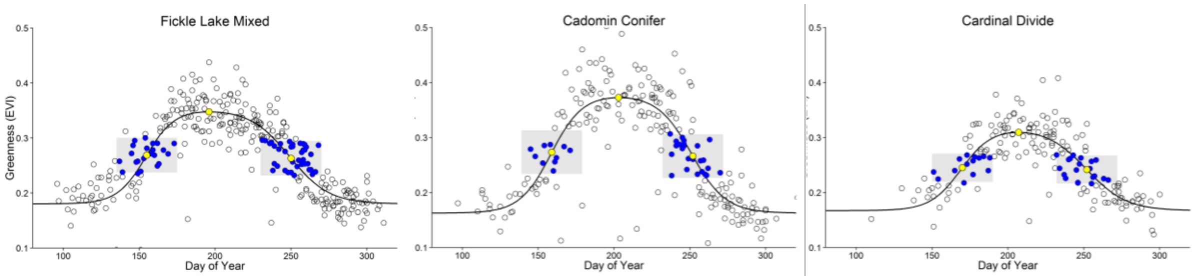

Figure 6: Example Phenology curves and observations from the camera locations. Blue dots indicate the points used for the annual phenology shifts.

Annual Variability. Comparison of the annual adjusted Landsat phenology with the camera observations confirms that annual corrections of the phenological transition dates decreases the bias between Landsat and Camera data. Annual transition dates are not always available however for all pixels because of a lack of observations in the transition period or significant cloud cover. On average 40% of the area in any given year has data during the green-up phase, and 54% during senescence. More recently, when Landsat 5 and 7 were both operational better data coverage was obtained. Overall we did not find a significant ($p<0.05$) trend in either the timing of green-up or across the study area over the observation period.

Discussion. Conventional thought suggests that available Landsat time series have insufficient density to fit phenological curves for individual years. However by accumulating multiple years of observations dependable dates can be derived for the key transitions: green-up and senescence. In this study we found green-up dates are accurate to within a week compared to camera observation. For senescence, the accuracy is less, with differences as large as two weeks in some cases. The accuracies found however are similar to those found relating ground based cameras to field data over the same area (C. C. W. Bater et al., 2011; Nijland et al., 2012; Vartanian et al., 2014). Leaf unfolding has a much stronger signal in greenness (and especially infrared based vegetation indices like EVI) than fall discoloration. Annual corrections to green-up- and senescence dates derived by shifting the general phenology curve to fit available observations in the transition period as proposed by Melaas et al (2013) improves the accuracy by 2 and 1 days for green-up and senescence respectively as compared to the field camera derived dates. The correspondence between the Landsat data and the camera network is a good indicator of the ability of this method to capture the spatial patterns in phenology across the study area. The relation also suggests that

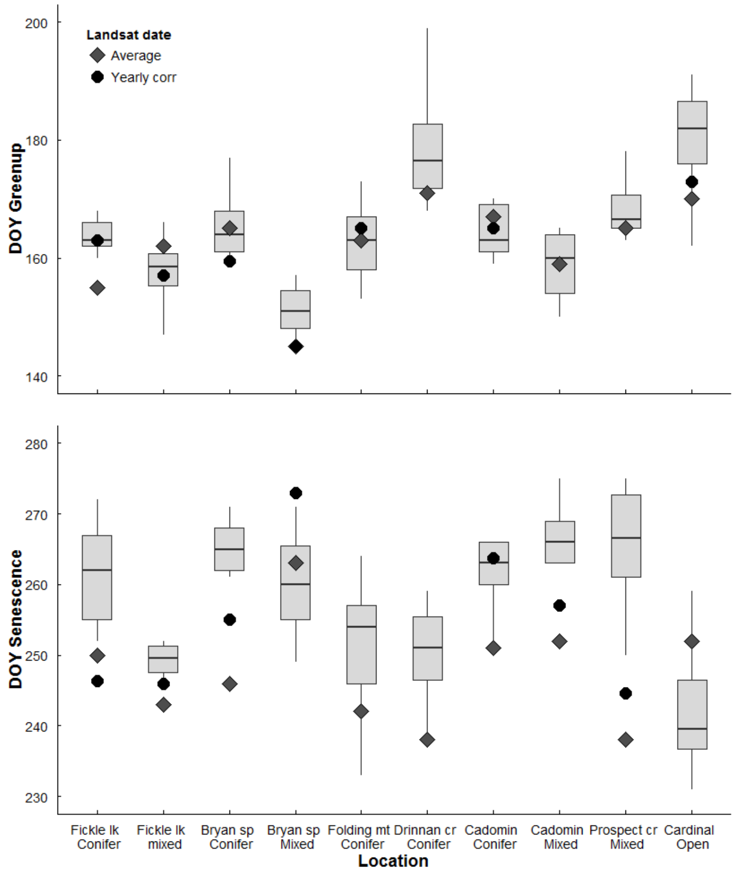

Figure 7: Phenological transition dates for the camera network and Landsat derived dates for the same locations. The boxplots represent the variability of different plant and tree species within the field of view of each camera.

Landsat imagery is either strongly influenced by understorey phenology which we hypothesize for the open coniferous forest common to our study area, or that understorey and overstorey phenology are synchronous. Spatial patterns in green-up and senescence show considerable fine scale variability on top of the general elevation dominated trends. The differences between adjacent sites may depend on vegetation cover or exposure which demonstrates Landsat superior capacity for upscaling phenological observations from fine scale camera network than coarser spatial resolution sensors, especially in heterogeneous landscapes.

Applications in habitat management. Effective management of wildlife in multi-use landscapes requires an in depth understanding of the behaviour and habitat requirements of the species of interest. Foraging and food availability are closely related to vegetation phenology, and are an important driver of animal movement patterns. For example, grizzly bear have a seasonally variable diet (Hamer and Herrero, 1987; Munro et al., 2006) and therefor seek different parts of the landscape driven by the availability of those foods. High spatial and temporal resolution phenology data can therefore contribute to improved dynamic wildlife habitat models (Nielsen et al., 2010) which support a better understanding of animal ecology and improve wildlife management. Landsat-derived phenological descriptors will inform our ongoing research into habitat selection by GPS satellite collared grizzly bears within the study area, and seasonal habitat selection models will be improved with this new knowledge.

Conclusions. We show the application of Landsat derived phenology curves on the east flank of the Rocky Mountains in Alberta, Canada and compare the results to phenology derived from a ground based camera network. Our results show that it is possible to expand the scope of Landsat derived phenology beyond the previously explored deciduous forest into mixed and coniferous stands. Areas with coniferous or herbaceous vegetation cover had fewer acceptable phenology fits than other landcover types as did areas with steep topography. However, even though only sparse data were acceptable in mountainous terrain they still give a good indication of phenology patterns in those areas where coarse spatial resolution methods may not resolve them. The case for using high spatial resolution data to deriver phenology curve is further strengthened by the level of spatial variability we find at fine scales. Correspondence between the satellite-derived vegetation or canopy dominated green-up and senescence dates and understory phenology as observed on the ground is significant with RMSE of 1 week for green-up and 2 weeks for senescence. Yearly adjustment of transition dates based on available observations in the transition period improved the agreement with field data with 2 and 1 days over average transitions dates derived from the whole time series from 1986 to 2014. The ability to derive high spatial resolution phenological curves from the Landsat archive and obtain yearly adjustments makes Landsat imagery a good candidate for upscaling ground based phenology networks to more comprehensive wall to wall coverage. Phenological information from Landsat improves our knowledge of spatial and temporal patterns in food availability, allowing for more informed management decisions regarding grizzly bear habitat in Alberta. Future work will focus on linking spatially continuous phenological information and habitat selection by grizzly bears.

Past-century decline in forest regeneration potential across a latitudinal and elevational gradient in Canada

Adam Erickson, Craig Nitschke, Nicholas Coops, Steven Cumming, Gordon Stenhouse

Ecological Modelling, 313, 94–102, 2015

Abstract. The regeneration niche of trees greatly narrows the fundamental niche and is sensitive to climatic change. Development from seed and phenology are regulated by biological and environmental controls, shaping forest successional pathways. We hypothesized that recent climate change is reducing regeneration suitability in northern forests. We used a process-based ecophysiological model to examine changes in forest regeneration conditions across an elevational and latitudinal gradient in Alberta, Canada from 1923 to 2012. We compared these results to a recent empirical study in the region to infer the recent drivers of regeneration change in northern forests. Our results suggest that these forests are experiencing climatically driven declines in conditions suitable for regeneration. Contrary to previous findings indicating poorer current conditions in low elevation forests, we found more stable regeneration potential there, attributable to a relative abundance of soil moisture. Rocky soils resulted in modeled losses of soil moisture at higher elevations, potentially preventing upslope migrations of species despite warming. We identify potential mechanisms driving unexpected tree regeneration patterns described in previous studies. Our simulations suggest a delayed response of forest regeneration to warming throughout the past 90 years.

Introduction. The widespread adaptation of trees to local climatic conditions (Alberto et al., 2013) indicates that tree phenology is intricately tuned to optimize fitness for local environmental conditions through gene expression, posttranslational modification, and, genetic and epigenetic inheritance (Cooke et al., 2012; Liu et al., 2010; Matzke and Mosher, 2014). Environmental effects are estimated to exert greater influence on plasticity than genetics in northern forests (Vitasse et al., 2013), while phenotypic variation reflecting phylogeographic origins (Alberto et al., 2013) is not necessarily adaptive (Duputié et al., 2015). Extreme weather events, such as frost or drought, occurring at critical times during tree development can have strong demographic effects on forests. Given the importance of fine-scale climatic and phylogenetic variability, high temporal resolution climate data (Cook et al., 2010) along with a range of aggregate species tolerances can aid in the modeling of these dynamics at the landscape scale, where individual-or population-level data is seldom attainable. We hypothesized that warmer conditions combined with changes in soil water balance (Dobrowski et al., 2013; Piedallu et al., 2013) and more rapid and severe extreme weather events (Allen et al., 2010; Kamae et al., 2014; Trenberth et al., 2014) are altering regeneration patterns in northern forests. Recent empirical evidence suggests that this shift is already occurring (Boisvert-Marsh et al., 2014; Lenoir et al., 2009; Urbieta et al., 2011; Zhang et al., 2015). However, direct measurement remains confounded by forest turnover, which can increase the amount of space available for recruitment (Carvalhais et al., 2014; Park Williams et al., 2013; Woodall et al., 2013; Zhu et al., 2014, 2012). Additional confounding factors include patterns of fine-scale climate (Dobrowski et al., 2013) and ontogenetic niche variation, whereby the niches of species can change throughout development (Bertrand et al., 2011a; Cavender-Bares and Bazzaz, 2000; Donohue et al., 2010; Eriksson, 2002; Niinemets, 2010; Urbieta et al., 2011). We suggest that changes to tree regeneration throughout north-ern forests in recent decades have been driven by interactions between climatic change and local soil patterns. To test this hypothesis, we used a species-specific ecophysiological model that explicitly represents major tree regeneration processes, based on forest gap models. We parameterized the model for tree species and soil textural classes across a 25.2 million hectare study area in Alberta, Canada, encapsulating an important elevational and latitudinal gradient. We used daily resolution historical weather station data for three decadal periods over the last century, and for the most recent decade, to model the effects of climatic change on forest regeneration throughout the past 90 years.

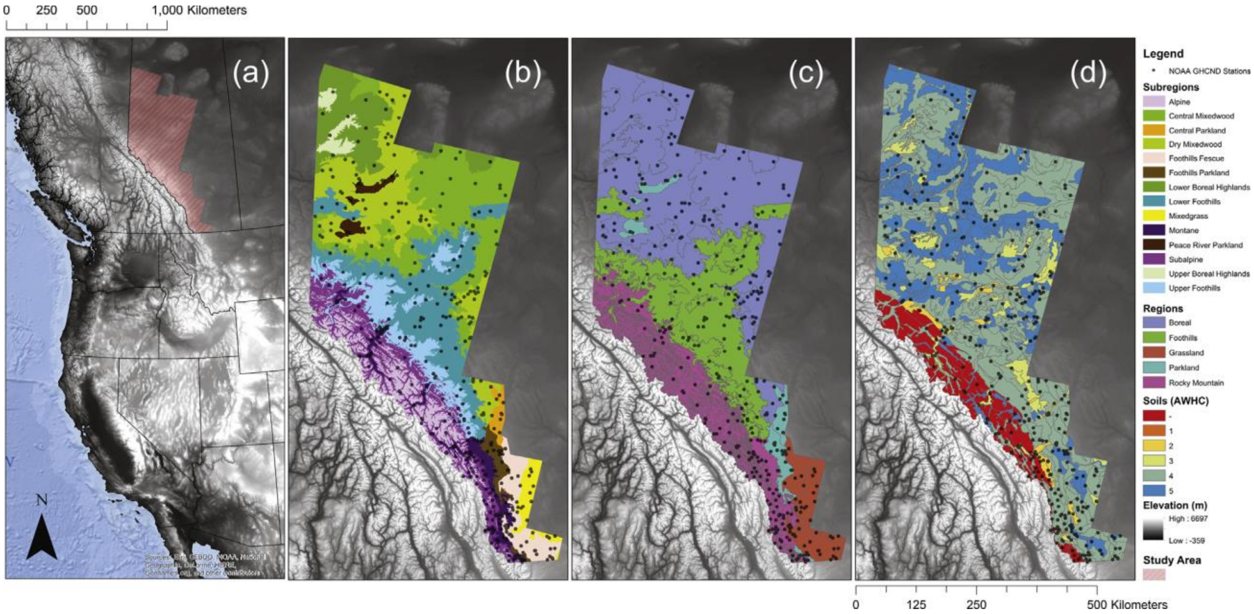

Fig. 1. Study area overlaid on 90-m resolution NASA SRTM topography: (a) study area geographic context within North America; (b) biogeoclimatic subregions and weather stations; (c) biogeoclimatic regions with subregion outlines and weather stations; (d) Soil regions with outlines and weather stations; available water holding capacity (AWHC) classes are shown, the most sensitive edaphic model parameter, with red representing bare rock or effectively zero. (For interpretation of the references to color in the figure legend, the reader is referred to the web version of this article.)

Methods. *Study area*. We applied the Tree And Climate Assessment Germination and Establishment Model (TACA-GEM) across fourteen biogeoclimatic regions of western Alberta, Canada (Natural Regions Committee, 2006) (Fig. 1), coextensive with ecoregions in the United States (Ricketts, 1999). The study area comprises a transition zone from boreal forest at lower elevations to higher elevation Cordilleran foothills and montane forests in the southern Canadian Rocky Mountains. We derived soil and climate parameters for thirteen natural subregions, excluding the treeless alpine subregion. Regional soil properties reflect a recent glacial history, primarily consisting of morainal and glacio-lacustrine parent materials, with gray luvisols and black chernozems representing the dominant soil types (Natural Regions Committee, 2006). Luvisols are periodically saturated and depleted of oxygen, whereas Chernozems occurs in semiarid and sub-humid climates, representing the dominant soil of the Canadian southern interior plains (Soil Classification Working Group, 1998). The region consists primarily of well-drained upland soils.

Elevational and latitudinal gradients segment the study area biogeoclimatically, with mean elevations ranging from 525 meters in the boreal to 2350 meters in the alpine. The study area covers a latitudinal gradient from 49° at the U.S. border to 58◦at the northernmost point (NAD83 datum). The heavily forested foothills region experiences higher levels of precipitation than surrounding areas, supporting productive lodgepole pine (*Pinus contorta* var. *latifolia*) forests and an active timber industry. While most Canadian provincial harvest levels remained stable over the past four decades, harvest increased approximately four-fold in Alberta (National Forestry Database, 2013), alongside a rise in oil, gas, and mineral extraction activities. Regionally abundant species include lodgepole pine (*Pinus contorta*), white spruce (*Picea glauca*), trembling aspen (*Populus tremuloides*), and black spruce (*Picea mariana*) (Natural Regions Committee, 2006; Zhang et al., 2015). Previous studies show that this region became warmer and drier throughout the 20th century (Luo and Chen, 2013; Peng et al., 2011).

TACA-GEM model design. The latest version of the Tree And Climate Assessment Germination and Establishment Model (TACA-GEM) presented herein builds on establishment-only TACA-EM (Nitschke and Innes, 2008) and extends previous TACA-GEM versions (Nitschke et al., 2012) with four improvements. First, establishment suitability is no longer governed by binary responses to growing degree days (GDD) and drought conditions for a given year. The GDD response functions from Zelig++ (Burton and Cumming, 1995), JABOWA (named for Janak, Botkin, and Wallis) (Botkin et al., 1972) and FORÊT (Shugart and West, 1977) are used to determine annual establishment suitability as a probabilistic function of temperature. Second, drought is no longer represented as the portion of the year where water deficit occurs per the actual-to-potential evapotranspiration ratio, but is now calculated based on the proportion of the year where soil water potential is equal or below the turgor loss point (permanent wilting) for a given species. Third, soil water potentials are calculated from soil water availability and soil texture class, using a reformulation of the van Genuchten soil water model (Van Genuchten, 1980). Species suitability is equal to one in years with no water deficit and declines to zero if the proportion of the year under water deficit exceeds a species-specific thresh-old. The fourth improvement to the model is the development of an extreme events module. The extreme events module modifies species regeneration by eliminating seedlings that regenerate in favorable years but are subjected to prolonged and/or extreme drought or frost events, which result in mortality over decadal time periods.

The TACA-GEM model focuses on species-specific responses through the use of logical submodels representing biological processes. The use of process-based species responses allows us to bridge the current knowledge gap related to fine-scale biological processes while minimizing cumulative model error. Such process-based models are particularly useful for balancing model specificity and generalizability (Levins, 1966) to infer broad-scale forest change, through a combination of biological appropriateness and computational efficiency. This paper implements the previously developed germination module (Mok et al., 2012) in North America, parameterized for 21 regional species either currently within the study area or with the potential to in-migrate from adjacent regions, based on published literature on species germination and seed ecology. We further provide an example of the three germination functions utilized in the model.

We used data from the National Oceanic and Atmospheric Administration (NOAA) Global Historical Climate Network Daily (GHCN-D) version 3.11 to parameterize daily minimum and maximum temperature, and precipitation sum, in the TACA-GEM model. The GHCN-D dataset is a global weather station database subjected to uniform quality assurance (Menne et al., 2012).

Using the R programming language (R Core Team, 2014), we computed daily weather values for the median decades of interest within 30-year periods, averaged across each natural subregion for each day, in order to provide model results comparable to recent vegetation modeling studies (Wang et al., 2012). We imputed missing values using a computationally efficient approximation of the expectation-maximization bootstrapping algorithm using the R Fast Imputation package (Honaker et al., 2011; Lounici, 2012). Our GHCN-D functions are available as part of the rnoaa package. We applied this approach to the 1923–1952, 1953–1982, and 1983–2012 periods by modeling their median decades (1933–1943, 1963–1972, and 1993–2002, respectively), as the model is designed for decadal periods. We modeled the most recent period (2003–2012) to offer the most accurate depiction of current regeneration conditions.

Soils parameters. We overlaid the biogeoclimatic natural regions and subregions of Alberta (Natural Regions Committee, 2006) onto Soil Landscapes of Canada (SLC) v3.2 data (Soil Landscapes of Canada Working Group, 2010) to generate soil textural class parameters for TACA-GEM. We characterized soils in each natural subregion based on the dominant soil type. Soil texture, rooting zone depth, percentage of coarse fragment material, available water storage capacity, and percolation rate were calculated based on corresponding SLC values. We obtained soil moisture regime and mean elevation parameters from the natural subregion summaries (Natural Regions Committee, 2006). Traditional soil textural classes were calculated using Agriculture and Agri-Food Canada particle size classes (Soil Classification Working Group, 1998). Soils were classified into textural groups based on SLC values for percent sand, silt, and clay, filtered by parent material texture. Percolation rates were calculated by subtracting available water holding capacity from field capacity for each natural subregion, equal to the soil permanent wilting point (Cassel and Nielsen Arnold, 1986). Organic soils were designated for one subregion, based on evidence provided in the biogeoclimatic region summaries (Natural Regions Committee, 2006).

Species parameters. Tree species modeled in the study included any presently extant or directly adjacent species, in order to account for potential in-migrations. Tree species biophysical parameters were derived from the literature and regional databases, following methods applied previously (Nitschke and Innes, 2008; Nitschke et al., 2012). Sources for species biophysical parameters used in the model are provided in the supplementary information.

Results. We found that tree regeneration suitability, modeled as the probability of reaching age ten, declined for most species in the study area (Figure 3 et al.). The establishment of new cohorts for most species was increasingly unlikely. Adding extreme climatic events (i.e., drought and frost) further reduced regeneration conditions, which were poorest in recent decades. We estimate that the regeneration niches of extant and adjacent tree species are largely out of equilibrium with climatic conditions and have been for decades, with regeneration conditions likely to worsen in the coming years. The frequency and magnitude of drought following germination was the most limiting factor affecting regeneration conditions, due to reduced soil moisture.

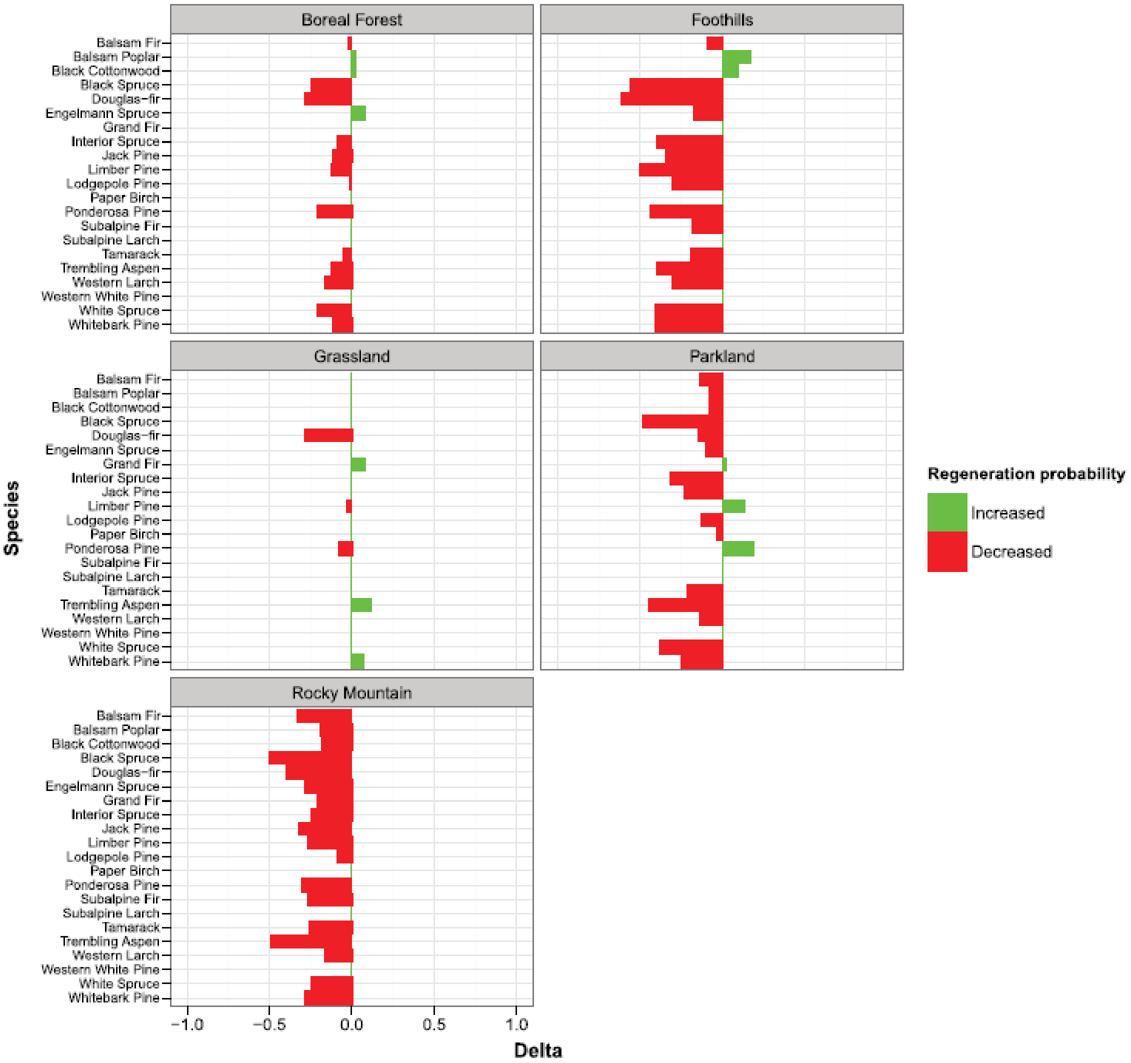

Fig. 3. Mean change in species regeneration probability (Delta) between the periods 1923–1952 and 1983–2012 including extreme events for the five regions; species that consistently failed to regenerate appear unchanged, as in the soil moisture-constrained Grassland region; a value of 1.0 represents a 100% change in regeneration probability; solid red = −1.0; none = 0; solid green = 1.0 (For interpretation of the references to color in the figure legend, the reader is referred to the web version of this article.).

We found that the most recent period modeled, 2003–2012, shows a slight deceleration in the rate of regeneration suitability change, likely attributable to a slowdown in warming (Kosaka and Xie, 2013). As multi-decadal warming continues unabated, modeled tree species are likely to fail to regenerate. An increasing magnitude of climatic disequilibrium is likely to reduce forest regeneration, which may be initiated through climate-driven changes to disturbance regimes (Magnani et al., 2007).

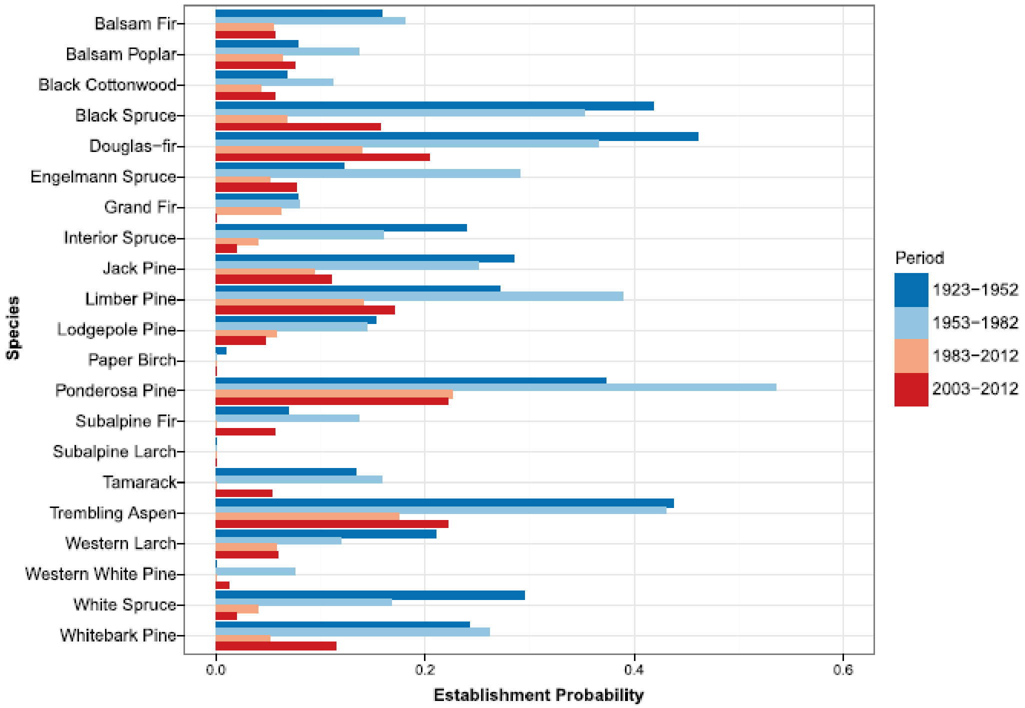

Fig. 4. Means species regeneration probabilities averaged across thirteen biogeoclimatic subregions; blue – 1923–1952; light blue – 1953–1982; light red – 1983–2012; red – 2003–2012; absent values represent regeneration failure. (For interpretation of the references to color in the figure legend, the reader is referred to the web version of this article.)

A significant mean decline in regeneration suitability was predicted across the full study period. Compared to simulations without extreme events, including extreme events in the simulations marginally decreased the probability of establishment (mean = 0.085, _ = 0.220; mean = 0.059, _ = 0.216) and the change in establishment across the full study period (mean = −0.138,_ = 0.228; mean = −0.142, _ = 0.248). More frequent drought, diminished germination success, and lengthened bud dormancy due to the failure to meet chilling requirements resulted in an overall decline in regeneration suitability. Species regenerational responses varied across space and time, often responding similarly in direction to climatic and edaphic conditions within regions and time periods. These trends (Figure 3) are indicative of directional climate change.

Conclusions. Based on our simulations, we conclude that warmer and more variable climatic conditions are diminishing the conditions for extant and adjacent tree species regeneration in Alberta, Canada. Some studies indicate that forest regeneration conditions should be improving at higher elevations and latitudes (Brubaker, 1986;Lenoir et al., 2009) and declining in lower elevation forests (Bertrand et al., 2011b; Loarie et al., 2009), while others provide mixed results potentially related to changes in human activity (Boisvert-Marsh et al., 2014). Our findings support a relative improvement in regeneration conditions in low-elevation northern forests (Crimmins et al., 2011; Dobrowski et al., 2013; Zhu et al., 2014, 2012). We found that changes to soil moisture conditions drove species regeneration niches toward the foothills and park-land regions, indicating that changes to soil water balance may drive future species migrations under warming (Crimmins et al., 2011; Piedallu et al., 2013). The inclusion of soil water balance is particularly important in mountain watersheds (Hwang et al., 2014) and in the Canadian boreal forest (Barnett et al., 2005), as it is the key limiting factor driven by climate. Our model results provide a potential explanation of complex tree regeneration pat-terns observed in previous studies (Boisvert-Marsh et al., 2014; Urbieta et al., 2011; Woodall et al., 2013; Zhang et al., 2015; Zhu et al., 2014, 2012), providing direction for future empirical work.

In the coming years, increases in the frequency of anthropogenic disturbances (Kurz et al., 2008; Park Williams et al., 2013) may accelerate the currently delayed regenerational response of forests by increasing the number of sites available for recruitment. Concurrently, warmer and wetter conditions projected for northern forests (Trenberth, 2011) may accelerate recruitment by increasing the rate of forest turnover (Carvalhais et al., 2014; Zhu et al., 2014). Due to the long-lived nature and relatively rapid dispersal ability of trees (Clark et al., 1998), future compositional changes will likely occur in pulses as climatic change intensifies. Directional changes to the region’s forests may occur through rare long-distance migration events (Clark et al., 1998) by species better adapted to low soil moisture, producing no-analog communities. Future empirical studies should investigate evidence of regenerational change in northern forests with ground plot data in connection with directly measured local climate data. Future modeling studies should incorporate important forest dynamics, such as competition, dispersal, and disturbance by fusing theoretical and empirical formulations with detailed remote sensing structural measurements. An improved understanding of forest regeneration may help forest managers to meet multiple-use goals, while providing a more complete picture of biospheric climate feedbacks.

Declining resilience of northern forests due to human influences on climate and wildfire

Adam Erickson, Nicholas C. Coops, Craig Nitschke, and Gordon Stenhouse

Submitted to Ecology Letters, 2015

Abstract. In western Canada, expanding human activity is theorized to shift the successional and evolutionary trajectory of forests. Forest dynamics are under a number of human influences, from regeneration to disturbance regimes. Regeneration underlies the migrational response of forests to directional change, modified by dispersal, competition, disturbance, soils, and light. Here, we fuse a process-based regeneration model with a cellular automaton-based forest dynamics model to probe the long-term resilience of forests in the southern Canadian Rockies. We show that a shift toward smaller, more frequent fires and diminishing regeneration conditions are reducing the ability of forests to track warming, amplifying climatic disequilibrium and reducing resilience. Tree species regeneration niches moved toward higher elevations and latitudes, driven by changes in soil water balance, as boreal fire regimes migrated northward. We anticipate that ecosystems to the south will migrate into the region in the coming years.

Introduction. Over the past 150 years, human activity has increased dramatically in forests worldwide, reflecting exponential-like population growth (Foley et al. 2005). Critically, global change conditions have the potential to reduce the resilience of northern forests to periodic perturbation, such as wildfire and drought (Davis & Shaw 2001). Determining when and where ecosystem shifts may occur is critical to management. Simulation models uniquely enable scientists to discern critical thresholds of forest change and their mechanisms. By running experiments *in silico*, the resilience of current landscape conditions can be tested under different scenarios. Here, we develop simulation scenarios based on variation in climate and fire conditions measured throughout the 20th and 21st centuries, probing for signals of directional change in forests of the southern Canadian Rockies.

Due to the higher velocity of warming at high latitudes, boreal temperature conditions and fire regimes are moving northward at rates of 430 m yr^{-1} (Loarie et al. 2009) and 2 km yr^{-1} (Erickson et al., *in preparation*), respectively. These rates are greater than paleo-rates of species range shifts inferred from the pollen record, while landscape fragmentation has been shown to reduce the migration rates of trees (Lazarus & McGill 2014). Together, these changes may amplify disequilibria. The prevalence of such disequilibria in forests is partly due to the long-lived nature of trees, which are able to tolerate wide climatic fluctuations once established (Svenning & Sandel 2013). Under persistent warming, changes to disturbance regimes can regulate species migration rates, and thus disequilibrium, by making sites available for recruitment. Direct measurement of species migrations and other forest dynamics have remained challenging due to the long time scales involved, incentivizing the development of mathematical models.

Here, we simulate a forested landscape in high spatial resolution (one-hectare cells) across a 25.2 million hectare latitudinal and elevational gradient at the nexus of the Canadian Rocky Mountains, boreal forest, and prairies. To determine the resilience of the current landscape under the continuation of recent historical climate and fire trends, we fuse a process-based tree regeneration model, TACA-EM (Nitschke & Innes 2008; Nitschke et al. 2012), with a cellular automaton-based forest dynamics hybrid model, LANDIS-II (Scheller et al. 2007). We initialized the landscape at year 2000 conditions using a rules-based reclassification of Canadian land cover data applied to a species distribution model (Gray & Hamann 2012). We classified historical conditions into the following three 30-year scenarios: Pre-Suppression Era (1923-1952), Early Suppression Era (1953-1982), and Global Change (1983-2012), corresponding to changes in fire suppression, climate, and human activity patterns (Erickson et al., *in preparation*). We added a Most Recent Decade (2003-2012) scenario, based on an observed rapid increase in fire frequency, decline in mean fire size, and climatic warming 'hiatus' with extreme summer temperatures (Kamae et al. 2014). We also add a contrast scenario, applying Pre-Suppression Era fire regimes to Most Recent Decade climatic conditions, as well as succession simulations without fire, to discern the relative influences of climate and fire on simulation results.

We simulated fourteen total scenarios for a period of fifty years at an annual time increment to determine current landscape resilience under the continuation of recent climate and fire trends. We applied two types of wildfire model: a statistical fire-spread model and a semi-mechanistic cost-path fire-spread model incorporating fire weather inputs that is used to dynamically model fuel conditions. All models used were developed and validated using empirical data for northern forests of North America, discussed in the Supporting Information. For both wildfire models, we developed a new validation technique that overcomes long-standing challenges in applying Monte Carlo signal processing methods to large stochastic landscape simulations (He & Mladenoff 1999).

Methods. We used TACA-EM to generate tree species regeneration probabilities for the succession submodel of LANDIS-II for each species, region, and period. We parameterized TACA-EM using tree species regeneration niche parameters from the literature and previous studies (Nitschke & Innes 2008; Nitschke et al. 2012), weather data from the NOAA Global Historical Climatology Network Daily dataset, and soil texture data based on a new classification scheme for the Soil Landscapes of Canada v3.2 database. For the biogeoclimatic and fire regions, we used a provincial classification scheme.

To initialize the landscape in LANDIS-II, we reclassified the best available Canadian land cover data, dated to year 2000 conditions, with forest composition defined based on the best available tree species distribution model (Gray & Hamann 2012). To parameterize tree species life history attributes in LANDIS-II, we used data from the literature and species compendiums. To parameterize the LANDIS-II fire submodels, we used historical wildfire polygon data from the Canadian National Fire Database. To calculate the fire weather index and fuel conditions, we used provincial historical fire weather station data and the Fire Behaviour Prediction System fuels classification scheme developed for Canada. We ran the simulations for four historical scenarios: Pre-Suppression Era (1923-1952); Early Suppression Era (1953-1982); Global Change (1983-2012); Most Recent Decade (2003-2012). This classification is based on an analysis of historical fire regimes (Erickson et al., *in preparatio*n). Additional materials and methods are available in the Supporting Information.

Results. Forest composition remained stable under the two most recent scenarios (1983-2012 and 2003-2102), but was less stable during previous scenarios (1923-1952 and 1953-1983). Pronounced compositional change of pyrogenic species under a larger annual area burned suggests that forests were already in climatic disequilibrium in the Pre-Suppression Era, with modeled regeneration conditions declining as warming accelerated. While the rate of migration for most species decreased across the entire study period, related to a decrease in fire mortality and its effects on recruitment rates, they maintained their general trajectory. A directional climatic signal is apparent in these migrational responses, with the rate of migration a function of mortality and warming rates. The contrast scenarios exhibit this finding, producing the greatest decline in forested area under large fires with recent warming.

Warmer conditions increased the relative abundance of drought-adapted species in our simulations, while cool-wet specialists declined. An elevational increase in fire (Erickson et al., *in preparation*) strongly affected Engelmann spruce (*Picea engelmannii*), a montane specialist, with species slowly and consistently following uphill. Montane trees are predominantly snow- and wind-, rather than fire-adapted, shifting forest composition as fire moves upland. At lower elevations, in the boreal forest, where species are strongly shaped by fire, human-driven fire regimes in recent decades slowed migrational responses, despite the highest level of warming.

Combined with empirical evidence for Canada (Zhang et al. 2015; Fisichelli et al. 2014; Leithead et al. 2012), our simulation results indicate that directional forest change is underway, with novel fire regimes reducing the ability of these forests to respond to warming through migration. Similar to other regions in the North American boreal, fire suppression likely explains the modest, rather than pronounced, increase in area burned under warming, combined with a demographic shift and related negative fire feedback (Héon et al. 2014; Kelly et al. 2013; Zhang et al. 2015).

Climatic warming is reducing the likelihood of forest regeneration. Our establishment model results suggest that tree regeneration conditions here are increasingly suboptimal. Species regeneration varied interregionally, while exhibiting a high degree of interspecific agreement in the direction and magnitude of response within regions. These results are supported by recent empirical observations on regeneration and demographic patterns in the North American boreal, which show declining regeneration conditions and recruitment rates (Fisichelli et al. 2014; Zhang et al. 2015; Leithead et al. 2012). Together with our results, these studies suggest that forest regeneration is following the direction of climatic gradients through species-specific ecophysiological niches. Both the boreal forest and its characteristic large stand-replacing fire regimes are tracking climatic gradients northward, matching satellite observations (Koven 2013). As fires also moved uphill, boreal forest species such as tamarack (*Larix laricina*) and black spruce (*Picea mariana*) followed, with a temporal lag regulating recruitment rates (Figure 3). This lag is likely the combined effect of seed dispersal and fire-related site availability.

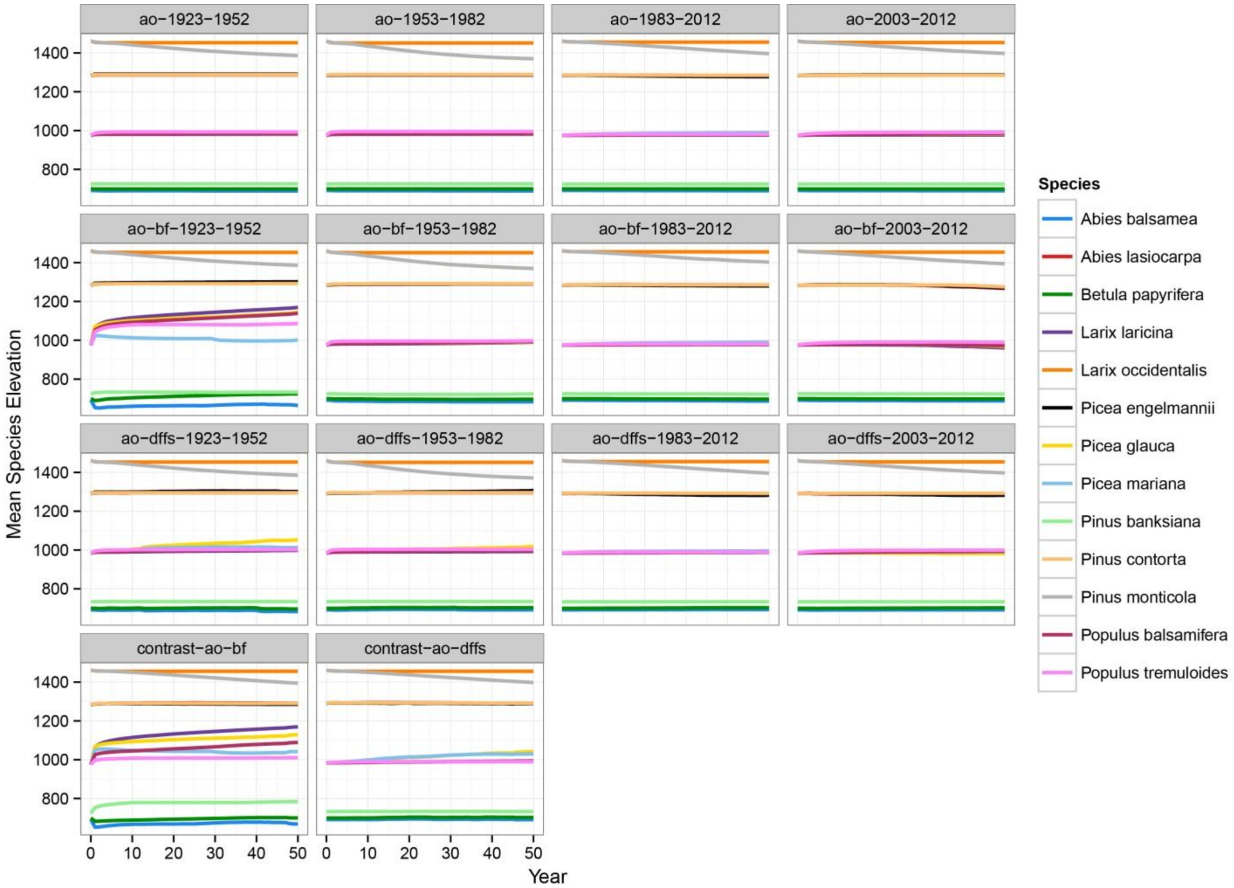

Figure 3. Simulated species mean annual elevation by scenario, 1923 to 2012: The plot titles indicate the LANDIS-II succession and disturbance models employed, followed by the period used for fire and climate parameterization (the initial landscape is fixed at year 2000 conditions): ao = Age-only succession model; bf = Base Fire model; dffs = Dynamic Fuels and Fire System model; contrast = 1923-1952 fire regimes applied to 2003-2012 climatic conditions

Anthropogenic fire regimes are limiting the ability of forests to track warming. Our simulation results show changes in forest composition and structure under the different scenarios (Figure 4). While these changes broadly differ in magnitude due to differences in disturbance rates, the direction of change is consistent across scenarios. Such changes to forest structure and composition carry implications for fire regimes, providing feedback mechanisms (Terrier et al. 2012; Rogers et al. 2015; Héon et al. 2014; Kelly et al. 2013).

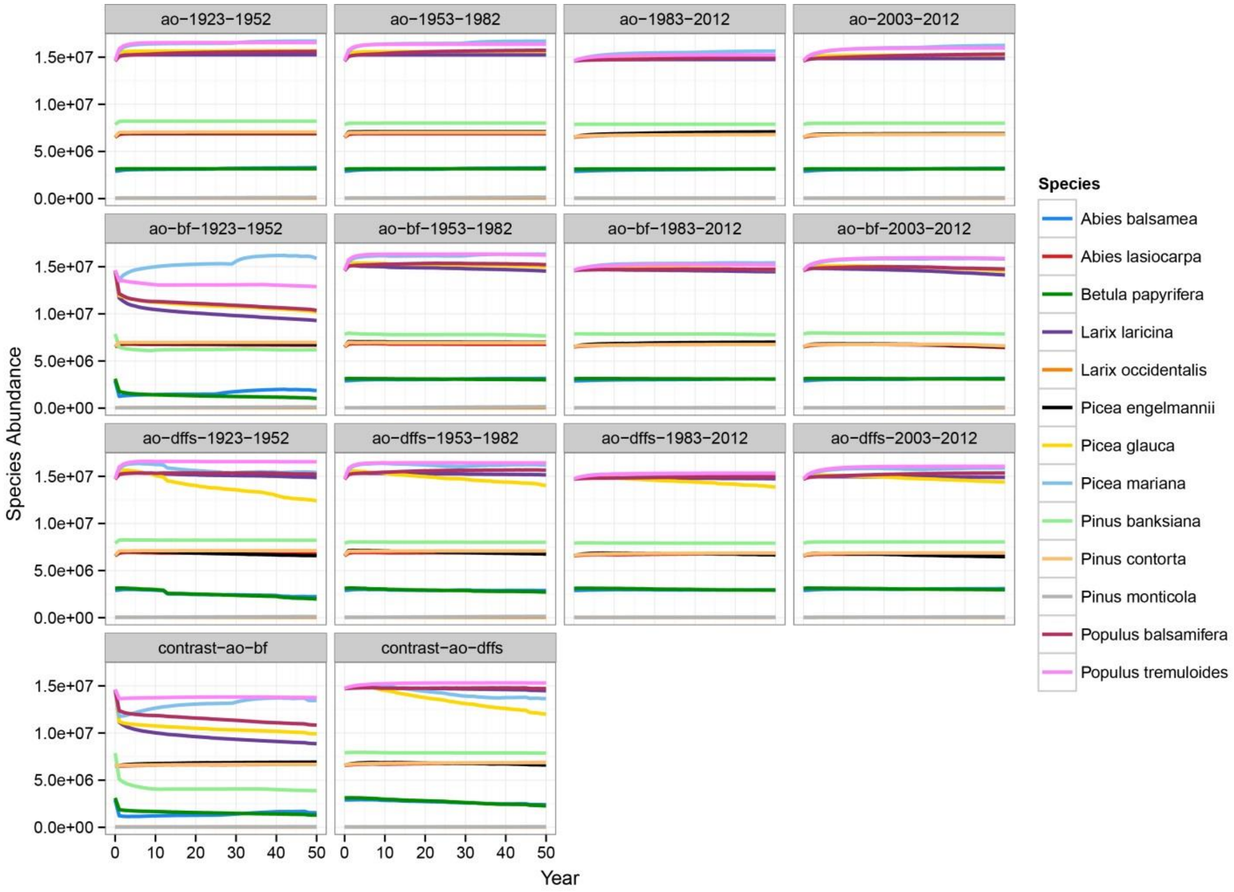

Figure 4. Simulated species abundance by scenario, 1923 to 2012: The plot titles indicate the LANDIS-II succession and disturbance models employed, followed by the period used for fire and climate parameterization (the initial landscape is fixed at year 2000 conditions): ao = Age-only succession model; bf = Base Fire model; dffs = Dynamic Fuels and Fire System model; contrast = 1923-1952 fire regimes applied to 2003-2012 climatic conditions.

Conclusions. We conclude that human-driven fire regimes have increased the magnitude of climatic disequilibrium in these forests in recent decades, supporting a recent empirical study in the eastern Canadian boreal (Leithead et al. 2012). This mathematical model result is due to the combined effects of two dynamics: (1) a more diffuse landscape structure pattern under human-driven fire regimes; (2) diminished species regeneration in all regions except for the boreal under warmer, wetter conditions. Changes to disturbance regimes made fewer sites available for recruitment under recent fire regimes, slowing migration rates, while regenerational disequilibria increased. The inability of species to respond to changing climatic conditions through migration suggests a pronounced shift in forest composition in the coming years, driven by migration and extirpation (Aitken et al. 2008).

Future directional forest change is likely to occur in pulses. In recent eras, fires were no longer concentrated in the boreal, where the ecological role of fire is well known (Rowe & Scotter 1973). Forest compositional change may occur in pulses where disturbances occur, concentrated around areas of human activity, such as roads, waterbodies, and work sites (Erickson et al., *in preparation*). Disturbances other than fire, such as harvest (Bond-Lamberty et al. 2007), drought (Anderegg et al. 2013; Michaelian et al. 2011), and insects (Kurz, Dymond, et al. 2008), may increase in importance, as boreal fire regimes move northward (Koven 2013).

In the short term, growing climatic disequilibrium may alter forest structure by reducing recruitment and stand density, as evidenced by recent empirical findings (Bond-Lamberty et al. 2014; Zhang et al. 2015). Reduced density and cover may provide a niche for migrant species from the south, while temporarily reducing the amount of carbon stored in northern forests. Long-term changes in northern forest structure and composition carry multiple implications for the earth's climate (Laothawornkitkul et al. 2009; Richardson et al. 2013; Mueller et al. 2012; Aponte et al. 2013). Long-term ground and remote sensing studies are required to monitor forest dynamics as warmer, wetter conditions continue at high latitudes in North America.

Northward-migration of boreal fires and emergence of Anthropocene regimes

Adam Erickson, Nicholas C. Coops, and Gordon Stenhouse

Abstract. Much attention has been paid to the effects of climatic change on fire regimes and carbon feedbacks in northern forests of North America(Tymstra et al. 2007; Magnani et al. 2007; de Groot et al. 2013; Bergeron et al. 2010; Kurz, Stinson, et al. 2008; Moritz et al. 2012; Koven 2013; Bond-Lamberty et al. 2007; Héon et al. 2014; Terrier et al. 2012; Kelly et al. 2013). Yet, these studies largely ignore non-climatic anthropogenic factors evident in the historical record that may equally explain recent fire regime variability(Bowman et al. 2011; Kasischke & Turetsky 2006). Here, we conduct an analysis of past-century fire regimes across a latitudinal and elevational gradient in western Canada. The region experienced intensifying anthropogenic activity in recent decades(Statistics Canada 2011; Cross & Bowlby 2006), serving as a model of future continental conditions under current anthropogenic trajectories. We found that fire regimes here shifted from large, lightning-caused fires in remote areas to more frequent, smaller, human-caused fires in anthropogenic corridors. Over the past half-century, annual fire seasons lengthened (mean = +1 day/year) due to rising temperatures (mean = +) and human-caused ignitions (mean = +). Fires occurred more frequently at higher latitudes and lower elevations. Area burned increased at higher elevations and declined at lower elevations, where suppression is prevalent. While warming conditions produced more severe fuel conditions, other factors, such as fire suppression(Cumming 2005), industrial and recreational activity(Magnani et al. 2007), and a forest demographic shift(Zhang et al. 2015; Héon et al. 2014) likely attenuated fuel conditions. We provide the first evidence of a northward migration of boreal fire regimes, accelerated by a southern boreal transition to Anthropocene fire regimes without historical analogue.

Introduction. We examine evidence of the northward migration of boreal fire regimes and the emergence of Anthropocene fire regimes in the southern boreal. We estimate that the northward movement of boreal climate and fire conditions are indicative of a northward boreal forest migration, given the climatic-pyrogenic niche of these forests(Rogers et al. 2015; Koven 2013). Our results show that increased human activity fundamentally shifted fire regimes in western Alberta toward more frequent and smaller fires at lower elevations near human activity, increasing in area burned only at higher elevations, reducing fire-related forest turnover despite warmer and wetter conditions(Carvalhais et al. 2014). Canada-wide, the average latitude of fires increased linearly throughout the past century, while fire frequency and size increased as a lower rate with greater variability.

Methods. For our historical fire regime data, we used the latest Canadian Forest Service's National Fire Database (NFDB) spatial wildfire polygon and point data(Canadian Forest Service 2015). The NFDB was formerly known as the Large Fire Database, or LFDB, and now contains fires of all sizes. The NFDB contain fires from 1919 through 2014, including 97% of the area burned in Canada(Stocks et al. 2002; Bond-Lamberty et al. 2007). The data is assembled from a variety of sources and undergoing extensive validation(Gralewicz et al. 2012; Goetz et al. 2006; Parisien et al. 2006; Canadian Forest Service 2015; Stocks et al. 2002), representing the best long-term fire data available in Canada. While remote sensing disturbance detection may produce more precise fire patterns, the classification of disturbance types currently contains a high level of uncertainty. The national fire perimeter data was created through a joint provincial-federal government disturbance mapping effort, using high-resolution historical orthorectified aerial photographs and Landsat scenes combined with expert-based manual fire delineations. The data indicates expected patterns of improved monitoring over time. The NFDB incorporates spaceborne remote sensing disturbance detection for recent decades using Landsat, providing greatly improved temporal resolution compared to airborne remote sensing, at the cost of spatial resolution.

We combined NFDB fire perimeter data with NASA Shuttle RADAR Topography Mission (SRTM3) version 2 data, processed using standard correction techniques(Reuter et al. 2007), and Natural Subregions of Alberta biogeoclimatic regions(Natural Regions Committee 2006), to analyze historical regional fire distributions. The 30-year temporal scale of the climate-fire scenarios was selected to align with known historical changes to fire management, as well as the widespread use of 30-year climate normals(Wang et al. 2012). We focus on management, annual fire frequency, and area burned change points relative to 30-year time periods. Our expert-based temporal classification is inspired by fuzzy logic change-point classification(Kumar & Wu 2001), based on the relative membership of observations to fuzzy sets.

Results and Discussion. Our results indicate that the application of historical climate-fire correlations to general circulation model projections to estimate future fire regimes, absent changes to anthropogenic trajectories, carries diminished predictive power in the Anthropocene. Short-term fire forecasts in northern forests should include spatially explicit dynamics of human-caused ignitions, fire suppression, and structural-demographic changes to fuels in industrial forests. Long-term forecasts should further include forest compositional change impacts on fuel conditions(Terrier et al. 2012), as well as coupled climatic feedbacks(Amiro et al. 2006). We observed significant changes to annual fire frequency, total area burned, and mean fire size across the 91-year period from 1923 to 2014 (Figure 2). These patterns differ from other recent studies in the North American boreal(Kasischke & Turetsky 2006; Stocks et al. 2002), which show a rapid rise in mean fire size and annual area burned, based analyses of a previous historical fire database. Our results show greater agreement with paleo-reconstruction results from Alaska(Kelly et al. 2013) and recent analyses indicating the presence of negative wildfire feedback mechanisms in the North American boreal(Héon et al. 2014; Rogers et al. 2015). While temperatures increased, fires grew more frequent and smaller, likely attributable to a combination of fuel limitations and fire suppression near built-up areas.

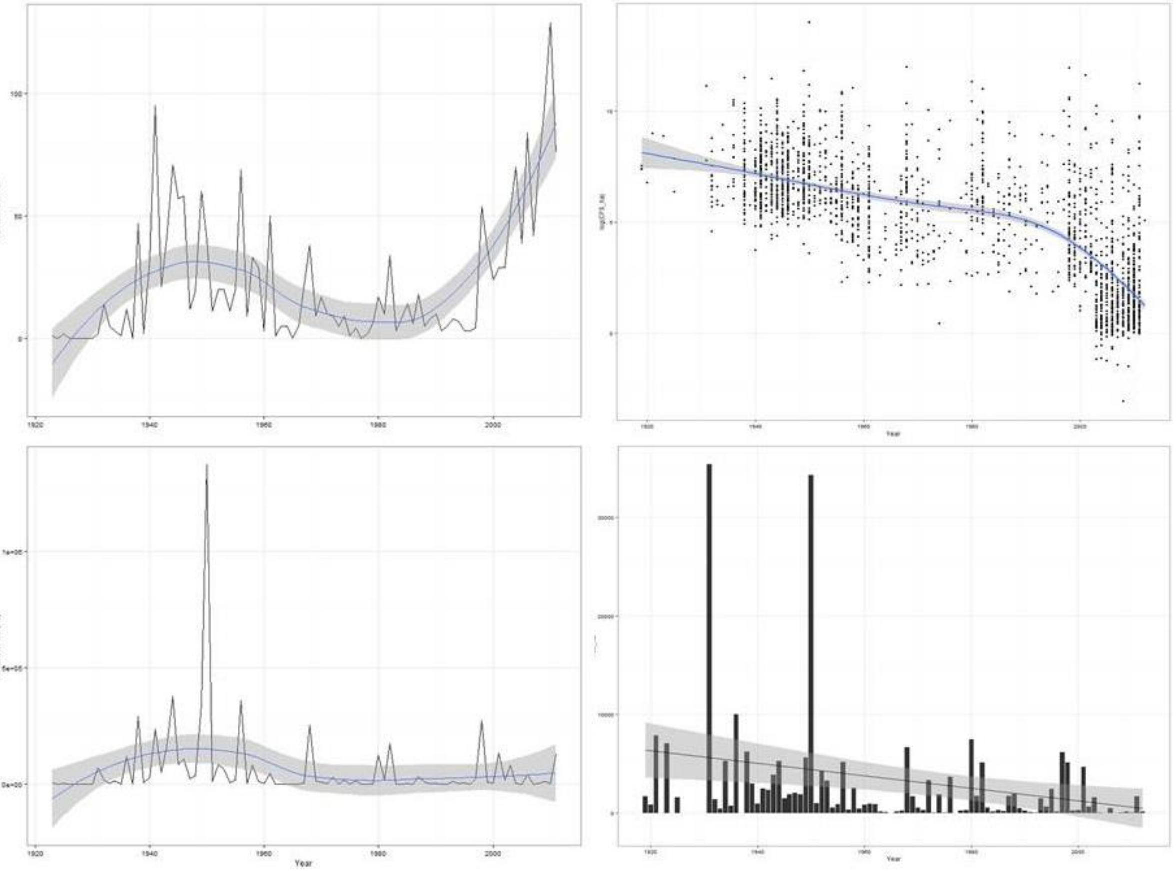

Figure 2. Historical wildfire distribution, 1919 to 2014: (a) annual number of fires; (b) log-transformed fire size by year; (c) annual area burned; (d) mean fire size by year.

The 1923-1952 'pre-suppression' period is characterized by relatively frequent fires and the largest annual area burned, while the 1953-1982 'early suppression' period shows a sharp decrease in fire frequency and annual area burned, with the lowest overall rates of each. The 1983-2012 'Anthropocene' period exhibits a rapid increase in fire frequency while the annual area burned remained relatively flat. The most recent decade, 2005-2014, shows an unprecedented increase in fire frequency coupled with only a modest increase in annual area burned.

Mean, maximum, and minimum fire sizes declined across the full study period, while the frequency of ignitions increased rapidly in recent decades. An increasing annual rate of fire frequency since 1980 corresponds with exponential-like population growth and economic activity in Alberta(Statistics Canada 2011) combined with rapid warming(Karl et al. 2015) (Figure 2a). The ratio of human- to lightning-caused fires increased from 1:1.10 to 1:1.69 (+65%) between the 1923-1952 and 1983-2012 periods. A spatial analysis of historical ignitions in the study area (an important grizzly bear conservation area shaped by the footprint of Landsat tiles), based on Canadian National Fire Database point data demonstrates that frequent small fires are concentrated around human activity, typically near roads and in river valleys (fire distance from roads: mean = 2,214 m, standard deviation = 4,844 m; fire distance from roads or surface water: mean = 297 m, standard deviation = 363 m), supporting a human origin. Between the 1980s and 2000s, while Alberta's population doubled, the mean distance of fires from roads declined by 40%, from 2,349 to 1,401 meters. Concurrently, the mean annual fire frequency increased by 33%, from 6,035 to 9,054 fires. The mean distance of fires from roads and/or surface water (rivers and lakes) declined by 32% across the same 30-year period, from 318 to 216 meters.

We infer that growing human activity in these forests explains most of the increase in the frequency of small fires near roads and surface water, although warming increases both the frequency of lightning strikes and severity of fire weather conditions(Krawchuk et al. 2009). Yet, the effects of directional warming on fire regimes appear to have been muted, rather than amplified, by human activity. This conclusion is supported by the literature, with a non-linear U-shaped relationship shown to occur between human activity and the frequency of fire ignitions(Syphard et al. 2007; Parisien et al. 2012). Due to the relative remoteness of Alberta's burnable land and small urban area of impervious surfaces, we found a linear rather than a U-shaped distribution between the frequency of fires and indicators of human activity. The recent success of fire suppression efforts(Cumming 2005) partially accounts for the decline in mean area burned and only a relatively small increase in total area burned, despite warmer conditions with more frequent ignitions in recent years. Meanwhile, high-frequency small fires and extensive extractive activities have also likely reduced forest fuels, together explaining an observed demographic shift in these forests(Zhang et al. 2015).

Boreal fire regimes appear to be tracking a northward shift of boreal climatic conditions(Koven 2013), reducing the size and severity of fires in the study area, as southern boreal ecosystems transition to new states under Anthropocene fire regimes. Data from the east indicate that the in-migration of temperate species into the southeastern reaches of the American boreal is already underway(Fisichelli et al. 2014). Across the study period, fires occurred more frequently at higher altitudes and latitudes. We estimate that the reduced size of boreal fires observed here, despite warming and historically large fire years elsewhere in Canada, is attributable to four key factors: (1) reduced fuel loads from frequent small human-caused fires; (2) increased fire suppression; (3) reduced crown fuels due to extractive industry activities; (4) a northward and shift of boreal climatic conditions(Koven 2013), evidenced by changing wildfire patterns and climate analogue vectors(Koven 2013).

The increasing extent and magnitude of industrial activity, recreational usage, and road network expansion in formerly remote areas are combining with record temperature anomolies(Kamae et al. 2014) to produce frequent ignitions and small fires around areas of human activity. Harvest operations are widespread in these forests, reducing canopy fuels while providing new ignition sources. A temporal lag of large fires following periodic pulses in pest populations(Kurz, Dymond, et al. 2008), expanding to higher altitudes and latitudes under warming, may amplify fuel conditions and thus fire regimes and forest transition rates. The conditions may favor deciduous species in the southern boreal(Terrier et al. 2012), producing a negative climatic feedback through increased summer albedo(Amiro et al. 2006).

Literature Cited

Aber JS, Aber, SW, Buster L, Jensen WE, Sleezer RL. **2009**. Challenge of infrared kite aerial photography: a digital update. *Trans. Kans. Acad. Sci*. 112, 31–39.

Aitken SN et al. **2008**. Adaptation, migration or extirpation: climate change outcomes for tree populations. *Evolutionary Applications*. 1(1), pp.95–111.

Alberto FJ, Aitken SN, Alía R, González-Martínez SC, Hänninen H, Kremer A, Lefèvre F, Lenormand T, Yeaman S, Whetten R, Savolainen O. **2013**. Potential for evolutionary responses to climate change–evidence from tree populations. *Glob. Change Biol.* 19, 1645–1661. http://dx.doi.org/10.1111/gcb.12181

Allen CD, Macalady AK, Chenchouni H, Bachelet D, McDowell N, Vennetier M, Kitzberger T, Rigling A, Breshears DD, Hogg EH (Ted), Gonzalez P, Fen-sham R, Zhang Z, Castro J, Demidova N, Lim J-H, Allard G, Running SW, Semerci A, Cobb N. **2010**. A global overview of drought and heat-induced tree mortality reveals emerging climate change risks for forests. *For. Ecol. Manage*. 259, 660–684. http://dx.doi.org/10.1016/j.foreco.2009.09.001

Amiro BD et al. **2006**. The effect of post-fire stand age on the boreal forest energy balance. *Agricultural and Forest Meteorology*. 140(1–4), pp.41–50.

Amoroso MM, Daniels LD, Bataineh M, Andison DW. **2011**. Evidence of mixed-severity fires in the foothills of the Rocky Mountains of west-central Alberta, Canada. *Forest Ecology and Management*. Vol. 262(12), pp. 2240–2249.

Anderegg WRL, Kane JM, Anderegg LDL. **2013**. Consequences of widespread tree mortality triggered by drought and temperature stress. *Nature Clim. Change*. 3(1), 30–36.

Aponte C, García LV, Marañón T. **2013**. Tree species effects on nutrient cycling and soil biota: A feedback mechanism favouring species coexistence. *Forest Ecology and Management*. 309(0), 36–46.

Badeck FW, Bondeau A, Bottcher K, Doktor D, Lucht W, Schaber J, Sitch S. **2004**. Responses of spring phenology to climate change. *New Phytologist*. Vol. 162(2), 295–309.

Barnett TP, Adam JC, Lettenmaier DP. **2005**. Potential impacts of a warming climate on water availability in snow-dominated regions. *Nature*. 438, 303–309.

Bater CW, Coops NC, Wulder MA, Nielsen SE, McDermid G, Stenhouse GB. **2011b**. Design and installation of a camera network across an elevation gradient for habitat assessment. *Instrumentation Science and Technology.* Vol. 39, 231–247.

Bater CCW, Coops NC, Wulder MA, Hilker T, Nielsen SSE, McDermid G, Stenhouse GGB. **2011**. Using digital time-lapse cameras to monitor species-specific understorey and overstorey phenology in support of wildlife habitat assessment. *Environ. Monit. Assess*. 180, 1–13. doi: 10.1007/s10661-010-1768-x

Bauer SD, Korč F, Förstner W. **2011**. The potential of automatic methods of classification to identify leaf diseases from multispectral images. *Precision Agric*. 12, 361–377.

Bayer BE. **1976**. Color imaging array. In: US Patent 3971065. Eastman Kodak Company, Rochester, NY.

Bergeron Y et al. **2010**. Will climate change drive 21st century burn rates in Canadian boreal forest outside of its natural variability? Collating global climate model experiments with sedimentary charcoal data. *International Journal of Wildland Fire*. 19(8), 1127.

Berland A, Nelson T, Stenhouse G, Graham K, Cranston J. **2008**. The impact of landscape disturbance on grizzly bear habitat use in the Foothills Model Forest, Alberta, Canada. *Forest Ecology and Management*. 256(11), 1875–1883.

Bertrand R, Gégout J-C, Bontemps JD. **2011a**. Niches of temperate tree species converge towards nutrient-richer conditions over ontogeny. *Oikos*. 120, 1479–1488. doi: http://dx.doi.org/10.1111/j.1600-0706.2011.19582.x

Bivand R, Keitt T, Rowlingson B. **2013**. RGDAL: bindings for the Geospatial Data Abstraction Library. R package, version 0.8-9.

Boisvert-Marsh L, Périé C, de Blois S. **2014**. Shifting with climate? Evidence for recent changes in tree species distribution at high latitudes. *Ecosphere*. 5. doi: http://dx.doi.org/10.1890/ES14-00111.1

Bond-Lamberty B et al. **2007**. Fire as the dominant driver of central Canadian boreal forest carbon balance. *Nature*. 450(7166), 89–92.

Bond-Lamberty B et al. **2014**. Disturbance legacies and climate jointly drive tree growth and mortality in an intensively studied boreal forest. *Global Change Biology*. 20(1), 216–227.

Botkin DB, Janak JF, Wallis JR. **1972**. Some ecological consequences of a computer model of forest growth. *J. Ecol.* 60, 849–872.

Bowman DMJS et al. **2011**. The human dimension of fire regimes on Earth. *Journal of Biogeography*. 38(12), 2223–2236.

Brooker G. **2009**. Introduction to Sensors for Ranging and Imaging. SciTech Publishing, NC, USA.

Brubaker LB. **1986**. Responses of tree populations to climatic change. *Vegetatio*. 67,119–130.

Buil C. **2012**. IR-Cut Filter Removal Operation, Performances and Image Samples, http://www.astrosurf.com/buil/350d/350d.htm [access 2012/12/11].

Burton PJ, Cumming SG. **1995**. Potential effects of climatic change on some west-ern Canadian forests, based on phenological enhancements to a patch model of forest succession. *Water Air Soil Pollut*. 82, 401–414. doi: http://dx.doi.org/10.1007/BF01182850

Canadian Forest Service. **2015**. Canadian Wildland Fire Information System (CWFIS) Datamart.

Carvalhais N, Forkel M, Khomik M, Bellarby J, Jung M, Migliavacca M, [Mgr]u M, Saatchi S, Santoro M, Thurner M, Weber U, Ahrens B, Beer C, Cescatti A, Randerson JT, Reichstein M. **2014**. Global covariation of carbon turnover times with climate in terrestrial ecosystems. *Nature*. 514, 213–217.

Cassel DK, Nielsen Arnold, DRE-K. **1986**. Field capacity and available water capacity. In: Methods of Soil Analysis. Part 1. Physical and Mineralogical Methods., pp.901–926.

Cavender-Bares J, Bazzaz FA. **2000**. Changes in drought response strategies with ontogeny in *Quercus rubra*: implications for scaling from seedlings to mature trees. *Oecologia*. 124, 8–18. doi: http://dx.doi.org/10.1007/PL00008865

Ciarniello LM, Boyce MS, Seip DR, Heard DC. **2007**. Grizzly bear habitat selection is scale dependent. *Ecol. Appl*. 17, 1424–1440.

Clark TW, Paquet PC, Curlee AP. **1996.** Special section: large carnivore conservation in the rocky mountains of the United States and Canada. *Conserv. Biol*. 10(4), 936–939.

Clark JS, Fastie C, Hurtt G, Jackson ST, Johnson C, King GA, Lewis M, Lynch J, Pacala S, Prentice C, Schupp EW, Thompson Webb III, Wyckoff P. **1998**. Reid’s paradox of rapid plant migration. *Bioscience*. 48, 13–24. Copyright 169; University of CA. doi: http://dx.doi.org/10.2307/1313224.

Cleland EE, Chuine I, Menzel A, Mooney HA, Schwartz MD. **2007**. Shifting plant phenology in response to global change. *Trends Ecol. Evol*. 22, 357–65. doi: 10.1016/j.tree.2007.04.003

Coogan SCP, Nielsen SE, Stenhouse GB. **2012**. Spatial and temporal heterogeneity creates a "brown tide" in root phenology and nutrition. *ISRN Ecology*. 618257.

Cook BI, Terando A, Steiner A. **2010**. Ecological forecasting under climatic data uncertainty: a case study in phenological modeling. *Environ. Res. Lett*. 5, 44014.

Cooke JEK, Eriksson ME, Junttila O. **2012**. The dynamic nature of bud dormancy in trees: environmental control and molecular mechanisms. *Plant Cell Environ*. 35, 1707–1728. doi: http://dx.doi.org/10.1111/j.1365-3040.2012.02552.x

Coops NC et al. **2011.** Modeling the occurrence of 15 coniferous tree species throughout the Pacific Northwest of North America using a hybrid approach of a generic process-based growth model and decision tree analysis. *Appl. Veg. Sci*. 14(3), 402–414.

Coops NC, Duffe J, Koot C. **2010.** Assessing the utility of lidar remote sensing technology to identify mule deer winter habitat. *Can. J. Remote Sens*. 36(2), 81–88.

Coops NC, Hilker T, Bater C, Wulder MA, Nielsen SE, McDermid G, Stenhouse G. **2012**. Linking ground-based to satellite-derived phenological metrics in support of habitat assessment. *Remote Sens. Lett*. 3, 191–200.

Coops NC, Wulder MA, Duro D, Han T, Berry SL. **2008**. The development of a Canadian dynamic habitat index using multi-temporal satellite estimates of canopy light absorbance. *Ecol. Indic*. 8, 754–766.

Craighead JJ, Sumner JS. **1995**. The grizzly bears of Yellowstone 1959–1972. Island Press, Washington, DC, US.

Crimmins SM, Dobrowski SZ, Greenberg JA, Abatzoglou JT, Mynsberge AR. **2011**. Changes in climatic water balance drive downhill shifts in plant species' optimum elevations. *Science*. 331, 324–327, doi: http://dx.doi.org/10.1126/science.1199040

Cross P, Bowlby G. **2006**. The Alberta Economic Juggernaut: The Boom on the Rose. *Canadian Economic Observer*. (11-010), 3.1–3.12.

Cumming SG. **2005**. Effective fire suppression in boreal forests. *Canadian Journal of Forest Research*. 35(4), 772–786.

Daly C, Neilson RP, Phillips DL. **1994.** A statistical-topographic model for mapping climatological precipitation over. *J. Appl. Meteorol*. 33(2), 140–158.

Davenport IJ, Holden N, Gurney RJ. **2004.** Characterizing errors in airborne laser altimetry data to extract soil roughness. *IEEE Trans. Geosci. Remote Sens*. 42(10), 2130–2141.

Davis MB, Shaw RG. **2001**. Range Shifts and Adaptive Responses to Quaternary Climate Change. *Science.* 292 (5517), 673–679.

De Groot WJ, Flannigan MD, Cantin AS. **2013**. Climate change impacts on future boreal fire regimes. *Forest Ecology and Management*. 294(0), 35–44.

De'Ath G. **2002.** Multivariate regression trees: a new technique for modeling species-environment relationships. *Ecology*. 83(4), 1105–1117.

Dierschke H. **1972**. On the recording and presentation of phenological phenomena in plant communities. English translation of: Zur Aufnahme und Darstellung pha¨nologischer Erscheinungen in Pflanzengesellschaften. Translated by R.E. Wessell and S.S. Talbot. 1970, *International Symposium for Vegetation Science*, The Hague, NL.

Dobrowski SZ, Abatzoglou J, Swanson AK, Greenberg JA, Mynsberge AR, Holden ZA, Schwartz MK. **2013**. The climate velocity of the contiguous United States during the 20th century. *Glob. Change Biol.* 19, 241–251. doi: http://dx.doi.org/10.1111/gcb.12026

Donohue K, Rubio de Casas R, Burghardt L, Kovach K, Willis CG. **2010**. Germination, postgermination adaptation, and species ecological ranges. *Annu. Rev. Ecol. Evol. Syst*. 41, 293–319. doi: http://dx.doi.org/10.1146/annurev-ecolsys-102209-144715

Duputié A, Rutschmann A, Ronce O, Chuine I. **2015**. Phenological plasticity will not help all species adapt to climate change. *Glob. Change Biol.* doi: http://dx.doi.org/10.1111/gcb.12914

Elith J, Leathwick JR, Hastie T. **2008.** A working guide to boosted regression trees. *J. Anim. Ecol*. 77(4), 802–813.

Eriksson O. **2002**. Ontogenetic niche shifts and their implications for recruitment in three clonal *Vaccinium s*hrubs: *Vaccinium myrtillus, Vaccinium vitis-idaea,* and *Vaccinium oxycoccos*. *Can. J. Bot.* 80, 635–641. doi: http://dx.doi.org/10.1139/b02-044

Ferster C, Coops NC, Trofymow J. **2009.** Aboveground large tree mass estimation in a coastal forest in British Columbia using plot-level metrics and individual tree detection from lidar. *Can. J. Remote Sens.* 35(3), 270–275.

Festa-Bianchet M. **2010**. Status of the Grizzly Bear (*Ursus arctos*) in Alberta : Update 2010. Alberta Wildl. Status Rep. 37, 56.

Festa-Bianchet M, Ray J, Boutin S, Côté S, Gunn A. **2011**. Conservation of caribou (*Rangifer tarandus*) in Canada: an uncertain future. *Canadian Journal of Zoology*. 89: 419–434.

Fisher JI, Mustard JF, Vadeboncoeur MA. **2006**. Green leaf phenology at Landsat resolution: scaling from the field to the satellite. *Remote Sens. Environ*. 100, 265–279.

Fisichelli NA, Frelich LE, Reich PB. **2014**. Temperate tree expansion into adjacent boreal forest patches facilitated by warmer temperatures. *Ecography*. 37(2), 152–161.

Foley JA et al. **2005**. Global Consequences of Land Use. Science (New York, N.Y.), 309(5734), pp.570–4.

Franklin SE, Peddle DR, Dechka JA, Stenhouse GB. **2002**. Evidential reasoning with Landsat TM: DEM and GIS data for land cover classification in support of Grizzly bear habitat mapping. *Int. J. Remote Sens.* 23, 4633–4652.

Friedman J. **2001.** Greedy function approximation: a gradient boosting machine. *Ann. Stat*. 29(5), 1189–1232.

Friedman JH. **2002.** Stochastic gradient boosting. *Comput. Stat. Data Anal.* 38(4), 367–378.

Fu P, Rich PM. **2002.** A geometric solar radiation model with applications in agriculture and forestry. *Comput. Electron. Agric.* 37(1–3), 25–35.

Gao F, Masek J, Schwaller M, Hall F. **2006**. On the blending of the Landsat and MODIS surface reflectance: predict daily Landsat surface reflectance. *IEEE Transactions on Geoscience and Remote Sensing*. 44(8), 2207–2218.

Gardner JL. **1998**. Experimental evidence for edge–related predation in a fragmented agricultural landscape. *Australian Journal of Ecology*. 23(4), 311–321.

Garnier BJ, Ohmura A. **1968**. A method of calculating direct shortwave radiation income of slopes. *J. Appl. Meteorol*. 7(5), 796–800.

Goetz SJ, Fiske GJ, Bunn AG. **2006**. Using satellite time-series data sets to analyze fire disturbance and forest recovery across Canada. *Remote Sensing of Environment*. 101(3), 352–365.

Gordon IJ, Hester AJ, Festa-Bianchet M. **2004.** Review: The management of wild large herbivores to meet economic, conservation and environmental objectives. *J. Appl. Ecol*. 41(6), 1021–1031.

Graham EA, Hamilton MP, Mishler BD, Rundel PW, Hansen MH. **2006**. Use of a networked digital camera to estimate net CO^2 uptake of a desiccation-tolerant moss. *International Journal of Plant Sciences*. 167, 751–758.

Graham EA, Riordan EC, Yuen EM, Estrin D, Rundel PW. **2010**. Public Internet-connected cameras used as a cross-continental ground-based plant phenology monitoring system. *Global Change Biology*. 16(11), 3014–3023.

Gralewicz NJ, Nelson TA, Wulder MA. **2012**. Factors influencing national scale wildfire susceptibility in Canada. *Forest Ecology and Management*, 265(0), 20–29.

Gray LK, Hamann A. **2012**. Tracking suitable habitat for tree populations under climate change in western North America. *Climatic Change.* 117(1-2), 289–303.

Guisan A, Zimmermann NE. **2000**. Predictive habitat distribution models in ecology. *Ecol. Modell*. 135, 147–186.

Hamer D, Herrero S. **1987**. Grizzly bear food and habitat in the front ranges of Banff National Park, Alberta. In: Zager, P. (ed.) Proceedings of 7th international conference on bear research and management, pp. 199–213. International Association of Bear Research and Management, Williamsburg, VA, US and Plityice Lakes, YU, February and March 1986.

Hamer D, Herrero S, Brady K. **1991**. Food and habitat used by grizzly bears, *Ursus arctos*, along the Continental Divide in Waterton Lakes National Park, Alberta. *Canadian Field Naturalist*. 105, 325–329.

He HS, Mladenoff DJ. **1999**. Spatially Explicit and Stochastic Simulation of Forest-Landscape Fire Disturbance and Succession. *Ecology*. 80(1), 81–99.

Healy SP, Cohen WB, Yang ZQ, Krankina ON. **2005**. Comparison of tassled cap–based Landsat data structures for use in forest disturbance detection. *Remote Sensing of Environment*. 97: 301–310.

Héon J, Arseneault D, Parisien M-A. **2014**. Resistance of the boreal forest to high burn rates. *Proceedings of the National Academy of Sciences*. 111(38), 13888–13893.

Herfindal I, Tremblay JP, Hansen BB, Solberg EJ, Heim M, Saether BE. **2009**. Scale dependency and functional response in moose habitat selection. *Ecography* (Cop.). 32, 849–859.

Hilker T, Coops NC, Gaulton R, Wulder MA, Cranston J, Stenhouse G. **2011**. Biweekly disturbance capture and attribution: case study in western Alberta grizzly bear habitat. *Journal of Applied Remote Sensing*. 5(1), 053568.

Hilker T, Wulder MA, Coops NC, Linke J, McDermid G, Masek JG, Gao F, White, JC. **2009**. A new data fusion model for high spatial-and temporal-resolution mapping of forest disturbance based on Landsat and MODIS. *Remote Sensing of Environment.* 113(8), 1613–1627.

Hirakawa K, Wolfe PJ. **2008**. Spatio-spectral sampling and color filter array design. In: Lukac, R. (Ed.), Single-Sensor Imaging: Methods and Applications for Digital Cameras. CRC Press, Boca Raton, FL.

Huang Y, Thomson SJ, Lan Y, Maas SJ. **2010**. Multispectral imaging systems for airborne remote sensing to support agricultural production management. *Int. J. Agric. Biol. Eng.* 3, 50–62.

Hwang T, Band LE, Miniat CF, Song C, Bolstad PV, Vose JM, Love JP. **2014**. Divergent phenological response to hydroclimate variability in forested mountain watersheds. *Glob. Change Biol*. 20, 2580–2595, doi: http://dx.doi.org/10.1111/gcb.12556

Hyde P, Dubayah R, Peterson B, Blair JB, Hofton M. **2005**. Mapping Forest Structure for Wildlife Habitat Analysis Using Waveform Lidar: Validation of Montane Ecosystems. *Sierra.*

Ide R, Oguma H. **2010**. Use of digital cameras for phenological observations. *Ecol Inf*. 5, 339–347.

Imhoff MF, Sisk TD, Milne A, Morgan G, Orr T. **1997**. Remotely sensed indicators of habitat heterogeneity: use of synthetic aperture radar in mapping vegetation structure and bird habitat. *Remote Sens. Environ*. 60, 217–227.

Irish RR, Barker JL, Goward SN, Arvidson T. **2006**. Characterization of the Landsat–7 ETM +automated cloud-cover assessment (ACCA) algorithm. *Photogrammetry Engineering and Remote Sensing*. 72(10), 1179–1188.

Iverson LR, Prasad AM. **1998**. Predicting abundance of 80 tree species following climate change in the eastern United States. *Ecol. Monogr*. 68, 465–485.

Jiménez-Valverde, **2011.** Relationship between local population density and environmental suitability estimated from occurrence data. *Front. Biogeogr*. 3(2), 59–61.

Johnson CJ, Parker KL, Heard DC, Gillingham MP. **2002**. A multiscale behavioral approach to understanding the movements of woodland caribou. *Ecol. Appl*. 12, 1840–1860.

Julitta T, Cremonese E, Migliavacca M, Colombo R, Galvagno M, Siniscalco C, Rossini M, Fava F, Cogliati S, Morra U, Menzel A. **2014.** Agricultural and Forest Meteorology Using digital camera images to analyse snowmelt and phenology of a subalpine grassland. *Agric. For. Meteorol.* 198-199, 116–125. doi: 10.1016/j.agrformet.2014.08.007

Kamae Y et al. **2014**. Attributing the increase in Northern Hemisphere hot summers since the late 20th century. *Geophysical Research Letters*. p.2014GL061062.

Karl TR et al. **2015**. Possible artifacts of data biases in the recent global surface warming hiatus. *Science.*

Kasischke ES, Turetsky MR. **2006**. Recent changes in the fire regime across the North American boreal region—Spatial and temporal patterns of burning across Canada and Alaska. *Geophysical Research Letters*. 33(9).

Kauth R, Thomas G. **1976**. The tasseled cap – a graphical description of the spectral–temporal development of agriculture crops as seen by Landsat. Paper presented at the Symposium on Machine Processing of Remotely Sensed Data. Purdue University of West Lafayette, Indiana, June 26–July 1.

Keeling CD, Chin JFS, Whorf TP. **1996**. Increased activity of northern vegetation inferred from atmospheric CO^2 measurements. *Nature*. 382, 146–149.

Kelly R et al. **2013**. Recent burning of boreal forests exceeds fire regime limits of the past 10,000 years. *Proceedings of the National Academy of Sciences*. 110 (32), 13055–13060.

Knoth C, Prinz T, Loef P. **2010**. Microcopter-based color infrared (CIR) close range remote sensing as a subsidiary tool for precision farming. In: Proceedings of the Workshop on Remote Sensing Methods for Change Detection and Process Modelling, 49–54.

Konica Minolta. **1998**. Precise Color Communication. Konica Minolta Sensing Inc. Osaka, Japan.

Kosaka Y, Xie S-P. **2013**. Recent global-warming hiatus tied to equatorial Pacific surface cooling. *Nature*. 501, 403–407.

Koven CD. **2013**. Boreal carbon loss due to poleward shift in low-carbon ecosystems. *Nature Geoscience.* 6(6), 452–456.

Krawchuk M, Cumming S, Flannigan M. **2009**. Predicted changes in fire weather suggest increases in lightning fire initiation and future area burned in the mixedwood boreal forest. *Climatic Change*. 92(1-2), 83–97.

Kumar K, Wu B. **2001**. Detection of change points in time series analysis with fuzzy statistics. *International Journal of Systems Science*. 32(9), 1185–1192.

Kurz WA, Dymond CC, Stinson G, Rampley GJ, Neilson ET, Carroll AL, Ebata T, Safranyik L. **2008**. Mountain pine beetle and forest carbon feedback to climate change. *Nature*. 452, 987–990.

Kurz WA, Stinson G et al. **2008**. Risk of natural disturbances makes future contribution of Canada's forests to the global carbon cycle highly uncertain. *Proceedings of the National Academy of Sciences*. 105 (5), 1551–1555.

Landis JR, Koch GG. **1977**. An application of hierarchical Kappa-type statistics in the assessment of majority agreement among multiple observers. *Biometrics.* 33(2), 363–374.

Laothawornkitkul J et al. **2009**. Biogenic volatile organic compounds in the Earth system. *New Phytologist*. 183(1), 27–51.

Lazarus ED, McGill BJ. **2014**. Pushing the Pace of Tree Species Migration. *PLoS ONE*. 9(8), p.e105380.

LDP LCC. **2012**. Spectral Response, http://maxmax.com/spectral response.htm [access 2012/12/11].

Lee DS et al. **2004.** Four years of Landsat-7 on-orbit geometric calibration and performance. *IEEE Trans. Geosci. Remote Sens.* 42(12), 2786–2795.

Leithead M, Silva LR, Anand M. **2012**. Recruitment patterns and northward tree migration through gap dynamics in an old-growth white pine forest in northern Ontario. *Plant Ecology*. 213(11), 1699–1714.

Lelong CCD. **2008**. Assessment of unmanned aerial vehicles imagery for quantitative monitoring of wheat crop in small plots. *Sensors*. 8, 3557–3585.

Lenoir J, Gégout J-C, Pierrat J-C, Bontemps J-D, Dhôte J-F. **2009**. Differences between tree species seedling and adult altitudinal distribution in mountain forests during the recent warm period (1986–2006). *Ecography* (Cop.). 32,765–777, doi: http://dx.doi.org/10.1111/j.1600-0587.2009.05791.x

Levins R. **1966**. The strategy of model building in population biology. *Am. Sci.* 54,421–431.

Liu C, Lu F, Cui X, Cao X. **2010**. Histone methylation in higher plants. *Annu. Rev. Plant Biol.* 61, 395–420. doi: http://dx.doi.org/10.1146/annurev.arplant.043008.091939

Liang L, Schwartz MD, Fei S. **2011**. Validating satellite phenology through intensive ground observation and landscape scaling in a mixed seasonal forest. *Remote Sens. Environ*. 115, 143–157.

Liang L, Schwartz MD, Fei S. **2012**. Photographic assessment of temperate forest understory phenology in relation to springtime meteorological drivers. *Int. J. Biometeorol*. 56, 343–355. doi: 10.1007/s00484-011-0438-1

Linke J, McDermid GJ. **2012**. Monitoring landscape change in multi-use west-central Alberta, Canada using the disturbance inventory framework. *Remote Sensing of Environment.* 125, 112–124.

Linke J, Franklin SE, Huettmann F, Stenhouse GB. **2005**. Seismic cutlines, changing landscape metrics and grizzly bear landscape use in Alberta. *Landscape Ecology and Management*. 20, 811–826.

Loarie SR, Duffy PB, Hamilton H, Asner GP, Field CB, Ackerly DD. **2009**. The velocity of climate change. *Nature*. 462, 1052–1055. doi: http://dx.doi.org/10.1038/nature08649

Lounici K. eprint arXiv: 1201.2577.

Lu D, Weng Q. **2007**. A survey of image classification methods and techniques for improving classification performance. *Int. J. Remote Sens*. 28, 823–870.

Luo Y, Chen HYH. **2013**. Observations from old forests underestimate climate change effects on tree mortality. *Nat. Commun*. 4, 1655.

MacArthur R. **1972**. Geographical Ecology: Patterns in the Distribution of Species. Harper & Row, New York.

Magnani F, Mencuccini M, Borghetti M, Berbigier P, Berninger F, Delzon S, Grelle A, Hari P, Jarvis PG, Kolari P, Kowalski AS, Lankreijer H, Law BE, Lindroth A, Loustau D, Manca G, Moncrieff JB, Rayment M, Tedeschi V, Valentini R, Grace J. **2007**. The human footprint in the carbon cycle of temperate and boreal forests. *Nature*. 447, 848–850, doi: http://dx.doi.org/10.1038/nature05847

Magnussen S, Boudewyn P, Wulder MA. **2004**. Contextual classification of Landsat TM images to forest inventory cover types. *Int. J. Remote Sens.* 25, 2421–2440.

Manel S, Williams HC, Ormerod SJ. **2001**. Evaluating presence-absence models in ecology: the need to account for prevalence. *J. Appl. Ecol*. 38(5), 921–931.

Markham BL, Helder DL. **2011**. Forty-year calibrated record of earth-reflected radiance from Landsat: a review. *Remote Sens. Environ.* 12230–12240, 2012.

Martinuzzi S et al. **2009**. Mapping snags and understory shrubs for a LiDAR-based assessment of wildlife habitat suitability. *Remote Sens. Environ*. 113(12), 2533–2546.

Matzke MA, Mosher RA. **2014**. RNA-directed DNA methylation: an epigenetic pathway of increasing complexity. *Nat. Rev. Genet.* 15, 394–408.

McDermid GJ, Franklin SE, Ledrew EF. **2005**. Remote sensing for large-area habitat mapping. *Prog. Phys. Geog*. 29, 449–474.

McDermid GJ, Hall RJ, Sanchez-Azofeifa GA, Franklin SE, Stenhouse GB, Kobliuk T, LeDrew EF. **2009**. Remote sensing and forest inventory for wildlife habitat assessment. *For. Ecol. Manage.* 257, 2262–2269.

McLellan BN, Hovey FW. **1995**. The diet of grizzly bears in the Flathead River drainage of southeastern British Columbia. *Journal of Zoology*. 73: 704–712.

Means JE et al. 2000. Predicting forest stand characteristics with airborne scanning Lidar. *Photogramm. Eng. Remote Sens.* 66(11), 1367–1371.

Melaas EK, Friedl MA, Zhu Z. **2013**. Detecting inter-annual variation in deciduous broadleaf forest phenology using Landsat TM/ETM+ data. *Remote Sens. Environ.* 132, 176–185. doi: 10.1016/j.rse.2013.01.011

Melendez KV, Jones DL, Feng AS. **2006**. Classification of communication signals of the little brown bat. *J. Acoust. Soc. Am.* 120(2), 1095–1102.

Menne MJ, Durre I, Vose RS, Gleason BE, Houston TG. **2012**. An overview of the global historical climatology network-daily database. *J. Atmos. Ocean. Technol.* 29, 897-910. doi: http://dx.doi.org/10.1175/JTECH-D-11-00103.1

Menzel A. **2000**. Trends in phenological phases in Europe between 1951 and 1996. *Int. J. Biometeorol*. 44, 76–81.

Michaelian M et al. **2011**. Massive mortality of aspen following severe drought along the southern edge of the Canadian boreal forest. *Global Change Biology*. 17(6), 2084–2094.

Mok H-F, Arndt SK, Nitschke CR. **2012**. Modelling the potential impact of climate variability and change on species regeneration potential in the temperate forests of South-Eastern Australia. *Glob. Change Biol*. 18, 1053–1072. doi: http://dx.doi.org/10.1111/j.1365-2486.2011.02591.x

Monserud RA, Leemans R. **1992**. Comparing global vegetation maps with the Kappa statistic. *Ecol. Modell*. 62(4), 275–293.

Moritz MA et al. **2012**. Climate change and disruptions to global fire activity. *Ecosphere*. 3(6), part 49.

Morris D, Boyd D, Crowe J, Johnson C, Smith K. **2013**. Exploring the potential for automatic extraction of vegetation phenological metrics from traffic webcams. *Remote Sensing*. 5, 2200–2218.

Mueller K et al. **2012**. Tree species effects on coupled cycles of carbon, nitrogen, and acidity in mineral soils at a common garden experiment. *Biogeochemistry*. 111(1-3), 601–614.

Munro RHM, Nielsen SE, Price MH, Stenhouse GB, Boyce MS. **2006**. Seasonal and diel patterns of grizzly bear diet and activity in west-central Alberta. *J. Mammal*. 87, 1112–1121. doi: 10.1644/05-MAMM-A-410R3.1

Myneni RB, Keeling CD, Tucker CJ, Asrar G, Nemani RR. **1997**. Increased plant growth in the northern high latitudes from 1981 to 1991. *Nature*. 386, 698–702.

National Forestry Database. **2013**. Silviculture Statistics by Province/Territory1975–2011. Ottawa, Ontario.

Natural Regions Committee. **2006**. Natural Regions and Subregions of Alberta, Edmonton, Alberta.

Nesby R. **1997**. Alberta Vegetation Inventory. Final Version, 2.2. Alberta Environmental Protection, Edmonton, Alberta, Canada.

Nielsen S, Stenhouse GB, Boyce M. **2006.** A habitat-based framework for grizzly bear conservation in Alberta. *Biol. Conserv*. 130(2), 217–229.

Nielsen S, Boyce M, Stenhouse GB. Grizzly bears and forestry. I. Selection of clearcuts by grizzly bears in west-central Alberta. *For. Ecol. Manage*. 199(1), 51–65.

Nielsen SE et al. **2008**. Can natural disturbance-based forestry rescue a declining population of grizzly bears? *Biol. Conserv*. 141(9), 2193–2207.

Nielsen S. **2005**. Habitat ecology, conservation, and projected population viability of grizzly bears (*Ursus arctos* L.) in West-Central Alberta, Canada. PhD Dissertation, University of Alberta, Edmonton, AL, CA.

Nielsen SE, Munro RHM, Bainbridge E, Boyce MS, Stenhouse GB. **2004**. Grizzly bears and forestry: II. Distribution of grizzly bear foods in clearcuts of west-central Alberta. *Forest Ecology and Management*. 199, 67–82

Nielsen S, Boyce M, Stenhouse GB, Munro RHM. **2003**. Development and testing of phenologically driven grizzly bear habitat models. *Ecoscience*. 10, 1–10.

Nielsen S, Cranston J, Stenhouse G. **2009**. Identification of priority areas for Grizzly bear conservation and recovery in Alberta, Canada. *J. Conserv. Plan*. 5, 38–60.

Nielsen SE, McDermid G, Stenhouse GB, Boyce MS. **2010**. Dynamic wildlife habitat models: Seasonal foods and mortality risk predict occupancy-abundance and habitat selection in grizzly bears. *Biol. Conserv*. 143, 1623–1634. doi: 10.1016/j.biocon.2010.04.007

Niinemets Ü. **2010**. Responses of forest trees to single and multiple environmental stresses from seedlings to mature plants: past stress history, stress interactions, tolerance and acclimation. *For. Ecol. Manage.* 260, 1623–1639. doi: http://dx.doi.org/10.1016/j.foreco.2010.07.054

Nijland W. **2012**. Basics of Infrared Photography, Infrared light, http://www.ir-photo.net/ir imaging.html [access 2012/12/11].

Nijland W, Coops NC, Coogan SCP, Bater CW, Wulder MA, Nielsen SE, McDermid G, Stenhouse GB. **2013**. Vegetation phenology can be captured with digital repeat photography and linked to variability of root nutrition in *Hedysarum alpinum*. *Applied Vegetation Science*. 16, 317–324.

Nijland W, Coops NC, Nielsen SE, Stenhouse G. **2015**. Integrating optical satellite data and airborne laser scanning in habitat classification for wildlife management. *Int. J. Appl. Earth Obs. Geoinf*. 38, 242–250. doi: 10.1016/j.jag.2014.12.004

Nijland W, de Jong R, de Jong SM, Wulder MA, Bater CW, Coops NC. **2014**. Monitoring plant condition and phenology using infrared sensitive consumer grade digital cameras. *Agricultural and Forest Meteorology*. 184, 98–106.

Nitschke CR, Amoroso M, Coates KD, Astrup R. **2012**. The influence of climate change, site type, and disturbance on stand dynamics in northwest British Columbia, Canada. *Ecosphere*. 3, 11. doi: http://dx.doi.org/10.1890/ES11-00282.1

Nitschke CR, Innes JL. **2008**. A tree and climate assessment tool for modelling ecosystem response to climate change. *Ecol. Modell*. 210, 263–277. doi: http://dx.doi.org/10.1016/j.ecolmodel.2007.07.026

Parisien M et al. **2006**. Spatial patterns of forest fires in Canada, 1980–1999. *International Journal of Wildland Fire*, 15 (3), 361–374.

Parisien, M-A et al. **2012**. Spatial variability in wildfire probability across the western United States. *International Journal of Wildland Fire*. 21 (4), 313–327.

Park Williams A, Allen CD, Macalady AK, Griffin D, Woodhouse CA, Meko DM, Swetnam TW, Rauscher SA, Seager R, Grissino-Mayer HD, Dean JS, Cook ER, Gangodagamage C, Cai M, McDowell NG. **2013**. Temperature as a potent driver of regional forest drought stress and tree mortality. *Nat. Clim. Change*. 3, 292–297.

Pasher J, Seed E, Duffe J. **2013**. Development of boreal ecosystem anthropogenic disturbance layers for Canada based on 2008 to 2010 Landsat imagery. *Canadian Journal of Remote Sensing*. 39, 1–17.

Peng C, Ma Z, Lei X, Zhu Q, Chen H, Wang W, Liu S, Li W, Fang X, Zhou X. **2011**. A drought-induced pervasive increase in tree mortality across Canada’s boreal forests. *Nat. Clim. Change*. 1, 467–471.

Piedallu C, Gégout J-C, Perez V, Lebourgeois F. **2013**. Soil water balance performs better than climatic water variables in tree species distribution modelling. *Glob. Ecol. Biogeogr*. 22, 470–482. doi: http://dx.doi.org/10.1111/geb.12012

Pigeon KE, Nielsen SE, Stenhouse GB, Côté SD. **2014**. Den selection by Grizzly bears on a managed landscape. *J. Mammal.* 95, 559–571.

Pontius RG, Millones M. **2011**. Death to Kappa: birth of quantity disagreement and allocation disagreement for accuracy assessment. *Int. J. Remote Sens.* 32(15), 4407–4429.

Poynton C. **1995**. A guided tour of color space. In: Proceedings of the SMPTE Advanced Television and Electronic Imaging Conference, New Foundations for Video Technology, San Francisco, Feb. 1995, pp. 167–180.

R Core Team. **2014**. R: A Language for Statistical Computing.

R Development Core Team. **2012**. R: A language and environment for statistical computing.

R Development Core Team. **2013**. R: A Language and Environment for Statistical Computing, R Foundation for Statistical Computing, Vienna, Austria.

Rahbek C, Graves GR. **2001**. Multiscale assessment of patterns of avian species richness. *Proc. Natl. Acad. Sci. U. S. A.* 98, 4534–4539.

Reuter HI, Nelson A, Jarvis A. **2007**. An evaluation of void-filling interpolation methods for SRTM data. *International Journal of Geographical Information Science*. 21(9), 983–1008.

Rich P et al. **1994**. Using viewshed models to calculate intercepted solar radiation: applications in ecology. *Am. Soc. Photogramm. Remote Sens.* Tech. Pap. 524–529.

Richardson AD, Black AT, Ciais P, Delbart N, Friedl MA, Gobron N, Hollinger DY, Kutsch WL, Longdoz B, Luyssaert S, Migliavacca M, Montagnani L, Munger JW, Moors E, Piao SL, Rebmann C, Reichstein M, Saigusa N, Tomelleri E, Vargas R, Varlagin A. **2010**. Influence of spring and autumn phenological transitions on forest ecosystem productivity. *Philosophical transactions of the Royal Society of London*. *Series B, Biological Sciences*. 365, 3227–3246.

Richardson AD, Braswell BH, Hollinger DY, Jenkins JP, Ollinger SV. **2009**. Near-surface remote sensing of spatial and temporal variation in canopy phenology. *Ecological Applications*. 19(6), 1417–1428.

Richardson AD et al. **2013**. Climate change, phenology, and phenological control of vegetation feedbacks to the climate system. *Agricultural and Forest Meteorology*. 169(0), 156–173.

Richardson AD, Jenkins JP, Braswell BH, Hollinger DY, Ollinger SV, Smith ML. **2007**. Use of digital webcam images to track spring green-up in a deciduous broadleaf forest. *Oecologia*. 152, 323–334.

Ricketts TH. **1999**. Terrestrial Ecoregions of North America: A Conservation Assessment. Island Press, Washington, DC.

Roberts J, Tesfamichael S, Gebreslasie M, van Aardt J, Ahmed F. **2007**. Forest structural assessment using remote sensing technologies: an overview of the current state of the art. *South. Hemisph. For. J.* 69, 183–203.

Roever CL, Boyce MS, Stenhouse GB. **2008**. Grizzly bears and forestry: II. Grizzly bears habitat selection and conflicts with road placement. *Forest Ecology and Management*. 256, 1262–1269.

Rogers BM et al. **2015**. Influence of tree species on continental differences in boreal fires and climate feedbacks. *Nature Geosci*, advance.

Rogers LN. **1987**. Effects of food supply and kinship on social behavior, movements, and population growth of black bears in northeastern Minnesota. *Wildlife Monographs*. 51, 1–72.

Rowe JS, Scotter GW. **1973**. Fire in the boreal forest. *Quaternary Research*. 3(3), 444–464.

Scheller RM et al. **2007**. Design, development, and application of LANDIS-II, a spatial landscape simulation model with flexible temporal and spatial resolution. *Ecological Modelling*. 201(3-4), 409–419.

Schwalm CR et al. **2006**. Photosynthetic light use efficiency of three biomes across an east-west continental-scale transect in Canada. *Agric. For. Meteorol*. 140(1–4), 269–286.

Schwartz MD, Reed BC, White MA. **2002**. Assessing satellite-derived start-of-season measures in the conterminous USA. *Int. J. Climatol.* 22, 1793–1805. doi: 10.1002/joc.819

Sharma S, Couturier S, Côté SD, Cote SD. **2009**. Impacts of climate change on the seasonal distribution of migratory caribou. *Glob. Chang. Biol*. 15, 2549–2562. doi: 10.1111/j.1365-2486.2009.01945.x

Shugart HH, West DC. **1977**. Development of an Appalachian deciduous forest succession model and its application to assessment of the impact of the Chestnut Blight. *J. Environ. Manage.*

Sluiter R, de Jong SM, van der Kwast H, Walstra J. **2004**. Chapter 15: A Contextual Approach to Classify Mediterranean Heterogeneous Vegetation using the Spatial Reclassification Kernel (SPARK) and DAIS7915 Imagery. 291–310.

Soil Classification Working Group. **1998**. The Canadian System of Soil Classification: Third Edition.

Song C, Woodcock CE, Seto KC, Lenney MP, Macomber SA. **2001**. Classification and change detection using Landsat TM data: when and how to correct atmospheric effects. *Remote Sensing of the Environment*. 75(2), 230–244.

Sonnentag O, Hufkens K, Teshera-Sterne C, Young AM, Friedl M, Braswell BH, Milliman T, O’Keefe J, Richardson AD. **2012**. Digital repeat photography for phenological research in forest ecosystems. *Agric. For. Meteorol*. 152, 159–177.

Soudani K, Hmimina G, Delpierre N, Pontailler J-Y, Aubinet M, Bonal D, Caquet B, De Grandcourt A, Burban B, Flechard C, Guyon D, Granier A, Gross P, Heinesh B, Longdoz B, Loustau D, Moureaux C, Ourcival J-M, Rambal S, Saint André L, Dufrêne E. **2012**. Ground-based network of NDVI measurements for tracking temporal dynamics of canopy structure and vegetation phenology in different biomes. *Remote Sens. Environ.* 123, 234–245.

Statistics Canada. **2011**. 2011 Census, Ottowa, Ontario.

Stewart BP, Wulder MA, McDermid GJ, Nelson T. **2009**. Disturbance capture and attribution through the integration of Landsat and IRS-1C imagery. *Canadian Journal of Remote Sensing*. 35(6), 523–533.

Stocks BJ et al. **2002**. Large forest fires in Canada, 1959–1997. *Journal of Geophysical Research: Atmospheres*, 107(D1), 8149.

Svenning J-C, Sandel B. **2013**. Disequilibrium vegetation dynamics under future climate change. *American Journal of Botany*. 100(7), 1266–86.

Swets JA. **1988**. Measuring the accuracy of diagnostic systems. *Science*. (80-) 240(4857), 1285–1293.

Syphard AD et al. **2007**. Calibrating a forest landscape model to simulate frequent fire in Mediterranean-type shrublands. *Environmental Modelling & Software*. 22(11), 1641–1653.

Terrier A et al. **2012**. Potential changes in forest composition could reduce impacts of climate change on boreal wildfires. *Ecological Applications*. 23(1), 21–35.

Thuiller W. **2004**. Patterns and uncertainties of species' range shifts under climate change. *Global Change Biol*. 10, 2020–2027.

Trenberth KE. **2011**. Changes in precipitation with climate change. *Clim. Res.* 47, 123-138.

Trenberth KE, Dai A, van der Schrier G, Jones PD, Barichivich J, Briffa KR, Sheffield J. **2014**. Global warming and changes in drought. *Nat. Clim. Change*. 4, 17–22.

Tucker CJ. **1979**. Red and photographic infrared linear combinations for monitoring vegetation. *Remote Sens. Environ*. 8, 127–150.

Tymstra C et al. **2007**. Impact of climate change on area burned in Alberta's boreal forest. *International Journal of Wildland Fire*. 16 (2), 153–160.

Uemura S. **1994**. Patterns of leaf phenology in forest understory. *Can. J. Bot*. 72, 1560–1560. doi: 10.1139/b94-192

Urbieta IR, García LV, Zavala MA, Marañón T. **2011**. Mediterranean pine and oak distribution in southern Spain: was there a mismatch between regeneration and adult distribution? *J. Veg. Sci.* 22, 18–31. doi: http://dx.doi.org/10.1111/j.1654-1103.2010.01222.x

Van Genuchten MT. **1980**. A closed-form equation for predicting the hydraulic conductivity of unsaturated soils.

Vartanian M, Nijland W, Coops NC, Bater C, Wulder MA, Stenhouse G. **2014**. Assessing the Impact of Field of View on Monitoring Understory and Overstory Phenology Using Digital Repeat Photography. *Can. J. Rem. Sens*. 40, 85–91. doi: 10.1080/07038992.2014.930308

Verhoeven GJ, Loenders JO, Vermeulen F, Docter R. **2009**. Helikite aerial photography—a versatile means of unmanned, radio controlled, low-altitude aerial archaeology. *Archaeol. Prospect.* 16, 125–138.

Vierling KT, Vierling LA, Gould WA, Martinuzzi S, Clawges RM. **2008**. Lidar: shedding new light on habitat characterization and modeling. *Front. Ecol. Environ*. 6, 90–98.

Visser ME, Both C. **2005**. Shifts in phenology due to global climate change: the need for a yardstick. *Proc. Biol. Sci.* 272, 2561–2569. doi: 10.1098/rspb.2005.3356

Vitasse Y, Hoch G, Randin C, Lenz A, Kollas C, Scheepens JF, Körner C. **2013**. Elevational adaptation and plasticity in seedling phenology of temperate deciduous tree species. *Oecologia*. 171, 663–678. doi: http://dx.doi.org/10.1007/s00442-012-2580-9

Wang T et al. **2012**. ClimateWNA: High-Resolution Spatial Climate Data for Western North America. *Journal of Applied Meteorology and Climatology*. 51(1), 16–29.

Wang T, Campbell EM, O’Neill GA, Aitken SN. **2012**. Projecting future distributions of ecosystem climate niches: Uncertainties and management applications. *For. Ecol. Manage*. 279, 128–140. doi: http://dx.doi.org/10.1016/j.foreco.2012.05.034

Waring RH, Coops NC, Fan W, Nightingale JM. **2006**. MODIS enhanced vegetation index predicts tree species richness across forested ecoregions in the contiguous U.S.A. *Remote Sens Environ.* 103(2), 218-226.

White B et al. **2012**. Using the cartographic depth-to-water index to locate small streams and associated wet areas across landscapes. *Can. Water Resour. J.* 37(4), 333–347.

White RG. **1983**. Foraging patterns and their multiplier effects on productivity of northern ungulates. *Oikos*. 40, 377.

Willis KJ, Whittaker RJ. **2002**. Ecology–species diversity–scale matters. *Science*. 295, 1245–1248.

Wing BM et al. **2012**. Prediction of understory vegetation cover with airborne lidar in an interior ponderosa pine forest. *Remote Sens. Environ.* 124, 730–741.

Woebbecke DM, Meyer GE, Von Bargen K, Mortensen DA. **1995**. Color indices for weed identification under various soil, residue, and lighting conditions. *Transactions of the American Society of Agricultural Engineers*. 38(1), 259–269.

Woodall CW, Zhu K, Westfall JA, Oswalt CM, D'Amato AW, Walters BF, Lintz HE. **2013**. Assessing the stability of tree ranges and influence of disturbance in eastern US forests. *For. Ecol. Manage*. 291, 172–180. doi: http://dx.doi.org/10.1016/j.foreco.2012.11.047

Woodcock CE, Allen R, Anderson M, Belward A, Bindschadler R, Cohen W, Gao F, Goward SN, Helder D, Helmer E, Nemani R, Oreopoulos L, Schott J, Thenkabail PS, Vermote EF, Vogelmann J, Wulder MA, Wynne R. **2008**. Free access to Landsat imagery. *Science*. 320, 1011.

Wulder MA et al. **2008**. The role of LiDAR in sustainable forest management. *For. Chron.* 84(6), 807–826.

Wulder MA, White JC, Cranny M, Hall RJ, Luther JE, Beaudoin A, Goodenough DG, Dechka JA. **2008**. Monitoring Canada's forests. Part 1: Completion of the EOSD land cover project. *Canadian Journal of Remote Sensing*. 34(6), 549–562.

Wulder MA, Dechka JA, Gillis MD, Luther JE, Hall RJ, Beaudoin A, Franklin SE. **2006**. Operational mapping of the land cover of the forested area of Canada with Landsat data EOSD land cover program. *For. Chron.* 79, 1075–1083.

Wulder MA, White JC, Han T, Coops NC, Cardille JA, Holland T, Grills D. **2008c**. Monitoring Canada's forests: part 2: national forest fragmentation and pattern. *Can. J. Rem. Sens.* 34, 563–584.

Wüller D, Gabele H. **2007**. The usage of digital cameras as luminance meters. In *Electronic Imaging 2007* (pp. 65020U-65020U). International Society for Optics and Photonics.

Zhang C, Franklin SE, Wulder MA. **2004**. Geostatistical and texture analysis of airborne-acquired images used in forest classification. *Int. J. Remote Sens.* 25, 859–865.

Zhang J, Huang S, He F. **2015**. Half-century evidence from western Canada shows forest dynamics are primarily driven by competition followed by climate. *Proceedings of the National Academy of Sciences*. 112(13), 4009–4014.

Zhu K, Woodall CW, Clark JS. **2012**. Failure to migrate: lack of tree range expansion in response to climate change. *Glob. Chang. Biol.* 18, 1042–1052. doi: http://dx.doi.org/10.1111/j.1365-2486.2011.02571.x

Zhu K, Woodall CW, Ghosh S, Gelfand AE, Clark JS. **2014**. Dual impacts of climate change: forest migration and turnover through life history. *Glob. Change Biol*. 20, 251–264. doi: http://dx.doi.org/10.1111/gcb.12382.

Research Theme: Habitat

Nutritional landscapes of grizzly bear carrying capacity for population recovery

Authors*:* Scott E Nielsen, Sean CP Coogan, Claudia Lopez, Tyler J Bateman, Andrew CR Braid, Nikhil Lobo, Terry Larsen & Gordon B Stenhouse[2]

1. Background and objectives.

Grizzly bear populations in Alberta are listed as a threatened species. Bear populations in the Foothills and Mountains of west-central Alberta have some of the lowest densities in Alberta and other interior populations of North America (Ferguson & McLoughlin 2000; Garshelis *et al*. 2005; Mowat *et al*. 2005; ASRD 2010; McLellan 2011; Zedrosser *et al*. 2011). The problem has been attributed to human-bear conflicts such as poaching and road accidents (Benn & Herrero 2002; Nielsen *et al*. 2004a; ASRD 2010). This represents a top-down view of limitations in bear populations. Nevertheless, nutritional conditions in bear habitats may also play a role in the observed low densities in Alberta by affecting reproductive success of female bears and reducing densities of bears through lower carrying capacities (Munro *et al*. 2006; Nielsen *et al*. 2010; López-Alfaro *et al*. 2015; López-Alfaro *et al*. 2013). In this research theme we have taken the approach of mechanistically defining habitat for grizzly bears by understanding, modeling, and relating food resource supply to bear populations. Specifically, we focus on estimating macronutrients of key grizzly bear foods in space and time to relate to patterns in bear abundance, limitations in reproduction (denning constraints), and estimates of carrying capacity. Not all of the available resources (food) can however be consumed by bears. Because of this, we focus on understanding consumption of one critical food resource, buffaloberry (*Shepherdia canadensis*), by the community of frugivores (birds, small mammals, and bears).

2. Nutritional ecology of grizzly bear diets

2.1 Nutritional estimates of key grizzly bear foods

A cornerstone of research investigating the foraging behavior of any animal is the understanding of not only its diet, but also the nutritional properties of its diet. We published nutritional estimates of several grizzly bear food items collected by University of Alberta and Foothills Research Institute field biologists (Coogan *et al*. 2014). These estimates were first reported as part of an MSc thesis (Coogan 2012) at the University of Alberta under the supervision of Dr. Nielsen. The purpose of estimating these nutritional and energetic values was to incorporate these values within ecological models of bottom-up factors affecting grizzly bear populations and health and thus providing insight for use in management and conservation of Alberta's grizzly bear sub-populations. For instance, this includes habitat-based estimates of carrying capacity which can be used to help set recovery targets. The nutritional research included new estimates for little studied species, including buffaloberry (*Shepherdia canadensis*) alpine sweetvetch (*Hedysarum alpinum*), horsetails (*Equisetum* spp.), and cow parsnip (*Heracleum lanatum*) (Table 1 and Table 2).

2.2 Geometric modeling of macronutrients

Recent research has demonstrated the value of relating macronutrients (protein, lipids, and carbohydrates) to animal foraging behavior and evolutionary fitness. Much of this research comes from geometric analysis of the macronutrient balance of foods (Raubenheimer 2011; Simpson & Raubenheimer 2012). We published the results of a geometric analysis of the foods potentially consumed by grizzly bears in west-central Alberta, by incorporating nutritional estimates of foods (including those described above) with recent research on the macronutrient preferences of captive grizzly bears housed at the Washington State University bear facility in Pullman (Erlenbach *et al*. 2014). Bears studied by Erlenbach *et al*. (2014) self-selected diets high in non-protein energy (lipids and carbohydrates) relative to protein (17% protein to 83% non-protein on an energy basis), and these diets maximized mass gain per unit energy intake. Geometric analysis revealed that, in west-central Alberta, grizzly bears are more likely to be limited by foods high in non-protein energy than protein in terms of macronutrient balance. Bears were, however, potentially able to optimize their intake of macronutrients when fruit was available by consuming fruit and complementary foods, such as high-protein ungulates (e.g. moose, elk, and deer) with high carbohydrate fruits (Figure 1). This study therefore sheds light on the importance of fruit as a food resource in this, and likely other, ‘interior’ ecosystems that lack subsidies from marine resources such as salmon. Geometric analysis also provided insight into other aspects of grizzly bear food items. For example, the near optimal macronutrient balance of alpine sweetvetch (*Hedysarum alpinum*) roots may be a reason why so many bears rely heavily on this resource during spring and fall seasons (Munro *et al*. 2006; Coogan *et al*. 2012), and why the root may be able to sustain bears nutritionally during such times, particularly by taking advantage of spatial-temporal variations in peak protein availability based on phenology of plant (Figure 2a) and variations in its phenology by elevation (Figure 3). Selection of alpine sweetvetch habitat is observed by all sex-age classes of bears (Figure 2b). Beyond foods *per se*, this study also demonstrated how accounting for multiple macronutrients can inform bear foraging behavior.

3. Bioenergetic constraints to bear populations

Understanding how wildlife-habitat interactions affect individual fitness is an essential tool for successful conservation plans. A fundamental relationship is that individuals must transfer energy and matter from their environment to themselves in order to support the requirements for maintenance, reproduction, and activity (Barboza *et al*. 2009; Robbins 1993). These flows of energy and matter are restricted by the physiology of the individuals and the environmental conditions where animals live (Barboza *et al*. 2009; Garland Jr & Carter 1994). Because these constraint have the potential to affect reproductive success and they can also restrict our capacity to recover endangered populations.

Grizzly bear populations are widely distributed in the North Hemisphere, although many populations are threatened due to human-wildlife conflict (McLellan *et al*. 2008; ASRD & ACA 2010). Across its distribution, grizzly bear populations exhibit a wide variety of life history traits. For example, average litter size ranging from 1 – 3 cubs, inter-birth interval ranging from 2.3 – 4.4 years, and primiparity ranging from 3 to 8 years; these scale up to population effects where densities vary from 2 to 65 bears per 1000 km^2 for interior populations and up to 500 bears per 1000 km^2 for populations with access to salmon (Miller *et al*. 1997; Hilderbrand *et al*. 1999a; Hilderbrand *et al*. 1999b; Swenson *et al*. 2001; Miller *et al*. 2003; Garshelis *et al*. 2005; Stoen *et al*. 2006; Zedrosser *et al*. 2011; Mowat *et al*. 2013). These differences in life history traits and population parameters have been attributed to differences in food availability (Hilderbrand *et al*. 1999a; Bojarska & Selva 2012).

Reproductive success of female bears is affected by their ability to accumulate and transfer nutrients to offspring during lactation. Bears give birth to altricial cubs which they nurture for 2 to 5 month during hibernation (Oftedal *et al*. 1993; Atkinson & Ramsay 1995; Farley & Robbins 1995; Robbins *et al*. 2012), with lactation continuing through the active period until the next hibernation (Farley & Robbins 1995). During hibernation, bears use their body mass reserves to provide the energy and nutrients necessary for maintenance and reproduction (Farley & Robbins 1995). During the active period lactating females bears must therefore consume enough resources to supply the energy and nutrients required to support themselves and their offspring, as well as some additional reserves to support the following hibernation phase.

Previous research has shown several physiological, ecological, and environmental factors influencing body mass gains in grizzly bears. Among these factors are maintenance cost, reproductive investments (litter size, lactation periods), digestive tract capacity, foraging efficiency, food availability (length of the active/hibernation phase) and the nutritional characteristic of foods (energy and protein content, digestibility) (Pritchard & Robbins 1990; Farley & Robbins 1995; Welch et al. 1997; Rode & Robbins 2000; Felicetti *et al*. 2003; Robbins *et al*. 2004; Robbins *et al*. 2007; Robbins *et al*. 2012; Erlenbach *et al*. 2014;). In this study, we explored how the interactions among the physiology of grizzly bears and the nutritional quality of their habitat influence body mass dynamics and thus the reproductive success of female bears. To do this, we built several mechanistic simulation models using the software program Stella (Richmond & Peterson 1997; Costanza & Gottlieb 1998; Costanza & Voinov 2001) as part of a PhD Dissertation by Claudia López-Alfaro (2014) at the University of Alberta supervised by Dr. Nielsen. This dissertation was divided into four individual chapters representing separate scientific manuscripts for publication with the first two published (López-Alfaro *et al*. 2013; López-Alfaro *et al*. 2015) and the last two in preparation. A brief summary of each of these chapters is presented below as sub-sections.

3.1 Energetics of hibernation

Our first objective was to explore the energetic trade-offs faced by females during hibernation since this can constrain reproductive success of grizzly bears in different ecosystems. To address this goal we developed a bioenergetic model that simulates body mass loss during hibernation by considering the main physiological mechanisms that determine the use of lean and fat mass reserves (López-Alfaro *et al*. 2013). The model accounts for maintenance and reproductive cost and can be run under different scenarios representing reproductive strategies (i.e., non-lactating/lactating, litter size, and lactation period) and regional environmental conditions (i.e., hibernation length).

Using this model, we evaluated the energy and protein cost of reproduction for different reproductive strategies (litter size; lactation period during hibernation), demonstrated a relationship between denning body fat content, different reproductive strategies, and potential survival time (López-Alfaro *et al*. 2013; Figure 4).

3.2 Assessing the digestible energy and protein among bear diets

Our second objective was to examine the nutritional differences between brown bear diets of four well-studied bear populations in interior North America and relate differences in nutrition to differences in life history traits and population densities. This objective helps address questions around constraints in the diets (nutrition) of grizzly bears in Alberta and how this may limit reproduction and density (carrying capacity) thus informing population recovery goals. To address this objective, we built a mechanistic model to evaluate the temporal changes in the digestible protein (kg) and energy (kcal) available in one kilogram of fresh diet. Diets represented the combination of different food items (e.g., berries, vegetation, ungulates) by approximating the average food habits of bears in the different ecosystems. These ecosystems included the Mountains and Foothills in west-central Alberta (Munro *et al*. 2006), the Flathead River in southeastern British Columbia (McLellan & Hovey 1995), and both the historic (ca. 1977-87) and recent (ca. 2007-2009) Greater Yellowstone ecosystem (GYE) in the USA (Mattson *et al*. 1991; Fortin *et al*. 2013).

Model results revealed noticeable differences in the amounts of digestible energy and protein consumed by bears between ecosystems (López-Alfaro *et al*. 2015; Figure 5). Diets in Alberta (Mountains and Foothills) showed the lowest levels of digestible energy and protein in the active period. This is consistent with low reproductive rates and lower population densities observed in other interior ecosystems (Garshelis *et al*. 2005) helping support the suggestion of bottom-up constraints to Alberta grizzly bear populations (Nielsen *et al*. 2010; Nielsen *et al*. in review).

3.3 Energetics of brown bears, physiological, and ecological trade-offs

Our third objective was to develop a mechanistic model to simulate body mass dynamics of grizzly bears across the active period using different diets. The model considers the transfer of energy and protein from the environment to the individual, accounting for allocation in maintenance, growth, and reproduction. In total we simulated twelve bear diets varying the combination and amount of four common bear food groups: ungulates, green vegetation, fruits and seeds. We used this model to evaluate the requirements in energy (kcal) and protein (kg) for female bears under different reproductive strategies (i.e., lactating vs non-lactating females and different litter sizes).

Results demonstrated an interaction between the nutritional quality of the diet, the bear's digestive capacity and the individual requirements that constrain body mass gain (López-Alfaro 2014; López-Alfaro *et al*. in prep; Figure 6a). These constraints are especially strong when the nutritional characteristic of the bear diet are low in digestible energy and protein and/or when the individual requirements are high (e.g. lactating females or longest hibernation periods). These results identify the nutritional mechanisms influencing the observed rates of low reproductive success by female bears within ecosystems with poor habitat quality (nutritional values).

3.4 Bottom-up factors restricting population recovery in Alberta

Our final objective was to integrate the three component models addressed above to simulate the body mass dynamics of grizzly bears in Alberta. To address this objective we developed a model to simulate the gain and loss of lean and fat body mass from the beginning of the hibernation phase, through emergence and active period, and until the next denning (365 days). The model operates on a set of scenarios reflecting reproductive strategies (i.e., non-lactating/lactating, litter size, lactation period) and environmental conditions (i.e., hibernation length, different diets). Bear diets resemble the food habits of bears in Alberta. Different diet-scenarios were developed that vary consumption of key foods items (ungulates, berries) and length of food availability.

Model results demonstrate that the Foothill and Mountain ecosystems of west-central Alberta impose important nutritional restrictions for lactating females (López-Alfaro 2014; López-Alfaro *et al*. in prep; Figure 6b). First, during spring and summer lactating females use body mass reserves to support lactation. As a consequence, they need higher levels of fat and lean mass reserves for hibernation. Second, bears require several seasons to accumulate the necessary body mass reserves to support reproduction. This has a negative effect on the reproductive rate of bears because it increases the inter-birth interval. Our results also suggest that lactating females in west-central Alberta are not able to provide the same amount of energy and protein in their milk compared to what has been observed in captive bears.

This dissertation and publications on bioenergetics of grizzly bears by Claudia López-Alfaro (2014) suggests that the nutritional conditions in Alberta's ecosystems limit the reproductive rates of brown bears. From a management perspective there are two major consequences to these conclusions. First, there is a reduced carrying capacity for Alberta grizzly bears compared with other interior ecosystems (e.g. Flathead and the GYE) suggesting that caution should be used in setting recovery targets based on densities within other ecosystems. Second, the low reproductive rate observed in Alberta and supported by bioenergetic models here suggest that the recovery of grizzly bear populations in west-central Alberta will be slower than those observed elsewhere, such as the GYE or southwest Alberta which is connected to both the Flathead and Glacier National Park populations. Thus recovery of grizzly bears in the relatively unproductive ecosystems of much of Alberta will be a slow process. Areas connected to larger populations are expected to recover sooner.

4. Carnivory and frugivory resources affect patterns in local abundance of bears

Top-down factors are often considered of most importance in the management of grizzly bears (Boyce *et al*. 2001). Indeed, there is a common relationship found between road density (proxy for human-bear interaction) and human-caused grizzly bear mortality (Benn & Herrero 2002; Johnson *et al*. 2004; Nielsen *et al*. 2004a; 2008; Nielsen 2011; Boulanger & Stenhouse 2015). Bottom-up factors, however, should not be overlooked when considering grizzly bear conservation, as vital rates (Mattson *et al*. 1992; Pease & Mattson 1999), population abundance and dynamics (Hilderbrand *et al*. 1999; Pease & Mattson 1999; McLellan 2011), geographic distribution (Mattson & Merrill 2002; Bojarska & Selva 2012) and fitness proxies, such as body size (McLellan 2011; Nielsen *et al*. 2013; Erlenbach *et al*. 2014) and body fat percentage (Robbins *et al*. 2012), relate to dietary and nutritional conditions in bears. Factors related to both survival and food resource availability has been shown to improve accuracy of grizzly bear habitat quality estimates over top-down-based models alone (Nielsen *et al*. 2010).

Top-down and bottom-up factors acting on bear populations are not likely to be independent of each other as perhaps often assumed. Human-caused mortality of bears increases when natural food availability is low (especially during the hyperphagic period) since bears seek anthropogenic food sources (Mattson *et al*. 1992; Pease & Mattson 1999; Herrero & Higgins 2003; Gunther *et al*. 2004), or when bears choose to forage in areas associated with humans, such as attractive sinks (*sensu* Nielsen *et al*. 2006; Roever *et al*. 2008a; Northrup *et al*. 2012). A productive and nutritious food supply, however, may mitigate the effect of human-caused mortality in bears. For example, the nutritional quality of food resources often mitigates top-down pressures in herbivores (Schmitz 1998; Danner & Joern 2003), and this sort of relationship may be a reason why grizzly bears in some populations experiencing human-caused mortality can maintain high population densities (e.g. Mowat *et al*. 2005; McLellan 2011). It is therefore important that the distribution, abundance and nutritional aspects of food resources are well understood in order to better understand grizzly bear population dynamics and patterns in population size and local density (Lopez-Alfaro *et al*. 2015).

In the past, most field research relating food supply to bear population performance and density have focused on individual resources such as meat (Hilderbrand *et al*. 1999a; 1999b) or fruit (McLellan 2011). Although meat availability is commonly considered a major factor affecting variation in abundance of bears (Hilderbrand *et al*. 1999b), McLellan (2011) demonstrated that much of the positive relationship between amount of meat in diet and bear density is associated with the presence of salmon. In fact, the meat to bear density relationship does not hold up for interior populations lacking this marine (spatially-subsidized) resource (McLellan 2011).

Simply focusing on one resource or nutritional parameter (e.g. meat), however, may not be enough to resolve ecological relationships. Where a single optimally balanced food is not available, two foods can be considered complementary when they provide an animal with a blend of nutrients not found in either food alone, and that allows the animal to consume an optimal level of nutrients. The macronutrients (proteins, carbohydrates, and lipids), which are required for energy provisioning, as well as other purposes (e.g. lipids for cell membranes, and protein for lean mass), are a driving force behind food selection and foraging behaviour in several species (Rothman *et al*. 2011). This behavior also extends to predators (reviewed in Kohl *et al*. 2015), where nutrient-specific foraging has been linked to fitness (reproductive output) in an invertebrate carnivore (Jensen *et al*. 2012).

Studies of macronutrient self-selection in captive bears demonstrated that animals choose diets varying in protein to non-protein (lipid and carbohydrate) energy in proportions that optimized their energy intake and maximized mass gain, where mass gain was considered a proxy for fitness (Erlenbach *et al*. 2014). In the wild, macronutrients available to bears are often found in variable environments (Nielsen *et al*. 2013) among a diverse range of potentially complementary foods that vary in availability and nutrient content across both time and space (Nielsen *et al*. 2010; Mowat *et al*. 2013; Coogan *et al*. 2014). Bears, therefore, must forage across “complimentary landscapes” (Dunning *et al*. 1992) to obtain such foods. Two foods can be considered complementary when they provide an animal with a blend of nutrients not found in either food alone, and that allows the animal to consume an optimal level of nutrients. Bears in the captive trials preferred high lipid intake over carbohydrate when mixing their diets; however, bears consumed carbohydrate in the absence of lipid to compose the same preferred ratio of protein to non-protein energy, which may be an adaptive trait for bears residing in ecosystems in which high lipid resources are not readily available (Coogan *et al*. 2014). Given the variable nature of environmental conditions (Nielsen *et al*. 2013) and spatial patterns of resources available to grizzly bears (Nielsen *et al*. 2010; Coogan *et al*. 2012; Mowat *et al*. 2013), wild bears may be limited in their ability to consume complementary resources that represent optimal diets (Coogan *et al*. 2014) which may subsequently result in population-level effects.

Here we test whether local patterns in abundance of ‘interior’ grizzly bear populations are co-limited by the distribution and abundance of two complementary food resources — (fruit and ungulates) — while accounting for a well-known top-down factors (roads) affecting survival in bears. While other important foods in the ecosystem, such as herbaceous vegetation and roots (*Hedysarum* spp.; Coogan *et al*. 2012) provide bear with important sources of nutrients they were not the focus of this analysis — neither on their own are complimentary with ungulates because they likely do not contain enough lipid or carbohydrate to reduce the ratio of protein to optimal levels (Coogan *et al*. 2015).

Both fruit and ungulate meat are documented as a major component of the seasonal diets of interior grizzly bear populations in the Rocky Mountains of western North America (McLellan & Hovey 1995; Munro *et al*. 2006; McLellan 2011). They also provide complementary macronutrients (i.e. carbohydrate from fruit, and protein and lipid from ungulates) that may allow bears to optimize their diet and fitness when co-occurring (Coogan *et al*. 2014; Erlenbach *et al*. 2014). These contrasting nutritional characteristics (fruit vs. meat) allow us to explicitly estimate food abundance while at the same time implicitly account for macronutrient composition. This co-limitation hypothesis suggests that local abundance in bears should be higher in landscapes having simultaneously higher available ungulate and fruit resource supply. Bears should also be attracted to areas offering complementary resources due to nutrient-specific foraging behavior. We compared this co-limitation hypothesis against more standard single resource hypotheses that suggest resource supply in either meat (Hilderbrand *et al*. 1999a; 1999b) or fruits (McLellan 2011) alone affect local population density of bears. We test these hypotheses for a population of grizzly bears in west-central Alberta where we have information on local variation in bear abundance and mapped (modelled) abundance of meat and fruit resources in units (kcal) that are biologically relevant to measuring population responses.

4.1 Top-down models

Because grizzly bear survival and mortality risk in the region is strongly associated with the proximity of roads (Benn & Herrero 2002; Nielsen *et al*. 2004a; Nielsen 2011; Boulanger & Stenhouse 2015), average road density was estimated within a 7.44-km radius moving window (average daily movement of female and sub-adult grizzly bears in the study area during hyperphagia; Boulanger *et al*. 2013) to account for top-down factors affecting local abundance of bears through human-caused mortality (Boulanger & Stenhouse 2015).

4.2 Ungulate models

To represent carnivory resources of ungulate matter, local abundance (population density) of five ungulate species were modelled in the area: moose (*Alces alces*), elk (*Cervus canadensis*), bighorn sheep (*Ovis canadensis*), white-tailed deer (*Odocoileus virginianus*), and mule deer (*Odocoileus hemionus*). Abundance data (counts) were obtained from aerial surveys conducted by Alberta Environment and Sustainable Resource Development (AESRD). Local density of ungulates were estimated for the study area using GLMs fit to observed abundances of individual ungulate species using a set of environmental predictors (land cover, land use, and terrain). Conversions to total biomass were estimated for each species, including neonates, based on average body sizes by sex for each species using a literature review. Digestible energy (Dig E; kcal/kg) estimates for ungulates were based on regional ungulate biomass (kg) estimates. Regional biomass estimates were corrected for water and indigestible components using body composition estimates; however, since such estimates were to our knowledge not available for all species and age classes, the body composition estimates of whole ungulate was standardized using average percent body composition of moose (*Alces alces*) minus hide and injesta (injesta free body mass [IFB mass]; Hundertmark *et al*. 1997). We then applied a digestible energy (kcal/kg) conversion for meat (Pritchard & Robins 1990) to estimate ungulate digestible energy using the following equation:

Eqn. 2: Whole ungulate biomass (kg) × % IFB mass × % dry matter IFB × % ash free IFB × digestible energy (kcal/kg)

Specifically, percent IFB mass was 88.1, percent dry matter of IFB mass was 34.8, percent ash-free content IFB was 94.9 (100-5.1% ash), and digestible energy was taken as 6920 kcal/kg. Final model of ungulate energy were mapped in a GIS (Figure 7a).

4.3 Fruit models

A multi-stage statistical modeling approach was used to estimate the nutritional landscape in digestible energy (kcal) for buffaloberry (*Shepherdia canadensis*). Specifically, three sets of model responses representing different measures of buffaloberry responses were fit using generalized linear models (GLMs) and included: (1) the distribution (presence/absence) of buffaloberry at a site; (2) shrub abundance (density) conditional on being present; and (3) fruit abundance where present. Field plot data on buffaloberry presence, shrub abundance and fruit density were used to predict landscape variation in the availability of buffaloberry fruit using environmental spatial predictors. Environmental variables included land cover, climate, terrain, soils, and forest stand measures that have previously been found to be important predictors in the region for buffaloberry distribution (Nielsen *et al*. 2003; 2004c; 2010; Roberts *et al*. 2014). Following model development, model predictions (distribution, shrub density, and fruit abundance) were mapped at a 30-m resolution in a Geographic Information System (GIS). Predicted number of fruit per pixel (900 m^2) that represented an average yearly abundance were converted to dry biomass using the dry weight of buffaloberry fruit (Coogan *et al*. 2014) and then converted to maps of available digestible energy (Dig E; kcal/kg) using biomass to digestible energy conversion of:

Eqn. 1: Gross energy × % Digestible energy

Gross energy of buffaloberry fruit was estimated as 4310 kcal/kg, while percent digestible energy was estimated as 64.5% (Coogan *et al*. 2014) resulting in 2780 kcal Dig E/kg or on a per gram basis of 2.8 kcal Dig E/g. Final model of fruit energy were mapped in a GIS (Figure 7b).

4.4 Local patterns in grizzly bear abundance

In 2004, the minimum count of grizzly bears was estimated at 1138 lured hair-snag sites (Figure 8). Each site consisted of a single strand of barbwire set in a “corral” fashion (~100 m^2 in size) with a cow blood lure placed on a pile of brush in the middle of the corral to attract bears to the site. Bear hair was collected non-invasively on the barbwire as animals entered and/or left the corral. Each hair-snag sample represented a 2 week session where hair was collected at the end of the session with the sampling sessions lasting from 25 May to 17 July 2004 and a total of four possible sessions and sites per 49 km^2 (7x7km) grid cell. Hair samples were genosequenced by Wildlife Genetics International to identify the number of unique bears detected at each hair-snag site (see Paetkau 2003; Boulanger *et al*. 2004; and Proctor *et al*. 2010 for more details on DNA lab techniques). We used the number of unique bears at each sample site to represent local abundance in bears.

4.5 Single versus complementary resource hypotheses

We tested 6 a priori models predicting patterns of local grizzly bear abundance in grizzly bears (Table 3) to evaluate support for top-down only or single versus complementary resource hypotheses representing bottom-up regulation in bears. Models tested included a null model where local abundance was assumed to be constant across the landscape (mean abundance), a null landscape model where we accounted for sampling session (time) and the expected effect of top-down factors influencing survival of bears as measured by surrounding road density, as well as different combinations of food resource models. Combinations of food resource models differentiated the importance of carnivory (ungulate sources of meat at 7.44 km radius) versus frugivory (buffaloberry fruit at a 1.69 km radius) and when combined either an additive or multiplicative effect on local bear abundance thus testing single and complementary resource hypotheses. Note that for the complementary resource hypothesis we considered both an additive (meat + fruit) and a multiplicative (meat + fruit + meat×fruit) model to evaluate whether local abundance of bears increased more than expected in the presence of complementary foods (i.e. multiplicative model).

To evaluate these hypotheses, we used ordered logistic regression that predicted the probability of an increased count of bears (0, 1, 2, ≥3) at a sample site/session. We used the different landscape and sampling covariates for the different hypotheses as predictors of local abundance in bears. The ordinal model was used rather than a zero-inflated or negative binomial count model since the number of unique counts of bears at DNA hair-snag sites was low and the parallel assumption for ordered logistic regression was satisfied (Brant test of parallel regression assumption, $\chi^2 = 5.29$, $P = 0.726$, $df = 8$). To account for potential correlation among local hair-snag sites, the variance (standard errors) of parameters in the ordered logistic models was estimated using the 'clustered sandwich' approach (Rogers 1993; Williams 2000) that accounts for intergroup correlation. Cluster identity was identified here as individual 7x7 km DNA sampling cells originally used to allocate DNA hair snag sites across the study region. To evaluate support for our hypotheses, we ranked model fit of the data given a penalty for model complexity (principle of parsimony) using Akaike's Information Criteria (AIC, Burnham & Anderson 2002).

4.6 Results of complementary foods and patterns in bear abundance

Within the study area, high concentrations of digestible energy from ungulate matter were predicted to be within the mountainous western region of the Yellowhead population unit bordering Jasper National Park (Figure 7a). Some of the highest concentrations of ungulate resources in the area, however, occurred around specific locations such as the reclaimed Greg River/Luscar mine. Available digestible ungulate matter (kcal) was generally lower in the eastern foothills where elk and sheep were absent (sheep) or less abundant (elk). DNA hair-snag sites recorded areas of high local bear abundance (≥3 bears) in areas predicted to have relatively high amounts of digestible energy from ungulates. This is consistent with patterns of where three or more unique bears were detected at a site (Figure 8).

Spatial patterns in the digestible energy of buffaloberry fruit were more variable than that of ungulates. This reflects the more local scale in which buffaloberry resources were measured around DNA hair snag sites (1.69 km radius) and the scale of resource patches itself that relate to local variation in forest structure. Areas of high buffaloberry resources were predicted for both the mountains and foothills regions with the greatest abundance of fruit often following valley bottoms (Figure 7b). DNA hair-snag sites measuring local grizzly bear abundance were generally related to areas with buffaloberry fruit (Figure 7b) with exceptions to the relationship being more common in the east where road density was higher.

Models comparing local patterns in grizzly bear abundance supported a top-down (roads) and bottom-up (resources) hypothesis with the additive complementary resource model of ungulates and buffaloberry having an Akaike weight of 0.72 (Table 4). The multiplicative complementary resource model was the second most supported model at a ΔAIC of 1.95 and Akaike weight of 0.27 (Table 4). In comparison, the null landscape model representing the top-down hypothesis (road density and sampling session covariate) was much less supported at a ΔAIC of 49.63, thereby illustrating the strong effect of adding bottom-up factors measuring local resource supply. When considering only the single resource hypotheses, carnivory (ungulate matter) was more supported than frugivory (buffaloberry fruit) with a ΔAIC from the top complementary model being 8.92 and 35.71 respectively.

Model parameters confirmed the expected inverse relationship between road density and observed local abundance in grizzly bears. Specifically, each one unit increase in road density resulted in a 62.3% decrease (Odds ratio [e^β] = 0.516) in local abundance of bears (Table 5). Road density was highest in the north and east regions of the Yellowhead population unit, with an additional area of high density found in the southeast. In contrast, areas of low road density were located in the central and western regions of the study area adjacent to the Rocky Mountains. There was an inverse relationship between session number and bear abundance with a 35.6% decrease in odds (Odds ratio [e^β] = 0.695) in local abundance of bears at a site across each session period (Table 5).

Relationships between food supply and local abundance of bears predicted that for each 10-fold increase in buffaloberry food supply (log10[kcal of fruit] at 1.69 km radius around hair-snag sites), local abundance of bears increased by a factor of more than 2 (Odds ratio [e^β] = 2.125). On the other hand, each 10-fold increase in ungulate food supply (log10[kcal of ungulate meat] at 7.44 km radius around hair-snag sites) increased local abundance of bears by a factor of 59 (Odds ratio [e^β] = 59) demonstrating the importance per unit increase in ungulate matter on local bear abundance. However, standardized coefficients (e^βStdX) indicated that when considering a one unit standard deviation change in ungulate and fruit resources, both ungulate and buffaloberry food supply were similar in their effect on local grizzly bear abundance with standardized coefficients for both being 2.0 (2-fold increase in local bear abundance per standard deviation change in resource supply) (Table 5). Therefore, on a per digestible kcal basis, ungulates were 29.5 times more important in affecting local abundance of bears, although differences were similar when considering standardized changes in available resource supply.

Differences in the interpretation of the importance of individual resources are due in part to greater landscape variation in local fruit supply compared with that of the supply of ungulate meat that responded at broader spatial scales (Figure 7). Regardless, both factors were found to contribute to the observed patterns in local abundance of bears with model support of the complementary effect being 72 times more supported than the most supported single resource model of ungulate meat (Akaike weights; Table 2). Figure 9 illustrates graphically this additive complementary effect with the probability of observing at a hair-snag site either no bears or the largest count (≥3) of bears. Only in situations where both ungulate and buffaloberry resource supply are abundant are the counts of bears highest (Figure 9b). Note, however, that variation in buffaloberry food supply makes little difference in encountering high counts of bears unless moderate or high levels of ungulate resource supply are available, while increases in ungulate resources at lower to moderate buffaloberry resource supply increase the likelihood of encountering sites with locally high abundance of bears.

4.7 Discussion of complementary resources and limits to local bear abundance

We demonstrate here that local patterns in grizzly bear abundance were affected by both top-down and bottom-up factors, and specifically that areas high in energy from complementary resources (ungulates and fruit) were more important in predicting patterns of local abundance in bears than either food source alone. This supports a complementary resource hypothesis and more specifically that complementary foods macronutrients (i.e. carbohydrate from fruit, and protein and lipid from ungulates) support more bears by allowing bears to optimize their diet and fitness when co-occurring (Coogan *et al*. 2014; Erlenbach *et al*. 2014). Importantly, the availability of complementary foods was more important in explaining bear abundance than energy or protein intake per se; if energy or protein were more important, then bear density would have been strongly associated with high-ungulate areas regardless of fruit abundance. Our work, therefore, further supports the supposition that purely energy-or single nutrient-based foraging studies may be insufficient to accurately predict or understand animal foraging behavior (Illius *et al*. 2002; Simpson *et al*. 2004; Robbins *et al*. 2007; Jensen 2012; Erlenbach *et al*. 2014; Coogan & Raubenheimer In review) .

Although the co-limitation hypothesis of ungulate matter (meat) and fruit was most supported, our study suggested that ungulate matter was more important than fruits in predicting local abundance of grizzly bear. One reason may be the resource size and efficiency between kcals of different foods. For example, 1 kcal of ungulate meat is more likely to be associated with several other kcals of ungulate meat (e.g. a whole carcass), than is 1 kcal of fruit which is packed in a far smaller and less energy dense ‘package’. Meat also provides both protein and lipid to bears, thereby offering a source of two macronutrients in an easily digestible form — adequate protein intake is important for bears in order to support lean mass growth and lactation costs. Another explanation may be that the availability of fruit energy in the area is not enough to dilute the protein intake of grizzly bears to optimal levels (perhaps especially for highly carnivorous bears), such that bears are more likely to consume a high ungulate diet despite not being optimally balanced — being omnivores, bears should have a high tolerance to dietary imbalances (Raubenheimer & Simpson 1997). It may also be that the diet of grizzly bears has them in a ‘nutrient space’ (sensu Simpson & Raubenheimer 2012) that requires relatively little fruit to reach their optimal intake of non-protein energy (see Coogan *et al*. 2014). Carbohydrate is likely especially important in this ecosystem, because it may be the only means for bears to optimize their nutrient intake given the absence of high-lipid food items. Yet, despite the relative importance of one food over the other, both fruit and ungulates were better at predicting local bear abundance than either food resource in isolation and only when both were available at high levels were counts of bears high. Higher bear abundance in areas offering both meat and fruit supports our co-limitation hypothesis. Although the most supported model did not include an interactive (multiplicative) effect between fruit and ungulate calories, interactive effects of food resources have been shown to exist at the individual level and may not directly translate with patterns in local abundance. For instance, giant pandas have been shown to migrate between two habitats to balancing their intake of protein and the micronutrients phosphorous and calcium (Nie *et al*. 2014).

Although our focus is on local patterns in grizzly bear abundance, higher number of grizzly bears at hair snag sites may be due in part to females with offspring. Cub-of-the year and to some degree yearlings are unlikely to be captured by barbwire corrals since hair snag heights are high (0.5 m) relative to their size. However, if dependent offspring are being captured in barbwire corrals, then the relationship between increased local bear abundance and the availability of fruit and ungulate matter suggests that availability of complementary resources may also increases reproductive success and litter size and thus indicates areas of greater population performance. Indeed, female reproductive success of bears is influenced by their capacity to store both fat and lean mass before hibernation (Farley & Robbins 1995; López-Alfaro *et al*. 2013; Robbins *et al*. 2012), as well as the availability of food resources during the post-denning lactation (spring) period, especially food resources high in protein which have been found to be important for bears (Landers *et al*. 1979; Noyce & Garshelis 1998). Fruit consumption during summer and early fall is an important source of energy that allows grizzly bears to accumulate fat mass prior to denning (McLellan 2011), as well as optimize their macronutrient intake and mass gain when combined with complementary resources (Coogan *et al*. 2014; Erlenbach *et al*. 2014). These complementary resources are therefore likely critical to reproductive rates in bears, which are known locally to be among the lowest recorded for the species in the least productive high elevation environments where mean age of first reproduction was 6.7 years and mean age of first surviving litter was 8.4 years (Garshelis *et al*. 2005). These same high elevation habitats are also associated with smaller body sizes (Nielsen *et al*. 2013). This suggests strong bottom-up limitations in the population.

Our results support the hypothesis that bottom-up factors were offset partly by top-down factors that related to human-caused mortality of grizzly bears as indicated by the inverse relationship between road density and local abundance of bears. This work supports local recovery efforts for a threatened population of grizzly bears in Alberta by demonstrating that not only is access management of roads important (Nielsen *et al*. 2009), but also the distribution of food resources which affects the ability (carrying capacity) of the landscape to support more bears. Numerous studies have demonstrated negative relationships between grizzly bears and roads, including higher human-caused mortalities/lower survival (Benn & Herrero 2002; Johnson *et al*. 2004; Nielsen *et al*. 2004a; Nielsen 2011; Boulanger & Stenhouse 2015) and avoidance of habitats near roads (McLellan & Shackleton 1988; Mace *et al*. 1996; 1999; Apps *et al*. 2004). It should be noted, however, that grizzly bears can also be attracted to roads in areas with concentrated sources of food (Nielsen *et al*. 2004b; 2004c; Roever *et al*. 2008a; Roever *et al*. 2008b) resulting in attractive sinks (Nielsen *et al*. 2006; Northrup *et al*. 2012). It would be informative if future work examined from a more nutrient explicit perspective.

Our results suggest that conservation and management planning should consider the non-substitutability of habitats on which bears rely to balance their nutritional intake. When comparing the difference in support between bottom-up factors and top-down factors, bottom-up factors were more important in explaining local patterns in abundance of bears based on AIC values and standardized coefficients. This suggests that greater emphasis should be placed on bottom-up control of local bear populations and is supported by regional assessments of differences in bear density where the most productive ecosystems, especially those that benefit from spatially-subsidized marine resources of salmon, have the highest density of bears (Hilderbrand *et al*. 1999b; Mowat *et al*. 2013). Recovery efforts should acknowledge the presence of bottom-up limitations that affect the number of bears that can be supported and thus the degree to which population recovery targets can be set. To hasten population recovery and increase population sizes, forest harvesting and prescribed fire may be effective tools in managing the complementary resources of ungulates and fruit (Nielsen *et al*. 2004b), although access management would need to be considered.

Traditionally, resource co-limitation studies have often been applied to autotrophic and herbivorous consumers, where individual growth responses to specific nutrient-limitation scenarios have been examined (Elser *et al*. 2007; Simpson & Raubenheimer 2012; Sperfeld *et al*. 2012). Our results suggest that the concept of nutrient co-limitation is also relevant to larger scale population measures. For example, under Liebig's law of the minimum, a more traditional approach to resource limitation, growth is considered strictly limited by the most limiting nutrient. The co-limitation hypothesis suggests, however, that growth can be simultaneously limited by >1 nutrient (Sperfeld *et al*. 2012). The relationship between bear density and both fruit and ungulates (Figure 7) is similar to co-limitation patterns in interactive essential resources (see Figure 1b in Sperfeld *et al*. 2012), where areas of rounded probability isoclines indicate a smooth transition of limitation by fruit to ungulates and a range of resource availabilities where both resources are simultaneously limiting. Similarly, while macronutrient self-selection studies necessarily tend to focus on the behavioral and physiological responses of individual animals, our results suggests that fitness benefits of a mixed-diet can influence spatial patterns of population density across an ecosystem. We therefore not only demonstrate the importance of bottom-up regulation using grizzly bears, but also show that more refined approaches to bottom-up regulation rather than simply food availability, energy- or single nutrient-based models should be considered. Fundamentally, a bottom-up approach to ecology, management, and conservation relies on understanding the relationships between an animal, their habitats and food resources that provide the necessary nutrients and energy. Yet, lack of knowledge of the nutritional requirements of wild animals, and the nutrient content of foods they consume, often limits such an approach, and are therefore required to integrate nutritional parameters within studies. Our study demonstrates the importance of bridging this knowledge gap, in order to further develop an interactive and nutrient-specific approach to understanding the nutritional ecology of animals in the wild.

5. Bottom-up (habitat-based) estimate of carrying capacity for the Yellowhead Ecosystem

Although recovery plans for grizzly bears in Alberta have suggested specific actions for recovery, including defining core and secondary conservation areas based on road density thresholds of 0.6 and 1.2 km/km^2 respectively (Nielsen *et al*. 2009), actual recovery targets were not identified, nor were suggestions made on how to estimate those targets. One option is simply defaulting to the IUCN criteria of 1000 breading adults at provincial scales rather than population units. Biologically and in particular socially, such recovery targets may not be feasible or desirable for local management at the scale of population units. Alternative approaches to defining recovery targets are therefore needed, as well as management actions to facilitate that recovery and methods for monitoring populations to identify when populations are recovered.

To date, socially-based recovery targets have largely been inferred as default targets for defining recovery of populations within Alberta, acknowledging limitations in recovery based on the realities of current land use activities. This is particularly evident as it relates to ranching in the far southern Castle population where human-bear conflict rates are high and recent eastern expansion of populations observed (Northrup *et al*. 2012). Knowledge of biological targets would be, however, helpful to identify deficits between social and biologically-based recovery targets or in areas with fewer human-bears conflicts, targets that are based more around biological potential (i.e., carrying capacity).

Here we outline an approach for estimating biologically-based targets for recovery of grizzly bear populations in Alberta based on food resource supply (Nutritional landscapes). This approach assumes that populations of bears are limited by food resource supply (bottom-up limitations). Although most would agree that top-down factors limit populations of grizzly bears in Alberta due to human-caused mortalities (Benn & Herrero 2002; Nielsen *et al*. 2004a; 2008; Nielsen 2011), there is also evidence that populations are limited by food supply. For instance, grizzly bear body size and reproduction is among the lowest reported for this species in Banff National Park where bears are protected, but have access to limited food resources and short growing seasons (Garshelis *et al*. 2005; Nielsen *et al*. 2013). Indeed, when considering range-wide scales, when grizzly bears have access to marine subsidized resources body size and population density can increase over that of interior populations, such as Alberta, by a factor of 10 and 100-fold respectively.

5.1 Landscape carrying capacity modeling approach

A total of 2,782 field plots were completed over the Yellowhead, Grande Cache, and Swan Hills population units between 2001 and 2008. At each field plot, vegetation characteristics, including presence and abundance (cover or density) of critical grizzly bear foods, were measured (Table 6). We used a multi-stage statistical modeling approach whereby resource distribution (presence of each species) and abundance (cover or density of each species) where present were modeled using generalized linear models (GLMs) with the response variable representing field data and environmental predictors derived from a GIS. Predictor variables include: land cover, climate, terrain, soils, and forest stand measures, which were found to previously be important in predicting their distribution and abundance (Nielsen *et al*. 2003; 2004c; 2010; Coogan *et al*. 2012).

We used logistic regression (generalized linear model (GLM), family = binomial, link = logit) to estimate the probability of occurrence of major grizzly bear foods based on environmental site conditions. Fourteen candidate models were created using a combination of variables (multivariate and interaction terms). All model variables were uncorrelated (Pearson $|r| < 0.7$). Models were selected for species based on ΔAIC > 2 for the top ranked (lowest AIC) candidate model. In cases where the global model was the top model by < 2 ΔAIC, or within ΔAIC of the top model, the global model was chosen as the top model without model averaging. Top candidate models for each species were evaluated for model accuracy using the receiver operating characteristic (ROC) area under the curve (AUC) statistic. Optimal probability thresholds for classifying presence-absence of individual food resource patches were estimated by calculating the minimum absolute difference between sensitivity and specificity values. Occupancy model estimates were mapped in a GIS, where species occurrence probabilities were re-classified to binary presence-absence resource patches (30-m pixel) using the optimal probability thresholds.

Abundance models were estimated for each food item, again using generalized linear models (GLMs) but instead using a Gaussian family and identity link function and excluding observations where it was absent (i.e., abundance where present models). Response variables included percent cover of groundlayer species or the density of food items including shrubs, distinct herbaceous items or fruit. Cover values were converted to proportions and transformed to logit values prior to fitting GLMs. This ensured that extrapolations to new environmental space within the GIS didn't result in cover predictions that were less than 0 or greater than 100. Densities of items (shrubs, fruit or distinct herbaceous items like cow parsnip) were log transformed with a constant of 1 added prior to fitting GLMs. These transformations normalized the data. Like occupancy models, model selection for shrub and distinct herbaceous items was based on AIC and included the same set of 14 candidate models used for occupancy modeling. Candidate models for fruit density were, however, based only on two factors: shrub density or cover and canopy (including non-linear responses for canopy).

Models estimating population density of five common ungulates (moose, elk, bighorn sheep, white-tailed deer, and mule deer) were based on aerial survey data collected and provided to us by Alberta Sustainable Resource Development (also see section 4.2 above). Aerial surveys represented only a fraction of the total 'blocks' within the study area. To estimate abundance of ungulates across the entire landscape, generalized linear models (GLMs) were fit to abundance estimates within sampled blocks to environmental factors in that block that related to land cover, land use, and terrain. Biomass estimates of each species, including neonates, were based on a literature review.

We used ocular estimates of percent ground cover of herbaceous bear foods — horsetails (Equisetum spp.), cow parsnip (Heracleum lanatum), dandelion (Taraxacum officinale), and clover (Trifolium spp.) — within 1 m^2 circular quadrats from two study areas (Kakwa and Crowsnest Pass) during the summer of 2012. Herbaceous bear foods were collected for above-ground biomass estimation by clipping the aboveground part of each herbaceous species. Biomass clipping were collected in paper bags and allowed to air dry while in the field and field camp prior to laboratory analysis (some samples were also frozen until return to the lab). Biomass samples were oven-dried at 60°C for 48 hours in the laboratory, and weighed to a constant weight.

We used the *lmer* function from the package *lme4* in the Program R (Version 2.15.2) to create allometric generalized linear mixed-models (GLMMs; family=Gaussian, link=identity) relating dry herbaceous biomass to percent ground cover estimates. All models were regressed through the origin (i.e., intercept at zero) so that biomass estimates > 0 would not be given when absent (percent cover was zero). Models regressed through the origin were checked against models with intercepts to ensure that the model functions were similar. We used a random effect for sample plot to account for multiple samples per plot. We compared three candidate models using AIC: (1) null model (mean value); (2) biomass as a function of percent cover; and (3) biomass as a function of percent cover plus day past June 1st to account for the influence of collection date on biomass and percent cover. Allometric models were selected for species based on ΔAIC > 2 for the top ranked (lowest AIC) candidate model.

We combined literature from grizzly bear food studies (Hamer & Herrero 1987; Pritchard & Robbins 1990; Noyce *et al*. 1997; Welch *et al*. 1997; Swenson *et al*. 1999; Rode *et al*. 2001; Mattson *et al*. 2004) with laboratory measures of foods collected from the Yellowhead ecosystem between 2008 and 2010 (Coogan 2012; Coogan *et al*. 2014) to estimate energy digestibility (kcal) per dry weight gram of each food resource based on relationships from Pritchard & Robbins (1990). Energy and energy digestibility estimates for food items were based on single-sourced estimates or averaged across studies (methods are presented in detail in López-Alfaro *et al*. 2015).

We used a bioenergetic simulation model of grizzly bear growth to estimate total annual energy requirements for an average female grizzly bear. The model simulates the energy (kcal) requirement of active bears by integrating the main metabolic mechanisms that determine maintenance, reproduction, movement and growth costs for non-lactating and lactating bears. The model was developed in Stella 10 using a daily time step. We assumed 180 days of active period. Day one corresponds to den emergence and the final model simulation day corresponds to den entry.

Maintenance cost is a function of the body mass (BM in Kg, equation 1). Initial body mass for female was 102 kg and the denning body mass was 153 kg. Initial body mass for male was 195 kg and denning body mass was 225 kg. We assumed spring body fat content of 15% for all bears.

Eqn. 1: $\text{Kcal/day} = 61.9*\text{BM}0.77$ McNab (2008)

For a lactating female we assumed that she has two cubs of 60 days at emergence. Milk production cost was added based on Farley & Robbins (1995) study.

Movement cost is a function of the daily movement distance (km) and body mass (equation 2). Movement rates were estimated from bear data from the Foothills Research Institute, thus for females daily movement was estimated randomly from 3.5 km to 12 km and from 4.5 km to 9.5 km for males.

Eqn. 2: $\text{Kcal/kg/km} = 2.57*\text{BM}-0.316$ Robbins (1993)

Growth cost depends on the denning body mass reserves necessaries to support maintenance and reproduction cost during hibernation. For non-lactating females was assumed that they will reproduce during hibernation, consequently they need more body mass reserve to sustain reproduction. Therefore target body mass for non-lactating female is higher than for lactating females. Denning body fat mass for non-lactating female was 28% and for lactating female was 22%.

Spatial predictions of available energy (kCal) for each species of food item were estimated for the study area using a 30 m resolution (900 m^2 pixel). Recovery zones (watersheds) were used to summarize total available energy per management zone per species. Food item consumption rates were then fit for each food item to reflect the fact that bears don’t consume everything that is available. This ranged from 1% to 25% (neonates) of its availability.

5.2 Landscape carrying capacity results

Landscape GIS variables successfully predicted the distribution, abundance, and biomass of different grizzly bear food items. These were converted from biomass to energy and mapped across the region. Bioenergetic models indicated that the energy requirements for non-lactating females were 1,975,000 kCal/bear/180days, while for non-lactating females were 2,023,000 kCal/bear/180days. Energy requirements for lactating females are higher due to cost of milk production. Energy requirements for males were 2,815,000 kCal/bear/180days. Male requirements are higher due they large body mass. For estimating energetic-based carrying capacity, we used the average of male and lactating female grizzly bear energy requirements of 2,419,000 kCal/bear/year.

When considering the entire 19,942 km^2 Yellowhead study area that included all core, secondary and unranked conservation zones total potential carrying capacity (*K*) and thus the maximum possible biological recovery was estimated at 200 grizzly bears or a density of 10 bears per 1000 km^2 (Figure 10). Considering only the core and secondary zones, *K* was estimated at 139 bears or 11.7 bears per 1000 km^2. Carrying capacity of bears varied substantially, however, among conservation zones with some units near the upper parts of the Greg River (including the Greg River Mine) as high as 35 bears per 1000 km^2 (Figure 10).

5.3 Discussion of nutritional landscape carrying capacity estimates

Recovery targets based on food resource supply suggest that currently defined grizzly bear conservation zones in the Yellowhead population unit could biologically support about two-times the current number of bears in the area at 11.7 bears per 1000 km^2. Areas of very high predicted carrying capacity included the upper Greg River at 35 bears per 1000 km^2. These estimates also do not consider what is socially acceptable. Biological targets could therefore be considered the maximum possible with social carrying capacity reducing targets to that which is achievable given current land uses and human-bear conflict.

These models are also based on a number of assumptions that require further testing. One assumption is the consumption levels of different food items by grizzly bears. Not all resources available are consumed. One element of this is competition for resources by other species. Below we consider this for one critical food item – buffaloberry – by using experiments to estimate competition for buffaloberry by small mammals and birds.

6. Scramble competition of buffaloberry by bears, small mammals, and birds

Fruit are often an important late-summer food for bears (*Ursus* spp.) during the pre-hibernation period where energy requirements are high. In Alberta, *Shepherdia canadensis* [Nutt.] fruit have been a common late-summer energy source for both black and grizzly bears (Hamer & Herrero 1987; Raine & Kansas 1990; Munro *et al*. 2006). Habitat models that incorporate food resources (e.g., Nielsen *et al*. 2003; 2010) can be used to prioritize protection and restoration of key habitats (Braid & Nielsen 2015) and used to relate to patterns in population size, density and individual performance (Nielsen *et al*. in review). However, use of habitat models from estimates of resource supplies may be confounded by the utilization of food resources by animals other than bears. To avoid overestimates of resource availability there is the need to understand the competition of fruit resources among small mammal, bird, and bear consumers.

6.1 Experimental design

To address this issue we designed a series of experimental exclosures in Kananaskis Country during the summers of 2013-2014. Exclosures excluded different fruit consumers based on different sized fencing and exclosure types. For some shrubs we also used both motion-triggered and time interval camera traps to specifically identify the consumers of buffaloberry fruit. Exclosures were constructed around fifty buffaloberry shrubs over two years (25 per year for 2013, 2014). Four treatments were applied, consisting of combinations of chicken wire, fence, and netting: (1) chicken wire alone, (2) chicken wire and netting, (3) fencing alone, and (4) fencing and netting (Table 7; Figure 11). In each year, each treatment, including controls, had five replicates (shrubs).

To exclude small mammals, large mammals, and grouse, while allowing for the passage of small birds, chicken wire was erected in a square exclosure around the plants, supported by four metal stakes (Figure 11). All taxa were thought to be excluded when the chicken wire exclosure was paired with bird netting. A square exclosure of 2 x 4 inch metal fencing was meant to exclude only large mammals and grouse, while the fence paired with bird netting was thought to let small mammals pass through but to exclude birds.

In 2013, plots were located between 1335 and 1457 m in elevation (2013 floods restricted access to higher elevations), while elevation ranged from 1755 to 2040 m in 2014. Higher elevations in 2014 allowed for the assessment of whether different taxa at higher elevations had a smaller or greater effect on *Shepherdia canadensis* fruit depletion.

6.2 Analysis of fruit depletion by treatment

The first depletion rate was assumed as zero where all fruit were still on shrubs. In the subsequent time periods, depletion rates were calculated by first calculating change in fruit number by taking fruit number at time t and subtracting fruit number at t–1. This was standardized to depletion rates per day by dividing by the number of days since the beginning of the study for each year. Specifically, the equation for depletion rate was:

$$\text{Depletion Rate} = \frac{\text{Fruit Number}_t - \text{Fruit Number}_{t-1}}{\text{Days since beginning of study}_t - \text{Days since beginning of study}_{t-1}}$$

Because this equation creates negative depletion rates, we multiplied all values by –1 to standardize to a positive depletion rate for ease of interpretation.

To model fruit depletion over time, data were first transformed to approximate a normal distribution. Untransformed fruit numbers were not normally distributed (Shapiro-Francia W' = 0.76), while log transformed data approximated normality (W' = 0.97) (Shapiro & Francia 1972; Royston 1983; Royston 1991). Similarly, depletion rate data were not normally distributed (W' = 0.72), while log transformed data approached normality (W' = 0.95).

For 34 of the 50 study shrubs, final fruit counts in the last observation had not reached zero. Therefore, we extended the depletion data using the last calculated rate of depletion until fruit numbers reached zero. For example, a plant with 6 fruit remaining at the final count and a depletion rate of 2 fruit was extended by four days, three for the fruit number to reach zero, and a further day to reduce the depletion rate to zero.

We assumed depletion rates were non-linear in shape and best represented by a quadratic model of depletion by time (Figure 12). Because of large variations in depletion rates between shrubs, depletion curves did not follow accurately a simple quadratic form. We therefore used a linear model relating the loss of berries (log of berry count) over time (day number since start of experiment in the earliest of the two years [1 to 58]), elevation, and treatment (excluded taxa). An interaction term was also estimated between treatment and time since we expect change in fruit number by time to be affected by treatments where certain exclosures should reduce depletion rates over time. Exclosure treatments were analyzed relative to the control group (no fencing) to assess how much exclosures decreased loss in fruit numbers (depletion).

A one-way ANOVA was used to determine whether fruit numbers in the first time period differed significantly among treatment groups since this may confound results and interpretation of raw fruit numbers. No between-group (treatment) differences were found in the first time period for both with the untransformed and transformed data ($F > 0.56$).

6.3 Results of exclosure treatments

Loss of fruit number by time varied between years with a higher rate of loss in 2013 and overall lower number of fruit with a shallower slope of fruit loss in 2014 (Figure 13). Fruit number in 2013 was related to time ($\beta = –0.06$, $p < 0.001$), wire treatment ($\beta = –0.33$, $p = 0.083$), fence and net treatment ($\beta = –0.42$, $p = 0.028$), interaction between the wire treatment and time ($\beta = 0.01$, $p = 0.036$), and the interaction between time and the fence and net treatment ($\beta = 0.01$, $p = 0.032$) (Table 8). Elevation was not significantly related to fruit depletion in 2013 ($p > 0.8$). Overall the 2013 model explained 66% of the variation in the data ($R^2 = 0.66$). With a greater range of elevation in 2014 (and higher elevations overall), elevation was significantly related to fruit loss ($\beta = 0.003$, $p < 0.001$). As expected, time also predicted the change in fruit number ($\beta = –0.07$, $p < 0.001$), as did the wire treatment ($\beta = –0.82$, $p = 0.004$), the interaction between the wire treatment and time ($\beta = 0.03$, $p = 0.006$), and the interaction between the wire and net treatment and time ($\beta = 0.02$, $p = 0.036$) (Table 8). In 2014, the model explained 68% of the variation in the data ($R^2 = 0.68$).

Chicken wire and net treatment reduced fruit number relative to the control treatment in both years (Figure 14), but this difference was not significant in 2013. In 2014, this difference was accounted for in the interaction term between time and the wire and net treatment (Table 8, $\beta = 0.02$, $p = 0.036$).

Chicken wire alone reduced fruit loss in both years, most visible for 2014 (Table 8; Figure 14). Loss in fruit number over time in 2013 suggests that a small organism capable of passing the barriers effectively harvested berries from the plants in this year. Conversely, in 2014 all treatments had lower overall loss of fruit than the control treatment (Figure 14), although this was only reflected in the model in the wire, and wire and net treatment variables. In 2014, the chicken wire and net and the chicken wire alone were the most effective barriers to fruit loss, followed by the fence and the net treatment, and finally the fence alone (Figure 14).

Camera trap data revealed depletion by chipmunks, red squirrels, juvenile robins, gray jays, and other passerines (data not shown).

6.4 Discussion of patterns in fruit depletion by treatment

Model conditions for depletion rate and fruit number over time are represented in Figure 12 (see Figures section, below). Average fruit loss observed in both 2013 and 2014 (Figure 13) followed the general hypothesized model supporting our predictions (Figure 12). Heavy rains early in 2013 may have accounted for the early spike in depletion rates for that year, while the cold spring in 2014 may explain the later phenology observed in 2014. A number of factors may have affected differences in treatments. First, there may have been differences in rodent or bird densities among shrubs affecting foraging activity around the shrubs. Second, elevation may have changed densities for either rodents or birds, causing differences in treatment effects between the two years (elevations were higher in 2014). Third, phenology of fruit consumers (including recruitment of young) may have caused an interaction between treatment types and time.

7. Use of a reference population at carrying capacity for recovery targets

Although bioenergetics approaches can be used to estimate potential carrying capacity based on food resource supply, as pointed out above, that approach requires knowledge of general consumption rates of food items since not all resources available are consumed or available to grizzly bears if competing with other species (e.g. scramble competition for fruit). To address this challenge, we experimented with use of a reference population that is considered at carrying capacity to relate to background levels of food resource supply that is measured in consistent units (digestible energy) between food items. With a population estimate of grizzly bears for a reference area at carrying capacity, we can relate amount of digestible energy per bear, then use that same relationship in other areas to estimate potential biological carrying capacity. These estimates can then be used to help guide population recovery targets for management of the threatened bear population. Below we describe the approach used and results of this work.

7.1. Study area

Field plots were gathered between 2001 and 2009 in the Hinton to Kakwa region throughout the Grande Cache and Yellowhead population units. In total, 2782 plots (2614 plots for some species) were used for modeling plant occurrence and abundance. The large number of plots represents many years of sampling (Nielsen *et al*. 2003; 2004c; 2010; Roberts *et al*. 2014). Figure 15 illustrates the extent of the study area and the reference area (Willmore, Kakwa, and Rock Lake) used for establishing food supply and bear density estimates.

7.2 Plant species modeling

Predictor variables were included based on previously reported relationships with the grizzly bear food species included in this study (Table 1, Table 2; Nielsen *et al*. 2003; 2004c; 2010). Terrain variables included a compound topographic index (CTI) and a 30-m digital elevation model (DEM). CTI is an index of soil wetness (derived from the 30-m DEM) that is known to correlate with important soil characteristics that influence species distributions. Elevation is often used as a surrogate of climatic variables and has been an important predictor of occupancy and abundance of grizzly bear food species in previous studies. Linear and quadratic forms of CTI and elevation were considered for each species using univariate analysis, and the most-supported form (based on comparisons of Akaike's information criteria) was included in candidate models. A landcover classification derived from an integration of airborne laser scanning data and multispectral satellite imagery (from Nijland *et al*. 2015) was used to develop 14 dummy-coded (0/1) landcover variables. Two additional landcover classes, water and snow/ice, were considered non-habitat and were excluded from analyses. Moderate density conifer forest (mod_con), a common habitat type, was selected for use as a reference category and was withheld from all candidate models that included landcover variables. Pearson correlation (r) tests were used to assess linear predictor variables for collinearity, and only variables with $r \leq |0.7|$ were included in the same models. Interactions terms were included to account for possible variations in species responses to landcover types with changes in elevation. Because the alpine landcover types (alpine herbaceous and alpine barren) were delineated from their counterparts (herbaceous and barren) using a 1700-m elevation cutoff, the inclusion of interactions between landcover and elevation allowed for consolidation of the herbaceous and barren landcover classes (Table 10). Species models consisted of a series of nested models that represented occupancy and abundance (cover) given that it was present.

Occupancy was modeled for 20 grizzly bear food species as a function of terrain and landcover variables (Table 10) using logistic regression (0 – absent, 1 – present). Food species were selected based on reported presence in regional grizzly bear diets (Table 9; Munro *et al*. 2006).

A total of twelve a priori models were evaluated (Table 11) during model selection, and Akaike's information criterion (AIC) was used to identify the top model (given available data and variables included in candidate models) for each species. Perfectly avoided categorical variables (landcover classes) were forced into models to keep sample size consistent for all candidate models which is required for model selection using AIC. Receiver operating characteristic area under the curve (ROC AUC) estimates were used to assess model fit (Table 12). ROC scores between 0.5 and 0.7 indicated low model accuracy, scores ranging from 0.7 to 0.9 indicated moderate model accuracy, and scores greater than 0.9 were indicative of high model accuracy. A geographic information system (GIS) was used to map model estimates for each species. Equalized sensitivity-specificity probability thresholds were then used to determine optimal probability cut-off values for each food species, which were then used to generate binary occupancy maps (0 – absent, 1 – present). Finally, perfectly avoided landcover classes were masked out from binary occupancy rasters to ensure that non-habitat was not identified as suitable habitat (predicted presence).

Abundance (percent cover) was modeled for 18 grizzly bear food species using generalized linear models and the same suite of covariates and *a priori* candidate models that were used to model occupancy (Table 9, Table 10). Percent cover was converted to a proportion and normalized using an arcsine transformation. These values were converted to proportions (ranging from 0.001 to 0.999) using maximums of arcsine-transformed cover proportions. A logit-transformation was then used to bound the range of possible predictions between zero and maximum observed abundance values from field plots. This ensured reasonable estimates across the region avoiding extrapolation of large or small cover estimates for new environmental space. Top models for each food species were selected using AIC scores (Table 13). As with occupancy models, perfectly avoided categorical variables (landcover classes) were forced into models to keep observations consistent between candidate models. Model estimates were mapped in a GIS and back-transformed to obtain estimates of percent cover. These maps were then masked using binary occupancy rasters, along with perfectly avoided landcover classes, to force abundance estimates to zero in non-habitat.

Fruit density (number of fruit per 10 m^2) was modeled for nine fruiting species as a function of abundance (percent cover of plant in plot) and forest stand canopy cover using generalized linear models (Table 14). We hypothesized that species abundance would drive fruit production, and the influence of canopy cover on fruit production is well-documented (Martin 1983; Hamer & Herrero 1987; Hamer 1996; Nielsen *et al*. 2004c). Canopy cover was included in candidate models in both linear and quadratic forms to test for possible non-linear relationships between fruit production and canopy cover. Observed fruit densities (number of fruit per 10 m^2) from field plots were first normalized using a log transformation. These values were converted to proportions (ranging from 0.001 to 0.999) using maximums of log-transformed fruit densities, then logit-transformed to limit the possible range of predictions to those that were observed at field plots and avoid unreasonable fruit density estimates (i.e., negative values, very large values). Model estimates were mapped in a GIS and back-transformed to obtain estimates of fruit density per 10 m^2. Finally, maps of estimated fruit densities were masked with occupancy rasters to ensure fruit densities greater than zero were not predicted in non-habitat.

7.3 Ungulate and ant models

For modeling ungulate matter, we obtained aerial ungulate (goat *Oreamnos americanus*, sheep - *Ovis canadensis*, white-tailed deer - *Odocoileus virginianus*, mule deer - *Odocoileus hemionus*, elk - *Cervus canadensis*, and moose - *Alces alces*) survey data (counts) from the provincial government. Surveys were typically species specific and employed different methodologies such as Stratified Random Block (SRB), Distance Sampling, and complete Coverage), but all species were counted when observed and classified according to established protocols (i.e., male/female, adult/neonate, etc.). The dataset of ungulate counts were derived from 10 different aerial surveys (2007-2013) that occurred within specific management units across the study area and included: 1) winter bighorn sheep range; 2) summer goat range; 3) winter elk range; 4) moose/deer/elk within established WMUs. Counts of ungulates excluding neonates by species were summed at the scale of a SRB grid (~5' latitude x 5' longitude). In a GIS, we determined the quantities of various ungulate habitat attributes for the sampling grid that were associated with terrain (elevation, slope, aspect, and solar radiation), vegetation (Landcover), anthropogenic (cutblocks, linear features, agriculture, and open pit coalmine), and water (streams, lakes, and wetlands). We used logistic and negative binomial or zero-inflated negative binomial regression models to predict the distribution/abundance of ungulate species as a function of underlying habitat, but controlled for the potential effects of survey grid size (ha) and survey methodology (SRB vs. other). We used a purposeful approach to model selection and inference (Hosmer & Lemeshow 2000). For each species, the 'best' model was used to predict ungulate counts across the study area.

Models of ant abundance were similar to those of fruit abundance described above where density of mounds was estimated in the field at plots and transformations used to ensure a consistent range of predictions across the region. We used values from Swenson *et al*. (1999) to represent average dry grams of ants per nest (mounds) at 13 g and dry digestible energy at 4.2 kcal/g.

7.4 Conversion of food resource supply to digestible energy

Methods used to convert abundance of resources to digestible energy follow exactly as described in section 5.1 so they are not repeated here. Briefly, however, the general approach was to convert abundance of items to dry grams and from there convert to digestible energy. For example, ungulate counts were then converted to total biomass (digestible dry matter) by multiplying predictions by values (sex ratio, reproductive success, and summer/fall body mass) obtained from the dataset or from the literature (Mattson 1997; Knopf *et al*. 2010; Table 16). Maps of digestible energy were then produced for the entire region (Grande Cache and Yellowhead). Predictions of general food groups can be seen for ungulates (Figure 16), ants (Figure 17), roots (Figure 18), herbaceous plants (Figure 19), and fruit (Figure 20).

7.5 Nutritional landscape carrying capacity and its limitations

Using a population estimate of 153.8 grizzly bears in the reference area (Alberta Grizzly Bear Inventory Team 2009) and total dry digestible energy from the modeling process described above, potential carrying capacity for the Yellowhead and Grande Cache grizzly bear units were estimated at 26,502 and 32,444 respectively. When excluding food items with the highest spatial variability and potential uncertainty (ants and roots) and further changing total ungulate energy to neonate ungulate energy, carrying estimates were much smaller but still quite large at 1334 and 2359 bears for the Yellowhead and Grande Cache units respectively. Certainly these estimates are unrealistically high suggesting that the current method may be limited by its ability to accurately estimate spatial variation in some of the key resources across the larger region and in particular the use of the current reference area that is substantially different from most of the rest of the population units. Indeed, the reference area had an overall lower number of field plots, as compared to other parts of the study region. This suggests that model predictions may have led to a spatial bias in predictions. In particular, model estimates were most sensitive to four key food resources: ungulates, roots (*Hedysarum alpinum*), ants, and buffaloberry (*Shepherdia canadensis*). The reference area had low average food resource supply of all four of most critical resources (i.e. patch [900 m^2] mean (±SD) kcal for ungulates = 37.4 ±23.9; root = 0.11 ±0.31; ants = 28.1 ±65.5; and buffaloberry = 3.7 ±14.3). Root and fruit (buffaloberry) modeled distribution and abundance seemed reasonable, although total root digestible energy was very high making this parameter very sensitive. Ungulates and ants also strongly affected results and were especially low in total digestible energy for the reference area when compared to other units. For instance, the Yellowhead grizzly bear population unit had average patch kcal for ungulates of 135.2 ±76.8 and 183.8 ±208.4 for ants (Table 17). This is 3.6 and 6.5 times greater predicted resource supply in the Yellowhead than the reference population. Not surprisingly, estimates across all resource items increased population estimates. One item that was influential in total digestible energy for the Yellowhead and Grande Cache units, but was dramatically lower in the reference area, was roots of *Hedysarum alpinum*. Further work is needed to improve models, particularly for ungulates, while further estimates of biomass and energy values are needed to improve or validate root and ant models that had high total food supply. A high amount of ant biomass that rival or exceed ungulate biomass (Table 17, 18) is consistent with observations in Sweden where total available ant biomass of ants exceeded moose biomass (Swenson *et al*. 1999). Seasonal diets of grizzly bears in west-central Alberta is often dominated by ants prior to fruit ripening further supporting the importance of this resource and modeled available energy across the region. The overall high biomass of *Hedysarum alpinum* roots was also consistent with observed diets of bears in these areas where bears selected for this resource in the spring and late fall (Munro *et al*. 2006; Coogan 2012). Indeed, sweetvetch root quality peaks in the spring and late fall (Coogan *et al*. 2012), while bioenergetic macronutrient optimization models suggest that it is a near optimal food item balancing macronutrients (Coogan *et al*. 2014). More work is needed to better understand these resources.

Despite potential limitations in extrapolation from a reference population, mapped resource models show value locally in relating to patterns in bear abundance (see section 5 above) and have value in relating to population and animal-level performance (density, body size, health), especially since these models put everything on a standard currency of digestible energy.

8. Literature Cited

Alberta Environment and Sustainable Resource Development (2010) Status of the grizzly bear (*Ursus arctos*) in Alberta: update 2010. Alberta Wildlife Status Report No. 37 (ed. Fish and Wildlife Division). Alberta Sustainable Resource Development, Edmonton, Alberta, Canada.

Alberta Grizzly Bear Inventory Team (2005) 2004 population inventory and density estimates for the Alberta 3B and 4B grizzly bear management area. Alberta Sustainable Resource Development, Fish and Wildlife Division, Edmonton, Alberta, Canada.

Alberta Grizzly Bear Inventory Team (2009) Grizzly bear population and density estimates for the 2008 DNA inventory of the Grande Cache Bear Management Unit. Alberta Sustainable Resource Development, Fish and Wildlife Division, Edmonton, Alberta, Canada. 36 pages.

Apps CD, McLellan BN, Woods JG & Proctor MF (2004) Estimating grizzly bear distribution and abundance relative to habitat and human influence. *Journal of Wildlife Management* 68:138-152.

Atkinson S & Ramsay M (1995) The effects of prolonged fasting of the body composition and reproductive success of female polar bears (*Ursus maritimus*). *Functional Ecology* 9(4):559-567.

Barboza PS, Parker KL, Hume ID (2009) Integrative wildlife nutrition, Berlin; New York, Springer-Verlag.

Benn B & Herrero S (2002) Grizzly bear mortality and human access in Banff and Yoho National Parks, 1971–1998. *Ursus* 13:213–221.

Bojarska K & Selva N (2012) Spatial patterns in brown bear Ursus arctos diet: the role of geographical and environmental factors. *Mammal Review* 42:120-143.

Boulanger J, McLellan BN, Woods JG, Proctor MF & Strobeck C (2004) Sampling design and bias in DNA-based capture-mark-recapture population and density estimates of grizzly bears. *Journal of Wildlife Management* 68:457-469.

Boulanger J, Cattet M, Nielsen SE, Stenhouse GB & Cranston J (2013) Use of multi-state models to explore relationships between changes in body condition, habitat and survival of grizzly bears *Ursus arctos horribilis*. *Wildlife Biology* 19:274-288.

Boulanger J & Stenhouse GB (2015) The impacts of roads on the demography of grizzly bears in Alberta. *PLoS ONE* 9:e115535.

Boyce MS, Blanchard BM, Knight RR & Servheen C (2001) Population viability for grizzly bears: A critical review. *International Association for Bear Research and Management, Monograph Series* 4:1-45.

Braid ACR & Nielsen SE (2015) Prioritizing sites for protection and restoration for grizzly bears (Ursus arctos) in southwestern Alberta, Canada. *PLoS ONE*, in press.

Burnham KP & Anderson DR (2002) Model Selection and Multimodel Inference: A Practical Information-Theoretic Approach. 2nd Edition. Springer-Verlag, New York, New York, USA.

Coogan, SCP (2012) Getting to the root of the matter: grizzly bears and alpine sweetvetch in west-central Alberta. University of Alberta, MSc Thesis.

Coogan SCP & Raubenheimer D (2015) Might macronutrient requirements influence grizzly bear-human conflict? Insights from nutritional geometry. *Ecosphere*, in review.

Coogan SCP, Nielsen SE & Stenhouse GB (2012) Spatial and temporal heterogeneity creates a "brown tide" in root phenology and nutrition. *ISRN Ecology*, Article ID 618257:1-10.

Coogan SCP, Raubenheimer D, Stenhouse GB & Nielsen SE (2014) Macronutrient optimization and seasonal diet-mixing in a large omnivore, the grizzly bear: a geometric analysis. *PLoS ONE* 9(5):e97968.

Costanza R & Gottlieb S (1998) Modelling ecological and economic systems with STELLA: Part II. *Ecological Modelling* 112:81-84.

Costanza R & Voinov A (2001) Modeling ecological and economic systems with STELLA: Part III. *Ecological Modelling* 143:1-7.

Danner BJ & Joern A (2003) Food resource-mediated impact of predation risk on performance in the grasshopper *Ageneotettix deorum* (Orthoptera). *Oecologia* 137:352–359.

Dunning JB, Danielson BJ & Pulliam HR (1992) Ecological processes that affect populations in complex landscapes. *Oikos* 65:169-175.

Erlenbach JA, Rode KD, Raubenheimer D & Robbins CT (2014) Macronutrient optimization and energy maximization determine diets of brown bears. *Journal of Mammalogy* 95:160-168.

Farley SD & Robbins CT (1995) Lactation, hibernation, and mass dynamics of American black bears and grizzly bears. *Canadian Journal of Zoology* 73:2216-2222.

Felicetti LA, Robbins CT & Shipley LA (2003) Dietary protein content alters energy expenditure and composition of the mass gain in grizzly bears (*Ursus arctos horribilis*). *Physiological and Biochemical Zoology* 76:256-261.

Ferguson SH & McLoughlin PD (2000) Effect of energy availability, seasonality, and geographic range on brown bear life history. *Ecography* 23:193-200.

Fortin JK, Schwartz CC, Gunther KA, Teisberg JE, Haroldson MA, Evans MA & Robbins CT (2013) Dietary adjustability of grizzly bears and American black bears in Yellowstone National Park. *Journal of Wildlife Management* 77:270-281.

Garland Jr T & Carter P (1994) Evolutionary physiology. *Annual Review of Physiology* 56:579-621.

Garshelis DL, Gibeau ML, Herrero S & Gehrt (2005) Grizzly Bear Demographics in and around Banff National Park and Kananaskis Country, Alberta. *Journal of Wildlife Management* 69: 277-297.

Gunther KA, Haroldson MA, Frey K, Cain SL, Copeland J & Schwartz CC (2004) Grizzly bear-human conflicts in the Greater Yellowstone ecosystem, 1992-2000. *Ursus* 15:10-22.

Hamer D (1996) Buffaloberry [*Shepherdia canadensis* (L.) Nutt.] fruit production in fire-successional bear feeding sites. *Journal of Range Management* 49(6):520-529.

Hamer D & Herrero S (1987) Grizzly bear food and habitat in the front ranges of Banff National Park, Alberta. *Bears: Their Biology and Management* 7:199-213.

Hamer D & Herrero S (1987) Wildfire's influence on grizzly bear feeding ecology in Banff National Park, Alberta. *Int Conf Bear Res and Manage*.7:179-186.

Hamer D, Herrero S & Keith B (1991) Food and Habitat Used by Grizzly Bears, *Ursus arctos*, along the Continental Divide in Waterton Lakes National Park, Alberta. *Canadian Field Naturalist* 105:325-329.

Herrero S & Higgins A (2003) Human injuries inflicted by bears in Alberta: 1960-98. *Ursus* 14:44-54.

Hilderbrand GV, Jenkins SG, Schwartz CC, Hanley TA & Robbins CT (1999a) Effect of seasonal differences in dietary meat intake on changes in body mass and composition in wild and captive brown bears. *Canadian Journal of Zoology* 77:1623-1630.

Hilderbrand GV, Schwartz CC, Robbins CT, Jacoby ME, Hanley TA, Aurthur SM & Servheen C (1999b) The importance of meat, particularly salmon, to body size, population productivity, and conservation of North American brown bears. *Canadian Journal of Zoology* 77:132-138.

Hundertmark KJ, Schwartz CC & Stephenson TA (1997) Estimation of body composition in moose. Alaska Department of Fish and Game, Juneau, Alaska, USA.

Illius AW, Tolkamp BJ & Yearsley J (2002) The evolution of the control of food intake. *The Proceedings of the Nutrition Society* 61:465-472.

Jensen K, Mayntz D, Toft S, Clissold FJ, Hunt J, Raubenheimer D & Simpson SJ (2012) Optimal foraging for specific nutrients in predatory beetles. *Proceedings of the Royal Society B* 279:2212-2218.

Johnson CJ, Boyce MS, Schwartz CC & Haroldson MA (2004) Modeling survival: application of the Andersen-Gill model to Yellowstone grizzly bears. *Journal of Wildlife Management* 68:966-978.

Knoff KH, Knoff AA, Kortello A & Boyce MS (2010) Cougar kill rate and prey composition in a multiprey system. *Journal of Wildlife Management* 74:1435-1447

Kohl KD, Coogan SCP & Raubenheimer D (2015) Do wild carnivores forage for prey or nutrients? *BioEssays* 37:701-709.

Landers JL, Hamilton RJ, Johnson AS & Marchington RL (1979) Foods and habitat of black bears in Southeastern North Carolina. *Journal of Wildlife Management* 43:143-153.

López-Alfaro C (2014) Linking energetics of individuals to brown bear populations. PhD Dissertation, University of Alberta.

López-Alfaro C, Robbins CT, Zedrosser A & Nielsen SE (2013) Energetics of hibernation and reproductive trade-offs in brown bears. *Ecological Modelling* 270:1-10.

López-Alfaro C, Coogan SCP, Robbins CT & Nielsen SE (2015) Assessing nutritional parameters of brown bear diets among ecosystems gives insight into differences among populations. *PLoS ONE* 10(6):e0128088.

Mace RD, Waller JS, Manley TL, Ake K & Wittinger WT (1999) Landscape evaluation of grizzly bear habitat in western Montana. *Conservation Biology* 13:367-377.

Mace RD, Waller JS, Manley TL, Lyon LJ & Zuuring H (1996) Relationships among grizzly bears, roads and habitat in the Swan Mountains Montana. *Journal of Applied Ecology* 33:1395-1404.

Martin P (1983) Factors influencing globe huckleberry fruit production in northwestern Montana. *Int Conf Bear Res and Manage*. 5:159-165.

Mattson DJ, Blanchard BM & Knight RR (1991) Food-Habits of Yellowstone Grizzly Bears, 1977-1987. *Canadian Journal of Zoology* 69:1619-1629.

Mattson DJ (1997) Use of ungulates by Yellowstone grizzly bears *Ursus arctos*. *Biological Conservation* 81:161-177.

Mattson DJ, Blanchard BM & Knight RR (1992) Yellowstone grizzly bear mortality, human habituation, and whitebark pine seed crops. *Journal of Wildlife Management* 56:432-442.

Mattson DJ & Merrill T (2002) Extirpations of grizzly bears in the contiguous United States, 1850–2000. *Conservation Biology* 16:1123-1136.

Mattson DJ, Barber K, Maw R & Renkin R (2004) Coefficients of productivity for Yellowstone's grizzly bear habitat. US Geological Survey, Biological Science Report USGS/BRD/BSR-2002-0007, 76 pp.

McLellan BM (2011) Implications of a high-energy and low-protein diet on the body composition, fitness, and competitive abilities of black (*Ursus americanus*) and grizzly (*Ursus arctos*) bears. *Canadian Journal of Zoology* 89:546-558.

McLellan BN & Hovey FW (1995) The diet of grizzly bears in the Flathead River Drainage of Southeastern British-Columbia. *Canadian Journal of Zoology* 73:704-712.

McLellan BN & Hovey FW (2001) Habitats selected by grizzly bears in a multiple use landscape. *Journal of Wildlife Management* 65:92-99.

McLellan BN & Shackleton DM (1988) Grizzly bears and resource-extraction industries: effects of roads on behaviour, habitat use and demography. *Journal of Applied Ecology* 25:451-460.

McLellan BN, Servheen C, Huber D & Group ISBS (2008) *Ursus arctos*. IUCN Red List of Threatened Species. Version 2013.1.

McNab BK (2008) An analysis of the factors that influences the level and scaling of mammalian BMR. *Comparative Biochemistry and Physiology A* 151:5-28.

Merrill T, Mattson DJ, Wright G & Quigley HB (1999) Defining landscapes suitable for restoration of grizzly bears *Ursus arctos* in Idaho. *Biological Conservation* 87:231-248.

Miller SD, Sellers RA & Keay JA (2003) Effects of hunting on brown bear cub survival and litter size in Alaska. *Ursus* 14(2):130-152.

Miller SD, White GC, Sellers RA, Reynolds HV, Schoen JW, Titus K, Barnes VG, Smith RB, Nelson RR, Ballard WB & Schwartz CC (1997) Brown and black bear density estimation in Alaska using radiotelemetry and replicated mark-resight techniques. *Wildlife Monographs* 133:1-55.

Mowat G, Heard DC, Seip DR, Poole KG, Stenhouse G & Paetkau DW (2005) Grizzly *Ursus arctos* and black bear *U. americanus* densities in the interior mountains of North America. *Wildlife Biology* 11:31-48.

Mowat G, Heard DC & Schwarz CJ (2013) Predicting Grizzly Bear Density in Western North America. *PLoS ONE* 8:e82757.

Munro RHM, Nielsen S, Price M, Stenhouse G & Boyce M (2006) Seasonal and diel patterns of grizzly bear diet and activity in west-central Alberta. *Journal of Mammalogy* 87:1112-1121.

Nie Y, Zhang Z, Raubenheimer D, Elser JJ, Wei W & Wei F (2014) Obligate herbivory in an ancestrally carnivorous lineage: the giant panda and bamboo from the perspective of nutritional geometry. *Functional Ecology* 29:26–34.

Niljand W, Coops NS, Nielsen SE & Stenhouse G (2015) Integrating optical satellite data and airborne laser scanning in habitat classification for wildlife management. *International Journal of Applied Earth Observations* 38:242–250.

Nielsen SE, Boyce MS, Stenhouse GB & Munro RHM (2003) Development and testing of phenologically driven grizzly bear habitat models. *Ecoscience* 10:1-10.

Nielsen SE, Herrero S, Boyce MS, Mace RD, Benn B, Gibeau ML & Jevons S (2004a) Modelling the spatial distribution of human-caused grizzly bear mortalities in the Central Rockies ecosystem of Canada. *Biological Conservation* 120:101-113.

Nielsen SE, Boyce MS & Stenhouse GB (2004b) Grizzly bears and forestry I: selection of clearcuts by grizzly bears in west-central Alberta, Canada. *Forest Ecology and Management* 199:51-65.

Nielsen SE, Munro RHM, Bainbridge EL, Stenhouse GB & Boyce MS (2004c) Grizzly bears and forestry II: distribution of grizzly bear foods in clearcuts of west-central Alberta, Canada. *Forest Ecology and Management* 199:67-82.

Nielsen SE, Stenhouse GB & Boyce MS (2006) A habitat-based framework for grizzly bear conservation in Alberta. *Biological Conservation* 130:217-229.

Nielsen SE, Boyce MS, Beyer H, Huettmann F & Stenhouse GS (2008) Can natural disturbance-based forestry rescue a declining population of grizzly bears? *Biological Conservation* 141:2193-2207.

Nielsen SE, Cranston J & Stenhouse GB (2009) Identification of priority areas for grizzly bear conservation and recovery in Alberta, Canada. *Journal of Conservation Planning* 5:38-60.

Nielsen SE, McDermid G, Stenhouse GB & Boyce MS (2010) Dynamic wildlife habitat models: seasonal foods and mortality risk predict occupancy-abundance and habitat selection in grizzly bears. *Biological Conservation* 143:1623-1634.

Nielsen SE (2011) Relationships between grizzly bear source-sink habitats and prioritized biodiversity sites in central British Columbia. *BC Journal of Ecosystems and Management* 12:136-147.

Nielsen SE, Cattet MR, Boulanger J, Cranston J, McDermid GJ, Shafer AB & Stenhouse GB (2013) Environmental, biological and anthropogenic effects on grizzly bear body size: temporal and spatial considerations. *BMC Ecology* 13:31.

Nielsen SE, Coogan SCP, Larsen T & Stenhouse GB (in review) Complementary food resources of carnivory and frugivory affect local abundance of an omnivorous carnivore. *Oikos* (in review).

Northrup JM, Stenhouse GB & Boyce MS (2012) Agricultural lands as ecological traps for grizzly bears. *Animal Conservation* 15:369-377.

Noyce KV & Garshelis DL (1998) Spring weight changes in black bears in northcentral Minnesota: the negative foraging period revisited. *Ursus* 10:521-531.

Oftedal OT, Alt GL, Widdowson EM & Jakubasz MR (1993) Nutrition and growth of suckling black bears (*Ursus americanus*) during their mothers' winter fast. *British Journal of Nutrition* 70:59-79.

Paetkau D (2003) An empirical exploration of data quality in DNA-based population inventories. *Molecular Ecology* 12:1375-1387.

Pease CM & Mattson DJ (1999) Demography of Yellowstone grizzly bears. *Ecology* 80:957-975.

Pritchard GT & Robbins CT (1990) Digestive and metabolic efficiencies of grizzly and black bears. *Canadian Journal of Zoology* 68:1645-1651.

Proctor M, McLellan B, Boulanger J, Apps C, Stenhouse GB & Paetkau D (2010) Ecological investigations of grizzly bears in Canada using DNA from hair, 1995–2005: a review of methods and progress. *Ursus* 21:169-188.

Raine RM & Kansas JL (1990) Black bear seasonal food habits and distribution by elevation in Banff National Park, Alberta. *Bears: Their Biology and Management* 8:297-304.

Raubenheimer D (2011) Toward a quantitative nutritional ecology: the right-angled mixture triangle. *Ecological Monographs* 81:407-427.

Raubenheimer D & Simpson SJ (1997) Integrative models of nutrient balancing: application to insects and vertebrates. *Nutrition Research Reviews* 10:151-179.

Richmond B & Peterson S (1997) An introduction to systems thinking, High Performance Systems Hanover, NH.

Robbins C (1993) Wildlife nutrition and feeding. Academic Press, San Diego.

Robbins CT, Schwartz CC & Felicetti LA (2004) Nutritional ecology of ursids: a review of newer methods and management implications. *Ursus* 15:161-171.

Robbins CT, Fortin JK, Rode KD, Farley SD, Shipley LA & Felicetti LA (2007) Optimizing protein intake as a foraging strategy to maximize mass gain in an omnivore. *Oikos* 116:1675-1682.

Robbins CT, Ben-David M, Fortin JK & Nelson OL (2012) Maternal condition determines birth date and growth of newborn bear cubs. *Journal of Mammalogy* 93:540-546.

Roberts DR, Nielsen SE & Stenhouse GB (2014) Idiosyncratic responses of grizzly bear habitat to climate change based on projected changes in their food resources. *Ecological Applications* 24:1144-1154.

Rode KD & Robbins CT (2000) Why bears consume mixed diets during fruit abundance. *Canadian Journal of Zoology* 78:1640-1645.

Rode KD, Robbins CT & Shipley LA (2001) Constraints on herbivory by grizzly bears. *Oecologia* 128:62-71.

Roever CL, Boyce MS & Stenhouse GB (2008a) Grizzly bears and forestry. *Forest Ecology and Management* 256:1262-1269.

Roever CL, Boyce MS & Stenhouse GB (2008b) Grizzly bears and forestry: I: Road vegetation and placement as an attractant to grizzly bears. *Forest Ecology and Management* 256:1253-1261.

Rogers WH (1993) Regression standard errors in clustered samples. *Stata Technical Bulletin* 13:19-23.

Rothman JM, Raubenheimer D & Chapman CA (2011) Nutritional geometry: gorillas prioritize non-protein energy while consuming surplus protein. *Biology Letters* 7:847–849.

Royston P (1983) A simple method for evaluating the Shapiro-Francia W' test of non-normality. *The Statistician* 32(3): 297.

——— (1991) Estimating Departure from Normality. *Statistics in Medicine* 10(8):1283–1293.

Schmitz OJ (1998) Direct and indirect effects of predation and predation risk in old-field interaction webs. *American Naturalist* 151:327-342.

Shapiro SS & Francia RS (1972) An approximate analysis of variance test for normality. *Journal of the American Statistical Association* 67(337):215–216.

Simpson SJ & Raubenheimer D (2012) The nature of nutrition: a unifying framework from animal adaptation to obesity. Princeton University Press, Princeton, New Jersey, USA.

Simpson SJ, Sibly RM, Lee KP, Behmer ST & Raubenheimer D (2004) Optimal foraging when regulating intake of multiple nutrients. *Animal Behaviour* 68:1299-1311.

Sperfeld E, Martin-Creuzburg D & Wacker A (2012) Multiple resource limitation theory applied to herbivorous consumers: Liebig's minimum rule vs. interactive co-limitation. *Ecology Letters* 15:142-150.

Stoen OG, Zedrosser A, Saebo S & Swenson JE (2006) Inversely density-dependent natal dispersal in brown bears Ursus arctos. *Oecologia* 148:356-364.

Swenson JE, Jansson A, Riig R & Sandegren F (1999) Bears and ants: myrmecophagy by brown bears in central Scandinavia. *Canadian Journal of Zoology* 77:551–561.

Swenson JE, Sandegren F, Brunberg S, Segerström P & Segerstrøm P (2001) Factors associated with loss of brown bear cubs in Sweden. *Ursus* 69-80.

Welch CA, Keay J, Kendall KC & Robbins CT (1997) Constraints on frugivory by bears. *Ecology* 78:105-1119.

Williams RL (2000) A note on robust variance estimation for clustered-correlated data. Biometrics 56:645-646.

Zedrosser A, Steyaert SMJG, Gossow H & Swenson JE (2011) Brown bear conservation and the ghost of persecution past. *Biological Conservation* 144:2163-2170.

Tables and Figures

Table 1: Mean nutritional estimates for buffaloberry fruit (including seed) as a percentage of dry matter (in bold). Standard deviation (SD) and sample size (*n*) are also given. Table adapted from Coogan *et al*. (2014).

	Crude protein (%)	Crude fibre (%)	Ash (%)	Fat (%)	Total dietary fibre (%)	Available carbohydrate (%)
	mean (*SD*) *n*					
1. *Shepherdia* **2.** *canadensis*†	14.4 (3.6) 10	8.8 (1.7) 10	2.7 (0.7) 10	8.3 (1.1) 10	23.9 (2.7) 10	50.7 (6.5) 10
3. *Shepherdia* ***4.*** *canadensis*	19.8 (2.4) 8	10.1 (1.9) 8	3.0 (0.3) 8		26.3 (2.7) 8	

† *Indicates samples that were analyzed at an independent external laboratory*

Table 2: Monthly percent mean nutritional estimates (dry matter), standard deviation (*SD*), and sample size (*n*) of select grizzly bear food samples collected in west-central Alberta, Canada. Instances where standard deviation could not be calculated due to n = 1 are denoted by (-). Table adapted from Coogan *et al*. (2014).

Food item	**Estimate**	**May** **mean (*SD*) *n***	**June** **mean (*SD*) *n***	**July** **mean (*SD*) *n***	**August** **mean (*SD*) *n***	**September** **mean (*SD*) *n***
Cow parsnip (*Heracleum lanatum*)	Crude protein		26.8 (-) 1	15.1 (2.4) 3	9.7 (2.0) 4	
	Ash		12.2 (-) 1	19.9 (2.0) 3	19.5 (3.8) 4	
	Crude fibre		26.6 (-) 1	32.1 (1.9) 3	30.3 (6.9) 4	
	Total dietary fibre		57.1 (-) 1	67.5 (2.6) 3	64.7 (10.3) 4	
	Digestible protein		20.2 (-) 1	9.8 (2.1) 3	5.1 (1.7) 4	
	Digestible dry matter		21.9 (-) 1	7.5 (3.6) 3	11.4 (14.4) 4	
	Digestibly energy		26.2 (-) 1	14.3 (3.0) 3	17.5 (11.9) 4	
Clover (*Trifolium* spp.)	Crude protein	30.5 (-) 1	32.7 (5.6) 2	19.5 (3.5) 7	16.1 (1.5) 8	15.3 (0.9) 3
	Ash		10.0 (-) 1	10.1 (1.2) 6	9.2 (1.3) 5	9.1 (2.3) 2
	Crude fibre	14.7 (-) 1	13.2 (-) 1	26.5 (6.7) 5	29.8 (4.2) 4	29.0 (-) 1
	Total dietary fibre			56.1 (10.1) 5	60.9 (6.8) 4	60.4 (-) 1
	Digestible protein	23.4 (-) 1	25.4 (4.9) 2	13.7 (3.1) 7	10.7 (1.4) 8	10.0 (0.8) 3

	Digestible dry matter			23.3 (14.1) 5	16.6 (9.4) 4	17.3 (-) 1
	Digestibly energy			27.4 (11.7) 5	21.9 (7.8) 4	22.4 (-) 1
Dandelion (*Taraxacum officinale*)	Crude protein	29.8 (-) 1	19.9 (2.2) 4	16.1 (5.4) 2	9.7 (0.7) 3	
	Ash		15.4 (3.7) 4	16.4 (2.5) 2		
	Crude fibre		11.3 (0.8) 4	17.0 (1.3) 2		
	Total dietary fibre		34.9 (1.9) 4	43.6 (2.7) 2		
	Digestible protein	22.8 (-) 1	14.1 (2.0) 4	10.7 (4.7) 2	5.1 (0.6) 3	
	Digestible dry matter		52.8 (2.7) 4	40.7 (3.8) 2		
	Digestibly energy		51.9 (2.2) 4	41.8 (3.2) 2		
Horsetail (*Equisetum arvense*)	Crude protein	26.8 (-) 1	29.6 (-) 1	21.9 (2.2) 2	17.1 (4.3) 3	
	Ash	17.8 (-) 1	15.3 (-) 1	20.3 (1.5) 2		
	Crude fibre	19.4 (-) 1	16.5 (-) 1	22.1 (-) 1		
	Total dietary fibre	47.6 (-) 1		52.4 (-) 1		
	Digestible protein	20.2 (-) 1	22.7 (-) 1	15.8 (2.0) 2	11.6 (3.8) 3	
	Digestible dry matter	35.1 (-) 1		28.5 (-) 1		
	Digestibly energy	37.2 (-) 1		31.7 (-) 1		

Table 3: Set of hypotheses tested, model structure, and descriptions as it relates to testing top-down (mortality) and bottom-up (food resource supply) control in local patterns of grizzly bear abundance.

Hypothesis	*Model structure*	*Description*
Null	Null	No landscape pattern in bear abundance (mean count across study area)
Top-down	Null landscape (session + road density)	Bear abundance affected by sampling time and local patterns in mortality risk/survival (top-down regulation)
Top-down + Bottom-up (single resource – fruit)	Landscape + Fruit	Bear abundance affected by bottom-up regulation due to local variation in fruit abundance + Null landscape model
Top-down + Bottom-up (single resource – meat)	Landscape + Meat	Bear abundance affected by bottom-up regulation due to local variation in meat (ungulate) abundance + Null landscape model
Top-down + Bottom-up (complementary additive resources)	Landscape + Fruit + Meat	Bear abundance affected by the combined effect of fruit and meat (additive effect) + Null landscape model
Top-down + Bottom-up (complementary interactive resources)	Landscape + Fruit + Meat + Fruit×Meat	Bear abundance affected by the combined effect of fruit and meat (multiplicative effect) + Null landscape model

Table 4: Comparison of candidate models that explain local abundance in grizzly bears. Model selection results listing model log likelihoods (LL), model complexity (*K*), Akaike's Information Criteria (AIC), change in AIC (Δ AIC) and overall support (weights) of the models given data and models tested (w_i AIC). Most supported model in bold font.

Model	*Model LL*	*K*	*AIC*	*Δ AIC*	*w_i AIC*
Null model	-407.02	3	820.04	105.99	0.00
Null landscape (session + road density)	-376.84	5	763.68	49.63	0.00
Landscape + Fruit	-368.88	6	749.77	35.71	0.00
Landscape + Meat	-355.49	6	722.97	8.92	0.01
Landscape + Fruit + Meat	**-350.03**	**7**	**714.05**	**0**	**0.72**
Landscape + Fruit + Meat + Fruit$_X$Meat	-350.00	8	716.00	1.95	0.27

Table 5: Model parameters (β and SE) predicting local counts in grizzly bears as a function of sampling time (session), local mortality risk (road density within a 7.44 km moving window), buffaloberry fruit food supply (log10 digestible energy, kcal; 1.69 km radius), and ungulate (meat) food supply (log 10 digestible energy, kcal; 7.44 km radius). Odds ratio change in probability of count for a one unit change in variable (e^β) and a one standard deviation change in that variable (e^βStdX) are presented. Standard errors (SE) are based on cluster sandwich estimates using DNA cell as the cluster.

Model variable	β	SE	e^β	e^βStdX
Sampling session number (season)	-0.364	0.111	0.695	0.688
Mortality risk (road density)	-0.662	0.420	0.516	0.761
Buffaloberry food supply	0.754	0.273	2.125	1.994
Ungulate (meat) food supply	4.080	0.520	59.12	1.998

Table 6: List of critical grizzly bear food resources considered for models of local food supply in the Yellowhead ecosystem, Alberta.

Food Resource	Code	Food type
Shepherdia canadensis (buffaloberry)	SHCA	Fruit
Hedysarum alpinum (alpine sweetvetch)	HEAL	Root
Heracleum lanatum (cow parsnip)	HELA	Herbaceous
Vaccinium membranaceum (huckleberry)	VAME	Fruit
Vaccinium vitis-idaea (lingonberry)	VAVI	Fruit
Vaccinium scoparium (grouse whortleberry)	VASC	Fruit
Equisetum spp. (horsetail)	EQSP	Herbaceous
Trifolium spp. (clover)	TRIF	Herbaceous
Amelanchier alnifolia (saskatoon berry)	AMAL	Fruit
Arctostaphylos uva-ursi (bearberry)	ARUV	Fruit
Fragaria virginiana (strawberry)	FRVI	Fruit
Ribes spp. (currents)	RIBE	Fruit
Rubus idaeus (raspberry)	RUID	Fruit
Taraxacum officinale (dandelion)	TAOF	Herbaceous
Viburnum edule (highbush cranberry)	VIED	Fruit
Hymenoptera; Formicidae (ants)	ANTS	Animal
Ungulates (mostly moose *Alces alces*)	UNGL	Animal

Table 7: Treatment types for *Shepherdia canadensis* animal exclusion trials in 2013-2014 in Kananaskis, Alberta. Exclosures were used to manipulate the taxa of consumers of fruit. For each treatment the size of fencing and assumed taxa that were either included or excluded by treatment are listed.

Treatment	Size	Taxa excluded	Taxa Included
Control	–	None	Small mammals, small birds, large mammals, grouse
Fence	2×4-inch	Large mammals, grouse	Small mammals, small birds
Wire	1-inch	Small mammals, large mammals, grouse	Small birds
Fence and Bird Net	< 1-inch	Small birds, large mammals, grouse	Small mammals
Wire and Bird Net	< 1-inch	Small mammals, small birds, large mammals, grouse	None

Table 8: Model results for *Shepherdia canadensis* exclusion treatments from Kananaskis, Alberta in 2013–2014.

Year	Time (Interval)	Treatment Effects	Elevation
2013	**β** = –0.06, p < 0.001	Wire **β** = –0.33, p = 0.083 Fence and Net **β** = –0.42, p = 0.028 Wire*Time **β** = 0.01, p = 0.036) Fence and Net*Time **β** = 0.01, p = 0.032	N.A. (p > 0.8)
2014	**β** = –0.07, p < 0.001	Wire **β** = –0.82, p = 0.004 Wire*Time **β** = 0.03, p = 0.006 Wire and Net*Time **β** = 0.02, p = 0.036	**β** = 0.003, p < 0.001

Table 9: Species (food resources) used to estimate carrying capacity for grizzly bears in west-central Alberta, Canada.

Food Resource	**Code**	**Feeding Activity**	**Season of Use**
Amelanchier alnifolia (saskatoon)	AMAL	Frugivory	Late summer and fall
Arctostaphylos uva-ursi	ARUV	Frugivory	Spring, late summer,
Empetrum nigrum (crowberry)	ENIG	Frugivory	Late summer and fall
Equisetum spp. (horsetail)	EQUI	Herbivory (grazing)	Spring and summer
Fragaria spp. (strawberry)	FRAG	Frugivory	Late summer and fall
Hedysarum spp. (sweetvetch)	HEDY	Root digging	Spring and fall
Heracleum lanatum (cow parsnip)	HELA	Herbivory (grazing)	Spring and summer
Ribes spp. (gooseberry, currant)	RIBES	Frugivory	Late summer and fall
Rubus idaeus (raspberry)	RUID	Frugivory	Late summer and fall
Shepherdia canadensis	SHCA	Frugivory	Late summer and fall
Taraxacum officinale (dandelion)	TAOF	Herbivory (grazing)	Spring and summer
Trifolium spp. (clover)	TRIF	Herbivory (grazing)	Spring and summer
Vaccinium caespitosum (dwarf	VACA	Frugivory	Late summer and fall
Vaccinium membranaceum	VAME	Frugivory	Late summer and fall
Vaccinium myrtilloides	VAMY	Frugivory	Late summer and fall
Vaccinium scoparium (grouse	VASC	Frugivory	Late summer and fall
Vaccinium vitis-idaea	VAVI	Frugivory	Late summer and fall
Viburnum edule (low-bush	VIED	Frugivory	Late summer and fall
Ants in mounds	ANTS_M	Myrmecophagy	Summer

Table 10: Covariates used to model occupancy and abundance for grizzly bear food resources.

Category	Code	Name	Type	Units	Source
Terrain	cti	Compound topographic index	Continuous	Unitless	30-m digital elevation model
	dem	Digital elevation model	Continuous	Unitless	30-m digital elevation model
Landcover	cls_dec	Closed deciduous forest	Category	Binary (0/1)	Nijland et al., 2015
	cls_mix	Closed mixedwood forest	Category	Binary (0/1)	Nijland et al., 2015
	dns_con	Dense conifer forest	Category	Binary (0/1)	Nijland et al., 2015
	mod_con	Moderate conifer forest	Category	Binary (0/1)	Nijland et al., 2015
	op_con	Open conifer forest	Category	Binary (0/1)	Nijland et al., 2015
	op_dec	Open deciduous forest	Category	Binary (0/1)	Nijland et al., 2015
	op_mix	Open mixedwood forest	Category	Binary (0/1)	Nijland et al., 2015
	shrub	Shrub	Category	Binary (0/1)	Nijland et al., 2015
	wetl_op	Open wetland	Category	Binary (0/1)	Nijland et al., 2015
	wetl_tre	Treed wetland	Category	Binary (0/1)	Nijland et al., 2015
Simplified Landcover	lcsimp_bar	Simplified barren (alpine barren, barren)	Category	Binary (0/1)	Derived from Nijland et al., 2015
	lcsimp_hrb	Simplified herbaceous (alpine herb, herb)	Category	Binary (0/1)	Derived from Nijland et al., 2015

Table 11: Occupancy model AIC scores for grizzly bear food resources.

Model Number	Model Name	Species									
		amal	aruv	emni	equi	frag	hedy	hela	ribes	ruid	shca
0	Null	415.8	2056.6	815.3	3802.7	3482.1	2239.0	1497.1	2495.0	2242.6	2654.7
1	Terrain	404.3	2034.1	616.7	3647.6	3405.1	1838.9	1488.5	2384.2	2090.8	2633.4
2	Landcover	402.1	2039.5	739.8	3681.2	3363.6	2139.0	**1401.0**	2406.6	2112.9	2576.5
3	Terrain + Landcover	**400.7**	2015.2	**607.9**	**3584.8**	3326.6	**1813.7**	1402.5	**2347.7**	1987.6	2571.0
4	Terrain + Landcover + Interactions	401.4	**2004.6**	616.4	3602.8	**3321.7**	1815.0	1415.5	2359.2	**1983.7**	**2570.1**

Table 11 (Continued).

Model Number	Model Name	Species									
		taof	trif	vaca	vame	vamy	vasc	vavi	vied	ants_m	ants_w
0	Null	2551.7	2338.2	2607.5	1637.2	1817.9	646.9	3568.0	2368.2	520.1	1070.8
1	Terrain	2488.8	2263.8	2514.0	1549.7	1602.9	**630.6**	3336.6	2148.0	**494.1**	1073.2
2	Landcover	2383.0	2179.1	2541.6	1571.0	1777.2	648.9	3292.2	2146.5	513.6	**1052.2**
3	Terrain + Landcover	**2288.7**	**2053.7**	2481.2	**1514.2**	**1589.0**	636.2	3141.5	**2032.9**	499.0	1054.3
4	Terrain + Landcover +	2290.2	2056.3	**2478.6**	1526.9	1597.9	640.4	**3108.5**	2045.9	495.1	1070.0

Table 12: Selected statistics for top-ranked food resource occupancy models.

Species	**Prevalence**	***K***	**Model**	**LL**	**AIC**	**Probability**	**ROC**
Amelanchier alnifolia	0.0153	10	261.40	-189.35	400.71	0.0191	0.75
Arctostaphylos uva-ursi	0.1347	26	100.54	-976.32	2004.65	0.1410	0.66
Empetrum nigrum	0.0337	15	183.87	-287.94	607.88	0.0476	0.90
Equisetum spp.	0.4554	16	172.38	-1776.42	3584.83	0.4536	0.67
Fragaria spp.	0.3841	27	96.81	-1633.86	3321.72	0.4076	0.67
Hedysarum spp.	0.1410	16	172.38	-890.85	1813.71	0.1130	0.79
Heracleum lanatum	0.0769	11	250.73	-688.49	1400.97	0.0925	0.71
Ribes spp.	0.1836	16	163.38	-1157.85	2347.70	0.1924	0.68
Rubus idaeus	0.1534	26	100.54	-965.85	1983.70	0.1813	0.76
Shepherdia canadensis	0.1875	26	106.08	-1259.07	2570.14	0.2033	0.65
Taraxacum officinale	0.1748	16	172.38	-1128.35	2288.70	0.2114	0.74
Trifolium spp.	0.1508	16	172.38	-1010.83	2053.66	0.1710	0.76
Vaccinium caespitosum	0.3222	27	96.81	-1212.30	2478.59	0.2184	0.68
Vaccinium membranaceum	0.0874	16	172.38	-741.08	1514.16	0.1110	0.73
Vaccinium myrtilloides	0.1019	15	183.87	-778.52	1589.04	0.1421	0.78
Vaccinium scoparium	0.0268	4	653.50	-311.28	630.56	0.0321	0.64
Vaccinium vitis-idaea	0.3680	27	102.15	-1527.27	3108.54	0.3906	0.75
Viburnum edule	0.1679	15	174.27	-1001.43	2032.87	0.1570	0.76
Ants (mounds)	0.0207	4	653.50	-243.06	494.12	0.0261	0.71

Table 13: Abundance (percent cover) model AIC scores for grizzly bear food resources.

Model Number	Model Name	Species								
		amal	aruv	emni	equi	frag	hedy	hela	ribes	ruid
0	Null	38.06	1100.88	**306.34**	3348.30	2595.86	1048.56	**595.45**	**858.20**	1176.80
1	Terrain	34.65	1091.93	306.44	3307.58	2584.51	1050.59	599.28	861.30	**1165.62**
2	Landcover	**4.08**	1094.54	315.06	3327.91	2573.77	**1043.22**	600.34	870.86	1184.93
3	Terrain + Landcover	•	**1089.88**	318.05	3305.87	**2563.92**	1049.05	603.99	875.09	1175.56
4	Terrain + Landcover + Interactions[a]	•	1092.56	321.52	**3299.63**	2576.05	1055.67	602.07	885.84	1186.89

- Model complexity too low (< 1)

[a] Included interactions between elevation and each landcover class

Table 13: (Continued).

Model Number	Model Name	Species								
		shca	taof	trif	vaca	vame	vamy	vasc	vavi	vied
0	Null	1086.04	1298.98	1243.50	**1354.88**	721.16	906.42	**233.23**	2599.30	**255.00**
1	Terrain	1086.68	**1294.14**	1247.49	1354.89	**711.92**	**897.71**	238.19	2589.13	259.51
2	Landcover	1090.14	1304.55	**1197.82**	1363.85	731.18	911.45	247.69	2564.59	263.99
3	Terrain + Landcover	1090.11	1297.98	1199.81	1362.32	723.88	901.83	251.32	**2556.10**	269.15
4	Terrain + Landcover + Interactions[a]	**1082.77**	1311.90	1208.12	1374.84	735.80	909.42	266.30	2562.77	283.05

[a] Included interactions between elevation and each landcover class

Table 14: Selected statistics for top-ranked food resource abundance (percent cover) models.

Species	**n**	***K***	**Model Complexity**	**LL**	**AIC**
Amelanchier alnifolia	8	5	1.60	2.96	4.08
Arctostaphylos uva-ursi	349	15	23.27	-529.94	1089.88
Empetrum nigrum	75	1	75.00	-152.17	306.34
Equisetum spp.	1249	27	46.26	-1622.81	3299.63
Fragaria spp.	1002	16	62.63	-1265.96	2563.92
Hedysarum spp.	381	12	31.75	-509.611	1043.22
Heracleum lanatum	205	1	205.00	-296.73	595.45
Ribes spp.	369	1	369.00	-428.10	858.20
Rubus idaeus	390	5	78.00	-577.811	1165.62
Shepherdia canadensis	346	27	12.81	-514.38	1082.77
Taraxacum officinale	467	3	155.67	-644.07	1294.14
Trifolium spp.	412	12	34.33	-586.91	1197.82
Vaccinium caespitosum	519	1	519.00	-676.44	1354.88
Vaccinium membranaceum	239	3	79.67	-352.96	711.92
Vaccinium myrtilloides	280	3	93.33	-445.85	897.71
Vaccinium scoparium	69	1	69.00	-115.61	233.23
Vaccinium vitis-idaea	954	14	68.14	-1263.05	2556.10
Viburnum edule	81	1	81.00	-126.50	255.00

Table 15: Fruit model AIC scores for selected grizzly bear food resources.

Model Number	Model Name	Species			
		ribes	ruid	shca	vied
0	Null	1135.31	1405.83	1412.87	1072.19
1	Abundance[a]	**1127.75**	1285.73	1389.42	**1067.65**
2	Canopy Cover	1137.04	**758.21**	1413.07	1074.06
3	Canopy Cover + Canopy Cover^2	1137.23	758.33	1402.77	1075.87
4	Abundance + Canopy Cover	1129.50	1287.73	1390.60	1069.40
5	Abundance + Canopy Cover + Canopy Cover^2	1130.87	1289.23	**1378.57**	1071.39

[a] "Abundance" refers to percent cover of the species at any given site.

Table 16: Conversion of ungulate counts to total biomass (digestible dry matter) based on predictions by values (sex ratio, reproductive success, and summer/fall body mass) obtained from the dataset or from the literature.

	Species					
Measure	**Moose**	**Elk**	**Mule deer**	**White-tailed deer**	**Sheep**	**Goat**
Proportion of adults	n/a	n/a	n/a	n/a	0.78[a]	0.82[b]
Proportion of females	0.77[c]	0.88[c]	0.72[c]	0.81[c]	0.56[d]	0.66[b]
Reproductive rate	0.74[e]	0.79[f]	0.85[g]	1.00[h]	0.86[i]	0.5[j]
Twinning rate	0.15[e]	n/a	1.8[g]	2.08[h]	n/a	0.02[j]

[a] Festa-Bianchet et al., 1996 - Proportions based on the number of male and female (plus 18% removal of females) bighorn sheep ≥2yrs of age captured/observed at Ram Mountain, Alberta, 1973-1985.

[b] Festa-Bianchet et al., 1994 - Proportions based on the number of mountain goats ≥2yrs of age at Caw Ridge, Alberta, 1988-1993.

[c] Proportions, excluding sheep and goat, calculated from count data used in this study.

[e] Schwartz, 1992 - Reproductive rate proportion based on mean yearling and adult (≥2yrs) fecundity rates (calves/adult female) of a population near carrying capacity.

[f] Hebblewhite and Merrill, 2011 - Proportion based on mean pregnancy rates of subadult/adult (>1.5yrs) elk determined from PRS-B testing at Banff National Park, Alberta, 2002-2005.

[g] Anonymous, 1989

[h] Anonymous, 1995

[i] Festa-Bianchet, 1998 - Proportion based on the age-specific (≥ 2yrs) mean percent of lactating bighorn sheep females at Sheep River, Alberta, 1981-1985.

[j] Festa-Bianchet et al., 1994 - Reproductive rate proportion based on the number of kids produced by female mountain goats ≥2yrs of age at Caw Ridge, Alberta, 1988-1993.

Table 17: List of estimated (mean, SD and total) dry digestible energy (kcal) for the Reference Population (Willmore, Kakwa, Rock Lake). The percent of total provides easier comparisons among food items. Note the predicted strong affect ants, ungulates, and buffaloberry relative to the abundance of other items in this region.

Group	Species	Mean	SD	DDE (kcal)	%
Herbaceous	EQUI	0.00	0.01	1.10E+04	0.00
	TAOF	0.05	0.17	3.04E+05	0.07
	TRIF	0.30	1.27	1.88E+06	0.43
Roots	HEAL	0.11	0.31	7.06E+05	0.16
Fruit	FRVI	0.04	0.11	2.34E+05	0.05
	RIBE	0.04	0.12	2.35E+05	0.05
	RUID	0.02	0.09	9.76E+04	0.02
	SHCA	6.71	25.74	2.22E+07	5.03
	VAME	0.64	0.78	4.01E+06	0.91
	VAMY	0.01	0.08	4.50E+04	0.01
	VASC	0.17	0.15	1.06E+06	0.24
	VAVI	0.54	1.17	3.34E+06	0.76
	VIED	0.06	0.20	3.74E+05	0.08
Insects	Ants	63.38	147.52	1.75E+08	39.62
Animal matter	Ungulates	37.361	23.851	2.33E+08	52.57

Table 18: List of estimated (mean, SD and total) dry digestible energy (kcal) for the Yellowhead and Grande Cache population units. Total energy among units differs partly due to differences in sizes of population units. The percent of total per area and mean/SD provide easier comparisons among units. Note the strong affect of HEAL (*Hedysarum alpinum*).

		Yellowhead Population Unit				*Grande Cache Population Unit*			
Group	Species	Mean	SD	DDE (kcal)	%	Mean	SD	DDE (kcal)	%
Herbaceous									
	EQUI	0.02	0.05	4.79E+05	0.001	0.04	0.10	2.28E+06	0.00
	HELA	0.14	0.33	4.28E+06	0.006	0.29	0.44	1.55E+07	0.01
	TAOF	0.16	0.33	4.91E+06	0.006	0.19	0.36	1.01E+07	0.01
	TRIF	0.79	2.12	2.44E+07	0.032	1.05	2.56	5.60E+07	0.03
Roots									
	HEAL	2236.0	4003.0	6.93E+10	90.94	1464.6	3462.4	7.84E+10	46.95
Fruit									
	FRVI	0.13	0.18	3.95E+06	0.005	0.17	0.19	9.05E+06	0.01
	RIBE	0.10	0.17	3.18E+06	0.004	0.18	0.20	9.75E+06	0.01
	RUID	0.11	0.23	3.42E+06	0.004	0.23	0.31	1.24E+07	0.01
	SHCA	4.78	9.71	7.90E+07	0.104	4.49	11.54	1.28E+08	0.08

VAME	0.38	0.64	1.17E+07	0.015	0.37	0.62	1.95E+07	0.01
VAMY	0.33	0.64	1.02E+07	0.013	0.48	0.74	2.55E+07	0.02
VASC	0.08	0.13	2.48E+06	0.003	0.07	0.13	3.71E+06	0.00
VAVI	0.88	1.25	2.74E+07	0.036	0.84	1.23	4.47E+07	0.03
VIED	0.20	0.34	6.24E+06	0.008	0.40	0.39	2.12E+07	0.01
Insects								
Ants	183.77	208.04	2.53E+09	3.32	276.16	218.43	6.57E+09	3.93
Animal matter								
Ungulates	135.16	76.81	4.19E+09	5.50	147.82	97.50	7.98E+09	4.78

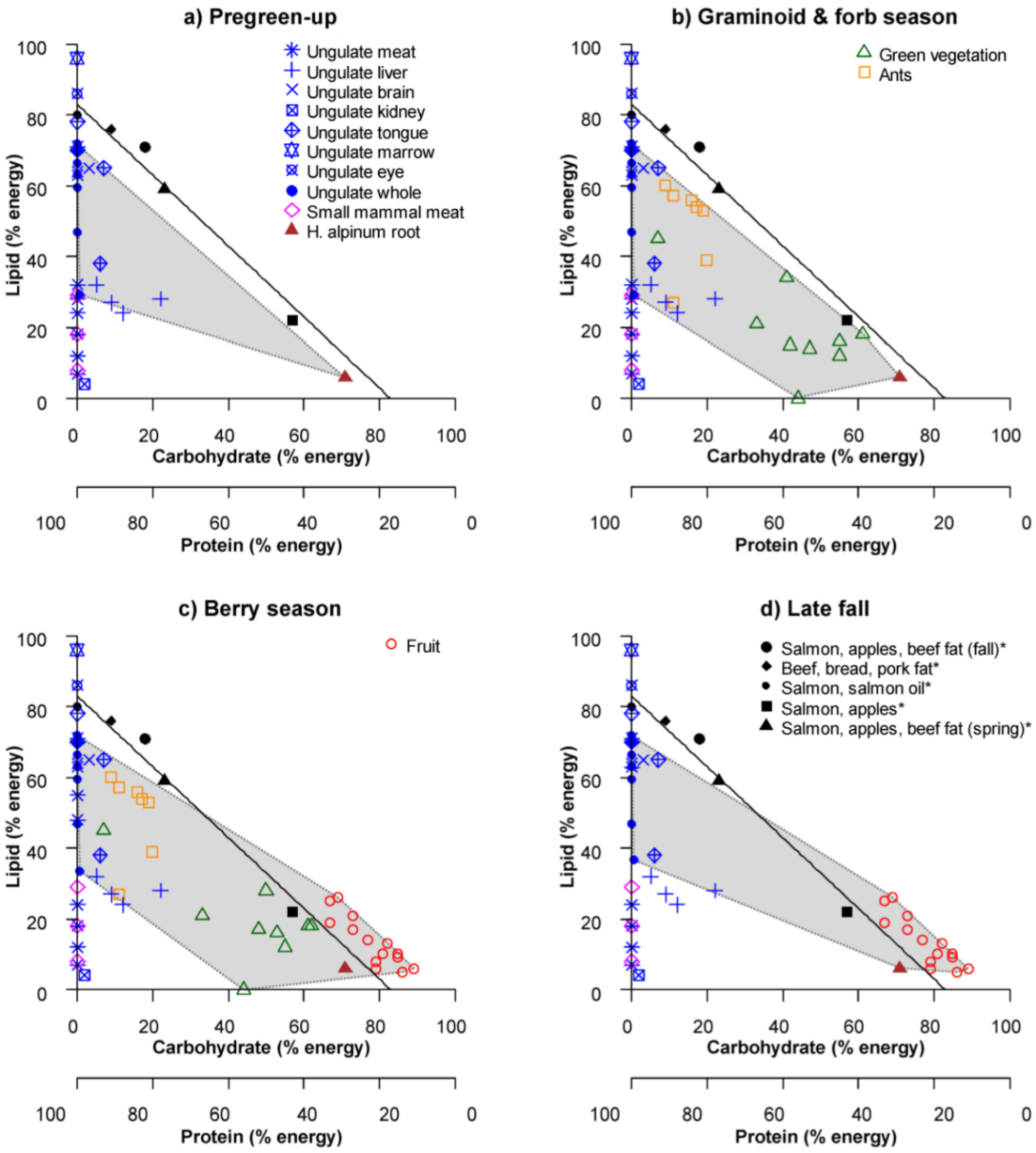

Figure 1: Right-angled mixture triangle illustrating macronutrient content of seasonally available foods consumed by grizzly bears in west-central Alberta, given as a percentage of metabolizable energy. In these figures, overlap between the shaded nutrient space polygon and the intake target (17% protein: 83% non-protein macronutrients) line (black line with a slope of -1) indicates that an optimal diet may be achieved. The closer an individual food point is to the intake target, the closer to optimally balance in its protein to non-protein energy. Food combinations shown in black (Figure 1d) are the point in nutrient space self-selected by captive bears (Erlenbach *et al*. 2014). Figure from Coogan *et al*. (2014).

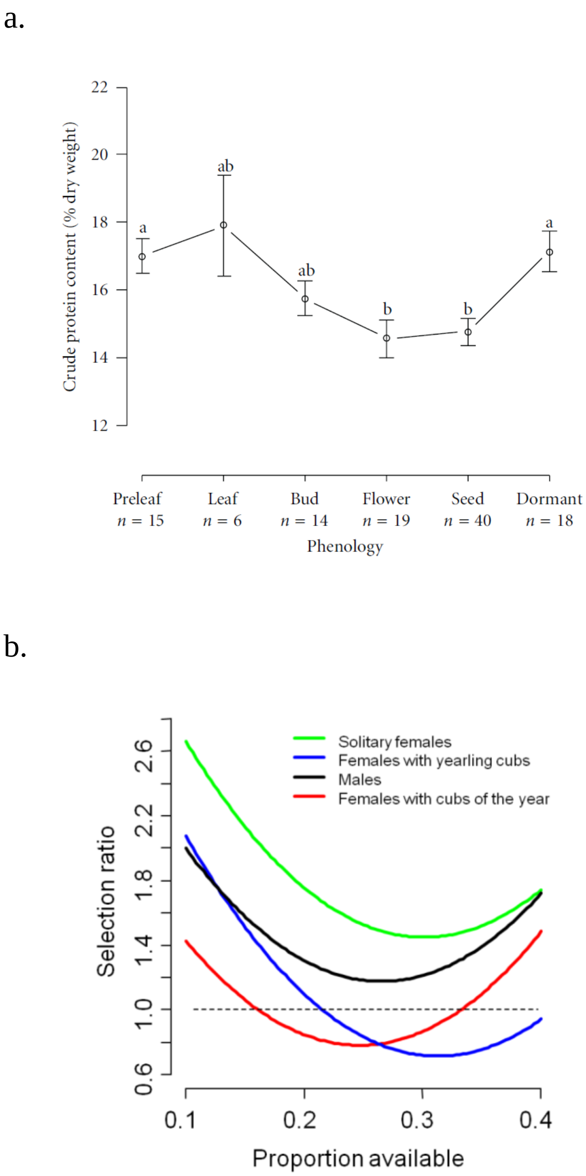

Figure 2: (a) Average crude protein content (% dry matter basis) of *Hedysarum alpinum* roots in west-central Alberta in different phenological stages. Error bars are 1 SE. Lower case letters indicate phenophases with significantly different levels of crude protein by phenophase. (b) Selection ratios of *Hedysarum alpinum* habitat as a function of proportion of habitat available by grizzly bears of different sex-dependency classes in the subalpine and alpine regions of west-central Alberta. Selection ratios above the dashed line (> 1) indicate selection, while those below the dashed line (< 1) indicate avoidance. Figures from Coogan *et al*. (2012) and Coogan (2012).

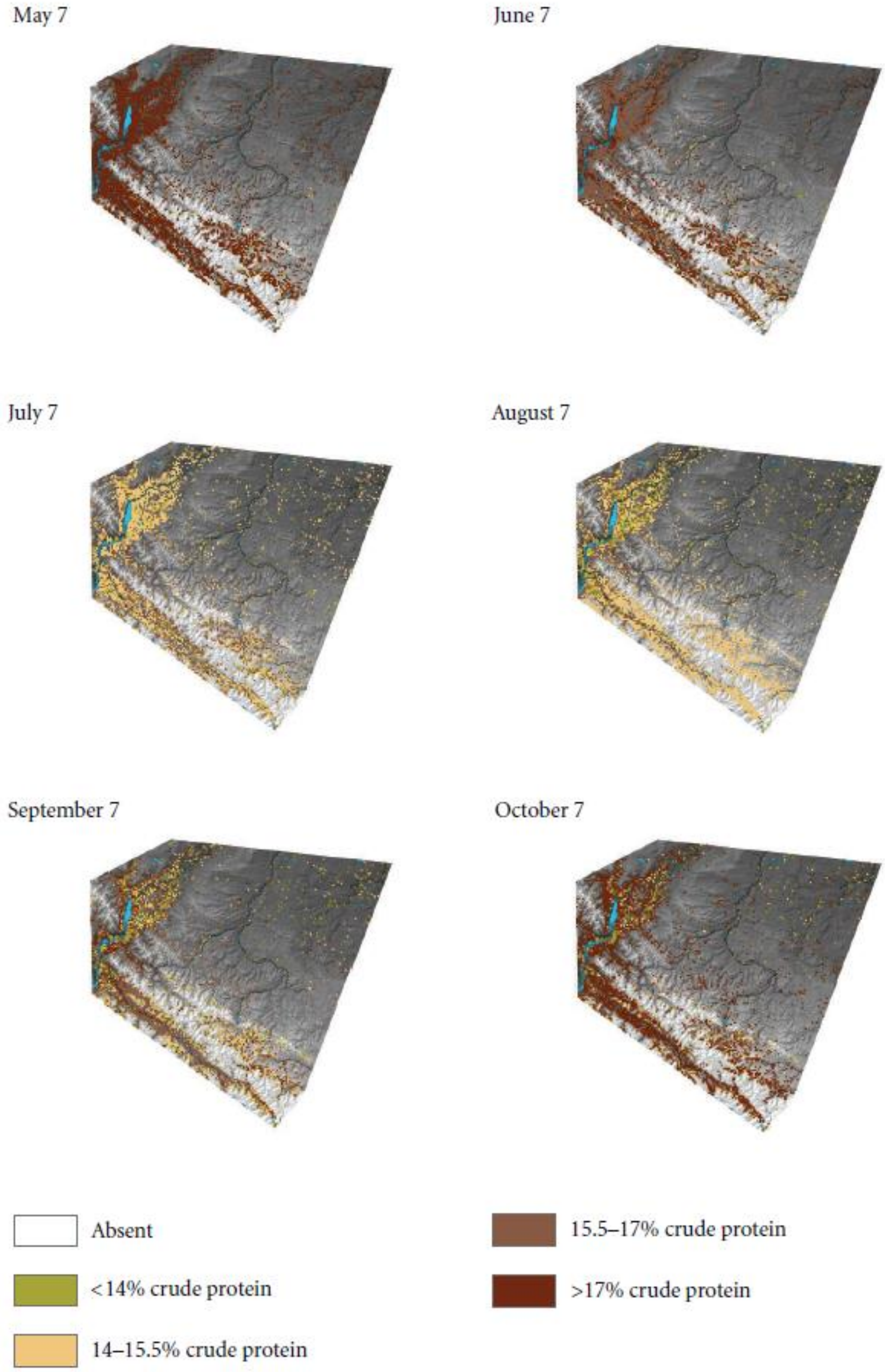

Figure 3: Nutritional landscape maps demonstrating "brown tide" patterns in west-central Alberta, Canada, by predicting the percent crude protein content of alpine sweetvetch (Hedysarum alpinum) roots from7 May to 7 October. Figure from Coogan *et al*. (2012).

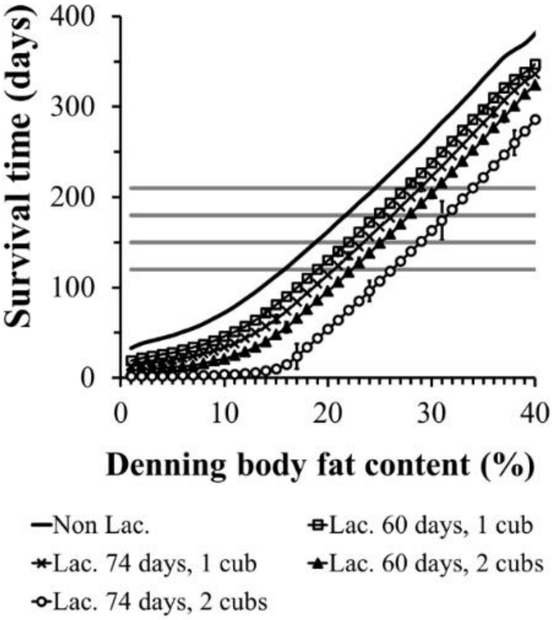

Figure 4: Estimated survival time for bears having different denning body fat content and experiencing different reproductive strategies. Lines represent the number of days before 30% of lean mass loss is reached (survival threshold). Initial body lean mass was 100 kg. Bars are three times SD. Horizontal grey lines represent a different length of hibernation (120, 150, 180 and 210 days). Figure from López-Alfaro *et al*. (2013).

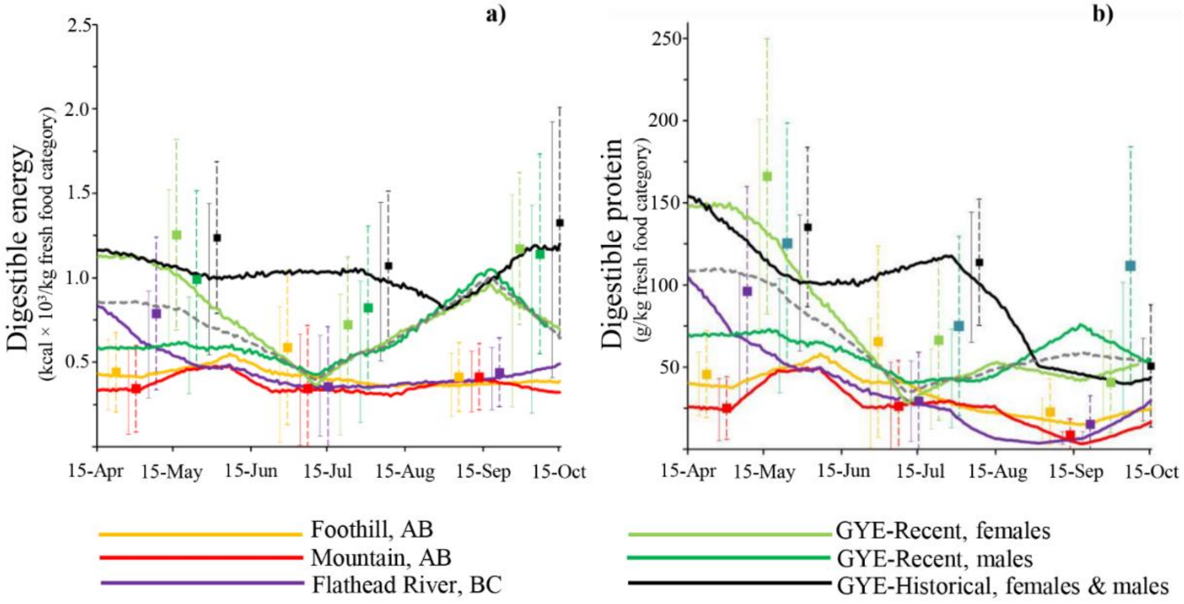

Figure 5: (a) Digestible energy (kcal) and (b) digestible protein (g) in one kilogram fresh grizzly bear diet across different 'interior' ecosystems in western North America. Ecosystem diets include the "Foothills" and "Mountains" of west-central Alberta (Canada), "Flathead" river drainage in southeast British Columbia (Canada) and the Greater Yellowstone Ecosystem (GYE, USA). For the GYE, we present the recent diets for both female ("GYE-Recent, female") and male ("GYE-Recent, male"), the average recent diet ("GYE-Recent"), and the historical diet "GYE-Historical, females & males" diets. Digestible energy and protein were estimated based on the proportion of digestible dry matter intake obtained from food habit studies in these ecosystems (e.g., Fortin *et al*. 2013; Mattson *et al*. 1991; McLellan & Hovey 1995; Munro *et al*. 2006) with fixed correction factors (CFs). Nutritional values were obtained randomly for a normal distribution curve estimated from the average and SD. Squares and dashed bars represent the results (average and ±1.96×SD) when CFs were allowed to vary (Table 1). Figure from López-Alfaro *et al*. (2015).

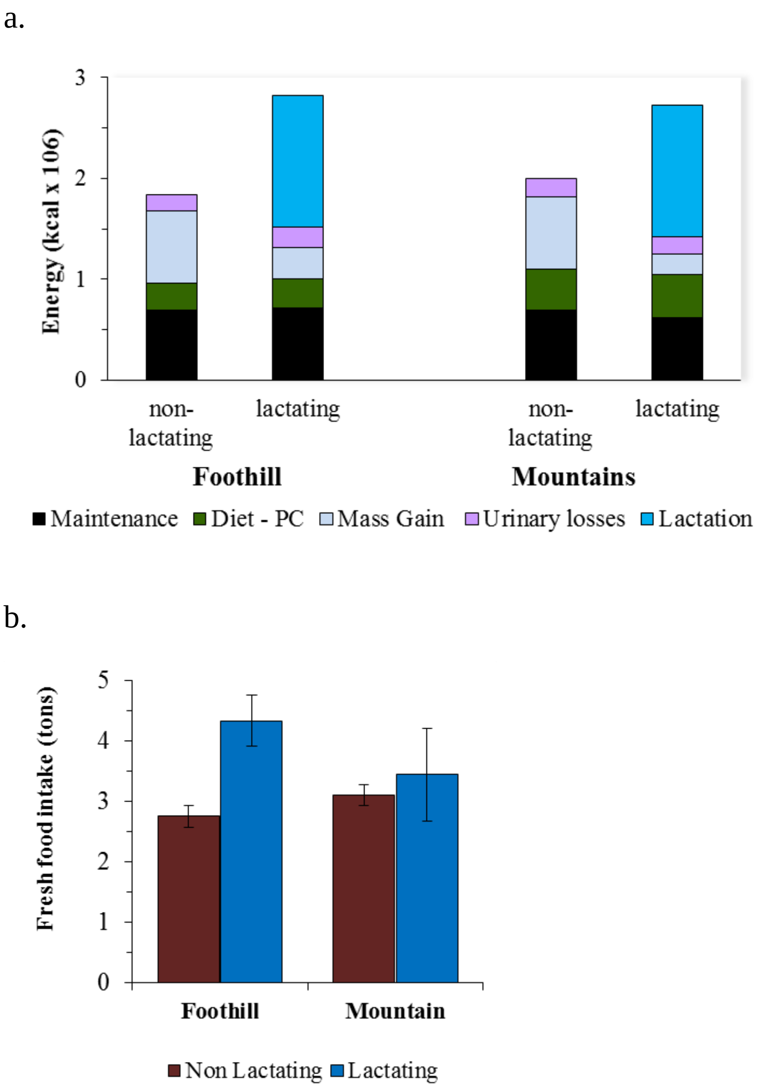

Figure 6: (a) Energy requirements for non-lactating and lactating bears under different diets. Energetic requirements are measure during the active period. Maintenance includes basic metabolic rate and activity cost in captivity. Diet represents the increase in maintenance cost due to the dietary protein content. Urinary losses are based on energy intake. Gain represents energy content of the lean and mass gain during the active period. Lactation represents the energy cost of milk production. (b) Food intake necessary to supply the energetic requirements of non-lactating and lactating females. Food intake resembles food habits of bears in the Foothill and Mountain ecosystems of Alberta. Figures from López-Alfaro *et al*. (In prep).

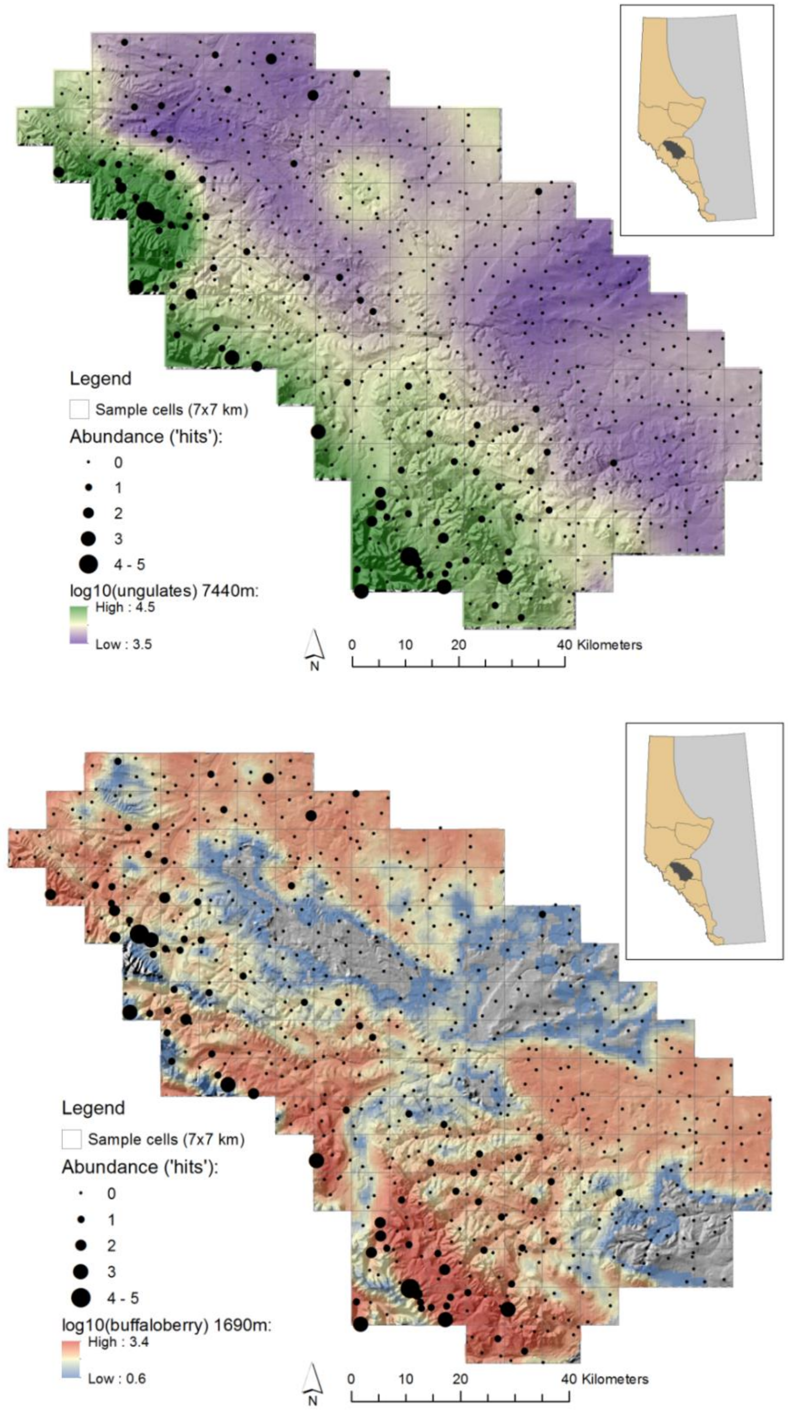

Figure 7: Patterns of grizzly bear abundance and predicted digestible energy for the two most dominant food resources: (a) ungulates (above) and (b) buffaloberry fruit (below) in the Yellowhead ecosystem, Alberta, Canada.

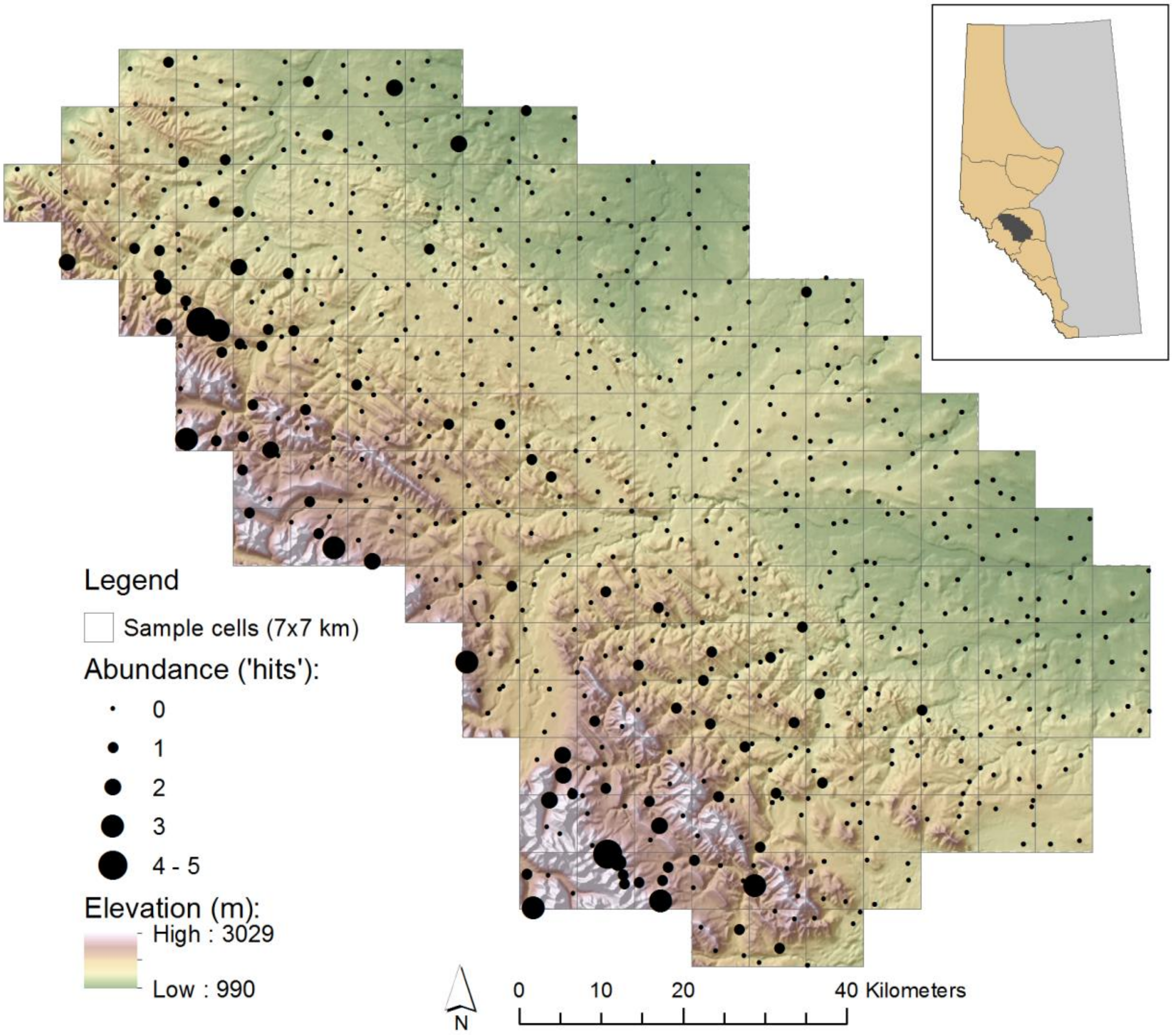

Figure 8: Location and terrain (elevation) of the Yellowhead grizzly bear study area in west-central Alberta, Canada illustrating DNA hair-snag sampling design (7x7km grid), location of hair-snag sites and number of unique grizzly bears detected at a site (size of points) in 2004. Inset map shows location of study area (gray) with respect to current grizzly bear range (orange) within the Province of Alberta.

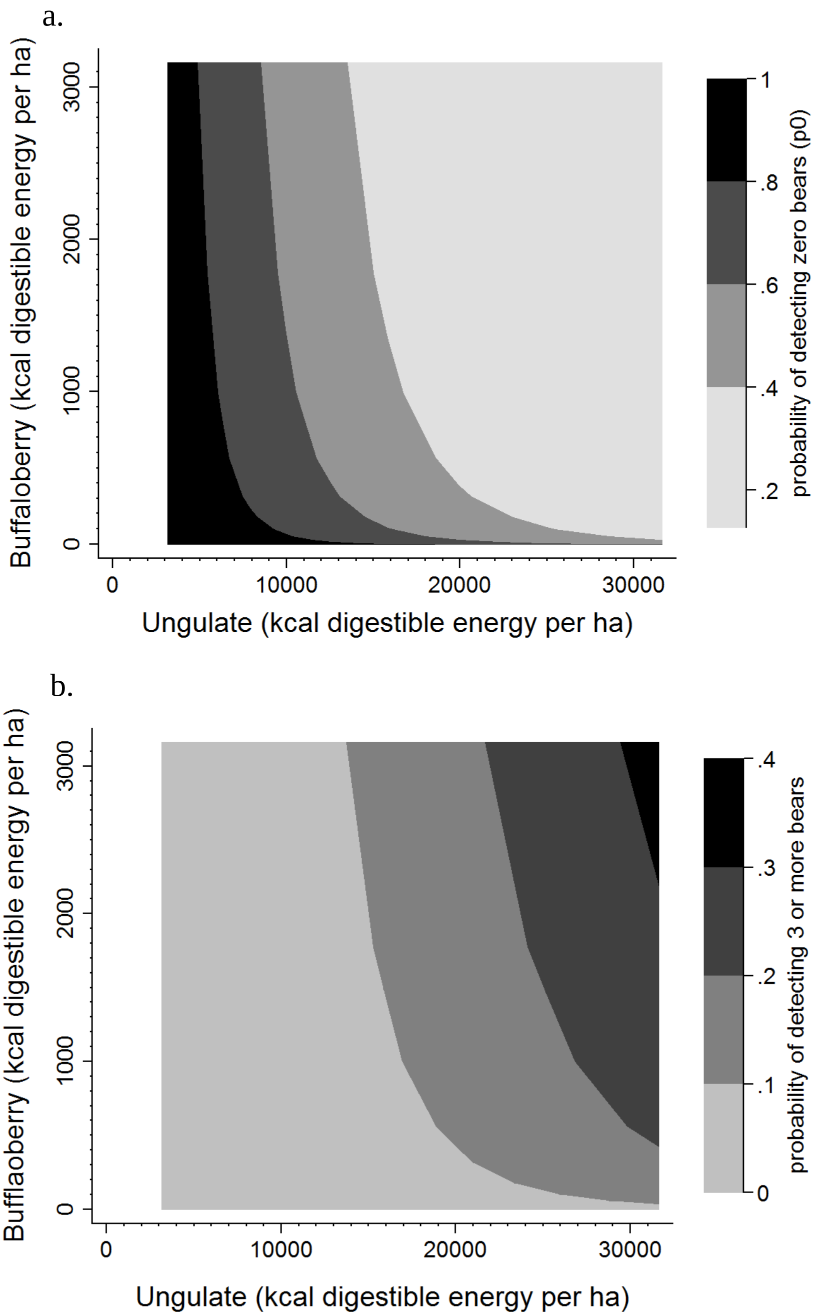

Figure 9: Predicted local abundance of grizzly bears as a function of trade-offs in available digestible energy (per ha) in ungulate and buffaloberry fruit resources. Model assumes no local roads (road density = 0) and the time of sampling being the first sampling session. Probability that a site has no grizzly bears (a.) and a count of ≥3 bears (b.) is illustrated as filled contours.

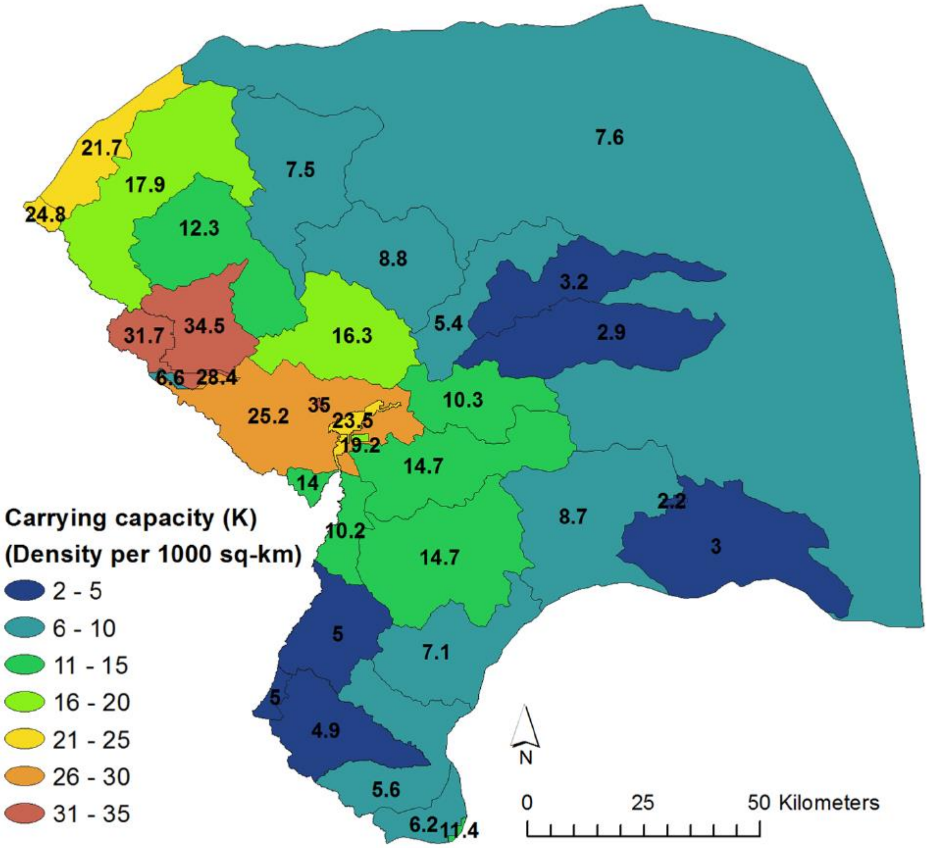

Figure 10: Predicted carrying capacity (*K*) of grizzly bear recovery zones for the Yellowhead ecosystem of Alberta using nutritional landscape models of kcal for critical grizzly bear foods, estimated consumption rates, and total annual bioenergetic needs.

Figure 11: Types of exclosures erected around *Shepherdia canadensis* shrubs in Kananaskis, Alberta, over a two-year study assessing exclusion of frugivorous animals. Photos: (a) Fence treatment; (b) Chicken wire treatment; (c) Combination of fence and netting; and (d) Combination of chicken wire and bird netting. The mist-netting (c and d) is not visible in the pictures.

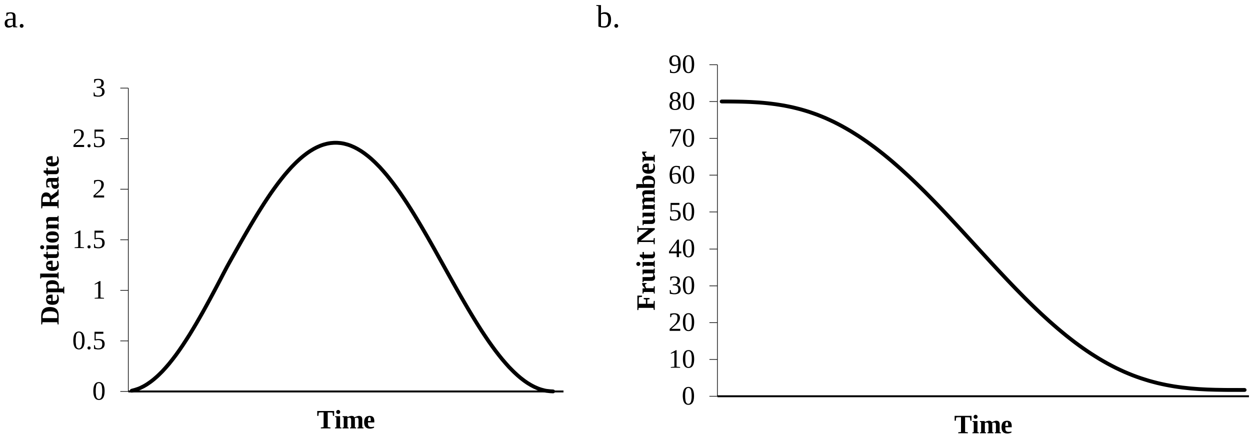

Figure 12: *A priori* model predicting depletion rate (a) and number of fruit (b) by time (mean number of fruit per shrub was 80).

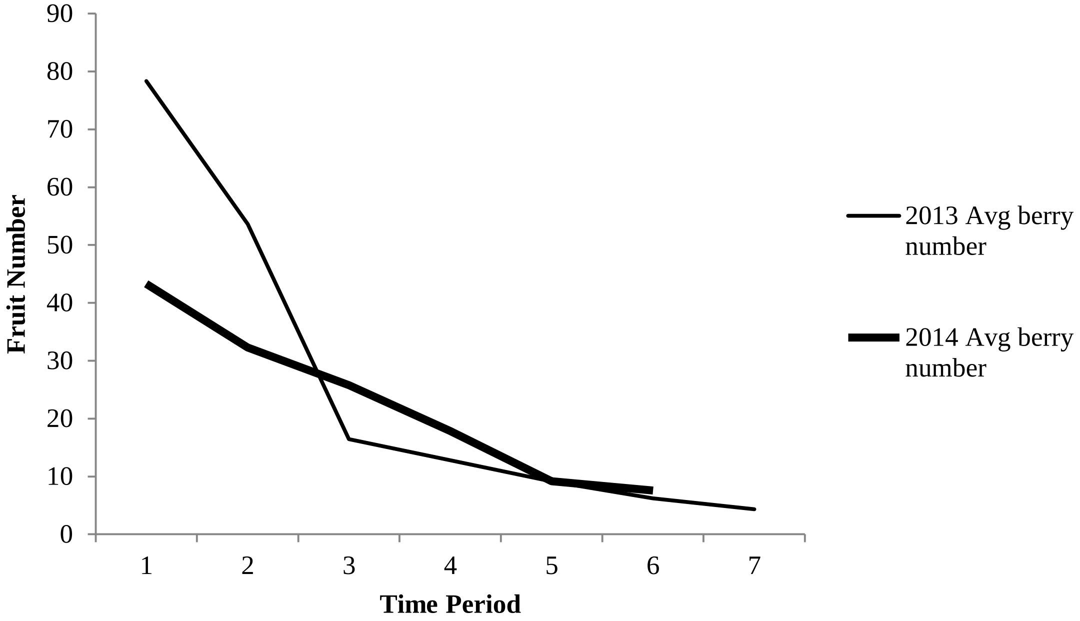

Figure 13: Average fruit number at seven subsequent time periods in 2014 and six in 2013.

a.

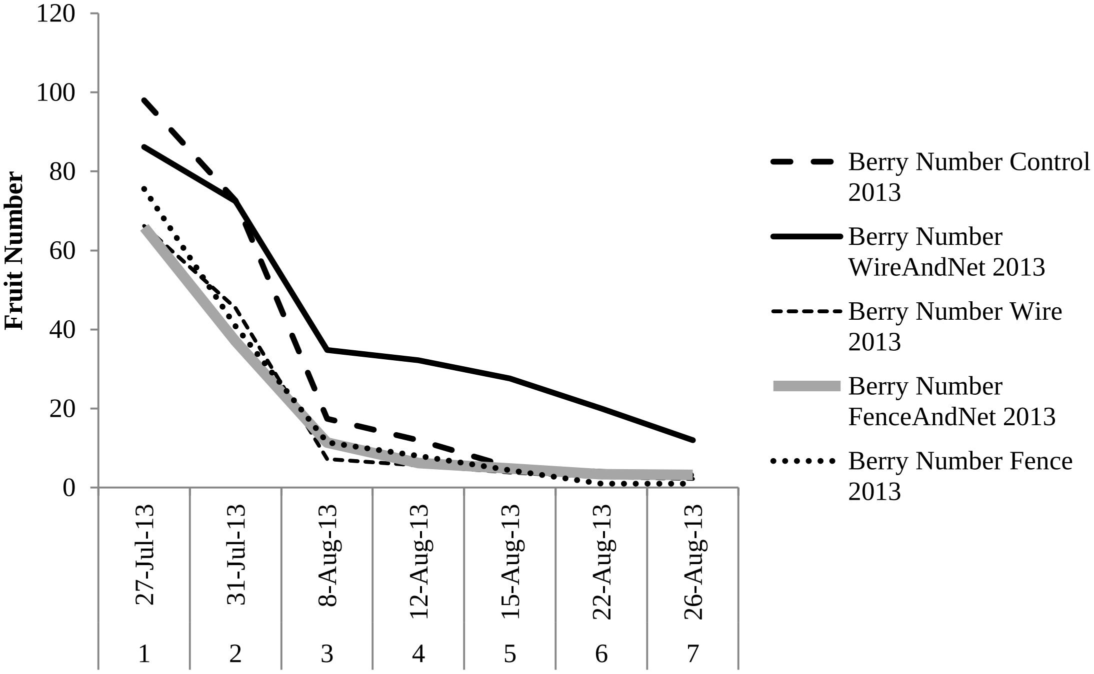

b.

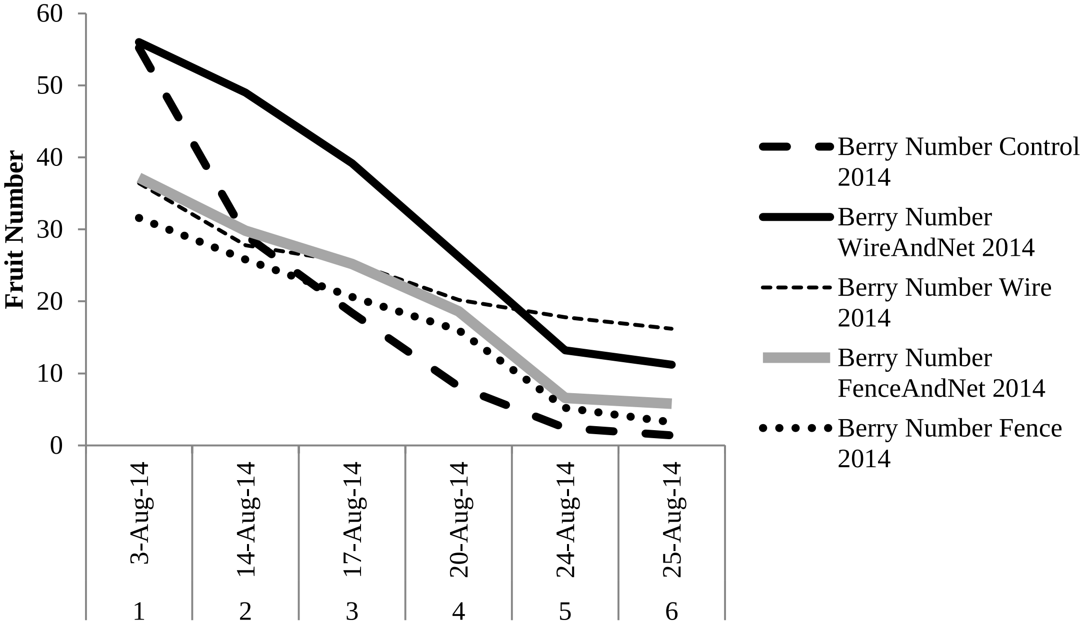

Figure 14: Loss of fruit in exclosure and control treatments by year (a. 2013; b. 2014).

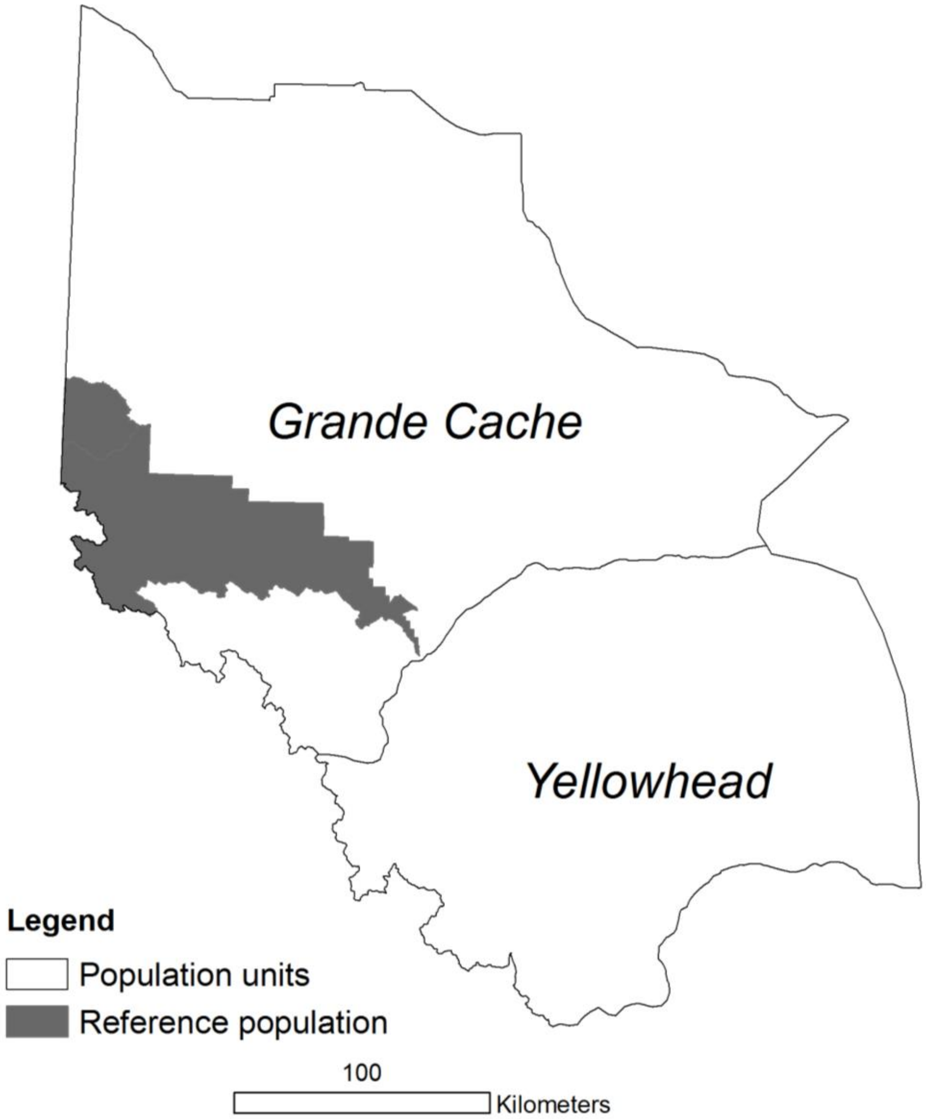

Figure 15: Study area for nutritional landscape estimates of carrying capacity using a reference population (in gray). Reference population represents Alberta Park sites in the foothills and mountains of the Grande Cache unit (Willmore Wilderness, Kakwa Wilderness, Rock Lake) where bear densities are highest.

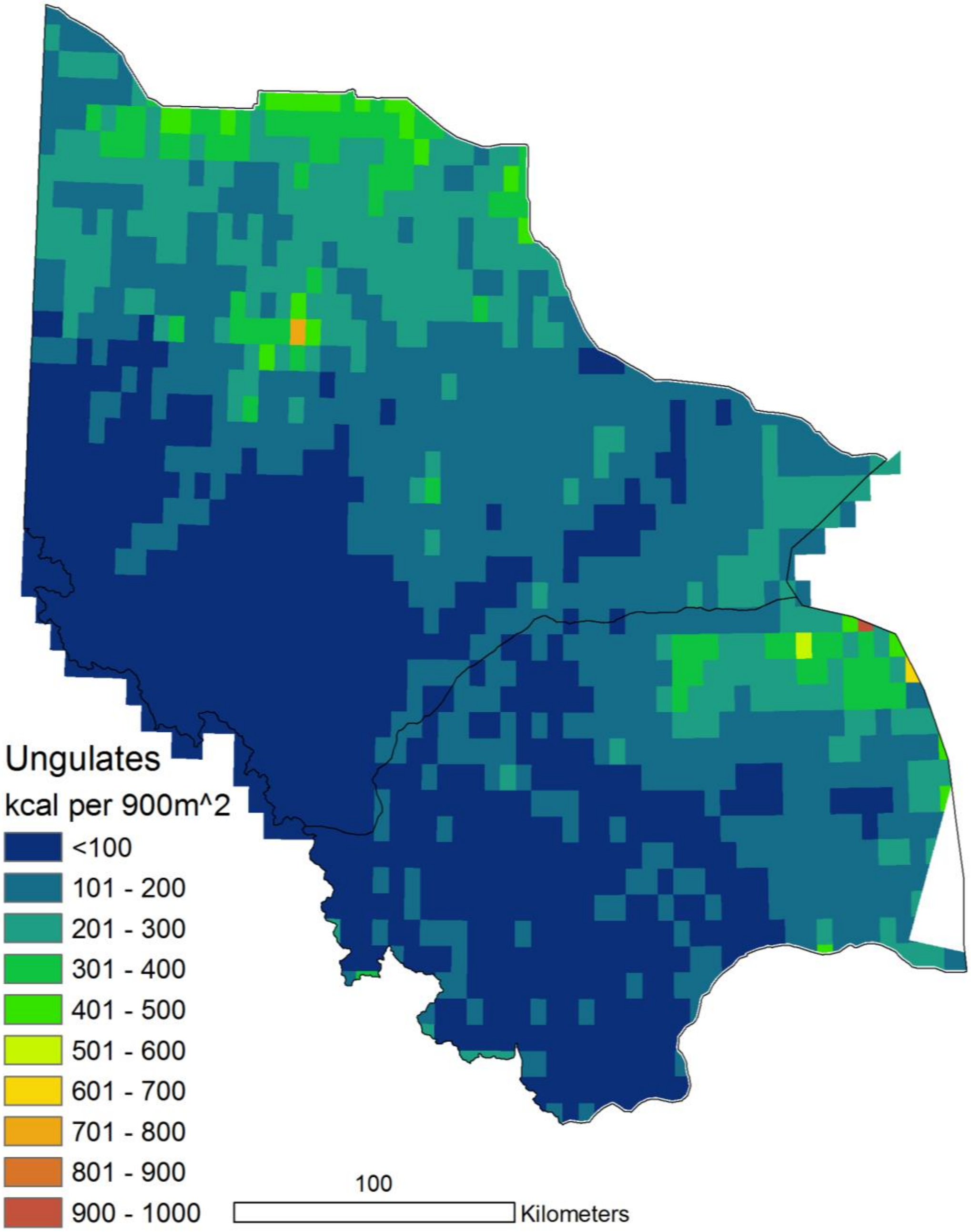

Figure 16: Digestible energy of ungulate matter in the Grande Cache and Yellowhead population units. Scale of 900 m^2 (30x30m) represents the resolution of other modelled food items (herbaceous, fruit, roots, and ants).

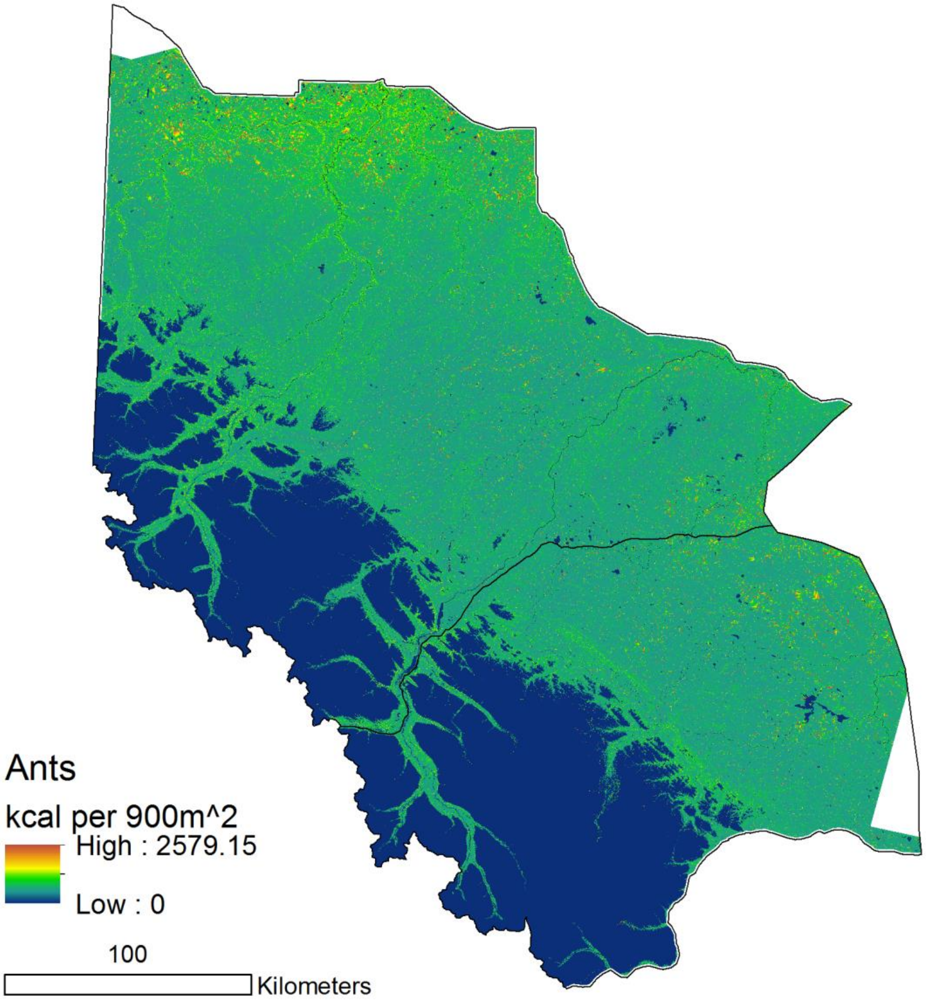

Figure 17: Digestible energy of ant matter in the Grande Cache and Yellowhead population units.

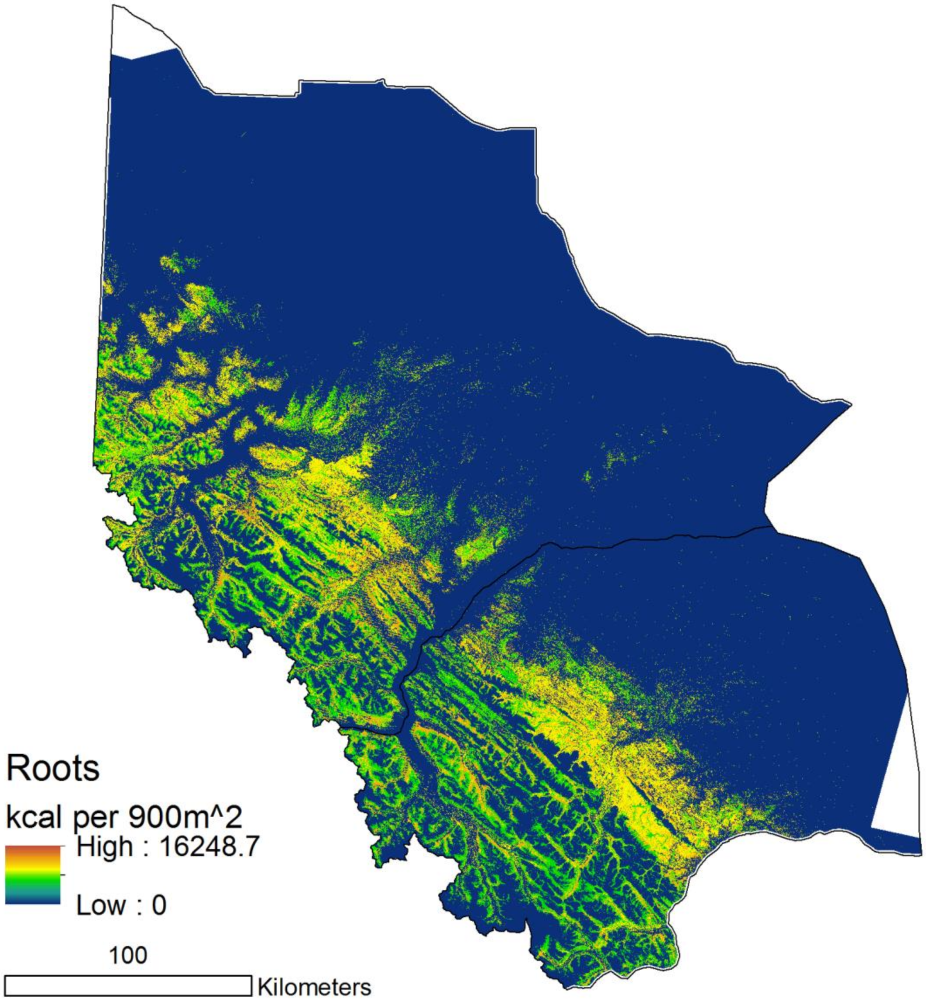

Figure 18: Digestible energy of root matter in the Grande Cache and Yellowhead population units. A single species, *Hedysarum alpinum* (alpine sweetvetch) was used for estimating root resources since it dominates the spring/fall diet of bears in the area.

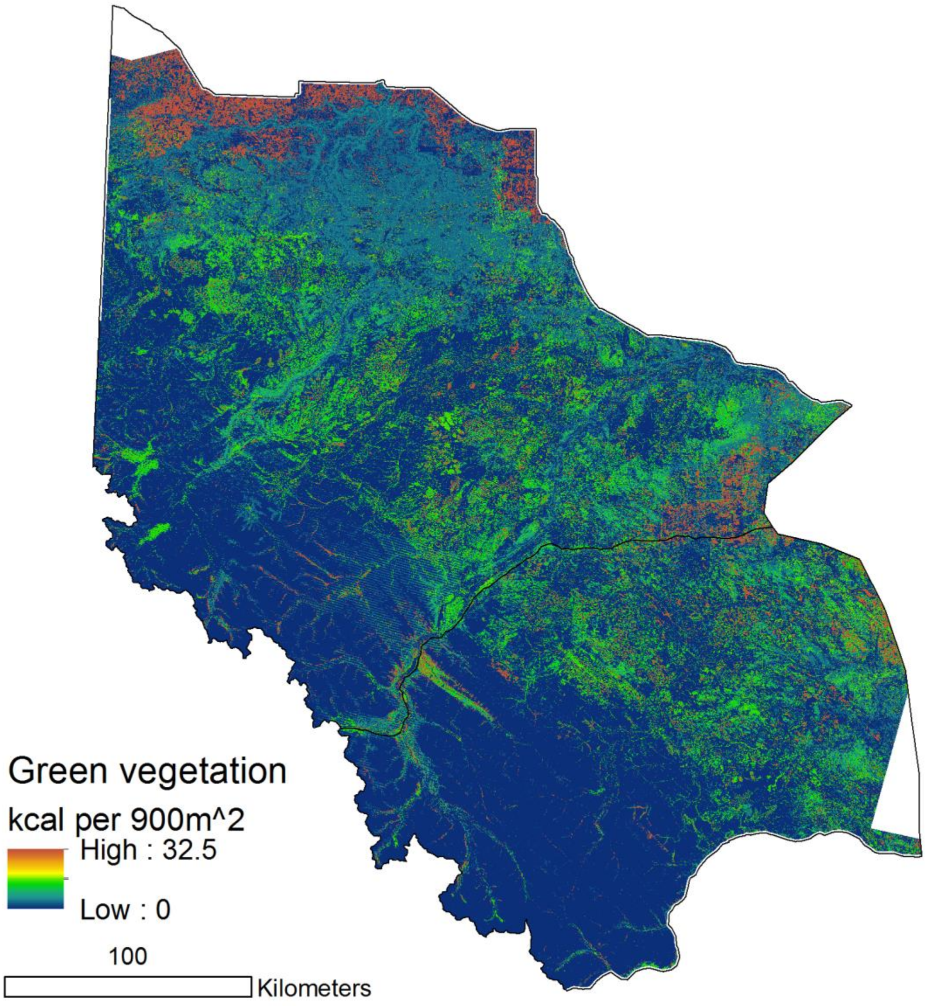

Figure 19: Digestible energy of green herbaceous matter in the Grande Cache and Yellowhead population units. This represents contributions from 4 species: *Equisetum arvense* (horsetail), *Heracleum lanatum* (cow parsnip), *Taraxacum officinale* (dandelion), and *Trifolium* spp. (clover).

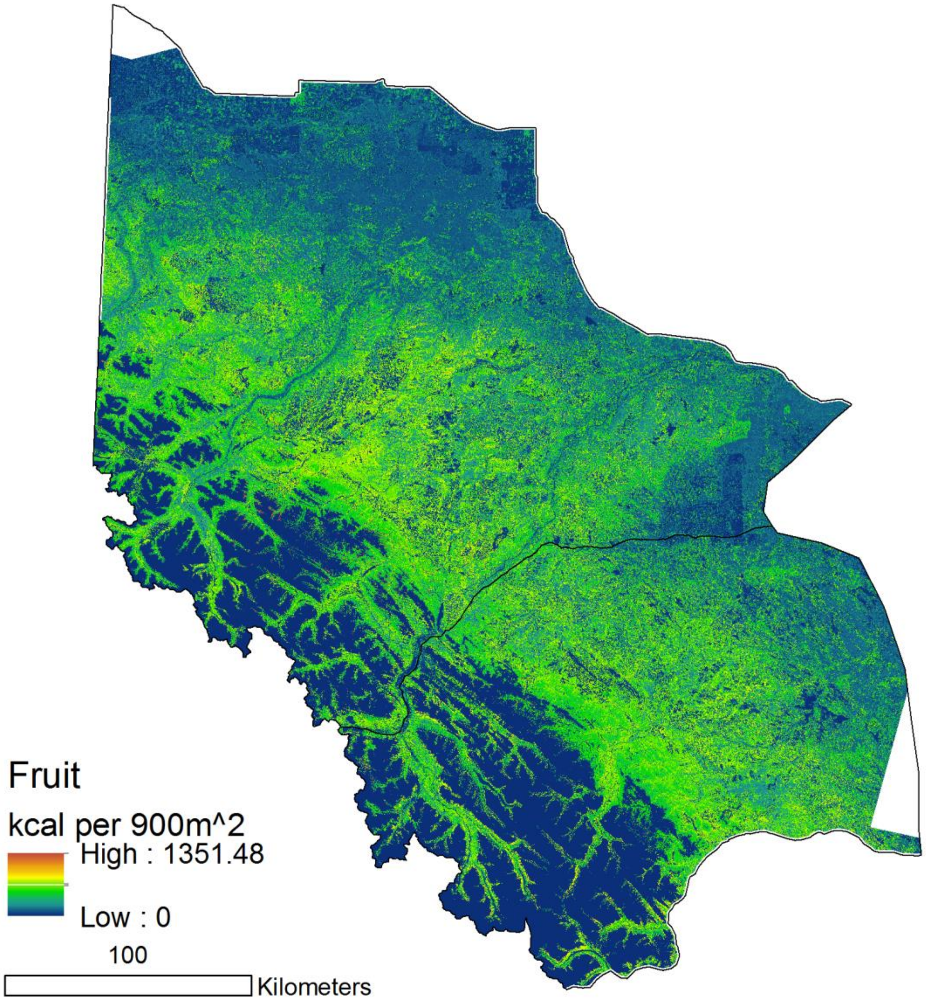

Figure 20: Digestible energy of fruiting resources in the Grande Cache and Yellowhead population units. This represents total fruiting biomass from nine species, although four species (*Shepherdia canadensis, Vaccinium membranaceum, Vaccinium myrtilloides, and Vaccinium vitis-idaea*) dominate the diets and biomass in the region.

Research Theme: Reproduction

The Measurement of Reproductive Hormones in the Hair of Brown Bears, and an Assessment of their Amounts in Relation to Reproductive Status, Stress, Body Condition, and Capture History

Authors: Marc Cattet and David Janz
With laboratory assistance by: Luciene Kapronczai and Gillian Cattet
And with collaborations by: Gordon Stenhouse, Joy Anne Erlenbach, Heiko T. Jansen, O. Lynne Nelson, Charles T. Robbins, Arne Söderberg, Andreas Zedrosser, and Jon E. Swenson

1. Introduction

In this study, we developed and validated laboratory techniques to accurately and reliably measure three steroid hormones – estradiol, progesterone, and testosterone – that are indicative of reproductive function in the hair of brown bears[1]. Although techniques to measure these hormones in other biological media, including blood serum and urine, are well established, the use of hair required the development of new procedures. Nevertheless, use of hair to potentially support the recovery of brown bears in Alberta offers several advantages over other biological media. Hair can be collected from animals without capturing them, e.g. with the use of hair traps (Woods *et al*., 1999). This avoids the potentially confounding influence of stress caused by capture and handling and, consequently, reduces the likelihood of adversely affecting the health and fitness of brown bears (Cattet *et al*., 2008). Hair is easy and inexpensive to prepare for storage; simply air-dry, seal in paper envelopes and store at indoor ambient temperature (Macbeth *et al*., 2010). Samples can be assigned to individual animals through DNA extraction and analysis (Proctor *et al*., 2010). Finally, because steroid hormones in hair do not degrade appreciably over time or after exposure to the environment (Macbeth *et al*., 2010), it opens the possibility of conducting analyses using archived samples, including museum specimens.

Although potential exists to evaluate a range of physiological functions through the analysis of hormones in hair (Stalder and Kirschbaum, 2012), our primary focus in this study has been reproduction because it is an important attribute of health (i.e., reproduction may cease when health is poor) and biological fitness in individual animals (Eberhardt, 2002; Zedrosser *et al*.,

---

[1] Brown bear and grizzly bear refer to the same species, *Ursus arctos*, with "brown bear" being the more general term applied to the species across its Holarctic distribution. Because we obtained hair samples from several sources, including outside of North America where the term grizzly bear is not used, we have opted to use "brown bear" for this report.

2013), and because it is required as a measurement to estimate reproductive rates at the population level (Garshelis *et al*., 2005). The detection and quantification of hormones in hair is in itself meaningless without verification that hormone levels truly reflect physiological and behavioral processes at the level of the animal. Accordingly, we sought to determine if changes in the reproductive status and annual activity pattern of eight captive adult brown bears housed at the Washington State University Bear Research, Education, and Conservation Center were matched by characteristic changes in the reproductive hormone profile (i.e., the relative amounts of the three hormones) of their hair. Confirmation of the biological validity of physiological indicators (often termed "biomarkers") also requires the evaluation of potentially confounding factors. Otherwise, the interpretation of hormone levels can be prone to error. Thus, we also assessed reproductive hormone levels in hair collected from 174 free-ranging brown bears in relation to: (i) the hair cortisol concentration, a recognized indicator of long-term stress (Macbeth *et al*., 2010; Bryan *et al*., 2013), (ii) body condition, an expression of energy status and potential indicator of nutritional stress (Cattet *et al*., 2002), (iii) various biological attributes; and (iv) capture history. We intentionally targeted stress and energy status because these factors are known to affect reproduction (Dickens *et al*., 2010; Robbins *et al*., 2012), and because they may also serve as important links between human-caused environmental change and depressed reproductive output (Acevedo-Whitehouse and Duffus, 2009; Semeniuk *et al*., 2012).

Herein we report on three years of research into the development of laboratory techniques to measure reproductive steroid hormones (estradiol, progesterone, and testosterone) in brown bear hair, and the verification of hair hormone levels in relation to the biology (in particular, the reproductive status), long-term stress, body condition, and capture history of the bears from which the hair was collected. We caution, however, that the findings presented in this report should be considered preliminary to the extent that the statistical analyses of data was completed recently, within the past few weeks. Thus, the interpretation of results has yet to benefit from crucial review and discussion among the various co-investigators and collaborators.

1.1 Statement of Objectives

Our three objectives under the Brown Bear Reproduction Theme were to:

1) Develop and validate non-invasive biomarkers of reproductive state that can be measured in brown bear hair.
2) Investigate the effect of long-term stress on reproduction
3) Develop multi-state models to identify dynamic relationships between demographic metrics, reproductive function, long-term stress, and environmental covariates.

2.Methods

2.1 Sources of brown bear hair

We obtained 264 hair samples collected from three independent projects studying brown bears in Canada, the United States, and Sweden from 2000 to 2015. In collaboration with Joy Anne Erlenbach and Drs. Heiko Jansen, Lynne Nelson, and Charles Robbins at the Washington State University Bear Research, Education, and Conservation Center, we obtained a total of 90 hair samples collected from eight captive adult brown bears (six females, two males) from April 2013 to February 2015. In collaboration with Drs. Arne Söderberg, Andreas Zedrosser, and Jon Swenson of the Scandinavian Brown Bear Research Project, we obtained a total of 133 hair samples collected from brown bears in Sweden, of which 63 bears were captured by remote drug delivery from helicopter from April 2000 to April 2007, and 70 bears were legally killed by hunters from August to October 2008. The remaining 41 samples were collected by the Foothills Research Institute Grizzly Bear Program from free-ranging brown bears in Alberta from June 2009 to September 2014. Of these samples, 16 were collected from bears captured by remote drug delivery from helicopter, 24 from bears captured by culvert trap, and one from a bear killed for wildlife management. In total, over the three projects, these samples represented 182 unique individual bears, from which 11 individuals were sampled on 2-13 occasions. Although hair collection methods varied slightly by project, hair samples were handled in a similar manner. They were placed into a paper envelope, the envelopes were left open for several hours to ensure that the samples were air-dried, and then they were sealed and stored under low light at room temperature (~20°C) until the time of laboratory analysis.

2.2 Laboratory analysis of hair hormone concentrations

We used guard hairs with the follicles removed in most cases to determine hormone levels, as recommended by Macbeth et al. (2010). However, follicles were retained for 34 samples from captive to allow paired comparisons with samples that had follicles removed, to determine if the presence of follicles significantly affected the measurement of hormone levels (see Table 3). Surface contamination was removed by washing hairs with methanol (three 3 min washes), as described in detail elsewhere (Macbeth et al., 2010). Following decontamination, hair was dried, ground to a fine powder using a ball mill, and weighed. Ground hair samples for determination of progesterone, testosterone, and cortisol were immersed in 0.5 ml of high-resolution gas chromatography-grade methanol, gently swirled (10 seconds), and placed on a slowly spinning rotator to extract for 24 hours. Following extraction, samples were centrifuged for 15 minutes at 2150 g, the methanol extract was removed, evaporated until dryness under nitrogen gas (38°C), and reconstituted in phosphate buffer (0.2 ml). Hormone levels were quantified as picograms of hormone per milligram of washed and dried hair (pg/mg) using commercially available enzyme-linked immunoassay kits, which we had previously validated for use in brown bears. The procedure for estradiol extraction followed similar steps. However, after testing several extraction solvents, we determined that use of tert-butyl methyl ether provided the most reliable results for estradiol.

2.3 Statistical analysis

We used linear mixed effects models (Zuur *et al*. 2009) in three separate analyses to evaluate relationships between hair hormone concentration, as the response variable, and a range of potential predictor variables (Tables 1, 3, and 5). The first analysis was restricted to data collected from eight captive bears at the Washington State University Bear Research, Education, and Conservation Center (Table 1). Our goal with this analysis was to determine if changes in the reproductive status and annual activity pattern of the captive bears affected the reproductive hormone profile of their hair in a consistent manner. We used hormone concentration in hair as the response variable and included reproductive hormone name (estradiol, progesterone, testosterone) as a categorical factor in the analysis. This approach allowed for comparison among the three hormones, which are known to be physiologically dependent, within a single model. However, because of differences in their range of concentrations, the concentration values for each hormone were standardized before the analysis such that a value of 0 represented the mean concentration for each hormone, i.e., 0.0133 pg/mg for estradiol, 4.78 pg/mg for progesterone, and 8.79 pg/mg for testosterone. Bear identification and sampling event were assigned as random effects. We used a stepwise backward-selection approach, starting with a global model containing all fixed effects and potential interactions. We then sequentially eliminated the least important variable or interaction based on a likelihood-ratio test, more commonly called a deviance test, that drops each explanatory variable in turn and each time calculates the difference in deviances and compares the difference to a Chi-square distribution (Zuur *et al*., 2013). The elimination of variables ceased, and the final model was determined, when the deviance statistic was at its lowest value.

We followed the same approach for the second analysis, but in this case the data was restricted to data collected from collected from 174 free-ranging brown bears that were either captured in Alberta or Sweden, or killed legally in Sweden (Table 3). Our intent with this analysis was two-fold. First, we wanted to determine if the reproductive hormone levels, as well as the cortisol levels, of free-ranging and captive bears were similar with respect to their absolute amounts, but also with respect to relative differences in hormone levels (hormone profiles) at different phases of the reproductive cycle and at different times of the year. Second, we wanted to determine if differences in hair cortisol concentration (a putative measure of long-term stress), body condition (as estimated by the body condition index [Cattet *et al*., 2002]), and/or capture history among bears influenced their reproductive hormone levels in a manner that could potentially alter reproductive activity.

With the third analysis, we used the same approach again but this time the response variable was the hair cortisol concentration (HCC) and the data set was comprised of information collected from 63 free-ranging brown bears, representing 20 family groups, captured in Sweden (Table 5). Each family group comprised an adult female with 1-3 yearlings. Our goal with this analysis was to determine if the HCC of yearlings was affected by the mother's HCC, as well by the age of the mother and/or the number of times that she had been captured.

Prior to each analysis, we evaluated respective data sets for (i) outliers within the response and predictor variables, (ii) homogeneity of variances, and (iii) collinearity among predictor variables. Following this, we centered continuous covariates to aid in the interpretation of parameter coefficients (Schielzeth, 2010). We used the ‘lme4’ package (Bates et al., 2015) in R 3.2.1 (R Core Team, 2015) for statistical analyses. Final models were validated by evaluating the distribution of standardized model residuals for normality, and by plotting standardized model residuals vs. the covariate values to ensure that the residuals were scattered at random around the horizontal line at zero (Zuur *et al*., 2009). We used the ‘ggplot2’ package (Wickham, 2009) in R 3.2.1 (R Core Team, 2015) for the graphical presentation of data and model results.

3. Results and Preliminary Interpretations

3.1 Detection and measurement of steroid hormones

Using the same extraction procedure that we developed for cortisol (Macbeth *et al*., 2010), we have validated progesterone and testosterone in brown bear hair for their accuracy and precision in the laboratory. Importantly, we can measure these hormones in similarly small quantities of hair compared to cortisol (i.e., 25 mg hair). Estradiol in hair proved to be more challenging, since it required the development of a new method that we determined through the comparative testing of a variety of different extraction solvents. We are now extracting estradiol from brown bear hair using tert-butyl methyl ether as the extraction solvent. However, relative to the other hormones, estradiol levels in brown bear hair are very low. Consequently, we require larger quantities of hair (50 mg) to ensure our concentration measurements are accurate. Nonetheless, we are now able to detect and measure the concentrations of four steroid hormones – cortisol, estradiol, progesterone, and testosterone – with 135-150 mg of guard hair. To provide a frame of reference for this quantity, it is similar to the amount of hair snagged from bears that encounter barbwire hair traps. What is most significant about this is it truly enables the application of these techniques to hair samples collected non-invasively, i.e., without capture, restraint, and handling. In recognizing this capability, hair samples collected during the 2014 brown bear DNA inventory in the Yellowhead Bear Management Area have been subdivided into two sets with one set used for DNA analyses in 2014-15 and the other set held for hormone analyses to be completed over the next 2 years.

3.2 Reproductive hormones in the hair of captive brown bears

Fluctuations in hair hormone concentrations over time appeared to coincide predictably with reproductive events (Fig. 1; Table 2). Hormone levels peaked in April immediately prior to breeding in both females and males, and then declined to the lowest levels from June to August (Fig. 2). Of exception were two females that bred successfully in May. Throughout pregnancy from June to November, progesterone levels in these females continued to rise to reach peak levels in September-October while estradiol levels declined to low levels from June to August, and then gradually increased during September to November. These changes over time in progesterone and estradiol levels are characteristic of pregnancy in many mammals, as measured in serum levels. Reproductive hormone levels in male and non-pregnant females changes similarly throughout the year. Notable however, because it stands in contrast to serum levels, is that mean testosterone levels were considerably greater in females than males (10.7 vs. 4.3 pg/mg). In all, this biological validation of reproductive hormone dynamics in the hair of captive brown bears was a necessary requisite to the interpretation of reproductive hormone levels in the hair of free-ranging brown bears exposed to diverse environmental factors. For 34 samples which were subdivided prior to hormone extractions into hair with follicles removed and hair with follicles intact, the hair with follicles intact consistently yielded higher concentrations of all three hormones (Table 2). In general, hair hormone levels tended to decrease with age, but at a more rapid rate with estradiol than with progesterone and testosterone (Table 2; Fig. 3).

3.3 Reproductive hormones in the hair of free-ranging brown bears

The ranges of estradiol and testosterone concentrations were similar between free-ranging and captive bears (estradiol: 4.3-26.1 pg/100 mg vs. 4.1-21.5 pg/100 mg; testosterone: 0.2-27.6 pg/mg vs. 0.8-25.0 pg/mg). However, the ranges of progesterone and cortisol concentrations were greater in free-ranging bears (progesterone: 0.3-17.4 pg/mg vs. 1.0-8.5 pg/mg; cortisol: 0.3-13.0 pg/mg vs. 0.1-2.5 pg/mg). We determined that seasonal differences in reproductive hormone levels of free-ranging bears did not fully match the pattern of changes seen in captive bears (Fig. 4). Mean estradiol and testosterone levels increased in all sex, age, and reproductive classes from April to October (Fig. 5). Mean progesterone levels increased from April to June, but decreased to lower levels from August to October (Fig. 5). The differences between free-ranging and captive bears appeared to be due to three potentially confounding factors – (i) the event experienced by a bear immediately prior to hair collection, (ii) its hair cortisol level, and (iii) its body condition (Table 4). Bears captured by culvert trap had greater hair hormone levels than measured in bears captured by helicopter or killed by hunters (Fig. 6). Given that the differences were similar across all four hormones, this was likely due to soiling of hair by urine, faeces and bait in culvert traps altering the permeability of hair allowing the influx of hormones from sebum and sweat, in addition to the blood circulation (Macbeth *et al*., 2010; Cattet *et al*., 2014). Estradiol and progesterone levels were inversely associated with cortisol levels, whereas the association between testosterone and cortisol was direct (Fig. 6). This suggests that under conditions of long-term stress (high hair cortisol levels), reproductive activity may be suppressed in females. Estradiol levels were inversely associated with body condition, whereas associations between progesterone and body condition, and between testosterone and body condition, were direct (results not shown). This suggests that reproductive activity could be suppressed in both sexes under conditions of nutritional stress (low body condition).

3.4 Maternal effects on the hair cortisol concentration of yearling brown bears

We determined that hair cortisol concentrations (HCC) in yearling bears were not associated with their mother's HCC (Table 6). However, yearling HCCs were significantly influenced by an interaction between the mother's age and the number of times that she had been captured (Fig. 7). In general, yearling HCCs were higher in family groups with older mothers than those with younger mothers. However, the magnitude of this age-related effect increased in direct proportion to the number of times a mother had been captured. Consequently, yearlings with mothers that had been captured many times (e.g., 6-8×) had greater HCCs than similar-age mothers that were only captured once or twice. Given the association between the HCC and reproductive hormone levels in the hair of yearlings (Fig. 8), it seems plausible that sexual maturation could be delayed for the offspring of mothers that have a lengthy capture history.

4. Deliverables and Outcomes

The deliverables of this research are:

- new laboratory techniques utilizing enzyme-linked immunoassays to accurately and reliably measure three reproductive hormones – estradiol, progesterone, and testosterone – in the hair of brown bears.
- The outcomes of this research are:
- verification that reproductive hormone dynamics in the hair of captive adult brown bears coincides with changes in their reproductive status and annual activity patterns;
- preliminary results to suggest that reproductive hormone profiles in the hair of free-ranging brown bears are influenced by other factors, including indicators of long-term stress (e.g., high hair cortisol concentration and/or poor body condition) that did not appear to be acting on captive bears; and
- evidence to demonstrate that hair cortisol levels in dependent offspring bears are directly influenced by their mother's age and capture history.

4.1 Some Concluding Remarks

Although at this time we are not yet able to demonstrate that reproductive hormone profiles in the hair of free-ranging brown bears can be used to distinguish among bears of different sex and age class and reproductive status, more research is clearly needed to aid in understanding how alterations in reproductive hormone profiles due to factors, such as long-term stress and body condition, may affect reproductive behavior and physiology. In addition, future sampling based solely on hair trapping (barbwire snags) and scheduled to coincide with critical reproductive cycle events throughout the year, especially for females, may help shed light on the applicability of this technique to help inform managers about the reproductive states of brown bears in a population.

Over the past 3 years, we have addressed two of our three research objectives; that is, to develop and validate non-invasive biomarkers of reproductive state that can be measured in brown bear hair, and to investigate the effect of long-term stress on reproduction. For the third objective, we had proposed to use multi-state modelling to assess temporal relationships between reproductive function and long-term stress in individual bears, environmental covariates, and measures of population performance (reproductive and survival rates) for brown bears within the Yellowhead and Grande Cache Bear Management Areas (BMA) of Alberta. With this analysis, individual female bears were to be followed through adulthood to ascertain how long-term stress and a suite of environmental variables, reflecting anthropogenic and natural landscape features, influence their transition between different reproductive states, i.e., pregnant, lactating, not reproductively active. We would then interpret the results of this analysis in light of our current understanding of survival and reproductive rates in the Yellowhead and Grande Cache BMAs (Boulanger and Stenhouse, 2014). At present, we have concurrent reproductive and long-term stress data from 35 candidate females that were captured multiple times (2-6×) from 1999 to 2014, which should be sufficient to conduct the multi-state analysis. What we did not anticipate, however, is the approximate 2-year time-lag that occurs between acquiring data from bears and compiling and preparing the data from their environment. Consequently, to avoid reducing sample size, which would limit model complexity, we are delaying this analysis until early next year when the full complement of environmental data will be available.

5. Literature Cited

Acevedo-Whitehouse K, Duffus ALJ (2009) Effects of environmental change on wildlife health. *Philosophical Transactions of the Royal Society B* 364: 3429–3438.

Bates D, Maechler M, Bolker B, Walker S (2015) lme4: Linear mixed-effects models using Eigen and S4. R package version 1.1-8, http://CRAN.R-project.org/package=lme4.

Boulanger J, Stenhouse GB (2014) The impact of roads on the demography of grizzly bears in Alberta. *PLoS ONE* 9(12): e115535. doi:10.1371/journal.pone.0115535

Bryan HM, Darimont CT, Paquet PC, Wynne-Edwards KE, Smits JEG (2013) Stress and reproductive hormones in brown bears reflect nutritional benefits and social consequences of a salmon foraging niche. *PLoS ONE* 8: e80537.

Cattet M, Boulanger J, Stenhouse G, Powell RA, Reynolds-Hogland MJ (2008) Long-term effects of capture and handling in ursids: implications for wildlife welfare and research. *Journal of Mammalogy* 89: 973–990.

Cattet MRL, Caulkett NA, Obbard ME, Stenhouse GB (2002) A body condition index for ursids. *Canadian Journal of Zoology* 80: 1156–1161.

Cattet M, Macbeth BJ, Janz DM, Zedrosser A, Swenson JE, Dumond M, Stenhouse GB (2014) Quantifying long-term stress in brown bears with the hair cortisol concentration: a biomarker that may be confounded by rapid changes in response to capture and handling. *Conservation Physiology* 2: doi:10.1093/conphys/cou026.

Dickens MJ, Delehanty DJ, Romero LM (2010) Stress: An inevitable component of animal translocation. *Biological Conservation* 143: 1329–1341.

Eberhardt LL (2002) A paradigm for population analysis of long-lived vertebrates. *Ecology* 83: 2841–2854.

Garshelis DL, Gibeau ML, Herrero S (2005) Grizzly bear demographics in and around Banff National Park and Kananaskis Country, Alberta. *Journal of Wildlife Management* 69: 277–297.

Macbeth BJ, Cattet M, Stenhouse GB, Gibeau ML, Janz DM (2010) Hair cortisol concentration as a non-invasive measure of long-term stress in free-ranging brown bears (*Ursus arctos*): considerations with implications for other wildlife. *Canadian Journal of Zoology* 88: 935–949.

Proctor M, McLellan B, Boulanger J, Apps C, Stenhouse G, Paetkau D, Mowat G (2010) Ecological investigations of brown bears in Canada using DNA from hair, 1995–2005: a review of methods and progress. *Ursus* 21: 169–188.

R Core Team (2015) R: A language and environment for statistical computing. R Foundation for Statistical Computing, Vienna, Austria. URL http://www.R-project.org/.

Robbins CT, Ben-David M, Fortin JK, Nelson OL (2012) Maternal condition determines birth date and growth of newborn bear cubs. *Journal of Mammalogy* 93: 540–546.

Schielzeth H (2010) Simple means to improve the interpretability of regression coefficients. *Methods in Ecology and Evolution* 1: 103–113.

Semeniuk CAD, Musiani M, Hebblewhite M, Grindal S, Marceau DJ (2012) Incorporating behavioral-ecological strategies in pattern-oriented modeling of caribou habitat use in a highly industrialized landscape. *Ecological Modelling* 243: 18–32.

Stalder T, Kirschbaum C (2012) Analysis of cortisol in hair – State of the art and future directions. *Brain, Behavior, and Immunity* 26: 1019–1029.

Wickham H (2009) ggplot2: Elegant Graphics for Data Analysis. Springer, New York, NY, pp 1–213.

Woods JG, McLellan BN, Paetkau D, Proctor M, Lewis D, Strobeck C (1999) Genetic tagging free-ranging black and brown bears. *Wildlife Society Bulletin* 27: 616–627.

Zedrosser A, Pelletier F, Bischof R, Festa-Bianchet M, Swenson JE (2013) Determinants of lifetime reproduction in female brown bears: early body mass, longevity, and hunting regulations. *Ecology* 94: 231–240.

Zuur AF, Hilbe JM, Ieno EN (2013) A Beginner’s Guide to GLM and GLMM with R – A frequentist and Bayesian perspective for ecologists. Highland Statistics Ltd, Newburgh, UK, pp 1–256.

Zuur AF, Ieno EN, Walker NJ, Saveliev AA, Smith GM (2009) Mixed Effects Models and Extensions in Ecology with R. Springer, New York, NY, pp 1–574.

6. Tables and Figures

Table 1. Variables evaluated as potential determinants of the reproductive hormone concentrations in hair samples collected from eight captive adult brown bears housed at the Washington State University (WSU) Bear Research, Education, and Conservation Center.

Variable	Variable type	Variable categories or range of values
Bear identification	categorical	name unique to each bear
Sex and reproductive status	categorical	female (not breeding), female (megestrol acetate), female (breeding), female (pregnant), female (lactating), male (not breeding), or male (breeding)
Adjusted age (age in years + ordinal date of sampling/365)	continuous	8.28 – 13.09
Year	categorical	2013 – 2015
Month	categorical	February, April, May, June, July, August, September, October, or November
Sampling event (unique to each bear and each sampling time)	continuous	1 – 90
Follicle removed prior to hormone analysis	categorical	yes or no
Reproductive hormone	categorical	estradiol, progesterone, or testosterone
Cortisol concentration (pg/mg of hair)	continuous	0.13 – 2.46

Table 2. Standardized coefficients (β_i), standard errors (SE), and significance (*p*) of linear mixed effects model variables describing reproductive hormone concentrations in hair samples collected from eight captive adult brown bears housed at the Washington State University (WSU) Bear Research, Education, and Conservation Center.

Fixed effects	β_i	SE	*p*
Intercept	-0.91	0.293	**0.009**
Sex and reproductive status (SRS)			
- female (breeding)	1.93	0.617	**0.002**
- female (lactating)	0.48	0.441	0.276
- female (megestrol acetate)	0.55	0.396	0.170
- female (pregnant)	-0.41	0.327	0.212
- male (not breeding)	1.60	0.577	**0.020**
- male (breeding)	1.41	0.810	0.090
- female (not breeding)	0		
Adjusted age (AA)	-1.26	0.217	**≤0.001**
Month			
- April	0.83	0.214	**≤0.001**
- May	0.60	0.433	0.169
- June	-0.18	0.286	0.519
- July	-0.02	0.279	0.957
- August	-0.08	0.199	0.706
- September	0.60	0.271	**0.028**
- October	0.46	0.201	**0.024**
- November	0.24	0.183	0.190
- February	0		
Follicle removed prior to hormone analysis			
- yes	0.36	0.109	**≤0.001**
- no	0		
Reproductive hormone (RH)			
- progesterone	-0.18	0.222	0.422
- testosterone	0.62	0.222	**0.006**
- estradiol	0		
Hair cortisol concentration (HCC)	0.14	0.085	0.102
Interactions[A]			
- SRS × RH			**≤0.001**
- RH × AA			**0.015**

- RH × HCC	0.101

[A] Significance (*p*) values for interactions between categorical factors are based on an analysis of variance (Type III ANOVA) of the fixed effects.

Table 3. Variables evaluated as potential determinants of the reproductive hormone concentrations in hair samples collected from 138 free-ranging brown bears that were either captured in Alberta (*N* = 32) or Sweden (*N* = 50), or killed legally in Sweden (*N* = 56).

Variable	Variable type	Variable categories or range of values
Bear identification	categorical	alpha-numeric code unique to each bear
Sex, age, and reproductive class	categorical	solitary adult female ((≥5 yrs), female with dependent offspring, juvenile female (<5 yrs), adult male (≥5 yrs), or juvenile male (<5 yrs)
Adjusted age (age in years + ordinal date of sampling/365)	continuous	1.28 – 22.67
Year	categorical	2000 – 2014
Month	categorical	April, May-June, August, or September-October
Sampling event (unique to each capture)	continuous	1 – 141[A]
Event preceding hair collection	categorical	capture by remote drug delivery from helicopter, capture by culvert trap, or death by gunshot
Number of captures per bear	continuous	1 – 8
Body condition index	continuous	-1.88 – 5.32
Reproductive hormone	categorical	estradiol, progesterone, or testosterone
Cortisol concentration (pg/mg of hair)	continuous	0.33 – 49.60

[A] The difference between number of bears (N = 138) and number of sampling events (N = 141) is explained by three bears in Alberta that were each captured and sampled on two occasions.

Table 4. Standardized coefficients (β_i), standard errors (SE), and significance (*p*) of linear mixed effects model variables describing reproductive hormone concentrations in hair samples collected from 138 free-ranging brown bears that were either captured in Alberta (*n* = 32) or Sweden (*n* = 50), or killed legally in Sweden (*n* = 56).

Fixed effects	β_i	SE	*p*
Intercept	0.62	0.231	**≤0.001**
Sex, age, and reproductive class (SARC)			
- juvenile female	-0.19	0.179	0.297
- female with dependent offspring	-0.12	0.201	0.539
- juvenile male	-0.42	0.179	**0.019**
- adult male	-0.24	0.169	0.151
- solitary adult female	0		
Month (M)			
- May-June	0.31	0.178	0.077
- August	0.37	0.224	0.099
- September-October	0.45	0.217	**0.038**
- April	0		
Event preceding hair collection (KC)			
- killed by hunter	-1.06	0.203	**≤0.001**
- capture by helicopter	-0.68	0.137	**≤0.001**
- capture by culvert trap	0		
Reproductive hormone (RH)			
- progesterone	0.46	0.224	**0.040**
- testosterone	0.08	0.224	0.724
- estradiol	0		
Hair cortisol concentration (HCC)	0.53	0.206	**0.009**
Body condition index (BCI)	-0.15	0.069	**0.037**
Interactions[A]			
- RH × SARC			**≤0.001**
- RH × M			**0.021**
- RH × HCC			**≤0.001**
- RH × BCI			**0.008**
- KC × HCC			**≤0.001**

[A] Significance (*p*) values for interactions between categorical factors are based on an analysis of variance (Type III ANOVA) of the fixed effects.

Table 5. Variables evaluated as potential determinants of the cortisol concentration in hair samples collected from 42 free-ranging yearling brown bears, representing 20 family groups that were captured in Sweden.

Variable	Variable type	Variable categories or range of values
Yearling's identification	categorical	alpha-numeric code unique to each bear
Sex	categorical	female or male
Adjusted age (age in years + ordinal date of sampling/365)	continuous	1.28 – 1.33
Mother's adjusted age	continuous	6.28 – 22.31
Year	categorical	2000 – 2007
Sampling event (unique to each family group)	continuous	1 – 20
Number of captures per mother	continuous	2 – 8
Mother captured in year of pregnancy	categorical	yes or no
Yearling's body condition index	continuous	-1.14 – 1.31
Mother's cortisol concentration (pg/mg of hair)	continuous	1.54 – 4.54

Table 6. Standardized coefficients (β_i), standard errors (SE), and significance (*p*) of linear mixed effects model variables describing the cortisol concentration in hair samples collected from 43 free-ranging yearling brown bears, representing 20 family groups that were captured in Sweden.

Fixed effects	β_i	SE	*p*
Intercept	1.84	0.321	**≤0.001**
Adjusted age	-0.12	0.121	0.311
Mother's adjusted age (MA)	-0.07	0.172	0.689
Number of captures per mother (MC)	0.13	0.173	0.459
Mother captured in year of pregnancy			
- yes	0.49	0.329	0.138
- no	0		
Interactions			
- MA × MC	1.13	0.200	**≤0.001**

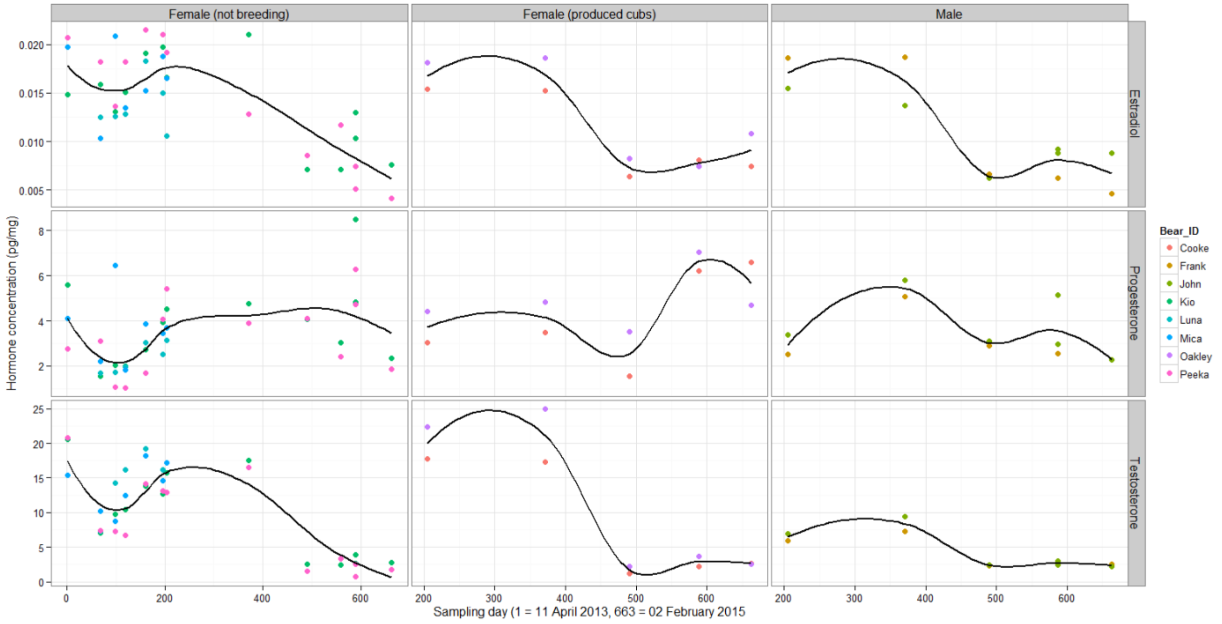

Figure 1. Changes in reproductive hormone concentrations in hair samples collected from eight captive adult brown bears from April 2013 to February 2015. A LOESS smoother with a span width of 0.75 was added to each panel to aid visual interpretation. Bear identification: Females (not breeding) – Kio, Luna, Mica, Peeka; Female (produced cubs) – Cooke, Oakley; and Male – Frank, John. Significant events in relation to sampling day: Onset of hibernation – days 196 and 559-561; Hibernation – days 587-589 and 663; Breeding – day 405; Pregnancy – days 490-589; and Lactation – day 663.

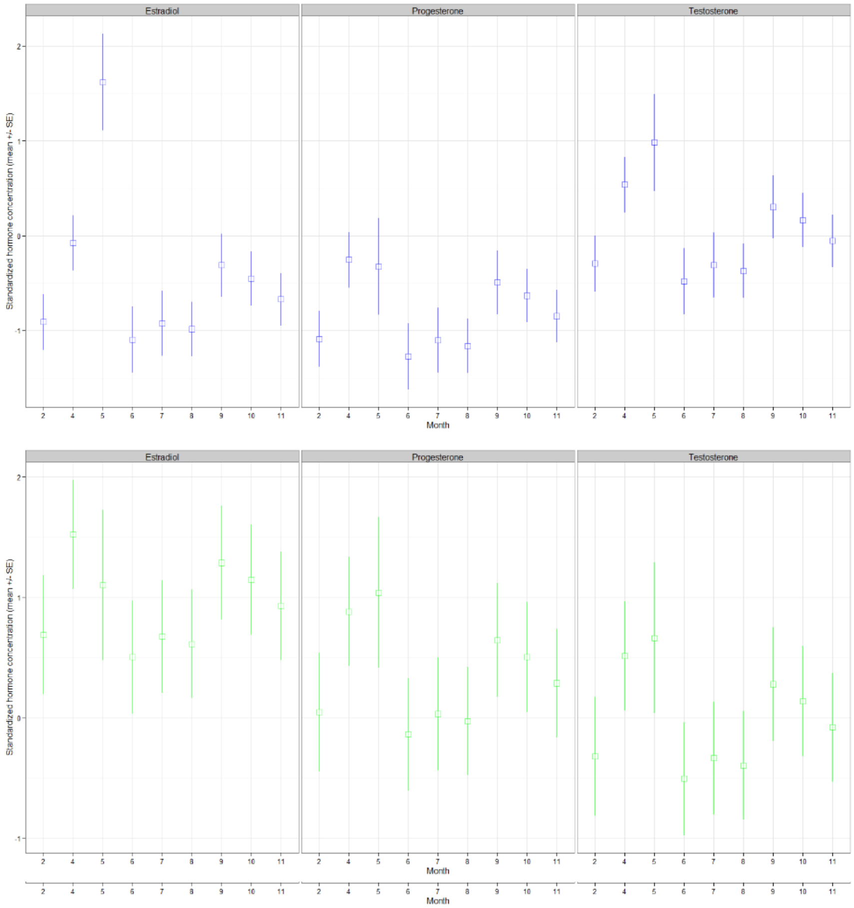

Figure 2. Reproductive hormone concentrations (mean ± SE) in hair samples collected from non-pregnant female (top panel - blue), pregnant female (middle panel – red), and male adult brown bears (bottom panel - green) as a function of month (February to November) as predicted from the linear mixed effects model in Table 2. The concentration values for each reproductive hormone were standardized prior to statistical analyses to allow comparison among the three hormones within a single model. The analyses are based on data collected from eight captive adult brown bears at 90 sampling events (6-13 events per bear) that occurred from April 2013 to February 2015. The plots are standardized for a 10.7 year-old brown bear with a hair cortisol concentration of 0.89 pg/mg. The standardized hormone concentrations are based on hair samples with follicles removed prior to laboratory analysis.

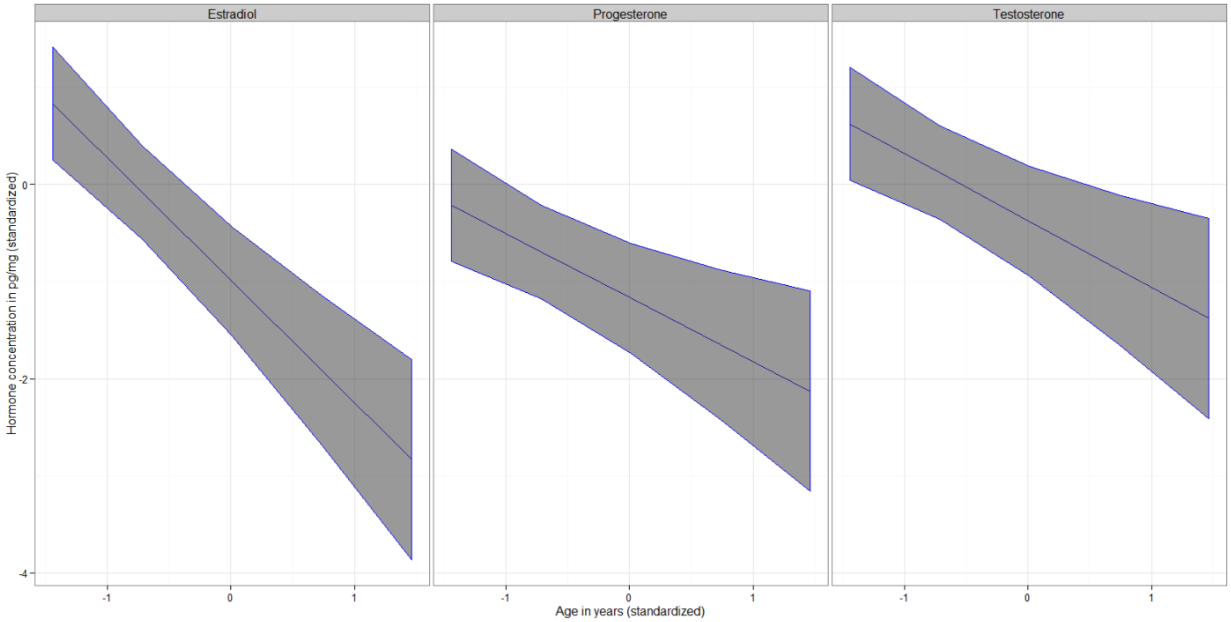

Figure 3. Reproductive hormone concentrations (mean ± 95% CI) in hair samples collected from adult brown bears as a function of age as predicted from the linear mixed effects model in Table 2. The concentration values for each reproductive hormone were standardized prior to statistical analyses to allow comparison among the three hormones within a single model. The analyses are based on data collected from eight captive adult brown bears at 90 sampling events (6-13 events per bear) that occurred from April 2013 to February 2015. The plots are standardized for non-breeding female brown bears ranging in age from 8.3-13.1 years, sampled in August, and with a hair cortisol concentration of 0.89 pg/mg. The standardized hormone concentrations are based on hair samples with follicles removed prior to laboratory analysis.

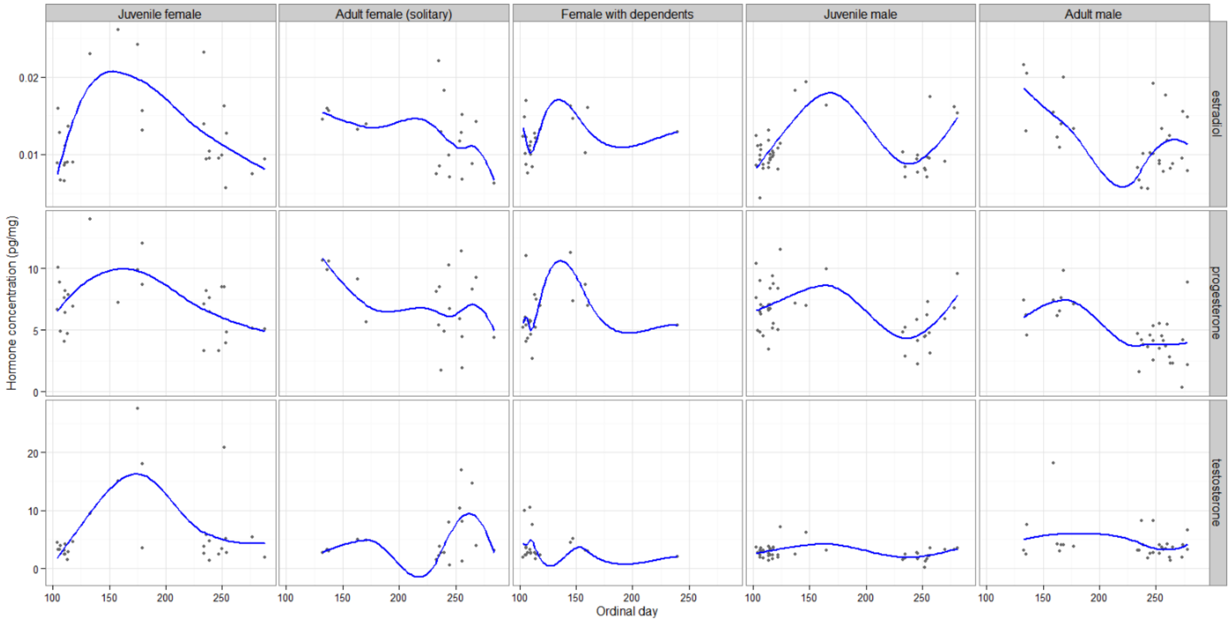

Figure 4. **Reproductive hormone concentrations by ordinal day in hair samples collected from 138 free-ranging brown bears from April 2000 to September 2014. A LOESS smoother with a span width of 0.75 was added to each panel to aid visual interpretation. Bears < 5-years in age are considered to be juveniles, whereas adults are ≥ 5 years. Calendar dates in relation to ordinal day: April 10 – day 100; May 30 – day 150; July 19 – day 200; and September 7 – day 250.**

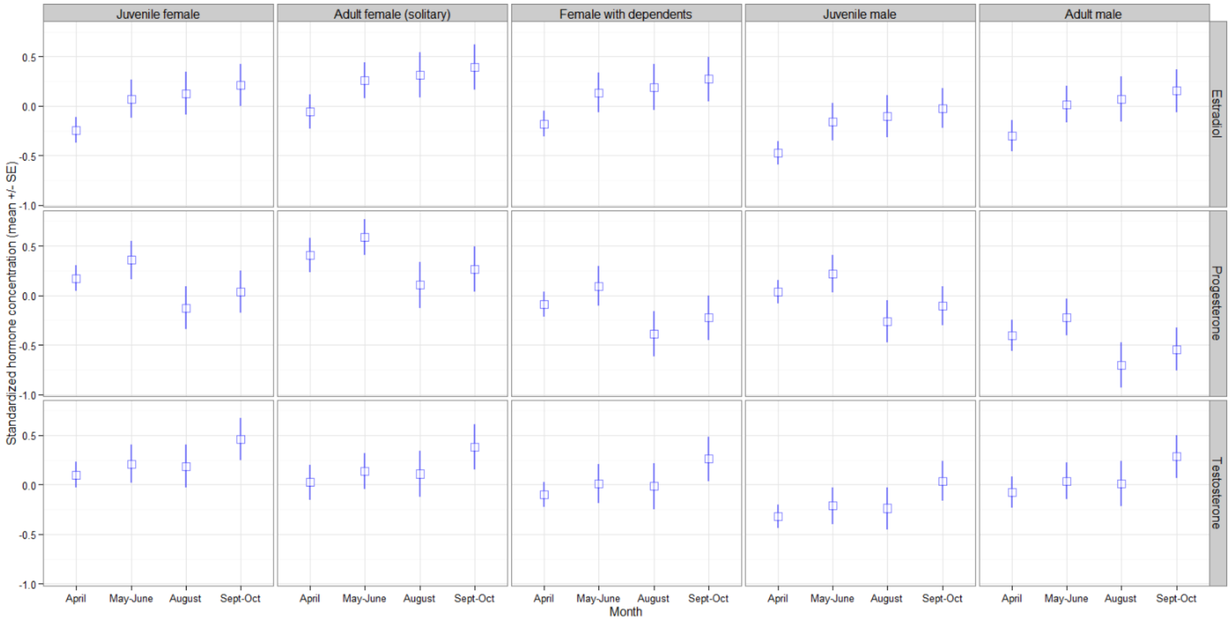

Figure 5. Reproductive hormone concentrations (mean ± SE) in hair samples collected from free-ranging brown bears as a function of sex, age, and reproductive class, and month as predicted from the linear mixed effects model in Table 4. The concentration values for each reproductive hormone were standardized prior to statistical analyses to allow comparison among the three hormones within a single model. The analyses are based on data collected from 138 free-ranging brown bears from April 2000 to September 2014. The plots are standardized for a brown bear, captured by remote drug delivery from a helicopter, with a body condition index of 0.80 and a hair cortisol concentration of 2.44 pg/mg.

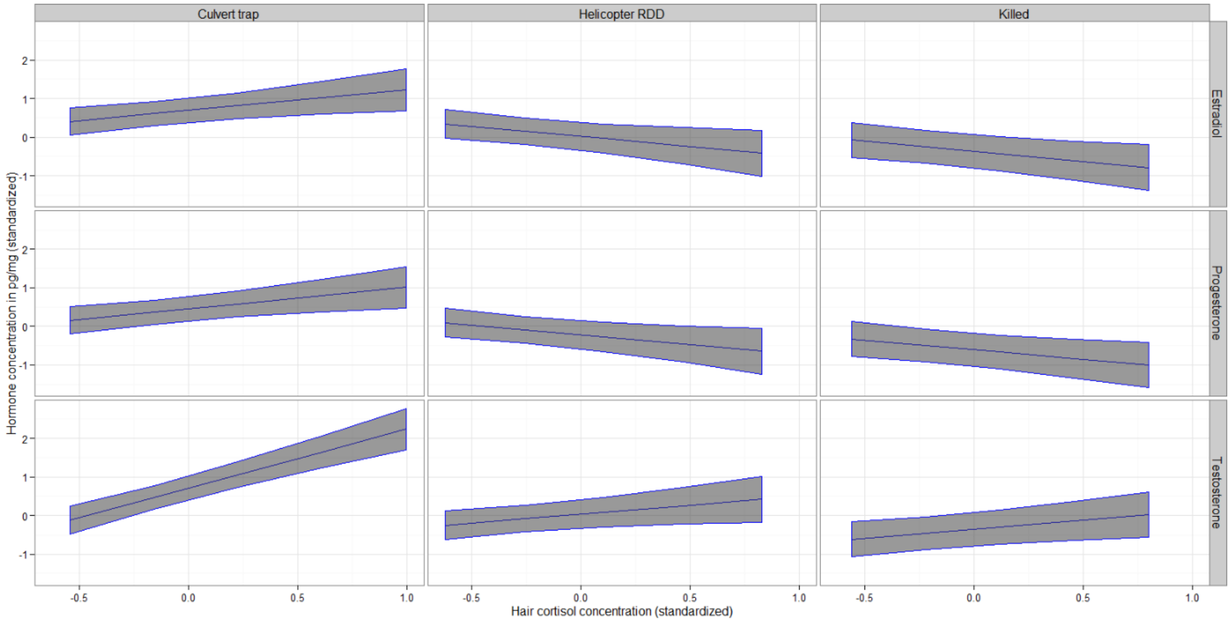

Figure 6. Reproductive hormone concentrations (mean ± 95% CI) in hair samples collected from free-ranging brown bears as a function of hair cortisol concentration, and the event preceding hair collection as predicted from the linear mixed effects model in Table 4. The concentration values for each reproductive hormone were standardized prior to statistical analyses to allow comparison among the three hormones within a single model. The analyses are based on data collected from 138 free-ranging brown bears from April 2000 to September 2014. The plots are standardized for an adult male brown bear, captured or killed in May-June, with a body condition index of 0.80.

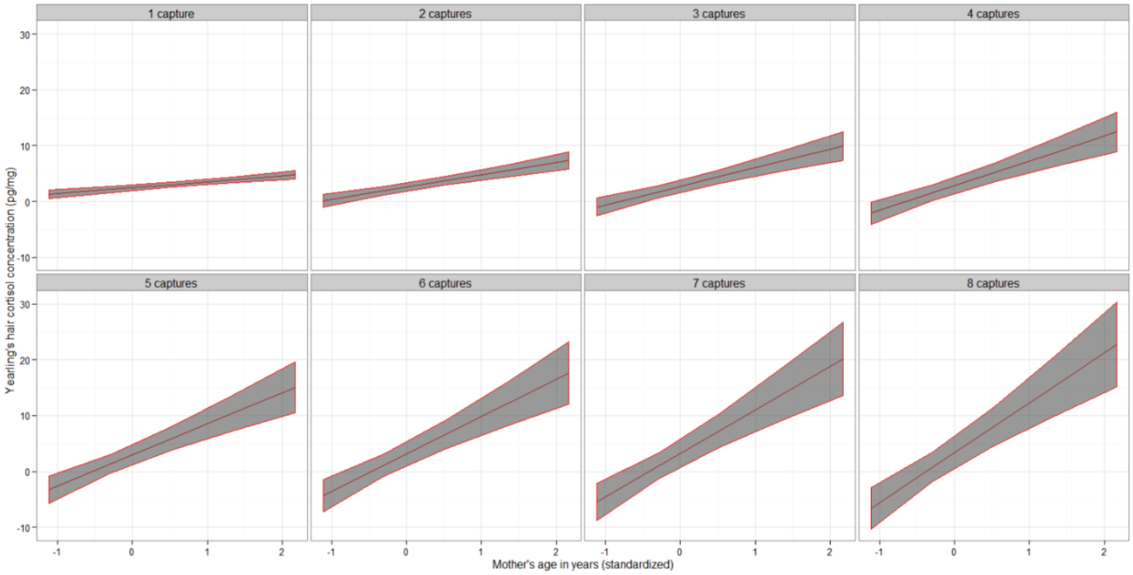

Figure 7. Cortisol concentrations (mean ± 95% CI) in hair samples collected from free-ranging yearling brown bears as a function of their mother's age, and the number of times that she had been captured as predicted from the linear mixed effects model in Table 3.2. The plots are standardized for adult female brown bears ranging in age from 6.3-22.3 years and yearlings that are 1.3-years old.

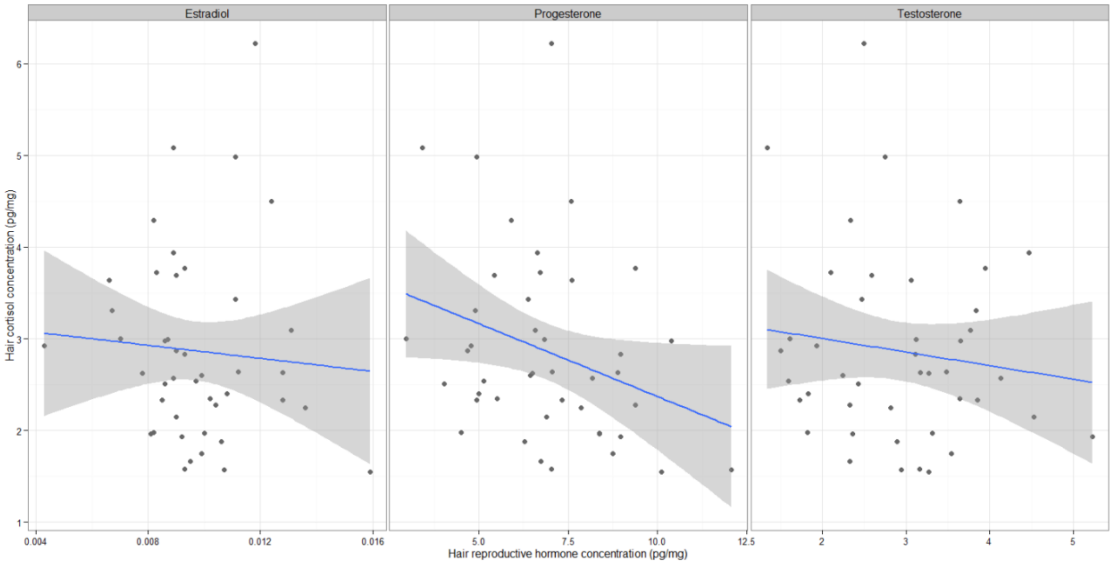

Figure 8. Cortisol concentrations in relation to reproductive hormone concentrations in hair samples collected from 42 free-ranging yearling brown bears, representing 20 family groups, captured in Sweden from April 2000 to April 2007. Fitted lines, based on simple linear regression, and 95% confidence intervals were added to each panel to aid visual interpretation.

Appendix A: Program Funding Partners

Government
Alberta Innovates Bio Solutions
Alberta Environment and Sustainable Resource Development
Parks Canada

Industry and Not for Profit Groups
Foothills Research Institute
Canadian Cooperative Wildlife Health Centre
Sundance Forest Industries Ltd.
Coal Valley Resources
Suncor Energy
Devon Canada
Canfor Forest Products
Grande Cache Coal Corp
Millar Western
Husky Oil
West Fraser
Teck Coal
Shell Canada
Weyerhaeuser Ltd
Conoco-Phillips
Encana
Canadian Natural Resources Limited
Spray Lakes Sawmills
Progress Energy Resources Corp.
Alberta Newsprint